Combination of computational and experimental approaches to rationalize and modify aldoxime dehydratase catalyzed reactions and their application

Dissertation

zur Erlangung des akademischen Grades
Dr. rer. nat.

Eingereicht von Hilmi Yavuzer
25.08.2021

Fakultät für Chemie
Universität Bielefeld

Erstgutachter: Prof. Dr. Harald Gröger
Zweitgutachter: Prof. Dr. Stephan Hammer

Termin der Disputation:
Ort: Bielefeld

Die vorliegende Arbeit wurde am Lehrstuhl für Industrielle Organische Chemie und Biotechnologie der Universität Bielefeld unter Leitung von Prof. Dr. Harald Gröger in der Zeit vom Januar 2018 bis September 2021 angefertigt. Die Arbeit wurde durch die Fachagentur für Nachwachsende Rochstoffe (FNR) (Fördernummer: 22001716) sowie durch die Europäische Kommission im Rahmen des ONE-FLOW Projekts finanziert (Fördernummer: 737266). Die Dissertation wurde selbstständig verfasst und hat in der gegenwärtigen oder einer anderen Fassung noch nicht einer anderen Fakultät oder Hochschule vorgelegen. Es wurden keine anderen als die in dieser Arbeit angegebenen Quellen und Hilfsmittel verwendet.

Hilmi Yavuzer

_____

Publikationen

Michael Hinzmann, Hilmi Yavuzer, Alessa Hinzmann, Harald Gröger
Discovery of novel aldoxime dehydratases with the 3DM system,
Manuskript in Arbeit.

Michael Hinzmann, Hilmi Yavuzer, Harald Gröger
Expanding the substrate scope of OxdRE towards benzylic aldoximes,
Manuskript in Arbeit.

Lukas Schober, Hilmi Yavuzer, Ana Maria Bago Rodriguez, Harald Gröger, Bernard P. Binks,
Pickering Emulsions enabling non-compatible chemoenzymatic two-step cascade towards n octanenitrile in batch and flow,
Manuskript in Arbeit.

Hilmi Yavuzer, Michael Hinzmann, Jianing Yang, Harald Gröger
Combination of structure-based sorting and in silico protein descriptors to increase the thermostability of enzymes,
Manuskript in Arbeit.

Hilmi Yavuzer, Jianing Yang, Lukas Schober, Harald Gröger
Rational biocatalyst design for a cyanide-free synthesis of long-chain fatty nitriles from their aldoximes,
Eur. J. Lipid Sci. Technol. Zur Veröffentlichung eingereicht.

Alessa Hinzmann, Hilmi Yavuzer, Yasuhisa Asano, Harald Gröger,
Improving Activity and Stability of Aldoxime Dehydratase OxdRE from Rhodococcus erythropolis by Directed Evolution,
ChembioChem. Zur Veröffentlichung eingereicht.

Hilmi Yavuzer, Yasuhisa Asano, Harald Gröger,
Rationalizing the unprecedented stereochemistry of enzymatic nitrile synthesis via a combined computational and experimental approach,
Angew. Chem. Int. Ed. **2021**, https://doi.org/10.1002/ange.202017234.

Carmen Plass, Alessa Hinzmann, Alessa, Michael Terhorst, Waldemar Brauer, Keiko Oike, Hilmi Yavuzer, Yasuhisa Asano, Andreas J. Vorholt, Tobias Betke, Harald Gröger
Approaching Bulk Chemical Nitriles from Alkenes: A Hydrogen Cyanide-Free Approach through a Combination of Hydroformylation and Biocatalysis,
ACS Catal. **2019,** https://doi.org/10.1021/acscatal.8b05062.

Vorträge

Hilmi Yavuzer, Yasuhisa Asano, Harald Gröger,
Rationalizing the unprecedented stereochemistry of resolutions with aldoxime dehydratases via molecular modeling,
37th Workshop, Graduate School of Chemistry and Biochemistry, November **2020**, Bielefeld.

Hilmi Yavuzer, H. D. Piyumi Wathsala, Fumihiro Motojima, Hiroaki Sasai, Yasuhisa Asano, Harald Gröger
Rationalizing the enantioselectivity of aldoxime dehydratases,
Cebitec Multistep Synthesis in Chemistry and Biology, November **2019**, Bielefeld.

Hilmi Yavuzer, Harald Gröger
Identification of new aldoxime dehydratases using 3DM as a bioinformatic tool
6th Cebitec Retreat, September **2019**, Bad Sassendorf.

Hilmi Yavuzer, Yasuhisa Asano, Harald Gröger
Rationalizing the enantioselectivity of aldoxime dehydratases,
5th Cebitec Retreat, September **2018**, Bad Sassendorf.

Hilmi Yavuzer, Yasuhisa Asano, Harald Gröger
Rationalizing the enantioselectivity of aldoxime dehydratases,
Molecular modeling workshop, März **2018**, Erlangen.

Posterpräsentationen

Hilmi Yavuzer, H. D. Piyumi Wathsala, Fumihiro Motojima, Hiroaki Sasai, Yasuhisa Asano, Harald Gröger
Rationalizing the enantioselectivity of aldoxime dehydratases,
Cebitec Multistep Synthesis in Chemistry and Biology, November **2019**, Bielefeld.

Hilmi Yavuzer, Yasuhisa Asano, Harald Gröger
Rationalizing the enantioselectivity of aldoxime dehydratases,
Molecular modeling workshop, März **2018**, Erlangen.

Danksagung

Zuallererst will ich meinem Doktorvater Prof. Dr. Harald Gröger danken, der mir die Möglichkeit gab mich mit spannenden Themen sehr frei zu befassen und mich in jeglicher Hinsicht weiterzuentwickeln. Herzlichen Dank für die gemeinsame Zeit, dein Vertrauen in meine Fähigkeiten und deine stetige Unterstützung für neue Ideen.

Herrn Prof. Stephan Hammer möchte ich für die sehr bereitwillige Übernahme des Zweigutachtens bedanken und für seine Unterstützung bei Fragen zu geeigneten analytischen Methoden.

Bei Prof. Yasuhisa Asano von der Toyama Prefectural University möchte ich mich neben der wertvollen Zusammenarbeit auf dem Themengebiet der Aldoximdehydratasen auch für seine unermessliche Gastfreundlichkeit in seinem Labor bedanken. お会いできて光栄でした。

Für die Finanzierung dieser Arbeit möchte ich mich bei der Fachagentur für Nachwachsende Rochstoffe (FNR) (Fördernummer: 22001716) sowie bei der Europäische Kommission im Rahmen des ONE-FLOW Projekts (Fördernummer: 737266) bedanken.

Während meiner Promotion hatte ich die Ehre großartige Studierende zu betreuen, die viele hervorragende Ergebnisse erzielt haben, weshalb ich mich ganz herzlich bei Caro Besse, Arne Merschel, Erich Gebel, Masaki Futrama, Katarina Klimova, Sören Jansen, Jianing Yang, Maximilian Böhm bedanken möchte

Für das Korrekturlesen dieser Arbeit möchte ich mich bei Dr. Alessa Hinzmann, Karla Wagner, Hannah Bork, Dr. Franziska Kühn, Dr. Daniel Bakonyi, Lukas Schober, Michael Hinzmann, Alina Nastke, Dr. Nadine Zumbrägel, Luisa Koch, Jannis Nonnhoff, Dr. Carmen Plass und Dr. Jana Löwe ganz herzlich bedanken.

Ein besonderer Dank gebührt allen ehemaligen und jetzigen IOCB (OC1) Mitgliedern, für die Unterstützung und dem fachlichen Austausch im Labor. Dabei will ich besonders Anika Hegemann und Thomas Geisler danken, weil ich mich bei unerwarteten Komplikationen stets auf euch verlassen konnte. Bei den ehemaligen Mitgliedern der IOCB, Dr. Daniel Bakonyi, Dr. Phillip Rommelmann, Dr. Florian Uthoff, Dr. Tobias Betke möchte ich mich für die vielen lehreichen Stunden bedanken. Dr. Nadine Zumbrägel, Dr. Franziska Kühn, Dr. Jana Löwe und Dr. Carmen Plass möchte ich mich für die aufregende und dynamische Zeit bedanken, nicht nur für die wissenschaftlichen Austausch, sondern auch für die wertvolle Zeit die wir als Freunde verbringen konnten. Karla Wagner, dir möchte ich für deine frohe Natur und stetige Hilfsbereitschaft danken. Die Welt braucht mehr Menschen wie dich! Michael Hinzmann, Lukas Schober und Alessa Hinzmann euch dreien möchte ich für die fortwährende und intensive Zusammenarbeit danken. Für die großartige Hilfe im Labor, ob es mal das gemeinsame Arbeiten am Wochenende oder das übernehmen von Experimenten war, will ich mich bei Jannis Nonnhoff, Luisa Koch, Alina Naskte, Karla Wagner und Hannah Bork bedanken. Für die Bewältigung des bürokratischen Aufwands und die Planung sämtlicher Veranstaltungen, will ich mich ganz herzlich bei Angelika Bendick bedanken. Ich bin überaus dankbar für alle Momente die wir als Arbeitsgruppe oder im Einzelnen hatten, vielen Dank Michael Hinzmann, Alessa Hinzmann, Lukas Schober, Jannis Nonnhoff, Alina Nastke, Alina Guntermann, Hannah Bork, Luisa Koch, Niklas Adebar, Tim Guntelmann, Laura Bernhard, Micol Santi, Jianing Yang und Dr. Anke Hummel.

Bei der Arbeitsgruppe von Prof. Dr. Stephan Hammer möchte ich mich ebenfalls bedanken. Ihr seid eine große Bereicherung für die Fakultät. Sebastian Gergel, Matúš Gajdoš, Cindy Klaus und Kai Schülke ich wünschte ihr hättet viel früher den Weg nach Bielefeld gefunden. Vielen Dank für das Nutzen von etlichen Sequenzierungsmarken, aber auch für die freudigen Abende die wir zusammen verbringen konnten.

Bei Manuela Koch und Nicole Hesse möchte ich mich für meine gesamte Zeit an der Universität bedanken. Beginnend vom Bachelorstudium bis zum Ende meiner Promotion konnte ich mich immer auf euch verlassen. Ich kann nicht in Worte fassen wie viel Ihr für Menschen wie mich bedeutet und welch eine große Unterstützung Ihr für alle Studierenden an der Fakultät seid. Ihr seid stets voller Tatendrang und immer auf unserer Seite! Vielen Dank für alles und macht genau so weiter!!!

Zu guter Letzt möchte ich mich bei meiner Familie und bei meinen Freunden bedanken, die mich tatkräftig auf meinem Weg begleitet haben. Besonders möchte ich mich bei meinen Geschwistern Münevver, Serdar und Mehmedarif sowie bei meinen Eltern, Zekiye und Mustafa bedanken, die mich selbstlos und ohne Bedingungen unterstützen und dabei selbst manchmal zu kurz kommen. Es ist schön mich immer auf euch verlassen zu können. Ein großes Dankeschön geht an meine langjährigen Freunde Kevin und Nils. Ich kann mich wahrlich glücklich schätzen euch an meiner Seite zu haben. Alina Nastke dir danke ich für die wundervolle Zeit und deine Freundschaft. Andrea ich danke dir vom ganzen Herzen für die gemeinsame Zeit in Bielefeld.

Von all den Dingen, die ich vermissen werde, wird es die Zeit sein, die wir als Gemeinschaft „Die drei Biochemiker und die Quasselstrippe“ verbracht haben. Michael, Alessa und Lukas wir haben etwa ein Drittel unseres Lebens sehr eng zusammen verbracht, uns den Gefahren und Herausforderungen des Lebens gemeinsam entgegengestellt. Nun geht jeder von uns, seinen eigenen Weg und ich danke euch, dass ihr mich zu dem gemacht habt der ich heute bin und ich weiß nicht, wo ich ohne euch drei heute wäre. Ich werde den Alltag mit Alessas zahllosen Niesern, Lukas unplatzierten Bemerkungen und Michaels „Dialekt“ wirklich vermissen. Michael auch unsere Wege trennen sich, mögest du Alessa die Stütze sein, die du für mich warst und sie dir dein Wegweiser, der ich für dich war. Solange wir alle Treu Seite an Seite stehen, werden wir den Rest des Weges, auch wenn es nicht mehr jeder Schritt ist, ihn dennoch gemeinsam bestreiten. Worauf ich mich bereits freue!

A true master is an eternal student

Master Yi

Sabreden derviş muradına ermiş

Türkisches Sprichwort

Table of contents

1 Aldoxime dehydratases: State of the art 1

2 Protein engineering with computational tools: State of the art 10

2.1 Overview computational tools guided protein engineering 10

2.2 Molecular modeling methods to improves substrate specificity and selectivity 11

2.3 Molecular modeling methods to improve stability and activity 15

3 Rationalizing the unprecedented stereochemistry of resolutions with aldoxime dehydratases via molecular modeling 17

3.1 Motivation 17

3.2 Biocatalytic dehydration of chiral nitriles 19

3.3 Development of a docking procedure 20

3.4 Modeling guided site directed mutagenesis of OxdRE 24

3.5 Summary and outlook for rationalizing the stereochemistry of aldoxime dehydratase 28

4 Chiral nitrile synthesis and formal double dynamic kinetic resolution 29

4.1 Motivation 29

4.2 Isomerization study with PPOX as standard substrate 31

4.3 Racemization of chiral aldoximes 33

4.4 Flow set up for the DDKR 40

4.5 Hydroformylation as alternative aldoxime synthesis 44

4.6 Expression optimization 45

4.7 Rational designed mutations 50

4.8 Smart library screening to increase the selectivity of OxdRE-L145F 55

4.9 Summary and Outlook for the chiral nitrile synthesis in a double dynamic kinetic resolution 63

5 Improving the biocatalytic transformation of non-soluble fatty aldoximes by targeting activity and stability of OxdB 66

5.1 Motivation 66

5.2 Solubility and enzyme substrate complex of fatty aldoximes 67

5.3 Increasing protein stability and in silico method development 69

5.4 Increasing the activity of OxdB by rational design 75

6 Compatibility of hydroxylamine and aldoxime dehydratase using Pickering emulsion in flow 78

6.1 State of the art and motivation 78

6.2 Pickering emulsion enabled combination of aldoxime formation and biocatalytic nitril synthesis in flow. 80

6.3 Addressing highly insoluble substrates with Pickering emulsions 83

6.4 Conclusion of Pickering emulsion mediated fatty nitrile synthesis 83

7 Summary and outlook 84

8 Zusammenfassung und Ausblick 89

9 Experimental section 94

9.1 Compounds 94

9.2 Chemical syntheses of substrates 94

9.3 Biochemical and molecular biological methods 115

9.4 Modeling with MOE (Molecular Operating Environment) 123
9.5 Rationalizing the unprecedented stereochemistry of resolutions with aldoxime dehydratases via molecular modeling.....131
9.6 Chiral nitrile synthesis and formal double dynamic kinetic resolution.....138
9.7 In silico method to increase thermostability of enzymes 168
9.8 Increasing the activity of OxdB by rational design.....193
9.9 Pickering emulsion mediated biotransformation 199
9.10 Combining Flow chemistry and Pickering emulsion with OxdB catalyzed octane nitrile synthesis 201
9.12 Analytic.....205
10 List of abbreviations.....208
11 Plasmids.....209
11.1 OxdB aldoxime dehydratase from *Bacillus sp.* as pUC18 construct.....209
11.2 OxdB aldoxime dehydratase from *Bacillus sp.* as pET28a construct.....211
11.3 OxdRE aldoxime dehydratase from *Rhodococcss erythropolis* as pET28a construct.....216
11.4 OxdA Plasmid aldoxime dehydratase from *Pseudomonas chlororaphis* as pET28a construct.....219
12 References 221

1 Aldoxime dehydratases: State of the art

Nitriles belong to a very fundamental class of molecules and play an important role in today's chemical industry. With a broad range of utilization, either as main product or as building block (e.g amines and acids) nitriles can be found in low prize high volume segment as solvents, polymers, adhesive and surfactants or in high prize low volume segment as pharmaceuticals.[1,2] Prominent examples for the bulk chemical sectors are acetonitrile and adiponitrile, which are produced in million ton scale per year.[1] In fine chemical sector nitriles are often found as fragrances such as dodecanenitrile, or cumin nitrile.[3] Besides those examples, nitriles are also important in complex molecules such as vildagliptin and saxagliptin, as they are both antidiabetic type 2 drugs with the sales exceeding 1 billion dollar per year. [4]

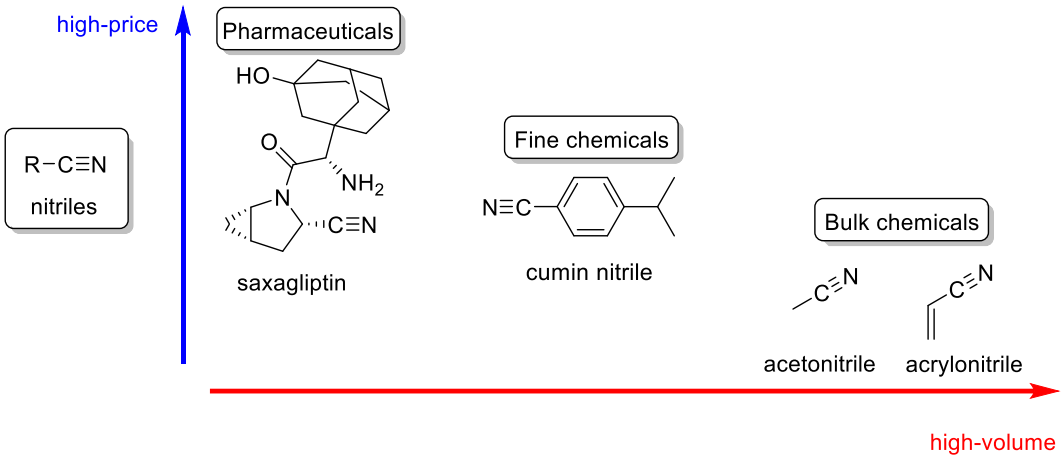

Scheme 1: Selected examples of nitriles in chemical industry with classification in low-volume high-price and high-volume low-price segment.

Over the decades various of methods have been developed to construct nitrile moieties. However, the established routes for the synthesis of nitriles need harsh and environmental harmful conditions, either high temperature like the ammoxidation or the use of highly toxic hydrogen cyanide or cyanide salts in substitution or addition reactions.[5,6] Besides, traditional routes do not provide a direct asymmetric nitrile synthesis. The optical pure nitriles are produced either by chiral nitrile precursors or by subsequent enantioselective transformation of racemic or prochiral nitrile. Thus, leading to a high demand in a sustainable as well as asymmetric nitrile synthesis, whereas many efforts were made to develop new strategies in the last decade.[7]

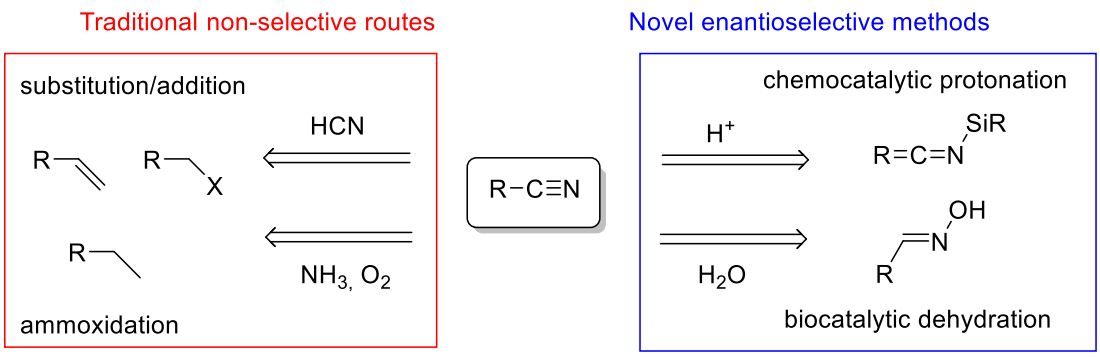

Scheme 2: Selected examples of novel and established methods for the synthesis of nitriles.

Among the variety of methods that have been reported, only a few covering the drawbacks of the established methods in terms of sustainability or enantioselectivity. One example is the aldoxime dehydratase catalyzed dehydration of aldoximes towards the corresponding nitriles, which were discovered by the *Asano* group in the late 90s.[8] Through their studies of nitrilase and nitrile hydratase-containing organisms that metabolize nitriles to amides or carboxylic acids, they were able to make the first finding of this class of enzyme, by predicting the existent of a nitrile generating enzyme in same pathway.[9]

Aldoximes themselves occur naturally in plants as growth, development and defense metabolite, which are produced from amino acids *via* Cytochrome P450 (CYP) proteins.[10] Microorganism such as *Bacillus subtilis* are able to convert those aldoximes to the corresponding nitrile. They discovered the first aldoximes dehydratase (OxdB) from *Bacillus subtilis* and showed the association of this enzyme class within the metabolism of nitriles and characterized the enzymatic properties as well as the recombinant expression of this protein.[11–13]

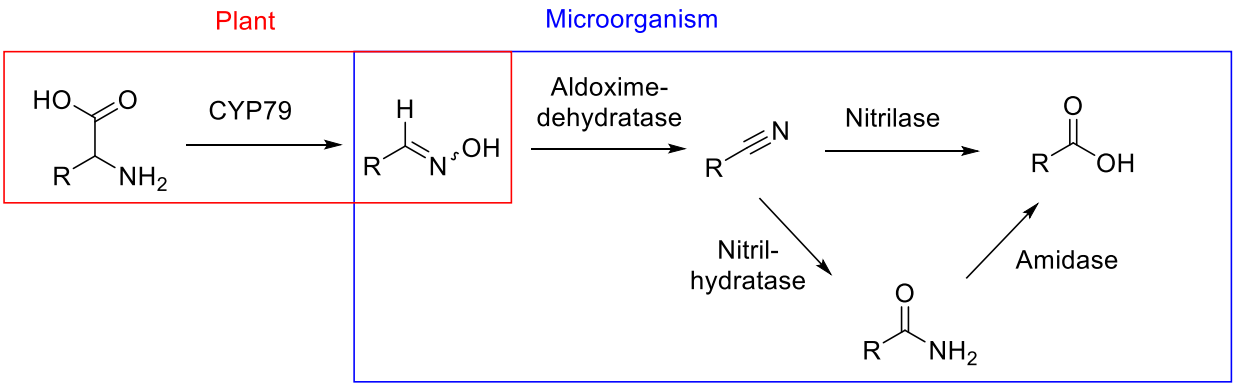

Scheme 3: Illustrated Aldoxime-nitrile pathway in microorganism as well as the formation of aldoximes in plants.

Aldoximes dehydratase contain heme b as prosthetic group and require microaerobic growth conditions to be expressed as soluble and correctly folded proteins.[13] With the discovery of the aldoxime dehydratase from *Rhodococcus sp*. (OxdRE) the *Asano* group were able to co-crystalize the enzyme with propanal oxime and butanal oxime, providing three different crystal structures and clarifying the Michaelis-complex of OxdRE. [14,15] The comparison of the co-crystal and ligand free crystal provided two different conformations of the enzyme. Proposing a conformational change induced by a bound substrate, leading to a closed entrance site of the enzyme.

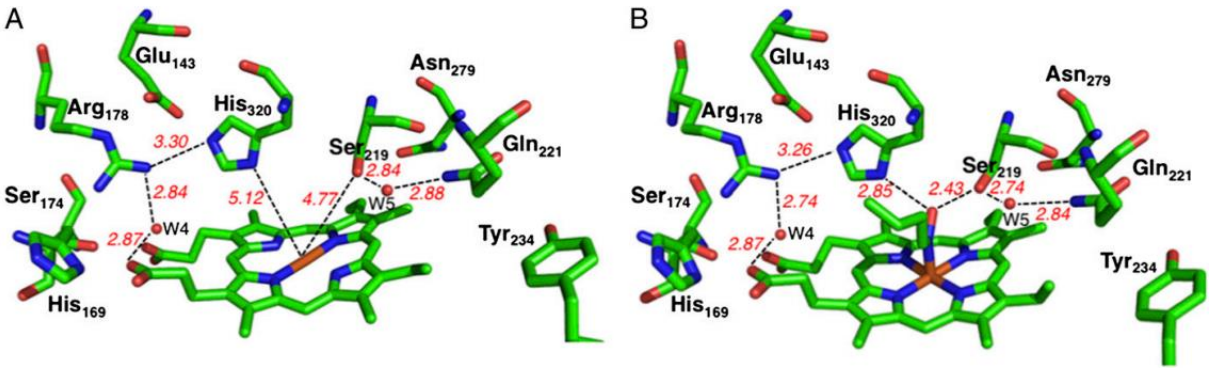

Figure 1: Schematic representation of the structural details of the aldoxime dehydratase active site. Hydrogen bonds are indicated as black dotted lines with distances in Ångstrom between atoms indicated in red. (A) OxdA, (B) OxdRE-substrate complex. (This figure was reprinted with the permission of PNAS). [16]

The *Kobayashi* group, later on provided a new crystal structure of the aldoxime dehydratase from *Pseudomonas chlororaphis* (OxdA) showing the sequential and structural homology of both aldoxime dehydratases (**Figure 1**).[16] The catalytic center is relatively large and close to the protein surface with a small entrance. The active site itself consists of the heme group, which is coordinated by the H169 and the backbone of M179 and G170. Whereas the iron itself is bound to the H299 (below the heme).[17] Besides the heme, the enzyme class has similar to oxidoreductase a catalytic triad consistent of R178, H320 and S219. With the preliminary work of the *Asano* group providing mutagenic analysis[18,19] and the co-crystal of OxdRE[14] in combination with the QM/MM study of the catalytic activity of Oxds from *Liang et al.*[15] a mechanism for the enzymatic dehydration (**Scheme 4**) could be proposed.[16] Aldoxime dehydratase contain a catalytic triad, consistent of an arginine (R178), histidine (H320) and serine (S219). S219 coordinates the substrate and increases its basicity, H320 acts as acid/base catalyst and its initial acidity is increased in the interaction with R178. In the initial state (**I**) the heme is present in its ferrous state (Fe^{+2}), allowing the migration of the substrate, which is then coordinated *via* the nitrogen at the ferrous center of the heme and by hydrogen bonds at the hydroxy functionality *via* H320 and S219 (**II**). Step 2 describes the Michaelis-complex or enzyme-substrate complex.

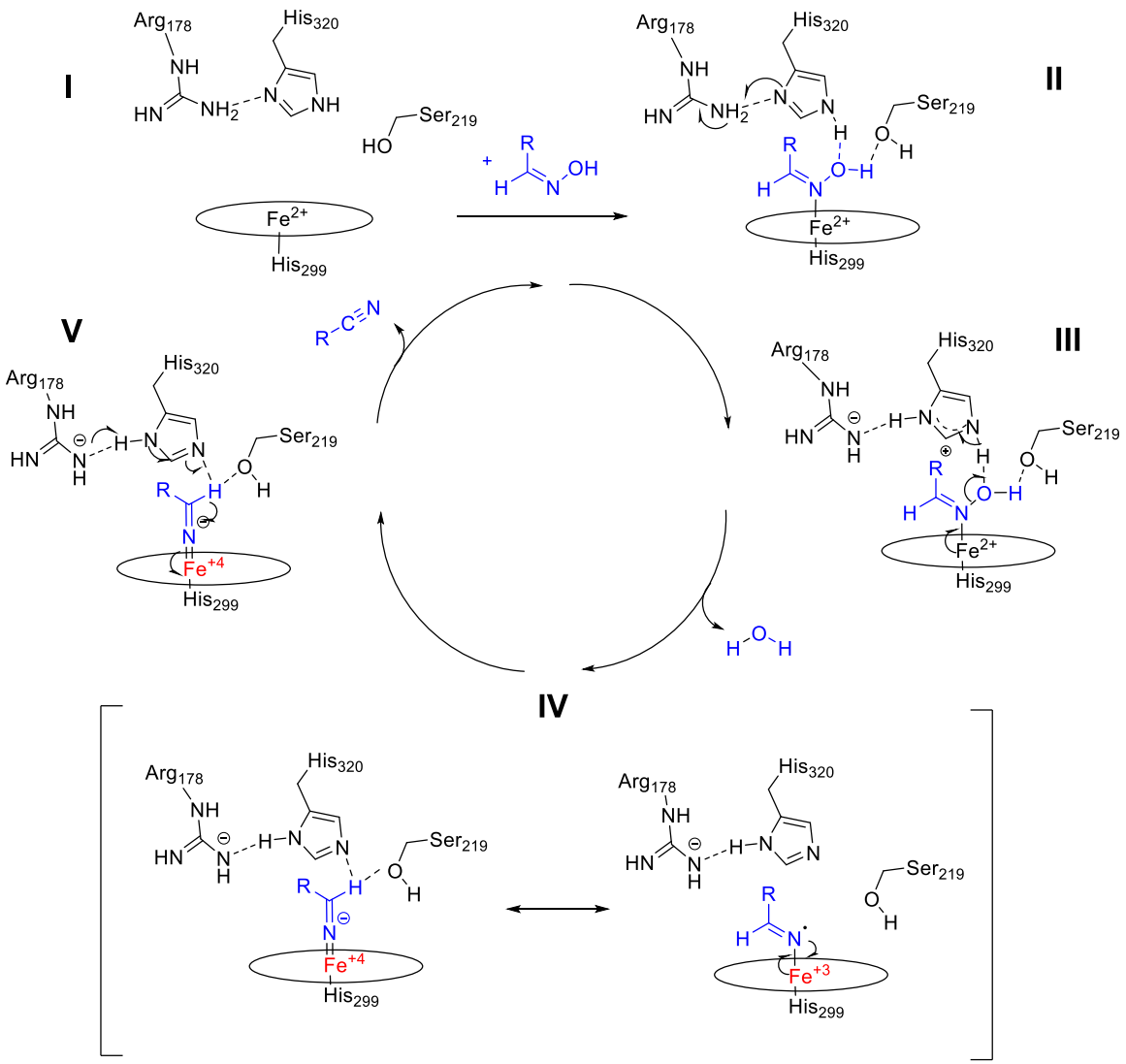

Scheme 4: Postulated mechanism of aldoxime dehydratase catalyzed dehydration of aldoximes towards the corresponding nitrile.

In the described mechanism, the reaction now proceeds with the protonation of the H320 by R178 increasing the acidity of H320. In the third step (**III**), the acidic H320 protonates the hydroxy group of the aldoxime, which has already an increased basicity due to its coordination by the S219 and the electron donation of ferrous center. The protonation then leads to an electron rearrangement, whereby water is formed as leaving group and iron is oxidized to Fe^{+3}. In the following transition state (**IV**), a rearrangement of the substrate due to the electron transfer from the ferric center to the nitrogen leads to linear orientation and the oxidation of the iron to Fe^{+4}. The C_{α}-carbon of the substrate in now spatial proximity to the H320 and S219, whereas the acidic C-H is coordinated by H320 and S219. The reprotonation of R178 causes the H320 to become basic and deprotonates the substrate (**V**). This electron rearrangement then leads to the formation of the nitrile, which leaves the active site and the enzyme returns to its initial state (**I**). For the reaction to proceed or the enzyme to be active the heme has to be in the ferrous state (Fe^{+2}), which is why the a microaerobic expression as well as the addition of reduction agents when using purified enzyme is necessary.[14] If the heme is present in the ferric state (Fe^{+3}) and used for the reaction with an aldoxime the oxygen of the hydroxyl group is bound to the iron, leading to the inactivation of the enzyme.[14,20]

With the recent report of a novel aldoxime dehydratase from *Bradyrhizobium sp.* (OxdBr)[21] in total only eight aldoxime dehydratases have been discovered yet. Excluding aldoxime dehydratase Oxd-YH3[12,22] from *Rhodococcus sp*, which could be stated homologue to OxdRE all know aldoximes dehydratase and their properties are shown in **Table 1**.

Table 1: Protein propeties of reported aldoximes dehydratases (Oxds).[23]

Properties	OxdA[24]	OxdB[13,19]	OxdFG[25]	OxdRE[19,26]	OxdRG[27]	OxdK[18]	OxdBr[21]
Molecular weight (kDA) native	76.4	42.0	34.1	80.0	80.0	85	77
Sequence	40.1	41,0	44.0	44.7	44.8	44.5	41
Subunits	2	1	1	2	2	2	2
Soret-peak (nm) Ferric form	408	407	420	409	409	409	404
Ferrous form	428	432	431	428	428	428	427
Optimum pH	5.5	7	5.5	8.0	8.0	8.0	7.0
Optimum temperature °C	45	30	25	30	30	20	40
Stability pH	6.0-8.0	6.5-8.0	4.5-8.0	6.0-9.5	6.0-9.5	5.5-6.5	7.0-8.0
Stability temperature °C	<40	<45	<20	<40	<40	<30	<30

Origin: OxdA from *Pseudomonas chlororaphis*, OxdB from *Bacillus sp*., OxdFG from *Fusarium graminearum*, OxdRE from *Rhodococcus erythropolis*, OxdRG from *Rhodococcus globerulus*, OxdK from *Pseudomonas sp. K-9*, OxdBr from *Bradyrhizobium sp*.

The general enzyme properties of the known aldoxime dehydratase are very similar. They have an average molecular weight of 40 kDa and are either present as monomers or dimers. The soret-peaks also appear in the same range for the ferric form at about 408 nm and the ferrous form at about 428 nm. In terms of activity, the optimum

reaction temperature ranges between 20-45°C and the optimum pH ranges from 5.5-8.0. Aldoxime dehydratases are in average stable at 30°C and a pH of 7.0-8.0.

For most of these enzymes, kinetic data were also collected and are summarized in **Table 2**. In general, there is no trend in K_M-values, although they vary from about 1 mM up to 11 mM, they remain in the same order of magnitude. With these data it could be shown very early that aldoxime dehydratase have a relatively large substrate spectrum, since cyclic, aromatic, heterocyclic, chiral and aliphatic aldoximes were successfully converted. The exact classification and applicability of aldoxime dehydratases in organic chemistry has been achieved in recent years through cooperation between the *Gröger* and *Asano* groups. Many milestones have been reached and aldoxime dehydratases have been established as biocatalysts for a cyanide-free alternative synthesis route.

Table 2: K_M-values of Oxds available in literature for a subest of susbtrates.

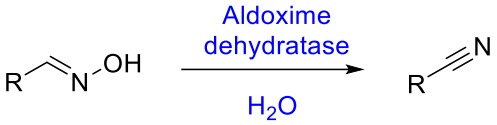

Substrate	K_M-value / mM					
	OxdB[13]	OxdA[24]	OxdRE[26]	OxdK[18]	OxdFG[25]	OxdRG[27]
Z-phenylacetaldoxime	0.87		3.2	0.99	3.52	1.40
Z-3-phenylpropionaldoxime	1.36		4.08	0.97	2.76	2.31
E/Z-4-phenylbutyraldoxime	5.24			0.88	1.79	
E/Z-2-phenylpropionaldoxime			10.0	4.07	3.71	11.9
Z-p-chlorophenylacetaldoxime	1.24					
Z-p-methoxyphenylacetaldoxime	3.08					
E/Z-indoleacetaldoxime	2.40				1.46	
Z-naphthoacetaldoxime	0.84					
E/Z-acetaldoxime		11				
E/Z-propionaldoxime	4.32		1.85	0.77		5.13
E/Z-n-butyraldoxime	11.1	0.25	4.34	2.16	2.87	1.73
E/Z-n-valeraldoxime	2.42		1.41	3.78	10.1	1.13
E/Z-isovaleraldoxime	3.58		6.66	1.33	2.66	3.97
E/Z-n-capronaldoxime	6.12			3.12	0.88	2.94
E/Z-isocapronaldoxime	2.98					6.76
E/Z-cyclohexanecarboxaldehyde oxime			1.25	5.96		1.13

Fatty nitriles play an important role in industrial chemistry within the production tree of fine and bulk chemicals,[1,2] the biocatalytic synthesis has to be able to compete with traditional synthesis in terms of productivity. For the synthesis of fatty nitriles OxdB happened to be the most suited variant, with high activity combined with the high stability *Hinzman et al.*[28] showed the applicability of this enzyme and reaching record numbers in terms of substrate loading for enzyme catalyzed reactions. For the best presented example of OxdB catalyzed reaction a substrate loading of 1.4 $kg \cdot L^{-1}$ with octanal oxime as substrate was reached, converting it into octanenitrile with 93% conversion (**Table 3**). Its worthy to mention that those number are enabled with the wild type of OxdB. Comparing to other enzymes with a heme group such as the CYP-monooxygenase superfamily, reactions usually take place for optimized mutants in mM range.[29] OxdB reaches similar potential as the nitrile hydratase, one of the most prominent example of an industrially applied enzyme, that is used for the synthesis of acrylamide from acrylonitrile.[30] The nitril hydratase reaches a space time yield of 0.1 $kg \cdot L^{-1} \cdot h^{-1}$ under industrially optimized

condition,[31] while the OxdB for the example of octane nitrile reached already under laboratory conditions a space time yield of 0.06 kg·L^{-1}·h^{-1} (**Table 3**).

Table 3: Preparative biotransfomation of aliphatic aldoximes to nitriles using OxdB as whole cell catalyst.[28]

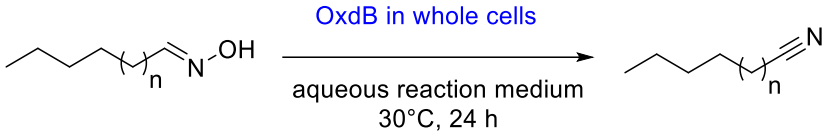

Entry	n =	Susbtrate loading / g· L^{-1}	Conversion /%	Yield /%
1	1	288	>99	81
2	2	342	>99	84
3	2	428	93	n.d
4	3	665	>99	98
5	3	1430	93	n.d

Besides the mono-nitriles also dinitriles play an important role as example adiponitrile is being produced annually in million ton scale,[1] the synthesis is carried out industrially mostly by the addition reaction of cyanide with butadiene.[6,32] Using aldoxime dehydratases, an alternative cyanide-free synthesis route was also demonstrated. Adiponitrile was successfully prepared on a preparative scale using OxdB. Quantitative conversion with a substrate loading of 50 g·L^{-1} was achieved.[33] With those mentioned examples of Oxd catalyzed dehydration of aldoximes, this enzyme class showed high potential to be applied in industry in the future.

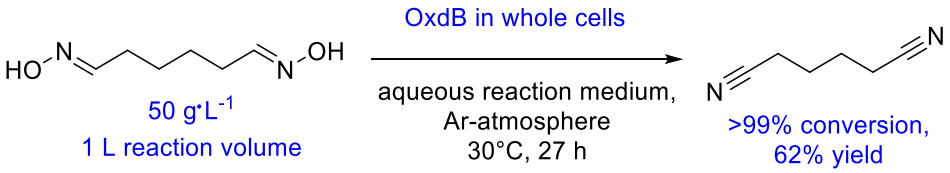

Scheme 5: Adiponitrile synthesis in water at 30°C using OxdB as whole catalyst on liter scale.[33]

Besides performance of catalyst also the stability, recovery and product purity are key features when it comes to economical and sustainable process. Immobilization techniques are usually applied to overcome such hurdles. There many different immobilization methods known, varying from covalent bound to a carrier, crosslinking of protein aggregates (CLEAs) and encapsuling techniques.[34] The methods also differ with formulation of the biocatalyst as pure enzyme, crude extract or as whole cells. Proven and well known examples are lipase B (*Candida antarctica*) and glucose isomerase (*T. oshimai*), with remaining residual activity of over 50% after 15 runs at high temperature exceeding 75 °C.[35] The use of a heterogenous catalyst in a reaction also enables a simple work up and recovery, increasing the economic benefits of a process. Therefore, immobilization techniques were also investigated for aldoxime dehydratase. So far two different yet similar approaches are reported so far namely silica coated alginate beads and superabsorber.[28,36] Both methods belong to the class of encapsulation techniques. From the perspective of using aldoxime dehydrases in water or two-phase systems and being able to reuse them, the silica alginate beads proved to be very suitable. With the investigation of different formulation of the biocatalyst they also showed that the enzymes were better suited as immobilized whole-cell catalysts than purified

proteins, which otherwise had only minimal residual activity. OxdB, for example, could be reused four times as an immobilized whole-cell catalyst (**Figure 2**).

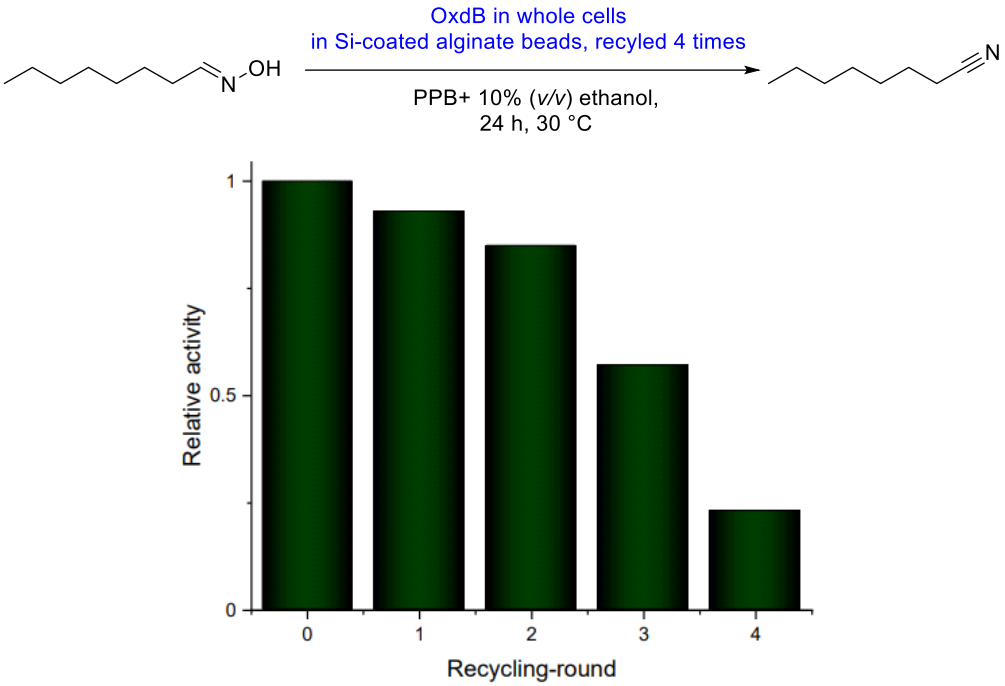

Figure 2: Recycling study of OxdB immobilized in calcium alginate beads coated with TEOS (Si-beads).[36]

With regard to the above-mentioned mono- and di-fatty aldoximes their overall solubility in water is very poor, therefore limiting the biotransformation in water. To overcome this hurdle immobilization technique were investigated to perform the biocatalytic reaction in organic solvent. For that, superabsorber as encapsuling technique enabling a solid water phase, was used to perform nitrile synthesis in pure organic solvent.[37] The superabsorber method enabled than also to use the enzyme as solid phase in a flow set up. The reported packed bed reaction also performed very well with high conversions (>95%) with a residence time of 30 mins for 100 mM octanal oxime. The same system was later also applied for segmented flow set up highlighting how robust and versatile aldoxime dehydratase can be used.[38]

In a total synthesis of a product, the optimization of one step does not necessarily lead to improvement of the entire synthesis. Thus, in the case of nitrile synthesis with aldoxime dehydratases, access to aldoxime and precursors was also an essential issue, as well as optimization of the entire cascade. Therefore, *Plass et al*.[39] showed that starting from petrochemicals as a resource for the production of nitrile, the entire cascade can be accomplished in one pot. In this way, the use of solvents for processing the intermediate steps can be avoided and the cost factor for chemicals in the bulk industry can be reduced considerably. The major problem was the synthesis of the aldoxime and the subsequent enzymatic dehydration. Since minimal excess (1 mM) hydroxyl amine already leads to inactivation of the enzyme. By a decomposition of the residual hydroxyl amine at 100 °C, the one-pot synthesis could be achieved. A preparative scale reaction with 1-octene as exemplified starting substance could be achieved with over 90% conversion and an isolated yield of 67%.

As alternative to petrochemicals as starting material, the synthesis of the aldehydes starting from alcohols, which in turn can be obtained from renewable resources, was also established. The known tempo oxidation[40] was

optimized for the substrate class overcoming the hurdle of over oxidation of alcohols to acids.[41] Subsequently they succeeded demonstrating the cascade reaction from alcohol to nitril in sequential type one-pot reaction, reaching quantitative conversion and very good yields for nitriles ranging from *n*-octanenitrile to *n*-dodecanenitrile.[42] In addition, the produced nitrile was at the same time used as a solvent. Thus, two different routes for the preparation of nitrile without the necessity to isolate intermediates, could be fully established.

Table 4: Chemoenzymatic cascades reaction towards aliphatic nitriles from two different feedstock, presenting an cyanide free altenative synthesis.

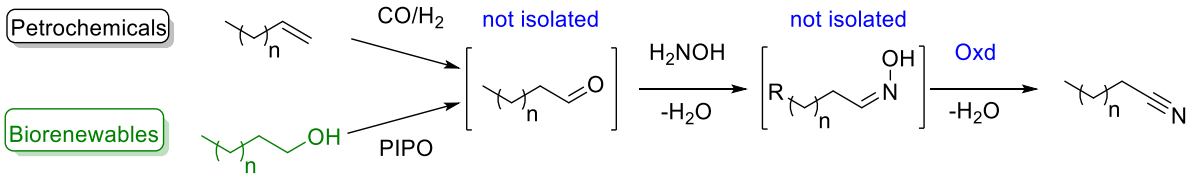

Entry	n =	Conversion to aldehyde /%	Conversion to aldoxime /%	Conversion to nitrile /%	Yield /%
1[a]	6	74	n.d	90	71
2[b]	3	99	99	92	60
3[b]	5	99	99	95	71
4[b]	9	99	99	93	63

[a] Conversion related to the hydroformylation pathway starting from 1-octene.[39] [b] Conversion related to the TEMPO oxidation pathway starting from the alcohol.[42] n.d = not determined.

In relation to the methods presented, dinitriles as well as branched nitriles were also successfully presented and indicate the versatility of this approach. With regard to the diversity of enzymatic nitrile synthesis, the synthesis of an aromatic nitriles was also achieved. Namely 2-furonitrile and pyronitrile were produced, concluding the first reported benzylic aldoximes conversion.[22,43] In particular, 2-furontrile is of industrial interest and is used in pharmaceutical and fine chemical segment. The synthesis of 2-furonitrile from furfural (biorenewable feedstock) represents an alternative cyanide-free synthesis route, since in comparison the industrial synthesis is carried out via ammoxidation at over 400 °C.[44]

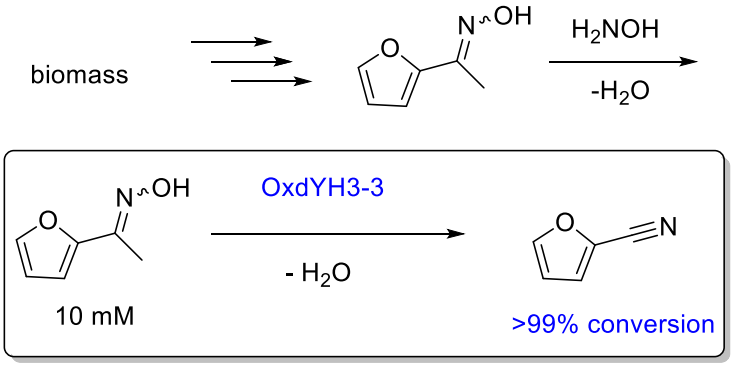

Scheme 6: Biocatalytic synthesis of 2-furonitrile starting from furfural, which can be obtained from biomass.[22,45]

The conversion of 99% at a substrate concentration of 10 mM could be shown with the aldoxime dehydratase Oxd-YH3. The low substrate concentration was due to the relatively low expression of the new recombinant, which is why the preparation of the aromatic nitriles could only be shown as proof of concept so far. Since this class of nitriles is of great interest for applications, there is still a high demand for this research field. A completely different property of aldoxime dehydratase and at the same time the main advantage of biocatalytic reactions from classical

chemical reactions in general, is the selectivity. Oxds are also enantioselective catalysts capable of producing enantiomerically pure nitriles. However, the selectivity of aldoxime dehydratase is a very special novelty.

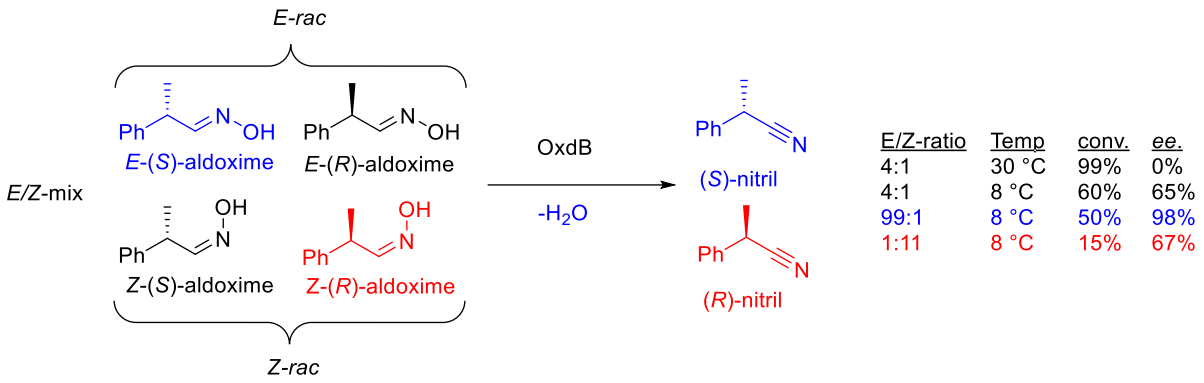

Scheme 7: Whole cell biotransformation of OxdB catalyzed dehydration of 2-phenylpropanal oxime (PPOX) in different *E/Z*-mixtures.[46]

The first reported enantioselektive dehydration of aldoxime was by *Metzner et al.*[46] showing high enantiomeric excess 98% *ee* could be reached when using low reaction temperatures and high *E/Z* ratio (99/1). Revealing that the enantioselectivity of the Oxd catalyzed dehydration is dependent on the *E/Z* ratio of the aldoxime and stating that low temperatures would decrease the isomerization rate.

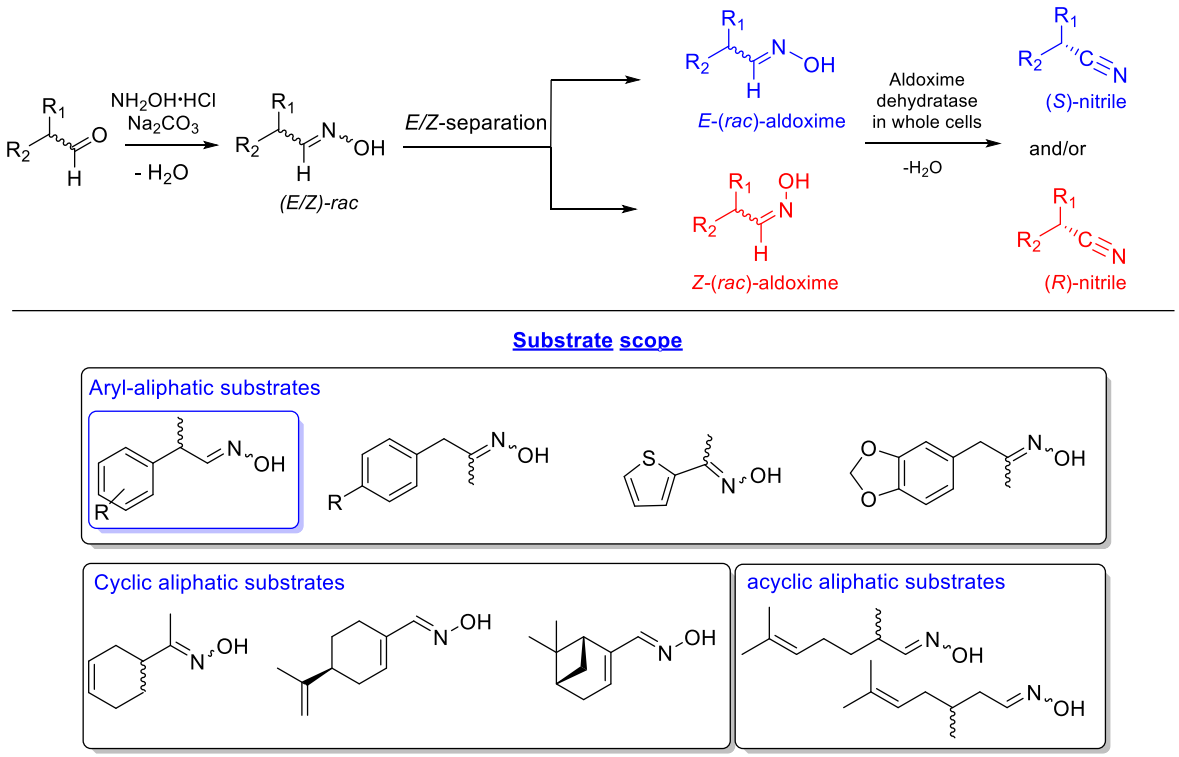

Scheme 8: Substrate scope of the synthesis of chiral nitriles with five different aldoxime dehydratases.[47]

With intensive investigation from *Betke et al.*[47] a broad substrate scope with 5 different aldoxime dehydratase as well as a detailed characterization of the enantioselectivity was achieved proposing a general concept. All five aldoxime dehydrataseS follow the same principle when chiral aldoximes are used for the reaction. When starting with an *E*-isomer, preferable the S-nitrile is formed and vice versa with the *Z*-isomer. Particular substrates with

their stereogenic center in α-position as well as a strong steric differentiation of the substituents at the chiral center showed high enantioselectivity in the reaction course, yielding the corresponding nitriles with up to 99% *ee*.[45] This phenomenon was later tailored and reported[48] as part of this work in chapter 1. This unique phenomenon brings the advantage in applied organic synthesis to be able to obtain opposite enantiomers with the same starting aldehyde in optical pure form. The use of this method for industrially relevant product is rather low, since low substrate loadings as well as the preparation of the substrate with multiple workup stages, as well as the isomerization are difficult to deal with. In addition, kinetic resolutions (KR) in general are non-elegant routes, with their naturally limitation of 50% yield.[49] The limitation of a KR can usually be addressed with a dynamic kinetic resolution, in which a second reaction is used to racemize the residual enantiomer.[50–53] In relation to the aldoxime dehydratase catalyzed reaction, however, a DKR would only solve this problem to a limited extent. Since the limit of this KR is not 50% but 25% if one assumes an *E/Z* proportion of 1/1. Which is why the reaction is so extremely unattractive for the preparation of product relevant nitriles. To realize, an attractive and elegant way for the preparation of chiral nitriles starting from aldoximes and using Oxds, a formal double dynamic resolution (DDKR) has to be developed and opens up an exciting and novel approach, which was also part of this work and will be discussed in chapter 4.

2 Protein engineering with computational tools: State of the art

2.1 Overview computational tools guided protein engineering

In the last decade, enzymes have found great value in industrial and pharmaceutical synthesis.[54] The development has been made possible by unprecedented advances in protein engineering that can modify naturally occurring enzymes in terms of substrate spectrum, specificity and selectivity.[55] In addition, ways have been developed to maintain the activity of the enzymes at elevated temperatures or under the influence of organic solvents.[56] The possibilities go so far that we have already reached the end of the third wave of biocatalysis.[57] One of the most important milestones reached was the development of directed evolution.[58,59] Enabled by high throughput assays, directed evolution can be performed to reach the desired properties of an enzyme with ease. But, depending on the targeted property and the fact that not all enzymes can be assayed in high throughput manner, the demand for computational analysis as alternative is very high.[60]

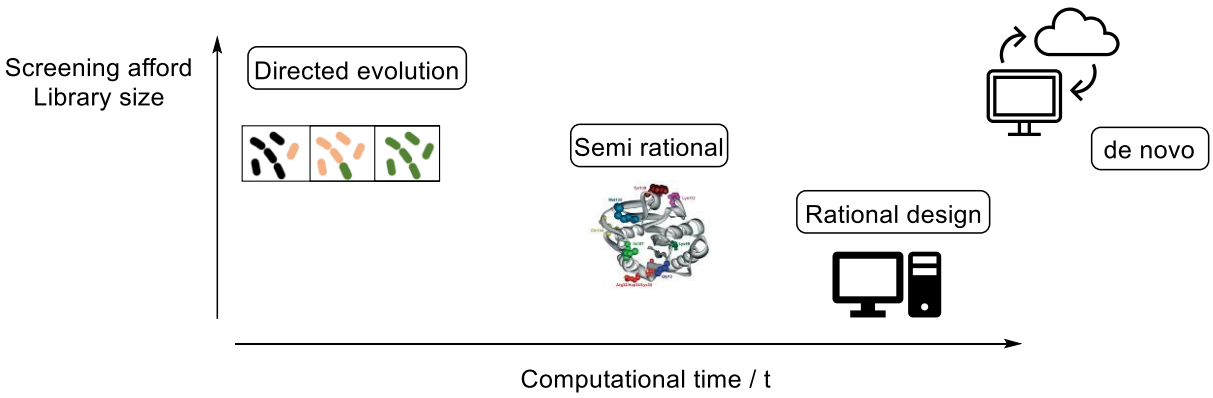

Figure 3: General overview about the screening afford versus the computational time of protein engineering approaches.

The computational tools for protein engineering are very diverse ranging from combinatorial[61] to fully rational[62] with widely varying approaches. The combinatorial methods are based on the random mutagenesis principle with the premise that the mutation space is reduced by rational design to have a feasible approach.[61,63,64]

While rational design does not require extensive screening, the enzyme must be fully understood at the molecular level (structure-activity-relationship, SAR). There are different types and approaches for rational design, whereas the application depends on the targeted enzyme property. Substrate specificity and enantioselectivity are often governed by steric factors of the active site, which is why docking simulation, MD-simulation and QM/MM-methods are suited for targeting those properties.[65] In addition, docking simulations provide general information about the active site and binding possibilities for the ligand.[66] Even though the number of available protein crystal structures increased in the last years, most of them are without direct information about substrate binding. Conventionally, those information's are gathered by preparing co-crystals either with the substrate or an inhibitor, but the generation of co-crystals are enormously tedious and often without success. The general success and convenience of docking simulations, has great importance especially in medicinal chemistry. Virtual screening method help in hit identification and in later stages also in lead optimization, thus improving drug development.[67]

2.2 Molecular modeling methods to improves substrate specificity and selectivity

For most cases the modification of the substate specificity and selectivity of an enzyme is the simplest property to target with docking simulation.[56] This applies specially when reaction mechanism and binding pose of ligands due to co-crystals are already available. For that, the essential step is the correct preparation of the active site in order to reimage the transition state of the reaction. With correctly defined geometries, such as binding angles and distances, a differentiation even between enantiomers of one ligand is possible.[68] Therefore, this method is highly dependent on the information's available. In most cases docking simulation, at least reveal a visualization of the binding pose.

This can be exemplified with the work of *Ghislieri et al*.[69] whereas basic docking experiments led to a hypothesis driven mutagenesis of the monoamine oxidase from *Aspergillus niger* (MOA-N). The enzyme was previously used to deracemize simple chiral amine with only one large moiety at the chiral center.[70] The modification led to an active site with much higher volume, leading to an enlarged substrate scope of the MOA-N mutant (**Figure 4**). The new developed mutant of MOA-N was able to selectively oxidize (*S*)-4-chlorobenzhydrylamine towards the ketone.

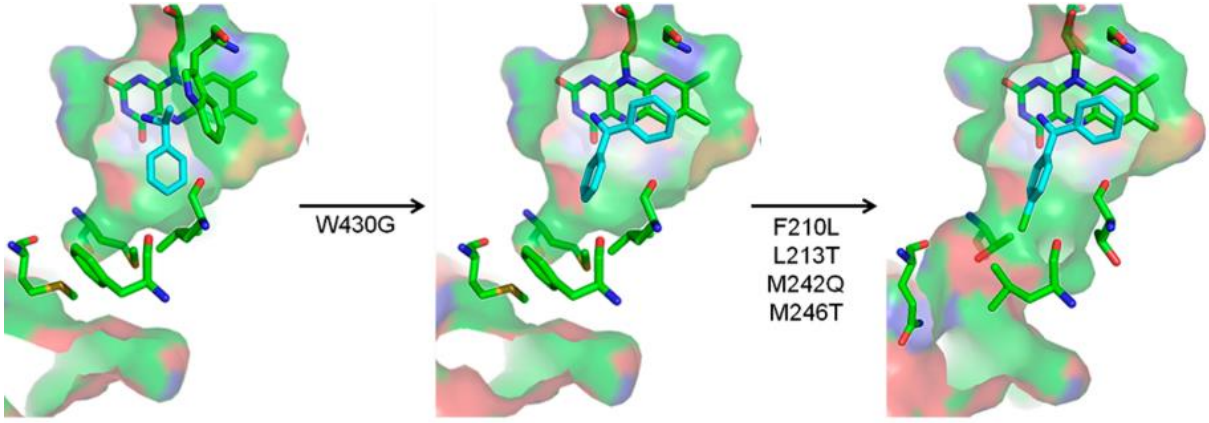

Figure 4: Modeled structure of the MOA-N and mutants with increased volume of the active site leading to improvement of substrate acceptance from (*S*)-phenylethylamine as ligand towards 4-chlorobenzhydrylamine. (This figure was reprinted with the permission of ACS). [69]

When docking is combined with saturated mutagenesis the binding poses are not required to be accurate to have sufficient improvement, especially when the active site or the substrate is large and multiple conformations are possible. The visualization leads to hypothesis guided complete or partial randomization of the identified hotspots, which represents a simple yet highly successful approach without deepening the understanding of the enzyme. For this purpose iterative saturated mutagenesis (ISM) became a broadly applied tool.[71] Besides the application in biocatalysis docking is a key tool in medical chemistry, whereas its used to screen large ligand- or receptor-libraries in the field of drug discovery and development. Furthermore, molecular modeling can also be applied to find certain features in nature. Starting from docking simulation the active site can be rationalized and the proposed or predicted changes in the essential amino acids can be screened in large sequence based[72] or structure based libraries.

But docking simulations have their limitations, which strongly dependent on the reaction and investigated property. Since it is well known that enzymes are not static catalysts and that their performance is more mechanical driven concerted dynamic interaction of all amino acids,[73] reactions proceeding in multiple dynamic transitions states or when the selectivity is depending on the migration of the ligand (tunnel), docking simulation alone cannot be applied to a rational improvement. Therefore, enzyme activity as well as stability are also properties, which usually cannot be addressed actively by docking simulations.

To address such properties as well as to include the dynamic nature of enzymes molecular dynamic (MD) simulations were invented.[74] One of the biggest pioneers in this field is *D. B. Janssen*, his group developed a molecular dynamic simulation to predict the enantioselectivity of an enzymatic reaction. Determining transitions states or binding motifs as near attack conformations (NAC) with docking simulation. In a subsequent MD simulation, the examined amount of time or the population rate of the ligand in this NAC were correlated with the enantioselectivity.[75,76] Whereas the enantioselectivity would be then calculated with $E^{predicted} = [NAC]^{P}/[NAC]^{D}$. P refers to the preferred enantiomer and D to the disfavored enantiomer. The method was designed with dehalogenase as example (**Figure 5**). The reason for that was, that for four different dehalogenases X-ray structures were available as well as experimental data of 45 substrates, which provided conversions and enantioselectivities ranging from E-values of 1-200, thus providing the perfect basis for *in silico* development.

Figure 5 shows the NAC determined via docking and the subsequently used MD-simulation to predict the enantioselectivity.

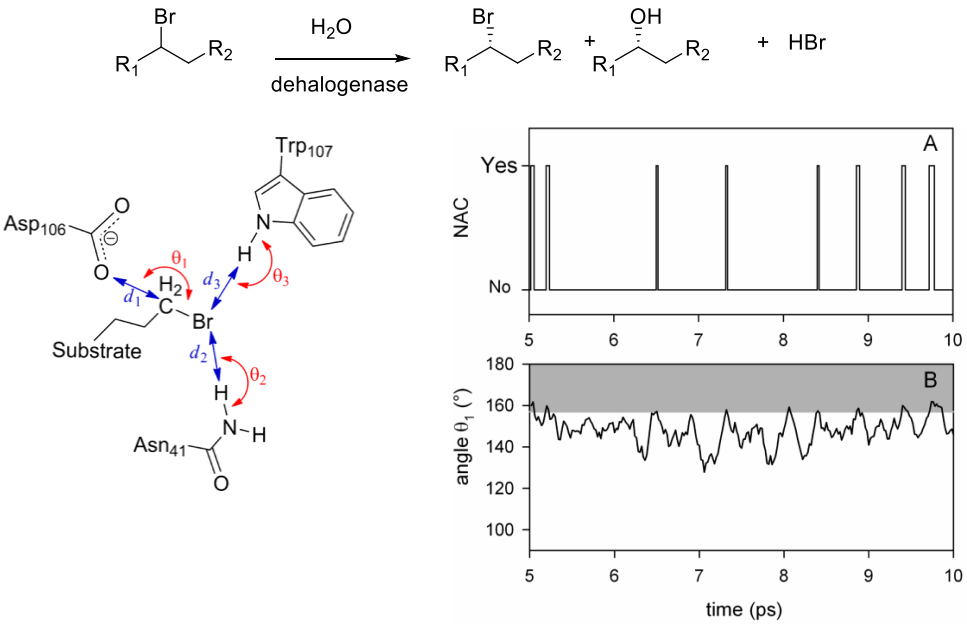

Figure 5: Schematic illustration of the dehalogenase catalyzed reaction. Geometries that were clarified to result in a near attack conformation (left). MD-simulation to determine the time spend in NAC (right). (This figure was reprinted with the permission of ACS). [75]

Important key players, that need to be mentioned when it comes to modern protein engineering are *Bornscheuer & Höhne*. Besides their utilization of automated HTS methods and bioinformatic tools they also showed many examples of molecular modeling guided protein engineering.[77,78] In one example they use MD-simulation for substrate specificity and activity modification of the transaminase from *Chromobacterium ciolaceum*, enabling the conversion of bulky ketones and increasing the activity by 200-fold.[79] Tailoring that the specificity is dependent on the tunnel leading to the active site of the enzyme. The MD-simulation guided trajectory of the ligand through the tunnel, led to rationalizing key amino acids and modifying them to improve the biocatalytic transamination. In **Figure 6** the modified positions of the transaminase (F88L, C418L) as well as the bound PMP at the end of the tunnel are shown.

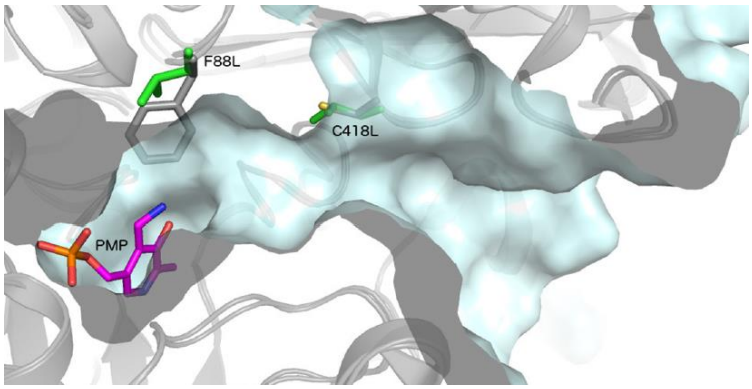

Figure 6: Illustration of designed mutant identified via MD simulation. (This figure was reprinted with the permission of ACS).[79]

MD-simulations are well suited to investigate complex enzymatic reactions and interactions. The costly computational times are gradually becoming a matter of the past with regard to the rapid development of chip technology.[80] This is also the case for quantum mechanical (QM) methods. While MD simulations are suitable for, as the name suggests, dynamic interactions, i.e. movements in general, QM methods are mainly used for the determination of transition states. Thus, QM methods can be used to gain a better understanding of the reaction steps and to formulate reaction mechanisms (**Scheme 9**).

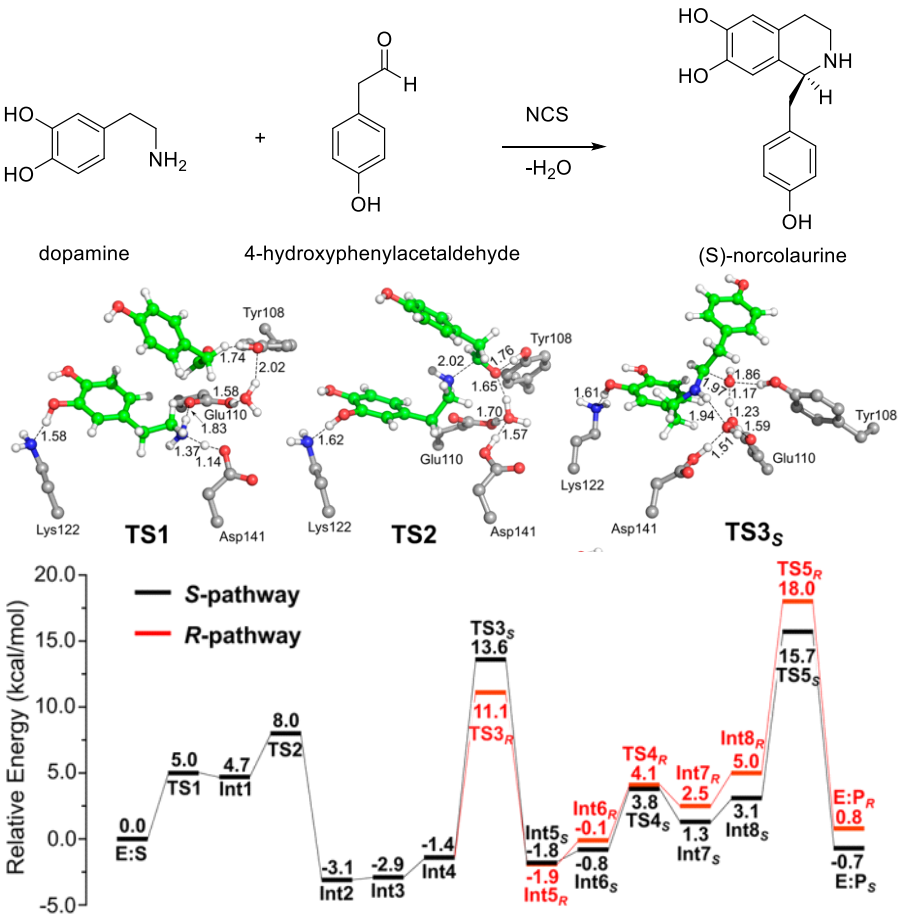

Scheme 9: Schematic illustration of the NCS catalyzed Pictet-Spengler reaction. Exemplified transition states as result of the QM-calculation as well as the energy profile leading to the formation of (*S*)- and (*R*)- products are shown in black and red, as illustrative example. (This figure was reprinted with the permission of ACS). [81]

Norcolaurine synthase (NCS) is able to convert dopamine and 4-hydroxypehnylacetalehyd to norcolaurine, however it was unclear how the reaction would proceed, which were the selectivity determining steps, which substrate would migrate first and how would the transition states look like. To clarify these questions QM methods were applied to determine energy profiles for each pathway and of the formed enantiomer. The extensive calculation led to the explanation and tailoring of the mechanism behind the NCS catalyzed reaction. This example clearly shows the strengths of QM methods, but with the drawback that QM methods alone are not suited for the application of a broad substrate classification, due to the long calculation time including only a specific subset of molecules. However, they deliver crucial mechanical inside especially when nothing else about the enzyme is known.[81] For an instance the characterization of the NCS enantioselectivity with docking or MD simulation would not have been possible for the exemplified reaction of norcoclaurine synthase. The revealed mechanism behind the NCS, provides the basis for subsequent work on substrate specificity and selectivity.

2.3 Molecular modeling methods to improve stability and activity

MD simulations are also used to identify dynamic, flexible regions of a protein. Changes in these regions can affect protein stability and activity, because catalysis requires certain flexibility of critical residues or parts of the protein. The improvement of the stability is a crucial point when it comes to biocatalysis, but besides the usage in organic chemistry, increasing the stability of an enzyme is always beneficial, since it promotes the evolvability.[82] At the same time, computer-based enhancement of stability (thermostability, solvent tolerance) is the most difficult task in terms of rational design. Since stability, unlike selectivity or specificity, does not depend on a few amino acids in a particular scaffold, rather the scaffold itself determines the stability. While our current understanding is not sufficient to represent an excellent tool for stability calculations, at the same time, many different approaches to predict and improve thermostability are available. On the bioinformatic level, it is possible to compare the target protein with thermophilic proteins either using a homology model or sequence based comparison.[83] Other structure-based methods refer to flexibility (B-fit), hydrophobic interaction in the protein core, disulfide bonds (FRESCO) or folding energies (FoldX).[56,84] The most successful way to enhance protein stability is to use small, but smart libraries.[85]

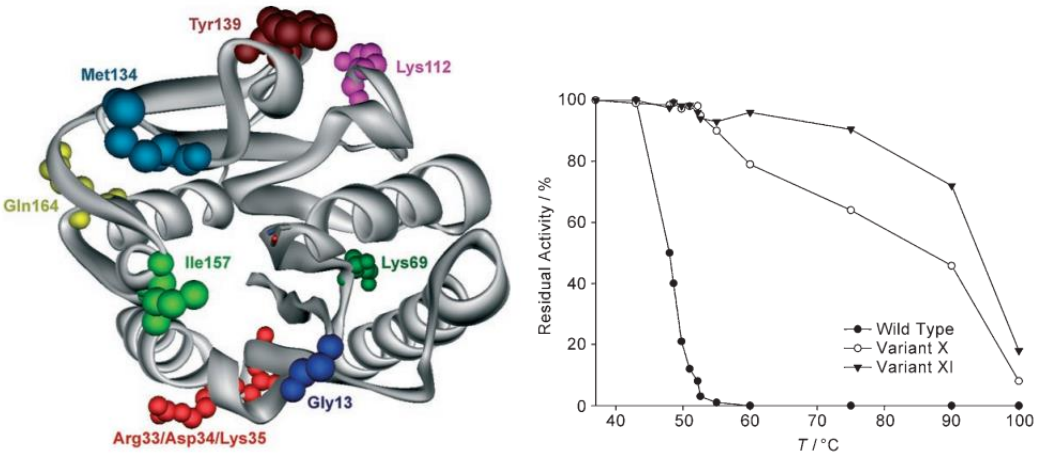

Figure 7: The defined mutation sites in Lip A that were chosen for saturation mutagenesis. Thermostability of the purified Lip A and mutants X and XI displayed as residual activity curves. (This figure was reprinted with the permission of Wiley-VCH).[85]

The libraries development can be achieved by using the named properties as an exploitation principle, to achieve a certain accuracy rather than just randomly screening. For an instance *Reetz et al*.[85] showed by using the B-factor as argument of the flexibility of a protein regions as criteria to define hot spots, which then were used to generate libraries. Those libraries were screened to identify improvement in thermostability. Lead mutants were then combined in a ISM to achieve final variants (X, XI) with highly improved thermostability from 50 °C (at 50% residual activity) to 95 °C (**Figure 7**).[85]

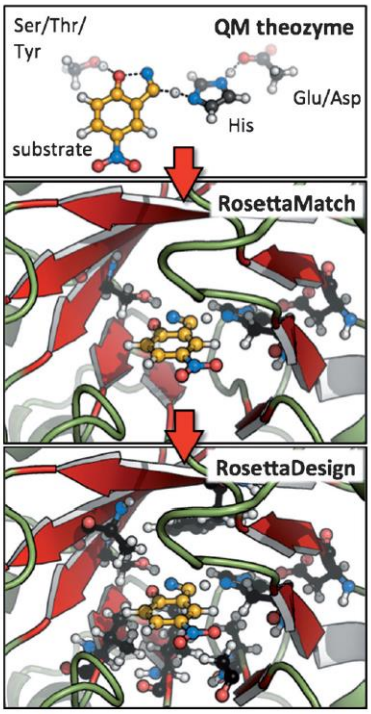

Figure 8: De novo design of an enzyme exemplified with Kemp eliminase. (This figure was reprinted with the permission of Wiley-VCH).[62]

Besides that, there are already a few examples exceeding the standard methods and examples and already emerging the fourth wave of biocatalysis.[57] Pioneer groups in the field of computational biochemistry achieved examples of *de novo* enzyme design. Starting from QM-calculations to define correct amino acids and ligand geometries for a defined and stable transition state of the target reaction. The obtained results lead to an theoretical active site of an enzyme, the theozyme.[86] This theozyme is then placed in protein scaffolds using RosettaMatch, the best starting points are then further optimized with RosettaDesign to achieve the correct amino acids in the predefined theozyme. After further *in silico* evaluations a few examples 10-100 variants are tested in wet experiments. With this method a few de novo designed enzyme were achieved: Retro aldolase,[87] Kemp eliminase[62,88] Diels-alderase.[89]

In this work, some of these presented methods and approaches are adopted in order to use them for the enzyme class of aldoxime dehydratase, approaching rationally the selectivity, activity and stability.

3 Rationalizing the unprecedented stereochemistry of resolutions with aldoxime dehydratases via molecular modeling

3.1 Motivation

Designing stereochemical processes is of utmost importance for the access to chiral building blocks needed for the production of fine chemicals and pharmaceuticals.[57,90,91] While over the last decades numerous examples with chiral chemocatalysts as well as enzymes, both representing fascinating chiral catalysts, exist, at the same time "by definition" there is one general limitation for any type of stereochemical process.[57,90,91] When starting from one (enantio)selective catalyst and a specific substrate, only one enantiomeric form of the product will be obtained. This is true for any type of asymmetric catalysis starting from prochiral substrates as well as for resolutions starting from racemic substrates.[57,90,91] In other words, when having only one enantiomerically pure form of a chiral catalyst in hand, only one enantiomeric form of the product will be accessible in the corresponding transformation.[3] Very recently, however, a unique enzymatic transformation which gave access to both enantiomeric forms of a chiral nitrile although starting from the *same* racemic aldehyde and utilizing the *same* enzyme were identified.[4] This unprecedented stereochemical phenomenon turned out to have its origin in the formation of racemic *E*- and *Z*-aldoximes as intermediates by simple condensation of the aldehyde as starting material and hydroxylamine.

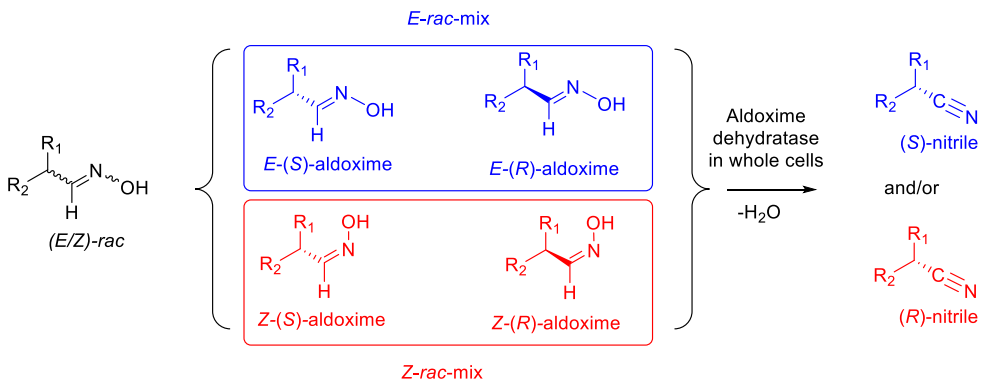

Scheme 1. Enantioselective dehydration of aldoximes towards the corresponding nitrile.

These racemic *E*- and *Z*-aldoximes serve as the "real" substrate for the enzyme and are enantioselectively dehydrated to the chiral nitrile. It is noteworthy that the enantiopreference of this enzymatic resolution then surprisingly does not depend on the absolute configuration of the stereogenic center at the aldoxime, but on the *E*- or *Z*-conformation of the aldoxime.

In detail, in the presence of the same enzyme, using the *E*-racemate as substrate then furnished the (*S*)-nitrile, whereas the (*R*)-nitrile was formed when starting from the *Z*-racemate (**Scheme 10**).[47] Thus, when separating these *E*- and *Z*-aldoximes, both racemates undergo dehydration with formation of the opposite enantiomers of the nitrile products, whereas using the non-separated racemic *E*/*Z*-mixtures would lead to more or less racemic nitrile products. The catalysts being capable of this unique transformation are members of the enzyme class of aldoxime dehydratase (EC: 4.99.1.5).[13,23,92] Although they have been known for over three decades, only 8 different enzymes have been published with only a little known about their nature. These heme containing enzymes convert aldoximes to the corresponding nitriles by release of water without any additional cofactor and contain a catalytic triad consisting of an arginine, histidine and serine or threonine. The substrate scope turned out to be very broad,[13,16,18,22,23,28,39,46,47,92,93] and among the resulting aliphatic and chiral nitriles are various important products for the chemical industry.

To gain insight into this exciting and very unusual stereochemical behavior of this class of aldoxime dehydratases, molecular modeling studies were performed, including *in silico* mutations and docking studies. In order to prove such data on rationalizing the selectivity of an aldoxime dehydratase, the computational studies were combined with laboratory experiments by preparing and characterizing the theoretically calculated enzyme mutants. Based on a general postulated mechanism for an aldoxime dehydratase by *Nomura et al*.[16] the focus of this work was rationalizing this unusual switch in enzyme selectivity by means of docking experiments. As a software MOE (Molecular Operating Environment)[94] was used to investigate protein-ligand structures. The software has already proven to be highly successful for a range of applications.[95,96,97] With the combination of wet experiments including a variety of mutants and substrates an approach to understand this unique and unprecedented behavior regarding the enantioselectivity of these enzymes was developed. Furthermore, the method should first be able to correctly predict the enantioselectivity of the reaction to then be able to predict mutants with increased or decreased enantioselectivity. By achieving a model with high accuracy in the enantioselectivity prediction, gaining a rational insight into stereochemical properties of such enzyme should be possible. The conducted computational as well as experimental work, which will be discussed in the next few chapters was successfully reported in *Angewandte Chemie*.[48]

3.2 Biocatalytic dehydration of chiral nitriles

To characterize the stereoselectivity of the aldoxime dehydratase from *Rhodococcus* sp. N-771 (OxdRE-WT)[26] for a model substrate as a basis for the molecular modeling studies, at first *ortho*-, *meta*- and *para*-fluoro-substituted phenylpropanal oximes (*rac*-2FPPOX, *rac*-3FPPOX, *rac*-4FPPOX) were synthesized and purified as racemic *E*- and *Z*-isomers according to previously developed protocols.[47,98] The isolated racemic *E*- and *Z*-isomers were subsequently used in biotransformations with *E. coli* BL21-STAR whole cells containing OxdRE in recombinant form (**Table 5**). The reactions with this wild-type enzyme proceed as expected as previously described,[47] thus furnishing the (*S*)-nitrile when starting from the *E*- isomer whereas utilizing the *Z*-isomer led to the (*R*)-nitrile. The determined E-values and the corresponding calculated energy values of these biotransformation experiments are given in **Table 5**.

Table 5: Biotransformations of various fluoro-substituted phenyl-2-propanal oximes as *E*- or *Z*-isomers with OxdRE-WT

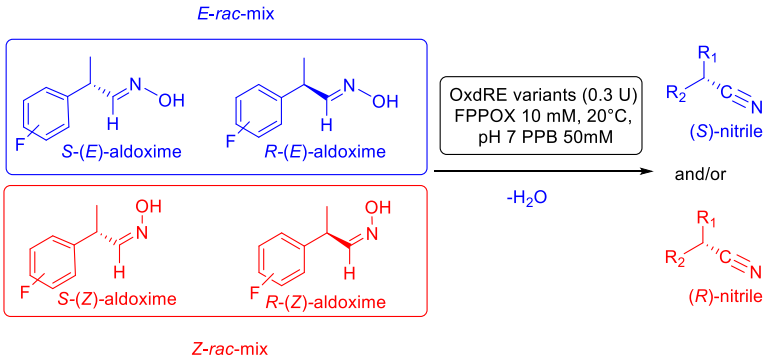

#	Name FPPOX	OxdRE-WT Con. / %	*ee* / %	E-Value	ΔΔG / kcal·mol^{-1}
1	2F-E	45	96 (*S*)	112	2.6
2	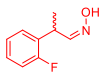 2F-Z	50	65 (*R*)	9	1.2
3	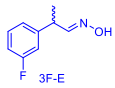 3F-E	48	96 (*S*)	146	2.7
4	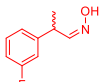 3F-Z	52	64 (*R*)	9	1.2
5	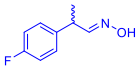 4F-E	34	93 (*S*)	44	2.1
6	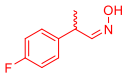 4F-Z	32	54 (*R*)	4	0.7

3.3 Development of a docking procedure

This aldoxime dehydratase from *Rhodococcus sp. N-771* (OxdRE-WT)[26] has been chosen for this study since crystal structures are available for this enzyme (PDB 3a15, 3a16, 3a17),[14] which served as an ideal starting point for the molecular modeling of the transition states when converting the various *E*- and *Z*-isomers. In detail, three different crystal structures are available, including two structures being co-crystallized with non-chiral substrates. Furthermore, crystal structures of two different conformations of the OxdRE are known, namely an "open" and "a closed" conformation. Since the available co-crystals were only found in "closed" conformation, the docking was performed using the closed conformation of OxdRE as this conformation appeared to be the one being relevant for the catalytic cycle. In order to find out which step in the reaction determines the selectivity, normally all intermediate states must be calculated. As in this case the enantioselectivity of the enzyme depends on the *E*- or *Z*-isomer of the substrate and due to the fact that this *E*/*Z* information only can play a role in the initial step of the catalytic mechanisms during the binding phase of the ligand, the binding energies of the ligands to rationalize the stereoselectivity of this enzyme class were calculated. The MM force field calculation was performed using data generated from preliminary experiments[47] and from this work. To find the correct protein-ligand-structures (pose) the co-crystal[14] with *n*-propanal oxime as ligand as a basis for this study was used. Based on the distances and angles of the co-crystal and the mechanism[16] for the dehydration, cut off values for a correct pose were calculated (**Figure 9a**).

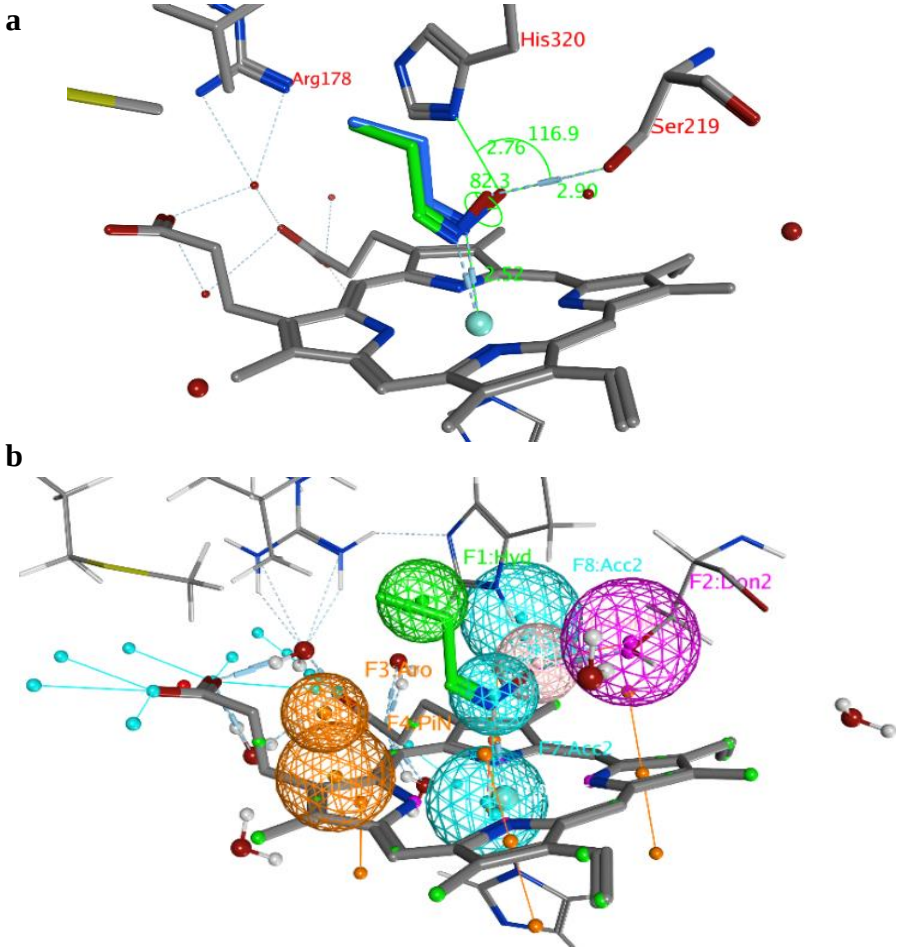

Figure 9. (a) Evaluating the docking results with redocking of propanal oxime; (b) pharmacophore generated with propanal oxime.

With the redocking of the *n*-propanal oxime the docking model as well as the calculation were evaluated and proven to be correct. To further refine, simplify and automate the docking simulation pharmacophores to obtain the correct pose of the ligands (**Figure 9b**) were generated. The pharmacophore can be used to define the binding motif such as the position of the functional group and its orientation. For example, a good pose is not just be described by the presence of the ligand inside the pocket, but by the orientation of the aldoxime ligand, in which the aldoxime function shows a specific position with specified angles (His-O-Ser ~115°), dihedrals (C-N-O-O, ~85°) and distances (Fe-N, ~2.5 Å; O-Ser, ~2.8 Å; O-His, 2.7 Å) towards the heme group and the catalytic triad. Only when these prerequisites are fulfilled, the subsequent dehydration step can proceed. With these defined parameters in hand, a pharmacophore query was created which then allowed to find ligand poses with this specified binding motif. Even though metalloenzymes are not well parameterized[99] a combination of MMF94 force field with the scoring functions London dG and Affinity dG proved to be suited for this purpose. The protein model was prepared using the preparation kit given by MOE.

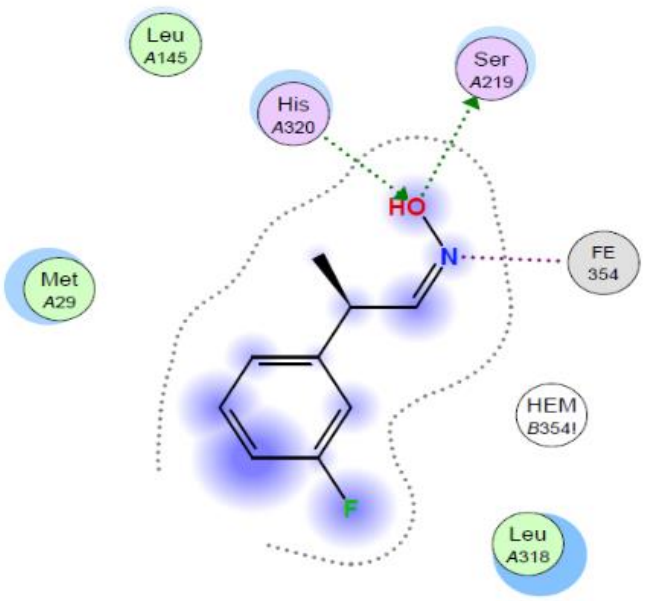

Figure 10: Ligand interaction pattern with (*R*,*Z*)-3FPPOX as an example bound in the active site of OxdRE-WT.

As a representative example, the 2D-figure in **Figure 10** shows the interaction pattern of the enantio- and diastereomerically pure ligand (*R*,*Z*)-3FPPOX with the active site of the enzyme OxdRE-WT. The ligand shows a hydrogen donation to the Ser219 and the H320 donates a hydrogen towards the oxygen of the ligand, while the nitrogen is coordinated by the Fe^{II}-metal center of the heme. The phenyl group of the ligand interacts with the porphyrin ring *via* π-π-stacking and the aldoxime function for each isomer is always in the same position.

Table 6: Comparison of docking experiments with OxdRE (3a17) and 2'-, 3'-, and 4'-fluorophenyl-2-propanal oximes FPPOX and the experimental biotransformation of OxdRE-WT with the various aldoximes.

#	Aldoxime	ΔG / kcal·mol^{-1}	ΔΔG / kcal·mol^{-1}	Prediction	Experiment
1	2F-ER	-7.30	1.87	(*S*)	(*S*)
2	2F-ES	-9.17			
3	2F-ZR	-6.24	1.64	(*R*)	(*R*)
4	2F-ZS	-4.60			
5	3F-ER	-7.68	1.98	(*S*)	(*S*)
6	3F-ES	-9.66			
7	3F-ZR	-6.28	1.51	(*R*)	(*R*)
8	3F-ZS	-4.77			
9	4F-ER	-7.07	2.65	(*S*)	(*S*)
10	4F-ES	-9.72			
11	4F-ZR	-5.88	0.92	(*R*)	(*R*)
12	4F-ZS	-4.96			

ΔG: Binding energy from docked ligand, ΔΔG: Difference of binding energies between two enantiomers of one isomer. Lower binding energy of one enantiomer corresponds to the formed enantiomer.

It is noteworthy that by means of this modeling tool, it was not only possible to predict the enantiopreference, but also to determine quantitatively the enantioselectivity of any aldoxime substrate of this study (**Table 6**). In detail, the calculated difference (ΔΔG) of the ligand binding energies (ΔG) were used to predict the enantiopreference and enantioselectivity. For example, the binding energy of (*S*,*E*)-3F of -9.66 kcal·mol^{-1} is lower than the binding energy of the opposite enantiomer (*R*,*E*)-3F with -7.68 kcal·mol^{-1} (**Table 6**, entry 7&8). Notably, the resulting calculated energy difference (ΔΔG) of 1.98 kcal·mol^{-1} corresponds very well with the experimental value of the enantioselectivity and the preferred formation of the *S*-enantiomer. The high accuracy is underlined when comparing the ΔΔG-values from the docking experiments (**Table 6**) with those obtained from the biotransformation experiments (**Table 5**) demonstrating a perfect agreement of the predicted enantio-preferences and a good agreement of the quantitative ΔΔG-values. By looking deeper into the final poses of the protein-ligand-structures and docked ligands, similarities between each substrate and its conformers (**Figure 11**) were revealed. The methyl group is exposed to M29, L145 and the H320. The general pose of the docked ligand does not vary from the position or the type of halogenation of the phenyl ring. Therefore, the halogenation has no direct effect upon the selectivity, however, it has a certain influence on the acceptance of a ligand. The enantiomeric excess can differ because the binding energies vary with the type and position of substituent on the phenyl ring.

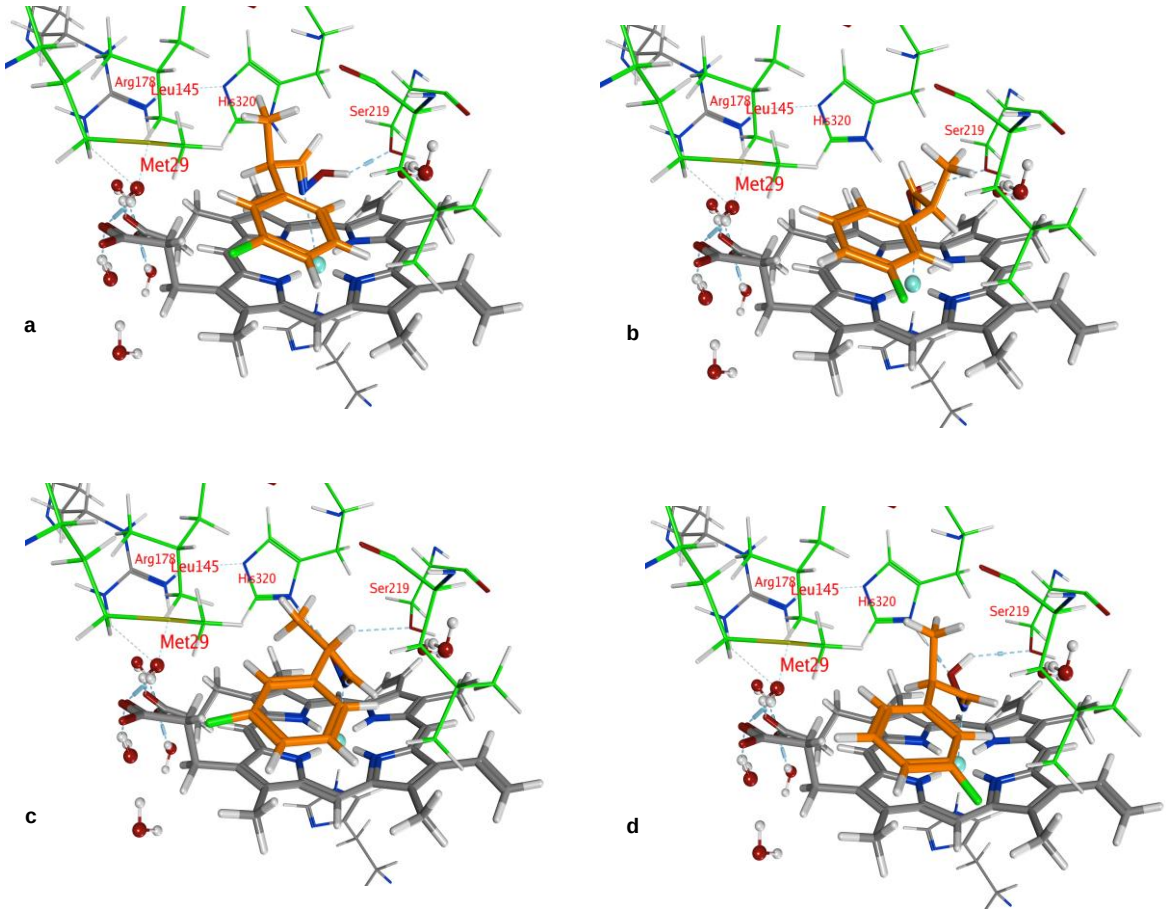

Figure 11. Protein-ligand-structure (pose) of 3-FPPOX conformers in the active center of OxdRE-WT. (a) 3-(*E*,*R*); (b) 3-(*E*,*S*); (c) 3-(*Z*,*S*); (d) 3-(*Z*,*R*).

Therefore, the halogenation has no direct effect upon the selectivity, however, it has a certain influence on the acceptance of a ligand. The enantiomeric excess can differ because the binding energies vary with the type and position of substituent on the phenyl ring. The methyl group is the only group which differs between the compared conformers in space and alignment. Based on that information, that the main reason for the selectivity with respect to an isomer the arrangement of the methyl group was claimed. The methyl group is always positioned in a cavity, which is formed by the amino acids M29, L145, A147 and H320, but for each conformer in a specific arrangement (**Figure 11**). In general, all PPOX-derivatives follow a certain alignment. The methyl group of the PPOX derivates is always in the cavity. However, while the methyl group of the ligands with *E*,*R*- and *Z*,*S*-conformations (not preferred) are closer to the H320 and L145, the methyl group of the ligand with *E*,*S*- and *Z*,*R*-conformation (preferred) are more in the middle of the pocket directing towards the cavity (**Figure 11**). The available data suggests that the position and orientation of the methyl group in relation to the cavity determines the selectivity (**Figure 11a**). The necessary alignment is only possible for the *E*-isomer in *S* configuration and for the *Z*-isomer only in *R* configuration. Due to the scoring function, however, it is not possible to determine the single contribution of each Van-der-Waals-(VdW)-interaction. Thus, a direct determination of the energy contribution of the methyl group was not possible. Another contribution leading to the observed selectivity could be related to the aldoxime function. Due to their small variation in the alignment, the aldoxime moiety could cause the energy gap ($\Delta\Delta G$) and with that the selectivity. Because of the perfectly designed model it is possible to determine single atom energy contribution due to the ligand interaction pattern illustrated in (**Figure 10**). Using the energy contribution, it has been successfully demonstrated that no correlation between energy contribution, selectivity and conformation

exists. Meaning the aldoxime functionality does not correlate with the selectivity. If for an instance the aldoxime functionality would have an impact upon the selectivity, then, when comparing ΔΔG values ($\Delta\Delta G_{NOH} = \Delta ES_{NOH} - \Delta ER_{NOH}$) for a pair of ligands, a sign reversal could be observed leading to an alternating graph when plotted against the selected ligand pairs. But **Figure 12** shows randomly distribution of the energy differences. Therefore, it was concluded that the arrangement of the aldoxime function is essential for the reaction, but insignificant for the differentiation between the enantiomeric pairs of an isomer.

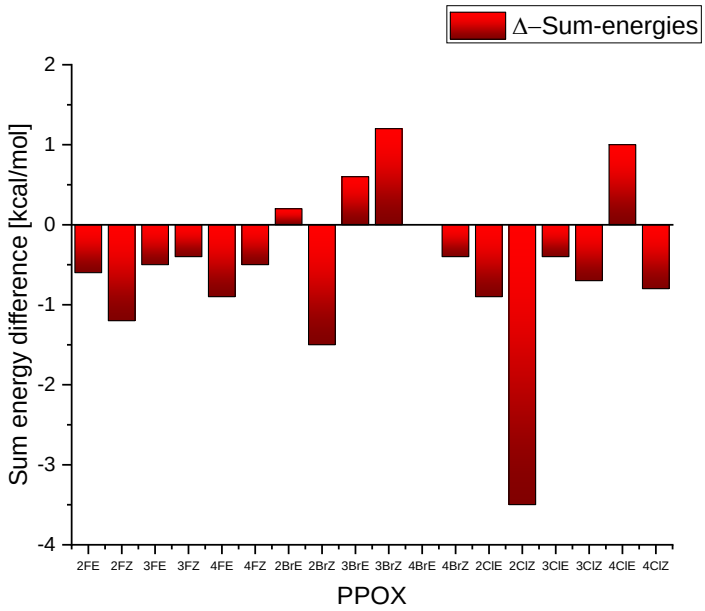

Figure 12: Energy contribution of the aldoxime function in dependency of the enantiomer formed

3.4 Modeling guided site directed mutagenesis of OxdRE

To prove the hypothesis about the methyl group being the main cause for the selectivity and in order to validate the modeling study further, the calculation as well as experimentally evaluation of various mutants with (i) a more enlarged or alternatively (ii) a tighter cavity in the active site, was initiated. Accordingly, these mutants then should lead to a decreased (in case of (i)) or increased (in case of (ii)) differentiation of the substrate enantiomers, and thus to a decrease of increase of the enantioselectivity. To start with the design of mutants with an enlarged active site (case (i)), *in silico* studies showed that mutants with such an increased size of the cavity goes in hand with a significant decrease of the ΔΔG-value.

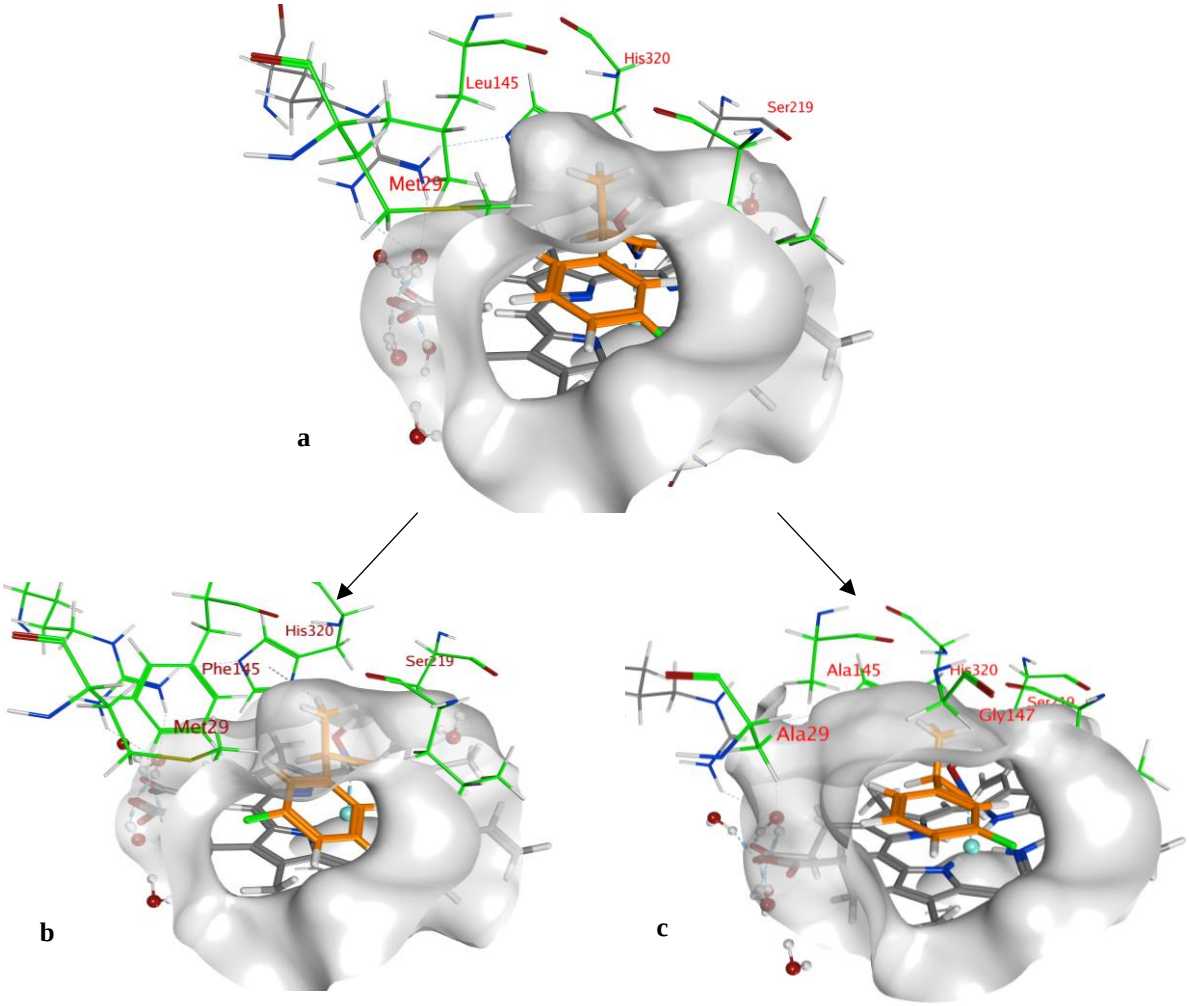

Figure 13. 3-(*R,Z*)-FPPOX bound in the catalytic center of OxdRE-WT (a), in L145F (b) and 3M (c). The methyl group is in the cavity, which is formed by the amino acids M29, L145, A147 and H320. The figure shows the docked position of the ligand 3-(*R,Z*)-FPPOX in three different OxdRE variants. The L145F has a smaller cavity the triple point mutant 3M (M28, L145A, A147G) has an increased cavity size

Consequently, such mutants then should lead to a lower selectivity. As described above, the cavity is formed by four amino acids. With A147 being already very small and M29 being highly flexible, L145 was the most promising mutation site, due to the highest steric contribution to the cavity. Mutating the proximal H320 to glycine or alanine also would increase the size of the cavity tremendously, but as part of the catalytic triad it is not possible to mutate the proximal H320 without creating a loss of function mutant.[100] However, the single point mutations of each position did not lead to a significant decrease of the ΔΔG-value except for the H320 mutation (*in silico*). Therefore, double and triple point mutations, whereas the triple point mutation showed a more significant decrease in the ΔΔG-value were designed. Based on the *in silico* analyses, the most promising mutant would have been the triple glycine mutant M29G/L145G/A147G (OxdRE-3G). However, in the wet experiments this mutant was found to be unstable, and the expressed protein could only be observed as insoluble protein (**Figure 14**).

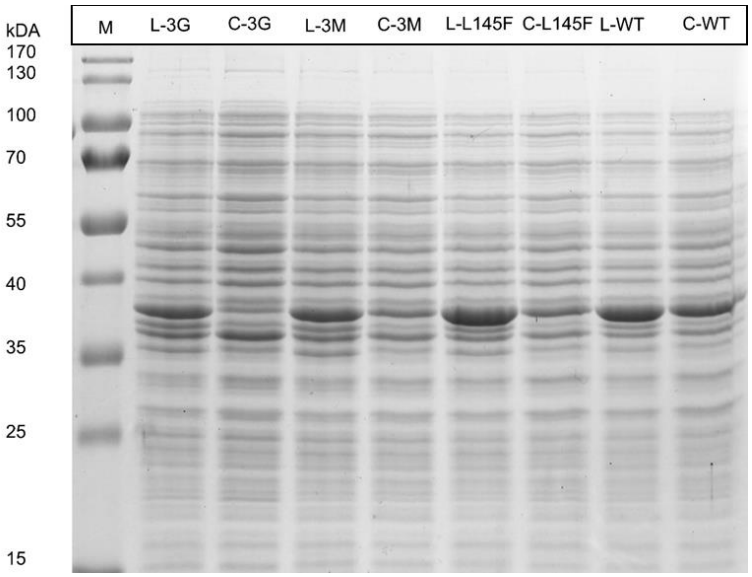

Figure 14: SDS-PAGE of OxdRE-WT (WT), OxdRE-L145F (L145F), OxdRE-M28/L145A/A147G (3M) and OxdRE-M29G/L145G/A147G (3G). C indicates crude extract while L indicates lysate. The SDS-PAGE show the over expression of the Oxds in general by the means of lysate solution with the comparison to the crude extract.

As alternative the M28/L145A/A147G (OxdRE-3M) mutant (**Figure 13c**) was generated. For the next step, the focus was to generate complementary mutation strategy, to create a variant with a decreased size of the cavity (case (ii)), thus making the active site more rigid. Accordingly, for the resulting biotransformation then an increased enantioselectivity can be expected. In order to decrease the size of the cavity, the position L145 turned out as the only option for a suitable mutation. In contrast, the amino acids M29 and A147 are not suitable for rationally decreasing the size of the cavity. The A147 mutations were all in the wrong orientation and not exposed to the active site. M29 was already one of the longest amino acids, which could reach the cavity. For Leu145 the most promising *in silico* mutation was found to be L145F (**Figure 13b**). Other amino acids were also tested *in silico*, but they were either too small, too large or changed the environment of the catalytic triad too much. The goal of this study (decreased cavity) was to gain an aldoxime dehydratase, which can convert only one enantiomer of four possible conformers (*ES*, *ER*, *ZS* and *ZR*). The *in silico* site directed mutation and the performed docking predicted, that the L145F mutant would be a promising candidate for a more enantioselective conversion of PPOX derivatives (**Figure 13b**). With these two optimized mutants in hand (addressing case (i) and (ii)), a detailed theoretical as well as experimental study was conducted (**Figure 15**). For a better comparison of the theoretical data with the experimental ones from the biotransformation, the E-values from the determined energy values ($\Delta\Delta G$) were calculated. As expected, the enantioselectivity (E-value) is much higher for the L145F mutant, while for the 3-M mutant the enantioselectivity is much smaller, which agrees with the proposed hypothesis. For example, for the two enantiomers of the 2F*E*-PPOX substrate a much higher enantioselectivity was determined in the docking experiment for the OxdRE-L145F mutant compared to the wild type and the mutant OxdRE-3M. In detail, the optimized mutant OxdRE-L145F shows an E-value of over 200 whereas OxdRE-WT and OxdRE-3M show much lower selectivities with E-values of 28 and 22 (**Figure 15a**). The docking data further predicts that in general the enantioselectivity for the conversion of the *Z*-isomer is lower than the conversion of the *E*-isomer. Thus, from these *in silico* experiments the prediction shows that the mutant L145F is about 10 times more selective than the wild type, while the 3M-mutant is about one third less selective.

In order to evaluate if the predictions and hypothesis are correct, *in vitro* mutations of OxdRE and biotransformation's were performed. The results from these *in vitro*, which are shown in figure 5b, agree with the theoretical data and also revealed interesting results.

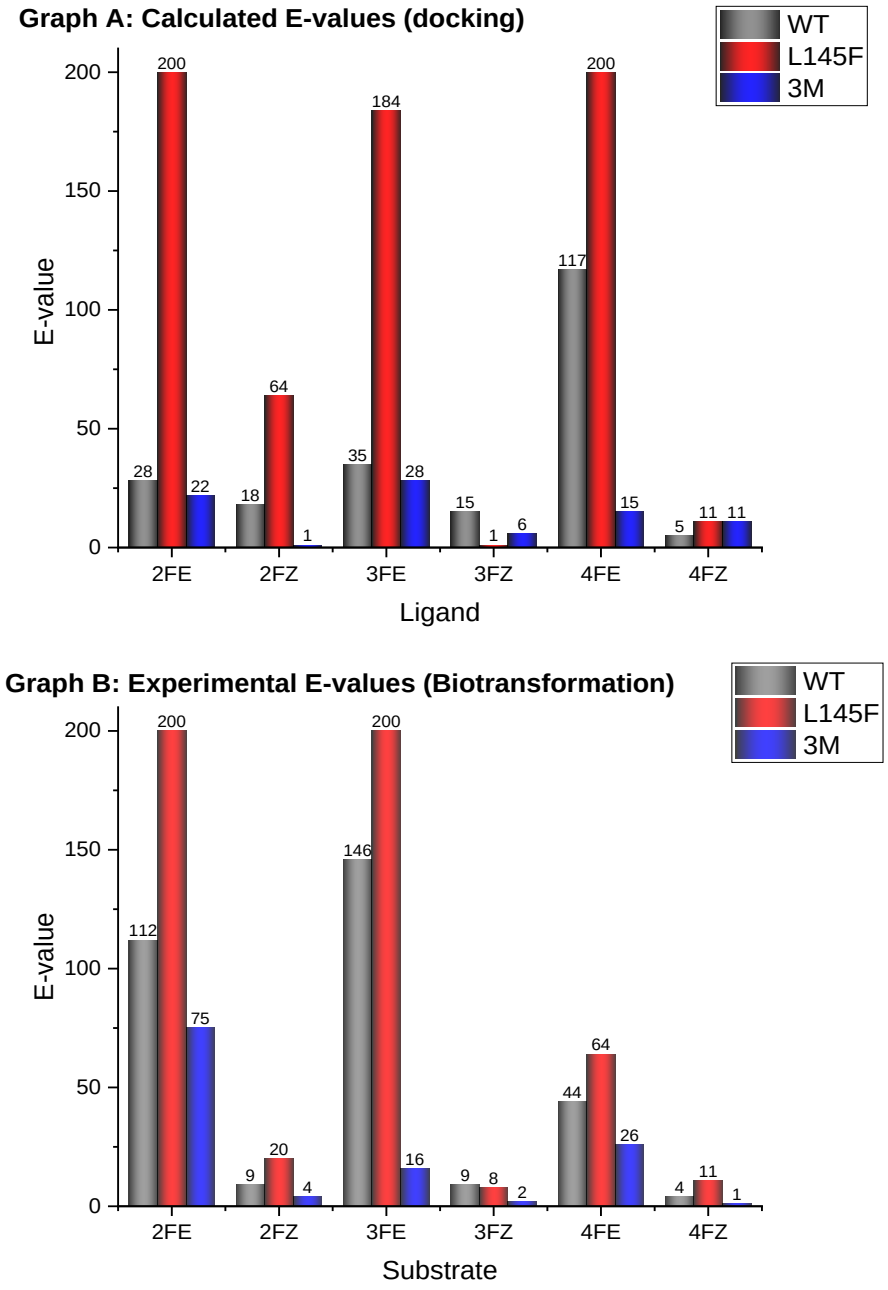

Figure 15. Graph A: Calculated E-values from the ΔΔG values of the docking data for the FPPOX derivatives with each enzyme. The graph was normalized to a maximum E-value of 200. Graph B: The E-values from the biotransformation of the FPPOX derivatives to their corresponding nitrile with the use of OxdRE-WT, OxdRE-L145F and OxdRE-3M. The graph was normalized to a maximum E-value of 200.

Although the E-values of the docking data are not exactly the same as the E-values of the biotransformation, both studies revealed the same tendencies and the calculation is consistent with the experimental data, showing highest E-values for the L145F mutant and lowest E-values for the 3M-mutant. The best example for increased selectivity is in case of the 2F*E*-PPOX substrate, whereas the L145F mutant has an E-Value of over 200 compared to the wild type with 112. The best example for decreased selectivity can be observed for the 3FE-PPOX, with the mutant 3M

being about 10 times less selective, than the wild type. The L145F mutant is still able to convert both isomers and not able to selectively convert an *E*/*Z*-mixture to the (*S*)-nitrile, but the selectivity is also for the mixture two times higher than the wild type, which will be discussed in Chapter 4. It is noteworthy that the selectivity could be increased just with one single point mutation and that with gained knowledge the enzyme can be engineered further.

3.5 Summary and outlook for rationalizing the stereochemistry of aldoxime dehydratase

In conclusion, the stereochemically unique and to the best of our knowledge unprecedented stereochemical phenomenon of aldoxime dehydratases, which can enantioselectively dehydrate aldoximes prepared from the same aldehyde to both enantiomeric forms of a chiral nitrile, has been rationalized by means of a molecular modeling study utilizing MOE as a software.

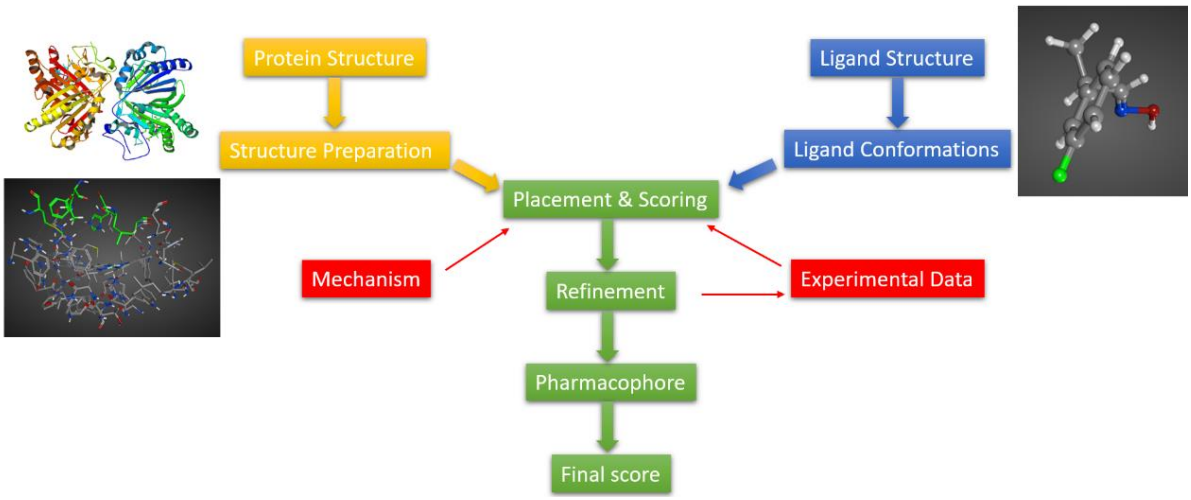

Figure 16: General flow chart for molecular modeling.

Thus, an optimal flow chart for modeling starting from protein and ligand structure, which were designed and prepared *in silico*, was utilized. By combining mechanism knowledge and experimental data a perfectly fitting model was accomplished. This modeling gave a detailed explanation why with the same enzyme the use of racemic *E*- and *Z*-aldoximes led to the opposite forms of the chiral nitrile. Furthermore, the modeling study was supported when designing mutants with an increased and decreased cavity, which showed the expected and theoretically predicted decrease and increase of the enantioselectivities also in the experimentally conducted biotransformations. In addition, based on this validated model it was possible to rationally design mutants with a decreased size of the cavity, which then gave superior enantioselectivities compared to the known wild-type enzyme with excellent E-values of up to E=200. Thus, this robust and validated model will also serve as a basis for predicting aldoxime dehydratase mutants with improved stereochemical properties activities and even stability.

4 Chiral nitrile synthesis and formal double dynamic kinetic resolution

4.1 Motivation

The kinetic resolution of aldoximes with Oxds require pure isomeric form either as *E*- or *Z*- aldoxime to obtain enantiomeric pure form of the corresponding nitrile.[101] Even though phenylpropanal oximes (PPOX) with a benzylic- and a methyl moiety can be purified into their isomers, the procedure even using automated column chromatography is very tedious and only in small amounts possible.[47] Furthermore, the isomers are in a long term instable and can only be stored in solution at -20 °C. From the chemical point of view, a kinetic resolution has the major drawback of being limited to maximum yield of 50%. In the case of aldoxime transformation with pure isomers, the maximum theoretical yield is even further limited. If, for simplification, assuming that the *E*/*Z* proportion is 50/50, the racemic mixture must first be purified into *rac*-*E* and *rac*-*Z*. Then, the substrate can be converted into the alleged nitrile in a kinetic resolution. In the case of *rac*-*E*, an ideal kinetic resolution would yield the pure *S*-nitrile and the remaining (*R*,*E*)-aldoxime with 25% each (**Scheme 10**). In reality, neither the enzyme is perfect, nor is the isomer ratio 50/50. For most phenylpropanal oximes, the thermodynamic equilibrium is about 70/30 (*E*/*Z*), whereas for fatty aldoximes, for example, it is 50/50 (*E*/*Z*). Since, the enzyme accepts both isomers of the PPOX as opposite enantiomers as substrate, using the substrate as *E*/*Z*-mixtures to increase the yield will lead to a racemate (when starting from a 50/50 *E*/*Z*-ratio).

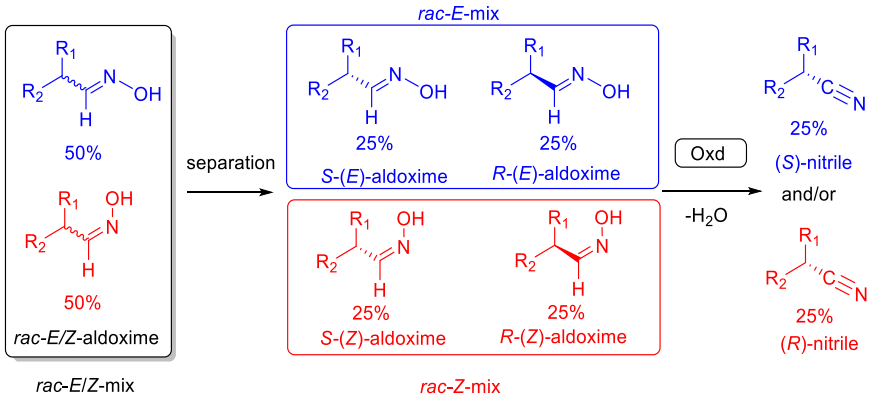

Scheme 10: Schematic illustration of a perfect kinetic resolution with pure *E*- or *Z*- isomer and an Oxd as catalyst

In addition, the substrate synthesis of the PPOX derivatives, is not only tedious in terms of downstream processing, but also inefficient due to the three subsequent steps with each step in average reaching only 50% yield, leading to an overall yield of only 7-25% (**Scheme 11**).[47]

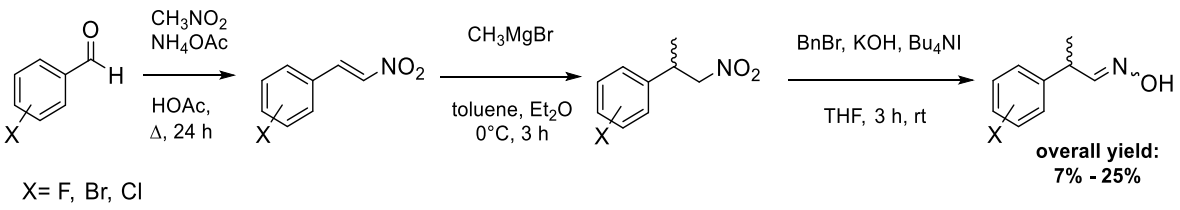

Scheme 11: Multistep synthesis of *rac*-(*E*/*Z*)-PPOX derivatives starting from benzaldehyde.[47]

With such low yields in the substrate synthesis as well as in the nitrile synthesis, the reaction is not suited for any kind of application. Nevertheless, a reaction to obtain chiral nitriles without the use of toxic substances such as cyanides and at the same time the possibility to provide them in a broad application is a very important research topic and at the same time the motivation of this work. In order to optimize the reaction, not only the biocatalytic process (**Scheme 10**) had to be optimized, but also the substrate synthesis (**Scheme 11**). Therefore, investigations were consulted to turn the kinetic resolution into a dynamic kinetic resolution (DKR). However, to improve the reaction to a DKR, a racemization method would have been needed, whereas the isomers remain stable. This option did not seem to be realizable, moreover it would increase the theoretical yield from 25% to only 50%. Instead, the already known isomerizability of aldoximes with a suitable racemization should be combined to develop a feasible method. Besides the development of a racemization/isomerization method also a suited biocatalyst for this purpose was essential. Therefore, an aldoxime dehydratase with regard to its selectivity, that separation of the *E/Z* isomer is no longer necessary, had to be designed. This would not only increase the theoretical yield from 25% to 100%, but would also be the first formal double kinetic racemate resolution (DDKR) (**Scheme 12**).

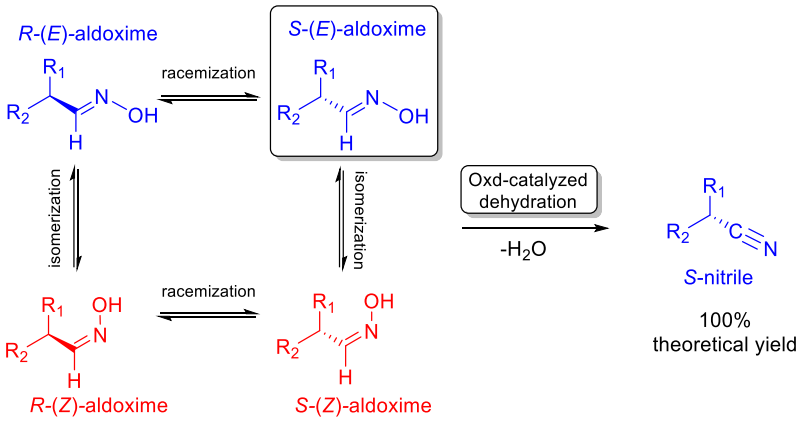

Scheme 12: Schematic illustration of a double dynamic kinetic resolution (DDKR) with *S*-nitrile as target product.

For that purpose, isomerization and racemization of chiral aldoxime with phenylpropanal oxime as the motif structure were investigated. Starting with kinetics for the isomerization of *rac*-(*E*)-**8** and *rac*-(*Z*)-**8** including a temperature, concentration and solvent profile. The biocatalytic dehydration of *rac*-(*E/Z*)-**8** was used to obtain the enantiomerically enriched (*R,E*)-**8** subsequently, (*R,E*)-**8** was used as a substrate for the racemization study. For the racemization itself thiazoles were investigated as racemization agent. The substrate synthesis was optimized using an alternative route including hydroformylation as key step starting from styrene derivatives. To optimize the enzyme and obtain a suitable catalyst for the reaction rational and semi-rational methods were used, including molecular modeling, site directed mutagenesis and saturated mutagenesis. As starting point OxdRE-L15F was chosen since the variant was already rationally modified with improved enantioselectivity.[101] After achieving all individual steps, the development of a process window to combine each step were also targeted. For this purpose, the combination of all steps was investigated in a flow set up.

4.2 Isomerization study with PPOX as standard substrate

The isomerizability of aldoxime is already well known and *S. Nsikabaka et al.*[102] were even able to develop a detailed mechanism in the aqueous milieu using DFT calculations. Based on this, the isomerization was quantified under different parameters. The resulting kinetic data and conditions should then be used in the DDKR.

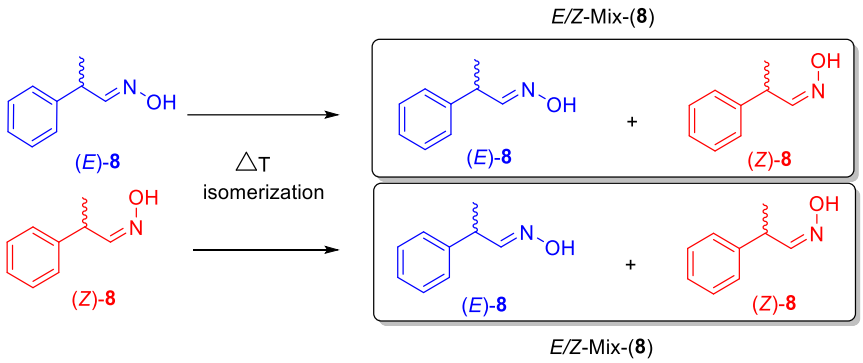

Scheme 13: Schematic illustration of the isomerization study with (*E*)-and (Z)-PPOX (**8**) into the *E*/*Z* mixture (thermodynamic equilibrium)

The following isomerization studies were always carried out with both isomers as starting point. To enable direct measurements the reactions were always carried out in deuterated solvents. The enzymatic dehydration of PPOX (**8**) was usually carried out with DMSO (10% *v/v*) as cosolvent and 10 mM substrate concentration, therefore the standard conditions were characterized showing the influence of DMSO first (**Figure 17**). Whereas isomerization occurs very slowly or not at all at 40 °C for all solvent ratios, therefore the reaction was repeated at 90 °C. The results indicate, that with increased DMSO concentration, the isomerization rate rapidly decreases. Moreover, the thermodynamic equilibrium is reached after 18 hours at 70/30 *E*/*Z*-ratio. With pure DMSO as solvent isomerization couldn't be observed. Since it was shown that DMSO has a negative influence on isomerization, the proportion of DMSO in the reaction solution was kept low at 10% for the further experiments

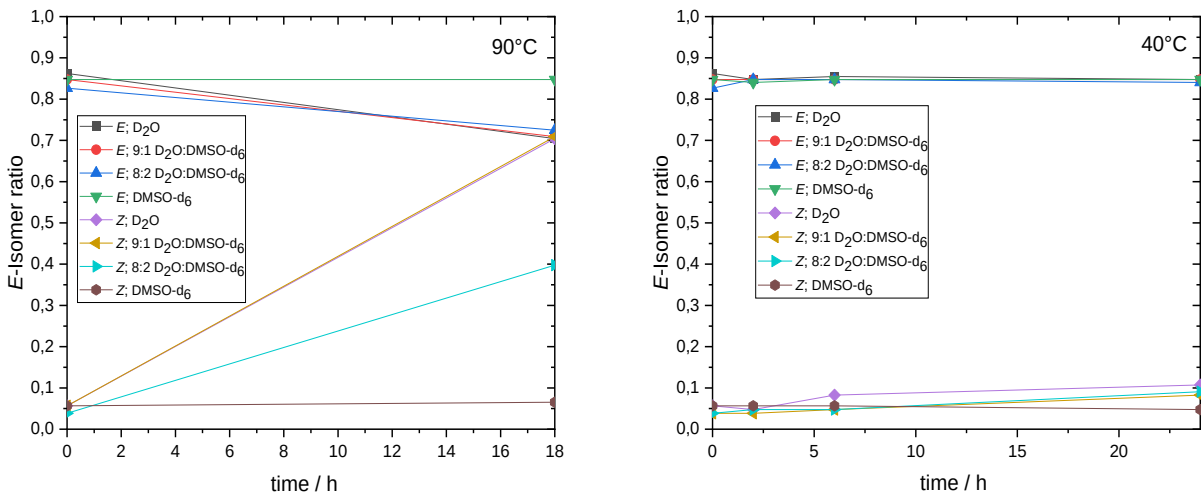

Figure 17 :Effect of DMSO on the isomerization rate of PPOX (**8**, 10 mM) at 40 °C and 90 °C.

The overall isomerization rate is quite low at 10 mM substrate concentration. The isomerization study at different temperature (**Figure 17**) indicated, that with more kinetic energy and thus accumulation of collisions, the isomerization rate increases. Therefore, increased substrate concentration should also amplify the isomerization rate.

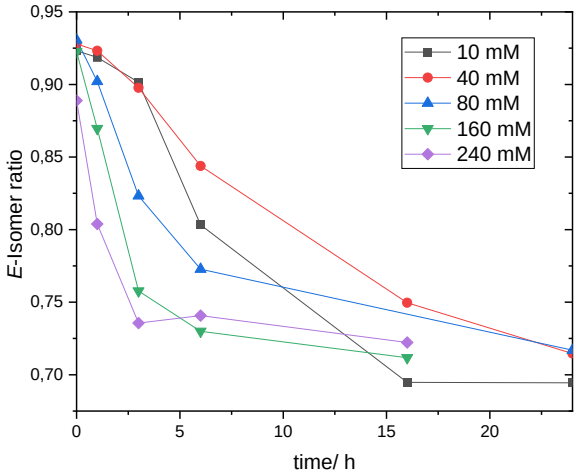

Figure 18: Concentration dependent isomerization rate of PPOX (**8**) at 100 °C in D_2O/DMSO (9:1)

To verify whether isomerization depends on substrate concentration, concentration dependent isomerization rate was measured. For this purpose, only *E*-(**8**) was used, due to the low excess to *Z*-(**8**). As expected, the rate of isomerization is dependent on the substrate concentration. The higher the substrate concentration, the faster the thermodynamic equilibrium is reached (**Figure 18**). In the case of 240 mM the equilibrium is reached after about 3 hours, while with 10 mM substrate concentration it takes about 15 hours to reach the thermodynamic equilibrium. Thus, a high substrate concentration coupled with a high temperature provides a process window in which isomerization can be coupled with enzymatic dehydration.

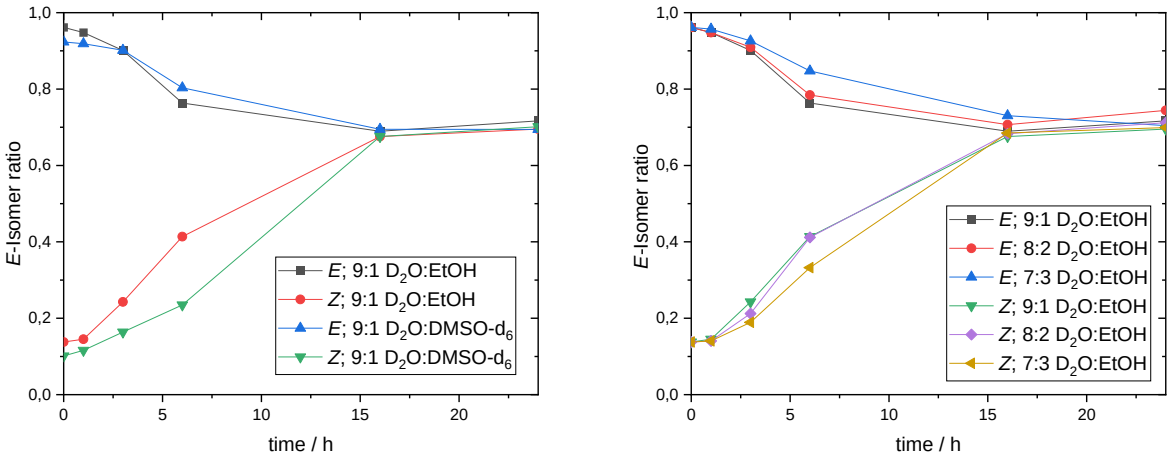

Figure 19: Comparison of isomerization rate with ethanol and DMSO as cosolvent using PPOX (**8**, 10 mM) at 100 °C

In the downstream process DMSO appeared to be tedious in terms of work up and substrate preparation, therefore a switch from DMSO to ethanol as cosolvent was desirable. In order to perform the reaction with ethanol, the influence of ethanol on the isomerization rate at different D2O/ethanol ratios and a comparison with DMSO were performed (**Figure 19**). It appeared that ethanol does not inhibit the isomerization rate even at higher ratios. In comparison with DMSO, ethanol does slightly improve the isomerization rate.

For the process discussed later, (chapter 4.4) the enzymes need to be immobilized in superabsorber using cyclohexane as solvent.[37] The isomerization and racemization will take place in a two-phase system containing water and cyclohexane. To verify whether isomerization can be combined with the reaction, cyclohexane as solvent was tested as well. Since the boiling point of cyclohexane is at 81 °C, the reaction was carried out at 80 °C instead of 100 °C (**Figure 20**). It appears that the isomerization in cyclohexane proceed as well, but slightly slower than in water. The reason for this, is probably based on the mechanism of isomerization of aldoximes, since the addition of water was postulated as an intermediate step.[102] In comparison, the isomerization in water is about twice as fast. With evidence, that isomerization also occurs in cyclohexane in a suitable time window and the possibility that it is much faster in a two-phase system than in pure cyclohexane, the isomerization study was completed. The next step was to develop a method for racemization.

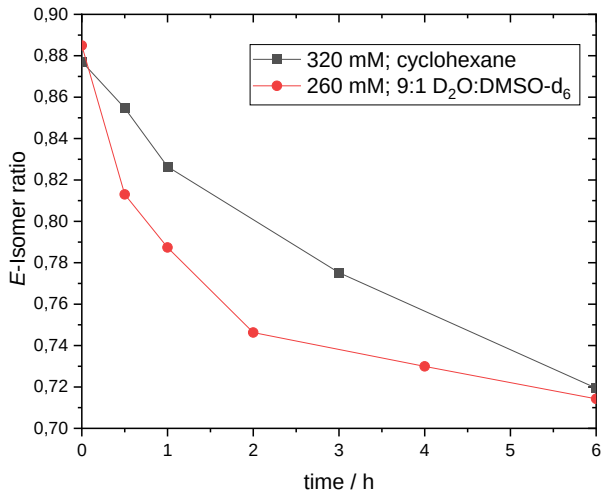

Figure 20: Isomerization rate of *E*-PPOX (**8**) in cyclohexane at 80 °C in comparison with 260 mM isomerization in D_2O/DMSO at 100 °C.

4.3 Racemization of chiral aldoximes

For the racemization of aldoximes a method had to be developed, which would release the hydrogen either as proton or hydride in a reversible reaction. Furthermore, the procedure must be selective for the substrate and not the product since both are present in the reaction solution at the same time. In view of this fact, only the carbon atom of the aldoxime/nitrile functionality remains as possibility to differentiate substrate and product and at the same time could potentially provide a racemization method. The idea was to use a nucleophile with excess to the aldoxime, but not the nitrile (**Scheme 14**). The nucleophile would bind to the positive polarized carbon atom of the aldoxime function (**I**) forming the amide structure **A**. The C_α proton could now tautomerize via a 1,3-H-shift (**II**) due to its spatial proximity to the negative charged amid leading to the intermediate **B.** In the next step (**III**)

the rearrangement of the electrons would lead to the leaving of the nucleophile, while forming a vinylic hydroxylamine **C**. In the last step (**IV**) the thermodynamically favored aldoxime could be formed in an imine-enamine tautomerization type rearrangement. In the case of the nitrile either step **I** or step **III** will not proceed. In step **I** the addition of a nucleophile on a CN-bond is very unlikely and even if the imine structure (**E**) is formed it is again quite unlikely to form the ketenimine derivative (**F**) in step **III**. All in all, if a suitable nucleophile is discovered it should only proceed with the aldoxime not the nitrile.

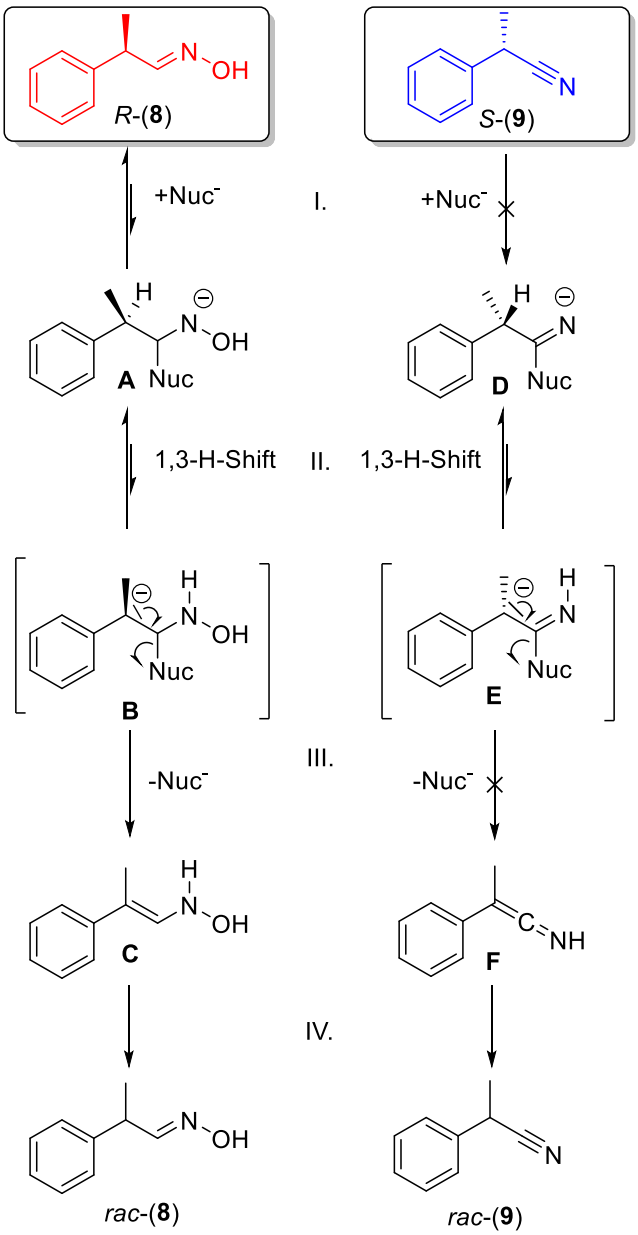

Scheme 14: Basic concept of theoretical racemization using a nucleophile with aldoxime and nitrile being present in the reaction solution

In literature reactions with similar mechanism do not exist for aldoximes yet, but for aldehydes, namely Stetter-reaction[103] and benzoin condensation[104]. Those reaction types are generally used to reverse the polarity of the carbonyls to subsequently form a C-C coupling. With consideration that aldehydes partly act similar to aldoximes, those reactions were investigated first. The Stetter-reaction was originally with the use of cyanide and thiazolium salts and later with N-heterocyclic carbenes (NHCs) also as asymmetric catalyst. In this work, the formulated

mechanism with thiazolium salts and NHC was particularly attractive.[105] With thiazoles being easily accessible and NHCs usually being used for asymmetric coupling, thiazoles were chosen to be investigated in this work. The mechanism behind the "Umpolung" or pole reversal with Thiazoles as well as NHCs in general is comparable to the proposed mechanism (**Scheme 15**).

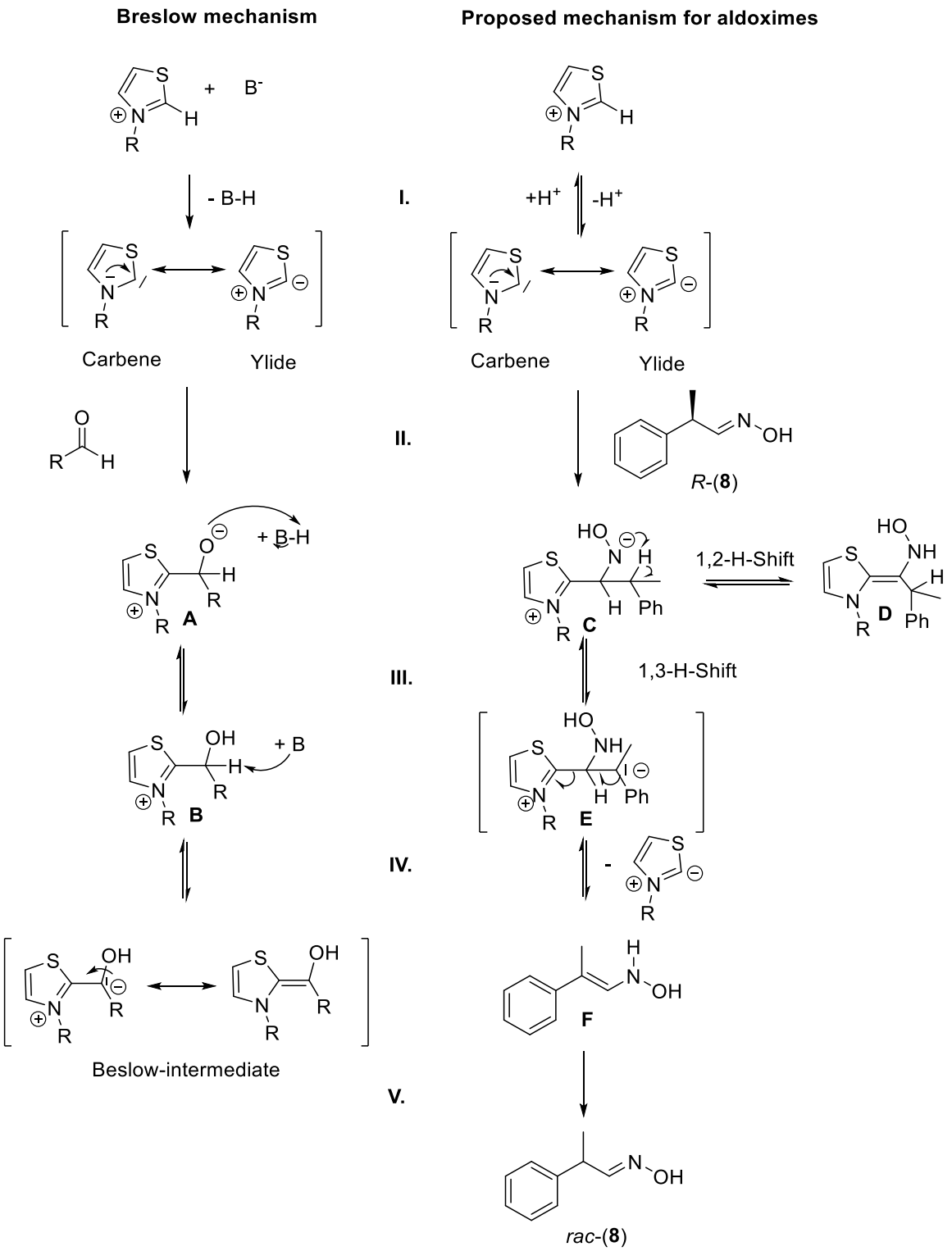

Scheme 15: Comparison of the postulated thiazole catalyzed "Umpolung" mechanism and formation of the Breslow-intermediate[106] with the proposed mechanism for racemization with thiazoles.

The thiazole catalyzed "Umpolung" starts with deprotonation of the thiazole using a base (**I**). In step **II** a nucleophilic attack of the ylide towards the carbonyl carbon with a follow up (**III**) protonation of the oxygen leads to the alcohol **B**. In the last step (**IV**) base catalyzed C_α deprotonation leads to the so-called Breslow intermediate.[105,106] In the proposed mechanism for aldoxime racemization, an additional base is not present. The thiazole should form the carbene-ylide mesomeres also in water to a small percentage, which could be accelerated with thermal energy (**I**). Step **II** would proceed exactly as for the aldehyde, leading to the amide **C**, a follow up 1,3-H-Shift (**III**) could lead to the carbanion **D** as intermediate. Subsequently electron rearrangement fueled by the proximity of the positive polarized C_α next to the carbanion would lead to the formation of the desired vinyl hydroxylamine **E** with the thiazole as leaving group (**IV**). In the last step as proposed before, the thermodynamically favored aldoxime could be formed spontaneously, in an imine enamine tautomerization type rearrangement leading to the compound **8**. It is also possible that in step **III** the Breslow-Intermediate is formed with the aldoxime by a 1,2-H-shift of the hydroxylamine **C**, but in a reversible reaction with a much lower probability of occurrence as well as the followed formation of the racemic substrate (**8**) a hydride ion had to be abstracted, which is again high unlikely. To verify the hypothesis, the enantiomeric enriched aldoximes first had to be obtained by doing preparative scale enzymatic dehydration of *rac*-(*E*)-(**8**) with OxdRE-WT (**Scheme 16**).

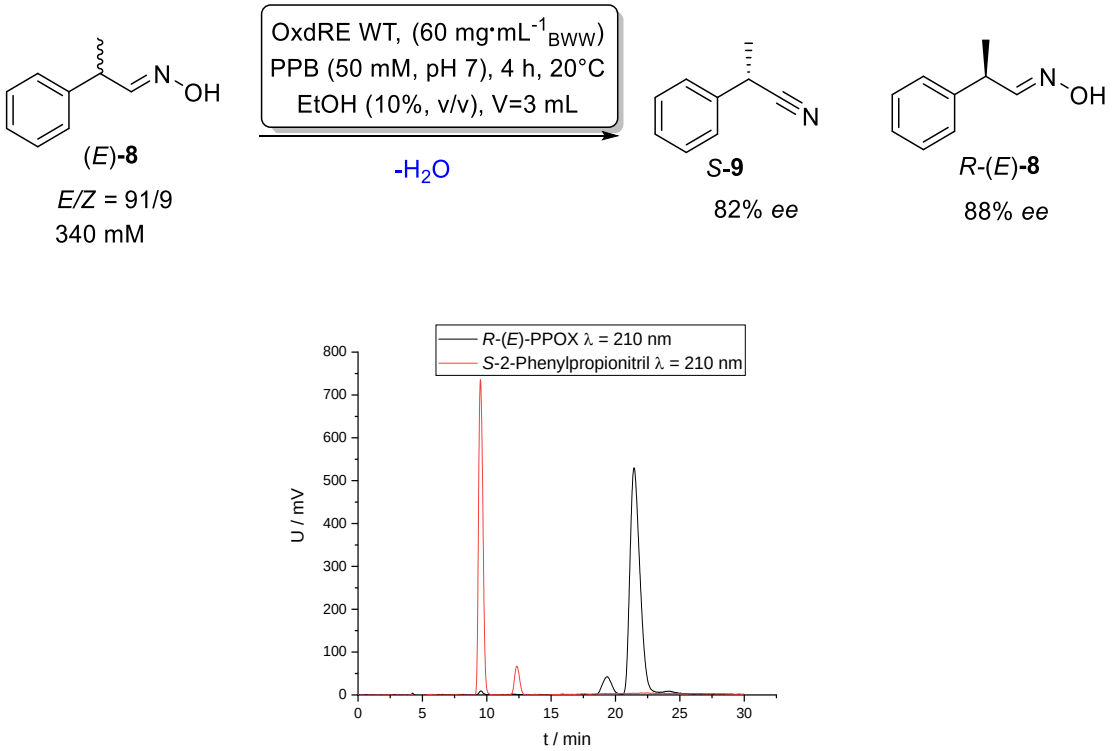

Scheme 16: Reaction scheme and HPLC chromatogram of the preparative scale reaction using rac-(*E*)-**8** and OxdRE-WT to obtain the enantiomerically enriched nitrile (S)-**9** and the aldoxime (*R*,*E*)-**8.**

The nitrile was obtained with 82% *ee* and the aldoxime with 88% *ee* (in a second experiment also with 68% *ee*). With the presented HPLC method, it was convenient to determine the *ee*-values for both the nitrile and the aldoxime. The aldoxime and nitrile was then used in a screening with eight different thiazolium salts and thiazoles. The screening was performed with 5 mM of aldoxime in water and 0.25 eq of thiazole derivative at 80 °C for 24 h (**Scheme 17**). From the eight tested thiazoles, N-allylbenzothiazolium bromide (**13d**), thiazole (**13g**), and thiamine hydrochloride (**13h**) showed a significant decrease of the *ee*-value (**Scheme 17**), revealing the possibility of

racemization of aldoximes with thiazoles. Thus, further investigations such as concentration, time dependency and compatibility with the reaction itself were carried out with the selected thiazoles (**13d**, **13g**, **13h**).

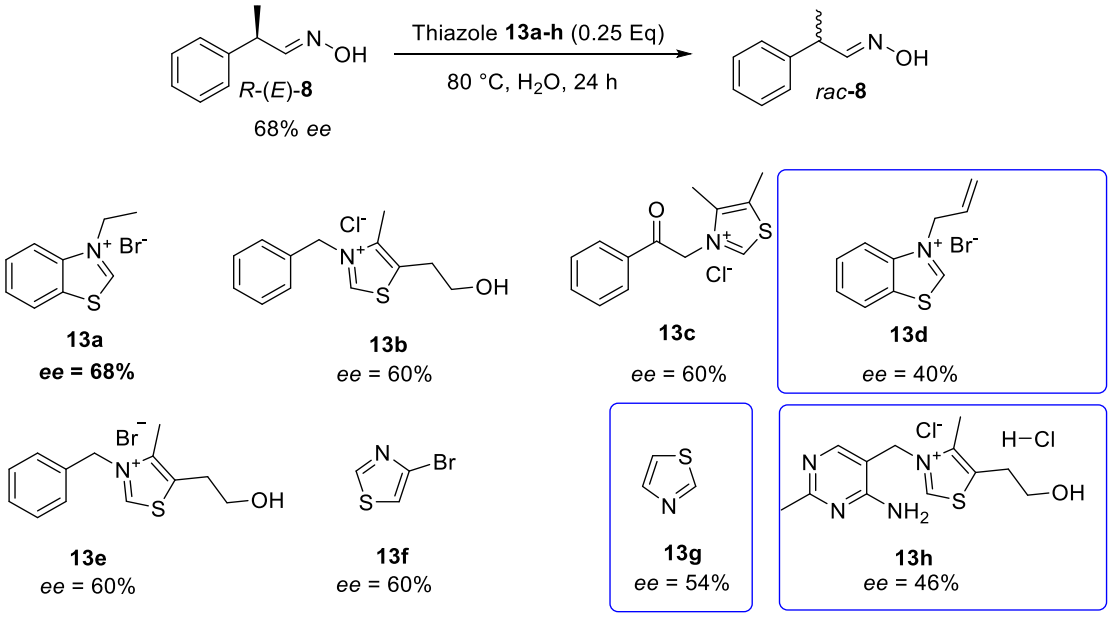

Scheme 17: Racemization screening of (*R*,*E*)-**8** (68% *ee*) with thiazole derivatives (**13a-13h**).

For the investigation of time and concentration dependency of thiazoles catalyzed racemization, *(R,E)*-**8** was used with a concentration of 5 mM and an *ee*-value of 88%. The reaction was carried out at 80°C for 72 h, showing the decrease of the enantiomeric excess of (*R*,*E*)-**8** over the time and in dependency of the thiazole equivalents used (**Scheme 18**). Thiamine hydrochloride (**13h**) and N-allylbenzothiazolium bromide (**13d**) demonstrate the highest racemization rate by reaching about 12% *ee* after 72 h with 1 equivalent.

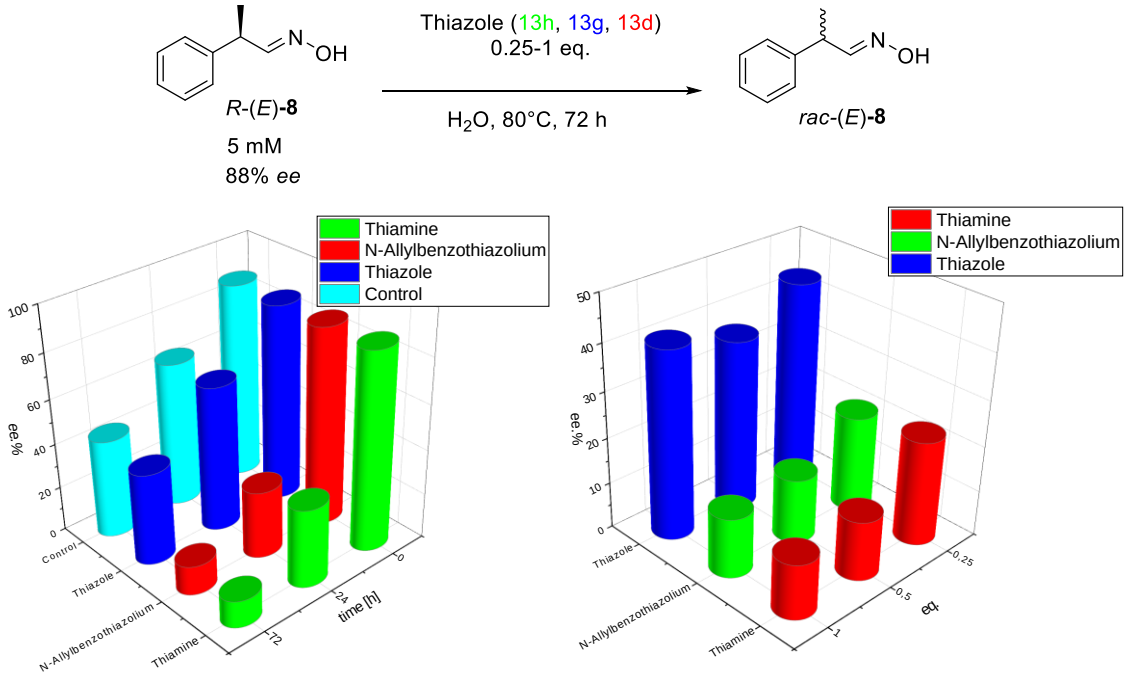

Scheme 18: Investigation of the racemization rate of *(R,E)*-**8** with thiazoles (**13h**, **13g**, **13d**) in dependency of time with 1 eq. of thiazole (left) and concentration after 72 hours (right).

The control reaction also indicates that the racemization of the stereocenter occurs even without the addition of thiazole derivatives. However, it is evident that with addition of thiazoles **13d** and **13h** almost complete racemization occurred. The addition of thiazole (**13g**) did not change the *ee*-values compared to the control reaction.

In the next step the compatibility of thiazolium salts **13d** and **13h** with the enzyme had to be investigated, to exclude inhibitory effect when using thiazoles as additives. For that biotransformation without and with the thiazoles **13d** and **13h** for 1 hour and 4 hours were performed, using OxdRE as biocatalyst and *rac*-**8** as substrate (**Scheme 19**). The control reaction (without thiazole) reached 50% conversion after one hour. N-allylbenzothiazolium bromide (**13d**) showed a much lower conversion reaching only 15% at 0.06 eq., further increasing the reaction time did also not increase the conversion meaning the enzyme was completely inactivated in a short time. Increasing the concentration of the thiazole **13d** further, lower conversions were reached. In case of thiamine hydrochloride (**13h**) 0.06 eq. had no effect and the reaction still reached same conversion as the control reaction without the addition of thiamine. When adding 0.25 eq or 1 eq. of thiamine, lower conversions were reached after 1 hour reaction time, however the enzyme was not deactivated since with longer reaction time of 4 hours the target conversion of 50% was still reached. Concluding that thiamine (**13h**) has small inhibitory effect, reducing the initial activity, but has no effect on the enzyme stability, whereas N-allylbenzothiazolium bromide (**13d**) strongly deactivates the enzyme. With regard to the racemization mechanism, it can be stated that the reaction rate presumably is only reduced by the interaction between thiazole and substrate and that thiamine, which occurs naturally in *E. coli*, has no influence on the enzymes stability.

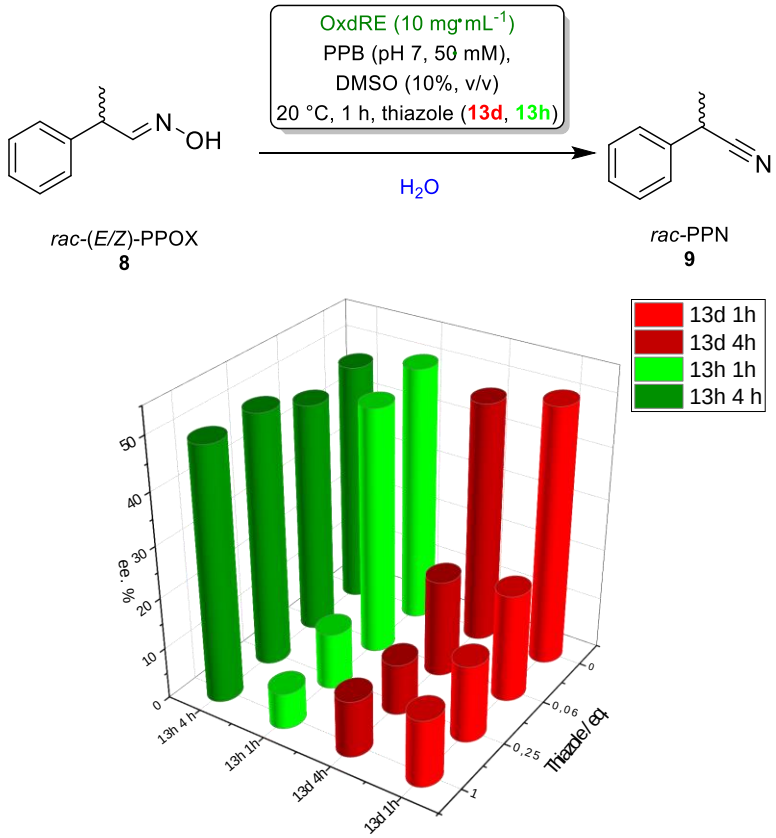

Scheme 19: Influence of N-allylbenzothiazolium bromide (**13d**) and thiamine hydrochloride (**13h**) on the OxdRE catalyzed dehydration of *rac*-**8**

To exclude the possibility that thiamine hydrochloride (**13h**) could racemize the nitril **9** also the racemization of *S*-(**9**) was investigated. The reactions were performed in PPB (50 mM, pH 6-7) at 80 °C. A racemization could not be observed after 24 hours (**Table 51**), therefore the racemization after 48 hours with different amounts of thiamine hydrochloride at pH 6 and pH 7 was investigated. The resulting data shows, that on the one hand the racemization is pH dependent and that on the other hand presumably the added thiamine even suppresses the racemization. From the available data this can only be speculated as thiamine itself possibly has no influence at all, but only the pH value and the duration of the thermal influence plays a role. Even if the necessary control reaction without thiamine as an additive is missing, the gradient clearly shows, that the racemization is not catalyzed by thiamine showing higher racemization at lower thiamine concentration.

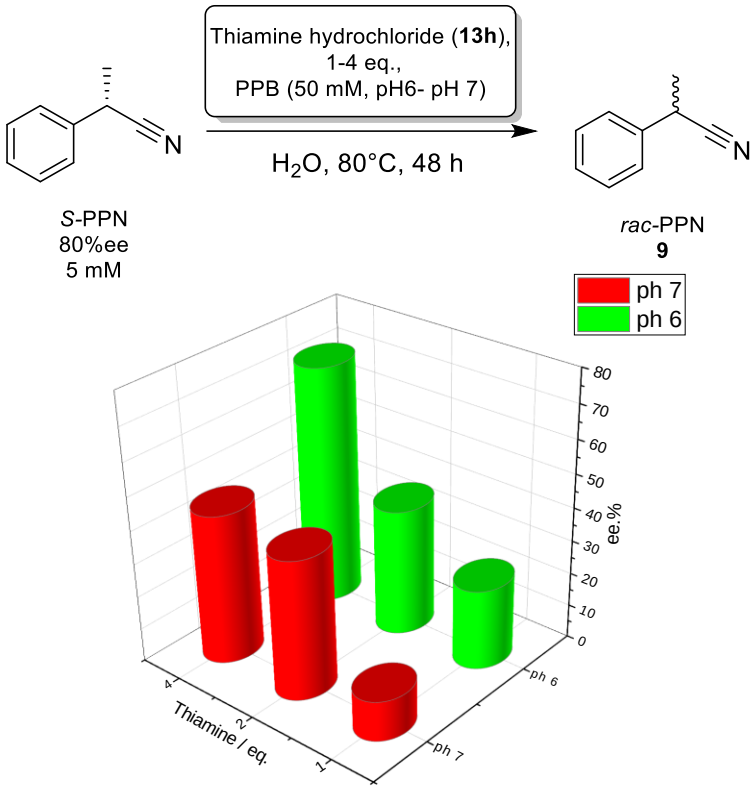

Scheme 20: Investigation of the racemizability of product *S*-**9**

For a proof of concept, it would be necessary to design the reaction in a time window of 24 hours. In 24 hours, a racemization of the nitrile does not occur, thus it does not pose a potential threat to the process. Additionally, the thiamine indicated a stabilization of the nitrile, which is also beneficial for the process, while the isomerization and racemization of the aldoxime takes place sufficiently. All in all, a suitable isomerization and racemization method was developed and will be used in the next chapter to present a proof of concept with respect to a formal double dynamic kinetic resolution (DDKR).

4.4 Flow set up for the DDKR

The challenging development of a working double dynamic kinetic resolution (DDKR) was studied with phenylpropanal oxime (PPOX). PPOX was a convenient starting point with phenylpropanal being commercially available. In the previous chapter's methods to racemize and isomerize aldoximes were described, since both methods require high temperatures, the enzymatic reaction needs to be separated. One possibility would have been a multi-sequential one-pot type reaction set up, with adding fresh enzyme to reaction after the thermal/chemical treatment, which would be repeated several times until the reaction reaches quantitative conversion.[50,51,107] With an immobilization method[37] for aldoxime dehydratase in cyclohexane being available and many examples of asymmetric synthesis in flow utilizing enzymes exist[52,108], a more elegant alternative was designed. By separating the two reactions (enzymatic dehydration, racemization/isomerization) in two different chambers (flask) and connecting those via pipes and using a peristaltic pump, the two reactions can be performed simultaneously in one-pot (**Scheme 21**). Using a superabsorber/cyclohexane mixture as biphasic system has two major advantages. One advantage is the high stability and convenient preparation of the immobilized cells, by simply using whole cell solutions and adding superabsorber until it is solidified.[37] Second advantage is, that the thiamine hydrochloride

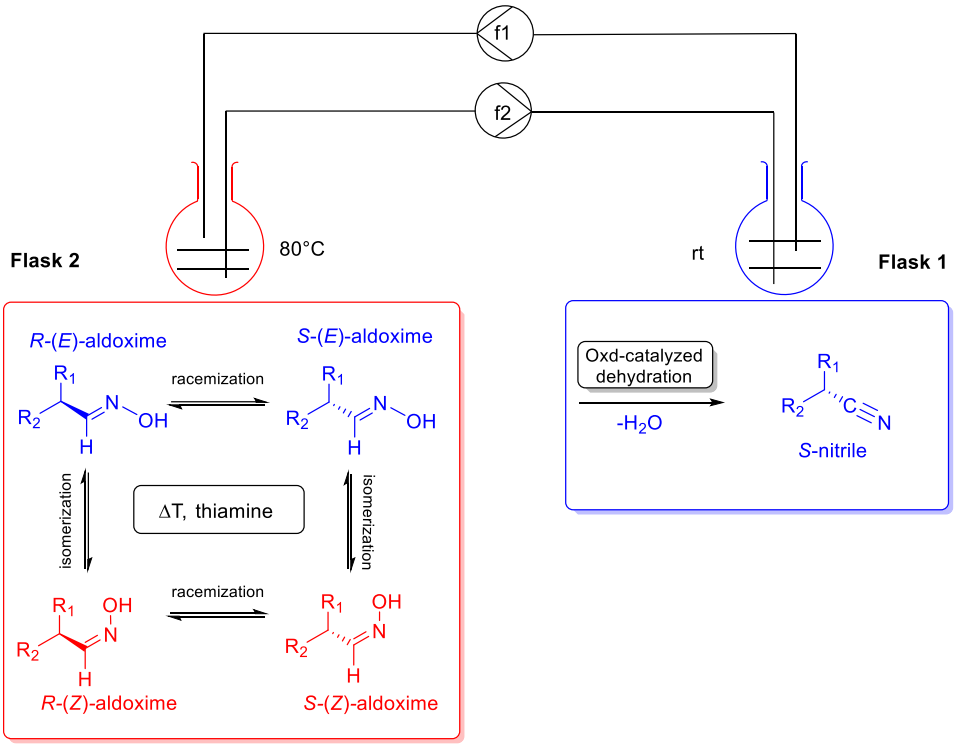

Scheme 21: Schematic illustration of DDKR using two reaction flasks as separation for the enzymatic dehydration and the chemical racemization/isomerization in a circular flow set up.

is basically insoluble in cyclohexane and remains in high concentration and without any influence on the enzyme, in the water phase of the racemization chamber. This leads to clean and pure transfer of cyclohexane containing substrate and product between the two reaction chambers, without any precipitation. Sampling and the work up were also straightforward and comfortable. Before setting up the flow reaction, the kinetical data of the enzyme in the superabsorber system was investigated (**Table 7**).

Table 7: Summary of reaction kinetics for each reaction step. Qualitative comparison to adjust the flow set up. The displayed graph showing incubation time dependent residual activity of OxdRE (20 mg· mL^{-1}) in superabsorber, at 20 °C with 10 mM *rac*-(*E*/*Z*)-**8**

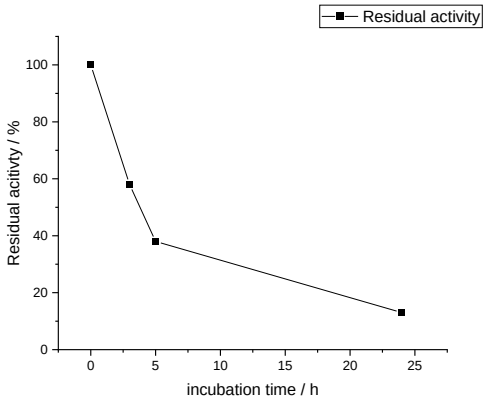

Reaction type	Reaction speed / µmol/h	Temperature / °C	Concentration / mM
Isomerization	0.46 (Z→E) 0.26 (E→Z)	100	10
Racemization (1 eq. Thiamin)	0.12	100	5
Biotransformation after 0h	3.6	20	10
Biotransformation after 3h	2.2	20	10
Biotransformation after 5h	1.4	20	10
Biotransformation after 24h	0.4	20	10
Biotransformation mean 0-24h	1.9-2.4	20	10

By incubation time dependent biotransformations, the degradation rate of the enzyme could be determined. Showing that, after 5 hours OxdRE-WT has still about 40% and after 24 hours only about 20% residual activity. Therefore, the whole process is limited to a reaction time of about 24 hours, besides with longer reaction time the product would as well racemize. By comparing the resulting kinetical data for each step, it appears that the enzymatic reaction is about 4 times faster than the isomerization and 10 times than the racemization (**Table 7**). Therefore, certain parameters were chosen for the flow set up (**Table 8**). The biotransformation itself was carried out in **Flask1** with a total volume of 5 mL while the racemization took place in **Flask2** with a total volume of 25 mL.

Table 8: Flow reaction results with 30 mL reaction volume and 17 hours reaction time.

#	Substrate	Enzyme	Volume / ml	Thiamin / eq.	Flow (f1/f2) / ml·min^{-1}	Bww/ mg·ml^{-1}	Sub. / mM	Conv. /%	*ee* %
1	PPOX	WT	30	0.5 eq.	0.6/0.35	20	10	87	7 (*rac*)
2	PPOX	WT	30	1.5 eq.	0.6/0.35	20	10	100	1 (*rac*)
3	4FPPOX	WT	30	1.5 eq.	0.6/0.35	20	10	92	15
4	4FPPOX	WT	30	1.0 eq.	0.6/0.35	20	10	83	36
5	3FPPOX	L145F	30	1.0 eq.	0.6/0.35	20	10	-	-
6	4FPPOX	WT	30	1.0 eq.	1.5/1.0	20	10	43	33

Therefore, the volume ratio between the two flasks was set to 1 to 4. In addition, the flow rate (f1, 0.6 mL·min^{-1}) from **Flask1** to **Flask2** was twice as high as the flow rate from **Flask2** to **Flask1** (f2, 0.35 mL·min^{-1}), which theoretically increased the total retention time of the substrate in **Flask2** 8-fold compared to **Flask1** as compensation for the higher transformation rate of the enzyme. Furthermore, the volume in each flask was kept constant by the height of the syringes.

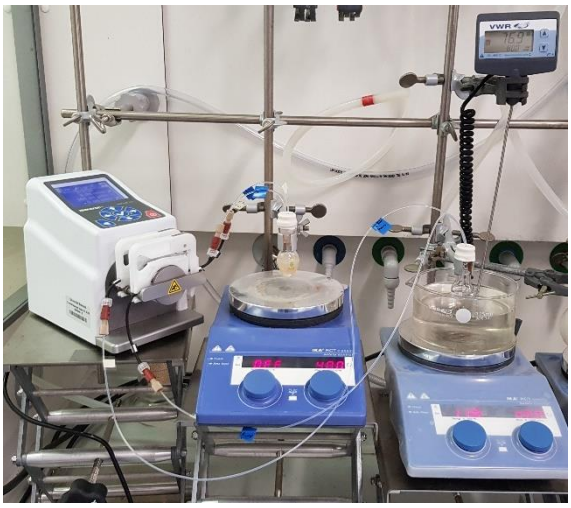

Figure 21: Foto of the used flow set up showing the two reactions in each flask (**Flask 1** left for the biotransformation, **Flask2** right for the racemization and isomerization) connected to a peristaltic pump.

Then the benchmark flow reaction was performed as described with OxdRE-WT (20 mg·mL^{-1}) and *rac*-(*E*/*Z*)-**8** (10 mM), showing in both cases (**Table 8**, entry 1 and 2) quantitative conversions yet with very low enantiomeric excess. The reason for that is, that the racemization is the rate limiting step and OxdRE-WT does not seem to have any significant preference, when comparing the isomers *E*-**8** and *Z*-**8**. For an instance substituted PPOX derivative such as FPPOX (**4**) does show significant difference in term of the used *E*- or *Z*- isomers. The *E*-isomer is converted much more selective than the *Z*-isomer (Chapter 3.2, **Table 5**). By using *rac*-(*E*/*Z*)-**4c** quantitative conversion could also be reached including moderate enantiomeric excess with 15% and 36%, from which it could be concluded that the designed set up and reaction are operating as planned. Even if the enantiomeric excess is still intermediate, the obtained results implicate a successful DDKR.

For a more detailed investigation, the flow reaction (**Table 8**, entry 4) and for comparison a batch reaction with same conditions were monitored over 17 hours. The resulting time course of the reaction implies that the enzyme is inactivated after 6 hours, resulting for the flow reaction over 80% conversion and for the batch reaction only 50% (**Figure 22**).

Furthermore, the comparison also shows the effect of the isomerization and racemization. While the batch reaction as kinetic resolution reaches only 50% conversion, the flow reaction as DDKR achieves 80%. The flow reaction or DDKR provides the enzyme with new preferred substrate *E-S* and *Z-R*, while in the batch reaction non preferred conformation *E-R* and *Z-S* accumulates and consequently limits the reaction. This can also be seen from the fact that an increased flow rate leads to a reduced conversion (**Table 8**, entry 6). Because higher flow rates mean shorter residence time in one flask. The residence time in **Flask2** is essential for the racemization and isomerization of the substrate.

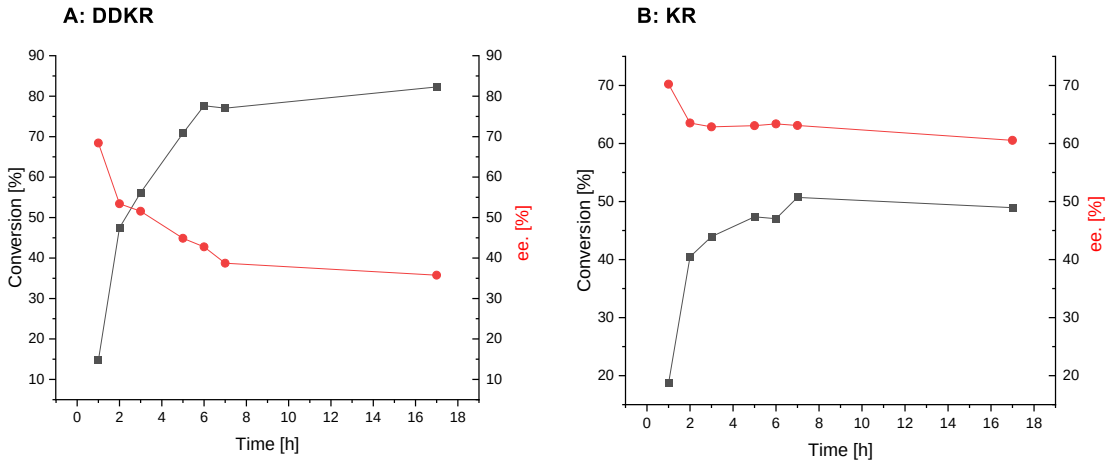

Figure 22: A: Time course of the DDKR with 4-FPPOX as substrate and OxdRE-WT as biocatalyst (left). B: Time course of the kinetic resolution of 4-FPPOX with OxdRE-WT as catalyst. Starting point with (70:30, E:Z).

To further increase the selectivity the rational designed mutant OxdRE-L145F (chapter 3), which showed significant increased selectivity, where used as possible biocatalyst. The investigations also revealed that the mutant reached highest selectivity with the substrate 3-FPPOX (**4b**). Thus, *rac*-(*E/Z*)-**4b** and OxdRE-L145F were used in the same flow set up, but unfortunately the reaction did not lead to any conversion. It was reasonable to assume that the relative instability of the mutant could be due to its extremely poor expression, which is why expression optimization was carried out (chapter, 4.6). However, before performing expression optimization, it was necessary to determine whether the problem of substrate concentration could be overcome. As mentioned before, the low substrate concentration leads to slow isomerization and probably also racemization. In order to increase the substrate concentration, the volume of the reaction was reduced, since the complex synthesis of substrates made them very difficult to access. However, the reduction in volume led to very poor unreproducible results. By adjusting the flow apparatus to the small volume many problems occurred, such as precipitation in the pipes, evaporation of cyclohexane and heat transfer from **Flask2** to **Flask1** inactivating the enzyme, which led to very low conversion even though high biocatalyst amount was used (**Table 9**).

Table 9: Flow reaction results with reduced volume using tubes instead of flask for the reaction separation.

Entry	Substrate	Enzyme	Volume /ml	Thiamin	Flow (f1/f2) /ml·min^{-1}	Bww/ mg·ml^{-1}	Sub. /mM	Conv. /%	ee %
1	PPOX	RE-WT	7	1 eq.	0.7/0.2	115	25	14	6 (*rac*)
2	4FPPOX	RE-WT	8	2.5 eq.	0.7/0.2	100	10	40	18
3	4FPPOX	RE-WT	8	2.5 eq.	0.7/0.2	100	10	47	17

As conclusion, the prior used flow set up with flaks as reaction chambers were superior. To increase the substrate concentration without to reducing the volume, the substrate synthesis had to be optimized. Therefore, an alternative

synthesis route starting from styrene derivatives over a selective hydroformylation towards the aldoximes in one pot were developed.

4.5 Hydroformylation as alternative aldoxime synthesis

The synthesis of the phenylpropanal oxime derivatives (PPOX) showed to be very tedious, following a three-step pathway starting from the commercially available substituted benzaldehydes. The overall isolated yield did not exceed 10% (this work) and hazardous and toxic chemicals as nitromethane or benzyl bromide have been applied following the reported protocol.[47,109]

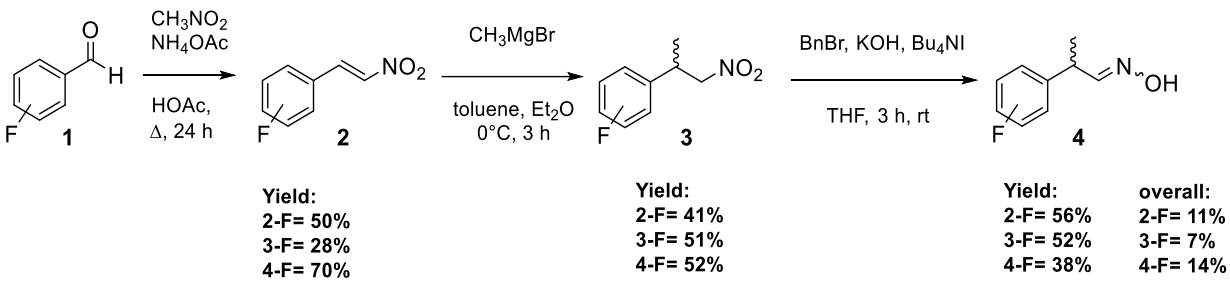

Scheme 22: Multistep synthesis of *rac*-(*E*/*Z*)-FPPOX derivatives (**4**) starting from benzaldehyde **1**.

The reaction (**Scheme 22**) proceeds over three steps, with each step including a work-up, isolation and purification of the intermediate. Since in every step only 50% yield could be obtained the overall yield for the target aldoxime (**4**) was between 7-14%. For some other PPOX derivatives, also an overall yield of 25% were shown to be possible.[47] The presented flow process (chapter 4.4) must be carried out at volumes of at least 30 mL and proceeds better with high substrate loading. Although, the aldoxime synthesis would not be suitable in any way for an industrial application with a yield of ~14%, the synthesis is too inefficient even for the laboratory scale, which is why an alternative route was first investigated.

In cooperation with *C. Plass* an alternative route opened up, by installing a high-pressure reactor with the possibility of utilizing syngas. This enabled a very simple, effective and selective substrate synthesis, without isolation of the intermediate aldehyde (**Scheme 23**). With styrene as starting material over a rhodium catalyzed hydroformylation with subsequent condensation of hydroxylamine the target aldoxime can be obtained without any isolation of the intermediate.

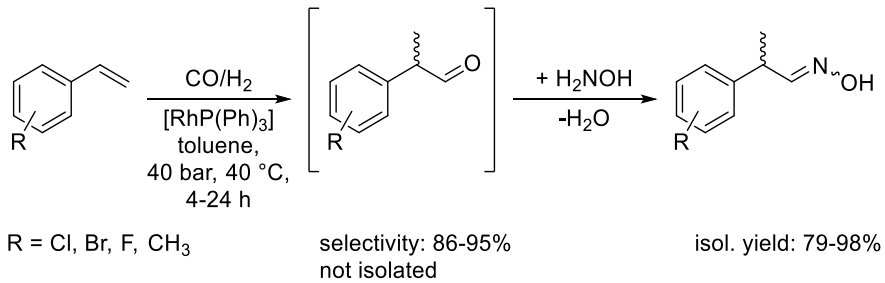

Scheme 23: General reaction overview of the synthesis of substituted phenylpropanal oximes.

Rhodium-catalyzed hydroformylation of styrenes preferably leads to the branched products.[110] This effect is argued in the literature by the formation of a stabilized π-benzylic species of the alkene catalyst complex.[111] This

effect has been described for different ligand types.[112] The regioselectivity is depending on the solvent as well as the reaction conditions.[113] For the desired oximes, hydroformylation and the oxime formation step were combined in a sequential one-pot mode to prevent work-up of the oxidation sensitive aldehydes. In the present work, a homogeneous hydroformylation setup applying the relatively cheap catalyst system of $[Rh(acac)](CO)_2/PPh_3$ under mild reaction conditions were used. This method led towards the target aldoximes with high selectivities and high yields, without any additional purification steps. All of the selected styrene derivatives were commercially available, presenting a convenient starting point. The two-step one-pot synthesis starts with hydroformylation of the styrene towards the corresponding aldehyde **6.** As side product the linear aldehyde is formed.

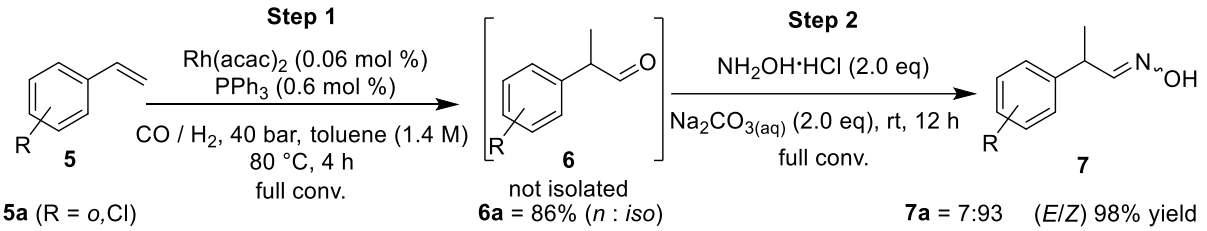

5a (R = *o*,Cl)	**6a** = 86% (*n* : *iso*)	**7a** = 7:93 (*E*/*Z*) 98% yield
5b (R = *m*,Cl)	**6b** = 94% (*n* : *iso*)	**7b** = 66:34 (*E*/*Z*) 86% yield
5c (R = *p*,Cl)	**6c** = 93% (*n* : *iso*)	**7c** = 68:32 (*E*/*Z*) 80% yield
5d (R = *o*,Br)	**6d** = 86% (*n* : *iso*)	**7d** = 20:80 (*E*/*Z*) 98% yield
5e (R = *m*,Br)	**6e** = 93% (*n* : *iso*)	**7e** = 65:35 (*E*/*Z*) 92% yield
5f (R = *p*,Br)	**6f** = 94% (*n* : *iso*)	**7f** = 66:34 (*E*/*Z*) 81% yield
5g (R = 1,4-Cl)	**6g** = 95% (*n* : *iso*)	**7g** = 43:57 (*E*/*Z*) 82% yield
5h (R = 1,4-F)	**6h** = 95% (*n* : *iso*)	**7h** = 54:46 (*E*/*Z*) 90% yield
5i (R = *o*, Me)	**6i** = 60% (*n* : *iso*)	**7i** = 1:99 (*E*/*Z*) 87% yield
5j (R = *m*, Me)	**6j** = 77% (*n* : *iso*)	**7j** = 69:31 (*E*/*Z*) 41% yield
5k (R = *p*, Me)	**6k** = 64% (*n* : *iso*)	**7k** = 67:33 (*E*/*Z*) 27% yield
5l (R = *o*, F)	**6l** = 64% (*n* : *iso*)	**4a** = 76:24 (*E*/*Z*) 79% yield
5m(R = *m*,F)	**6m**= 86% (*n* : *iso*)	**4b** = 66:34 (*E*/*Z*) 81% yield
5n (R = *p*, F)	**6n** = 94% (*n* : *iso*)	**4c** = 68:32 (*E*/*Z*) 89% yield

Scheme 24: Reaction scheme of aldoxime synthesis in a two-step one-pot synthesis.

The selectivity of the reaction can be determined via NMR. The aldoximes **7j** and **7k** were synthesized under neat conditions resulting in a low selectivity for the hydroformylation step and low yield for the subsequent aldoxime formation. By dilution of the starting material using toluene the selectivity can be increased dramatically. For non-optimized conditions selectivities from 60% up to 95% were reached. The selectivity should increase further with lower substrate concentrations, but for the purpose of this work further investigations were redeemed. In **Scheme 24**, all synthesized aldoximes are shown. Overall, the aldoximes were obtained in excellent yields and selectivities. To give a clearer picture about the advantage the alternative route provided in a rather unconventional comparison, with the multistep synthesis about 1 g of product could be obtained in a week while the hydroformylation route allowed the synthesis of about 20 g of product in a day.

4.6 Expression optimization

The previous cultivation of Oxds were performed either by AI or by IPTG induced expression. In each case, only a book part of the expressed protein was found in the soluble fraction. In order to optimize expression, Oxd expression was compared with heme containing enzymes namely the P450 monooxygenases. P450 superfamily are widely used and well characterized in terms of expression. It turned out that, for successful overexpression of P450 monooxygenases, the use of 5-aminolevulinic acid (5-ALA) and thiamine hydrochloride is essential.[114–116] The optimization was based on the fact that the heme production is the rate limiting factor. The heme production

in *E.coli* has already been widely investigated in many studies.[117] Thiamine or vitamin B1 is also essential for the heme production, by being incorporated in the PDH-complex, that is responsible for synthesis of succinyl-CoA, which is the precursor of 5-ALA.[118] Eight 5-ALA molecules form the protoporphyrin IX, which form by insertion of an iron ion heme.[119] Since 5-ALA has been shown to improve the expression of some P450 forms,[115,116,120] it has been tested whether 5-ALA also improves the expression of OxdRE, with being a heme protein like P450.[14] In addition to thiamine and 5-ALA, trace enzymes were also added in some reports, but the amount was not precisely quantified. [120,121] Besides, *Hara et al*. [119] reported that the trace elements had no significant influence on the synthesis of heme.

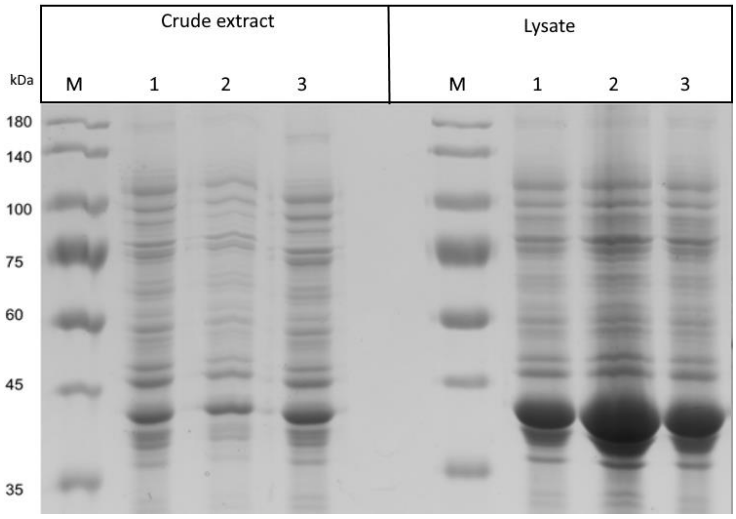

Figure 23: SDS-PAGE showing the expression of OxdRE-WT. M: Marker (*PageRuler Prestained, thermo scientific*), protein band located at 40 kDa. Comparison of expression with 1 mM thiamine and 5-ALA as well as 0.1 mM IPTG (1), standard expression with 0.1 mM IPTG (2) and standard expression with 1.5 mM IPTG (3).

The expression of OxdRE-WT was carried using the standard overnight expression at 20 °C in LB-Media with induction at 0.6 OD_{600}. Expression 1 was carried out with thiamine hydrochloride and 5-ALA (1 mM) as additives and induced with IPTG (0.1 mM). The expression 2 and 3 were carried out without any additional components but varying the used IPTG concentration for induction by 0.1 mM and 1.5 mM. The SDS-Page revealed no significant differences between the investigated expressions of OxdRE. Furthermore, in all three cases the largest portion of the expressed proteins are insoluble (**Figure 23**). When changing the expression system to auto induction to compare the influence of the addition of 5-ALA and thiamine hydrochloride again no significant difference can be observed (**Figure 24**). Concluding that, 5-ALA and thiamine hydrochloride did not increase the expression of OxdRE-WT.

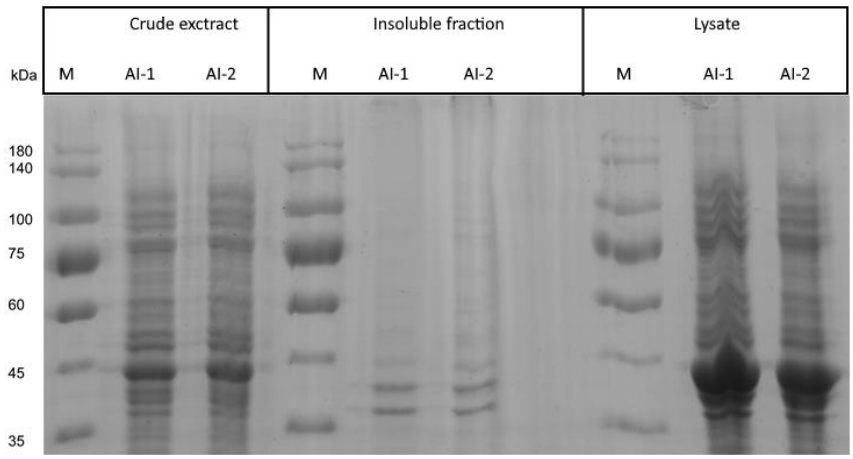

Figure 24: SDS-PAGE showing the expression of OxdRE-WT. M: Marker (*PageRuler Prestained, thermo scientific*), protein band located at 40 kDa. Auto induction expression with Thiamin and 5-ALA (1) compared with standard autoinduction expression of OxdRE-WT (2).

The SDS-PAGES revealed a crucial information about the expression of OxdRE-WT, namely that the expression does not perform poorly, but rather far too well. This peculiarity can be seen in the large protein bands of the lysate sample, which raises the question of why there is so little of the expressed protein in the soluble fraction (crude exctract). The following conclusions could be drawn: The enzymes are expressed too quickly. This is due to the fact that pET28a, which contains a T7 promotor is used as a vector. The T7-Promotor is very effective in producing the target protein. For most easily soluble proteins or simply foldable proteins without a prosthetic group, it is a great advantage leading to the target protein in high yields. However, the aldoxime dehydratases possess a heme group, which assumably slows the folding process. A comparatively slow folding process in the presence of a rapid expression machinery finally means the accumulation of unfolded proteins. The huge protein aggregates then stress the cell and could, under certain circumstances, have a negative influence on the folded proteins and thus affect the stability. Therefore, expression without any induction, with different cultivation time and incubation methods were investigated (**Figure 25**).

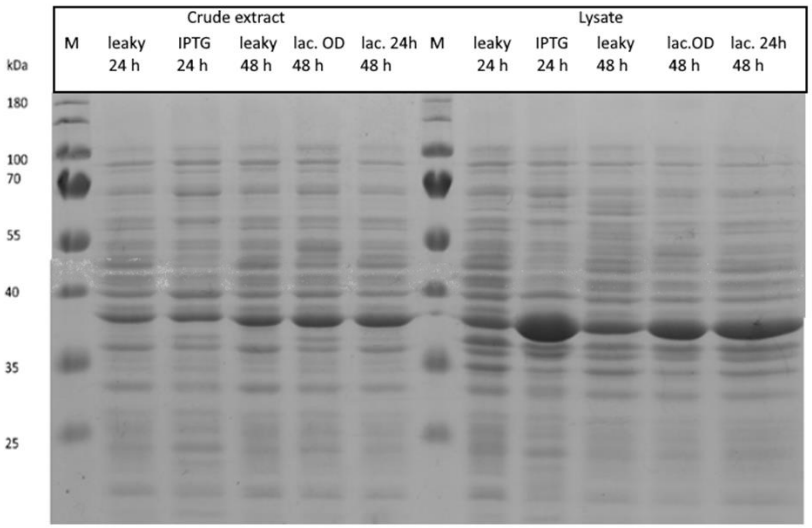

Figure 25: SDS-PAGE showing the expression of OxdRE-WT. M: Marker (*PageRuler Prestained, thermo scientific*), protein band located at 40 kDa. Comparison of different induction time and induction agent using standard expression protocol with leaky expression at 20 °C.

Its known that, *E.coli* pET-vektor expression with T7 promotors do have a basal expression,[122] which is usually unfavored and many examples of host cells to reduces this basal expression were designed.[123,124] However, for the cultivation of Oxds, the expression strategy using the basal activity could be a solution for the low expression. The so-called leaky expression[123] without any induction was compared with the standard expression using IPTG and lactose as induction agent. The cultivation was carried out at 20 °C in LB-media for 24 hours and 48 hours. Besides the induction at an OD_{600} of 0.6 also one culture was prepared, whereas the induction was performed after 24 hours. The crude extract and lysates of those cultures are shown in **Figure 25**. By comparing the protein bands for the 24-hour cultivation, the leaky expression is similar to the IPTG induced variant, which is already quite stunning, but much more important is the difference of the protein bands in the lysate. While in the case of leaky expression, the gemmate proportion of target protein is found in the soluble fraction, in the case of IPTG expression, as suggested, about 10 times the amount (visual estimation) is found in the lysate. The 48-h cultivation in general yielded in more protein, also the lactose induction seems to be less harsh then IPTG. In order to validate these findings, an activity test was carried out with the differently expressed enzymes. As the SDS-PAGE suggests, leaky expression was the best variant and IPTG induction in the logarithmic phase of E.coli (OD_{600}=0.6) was the worst. The leaky expression reached 90 % conversion while the IPTG induction only reached 19 %. The lactose induction in the stationary phase of *E. coli* also seemed to be an option. However, the approach was not pursued further since the lysate also showed significantly larger protein bands on the SDS-PAGE.

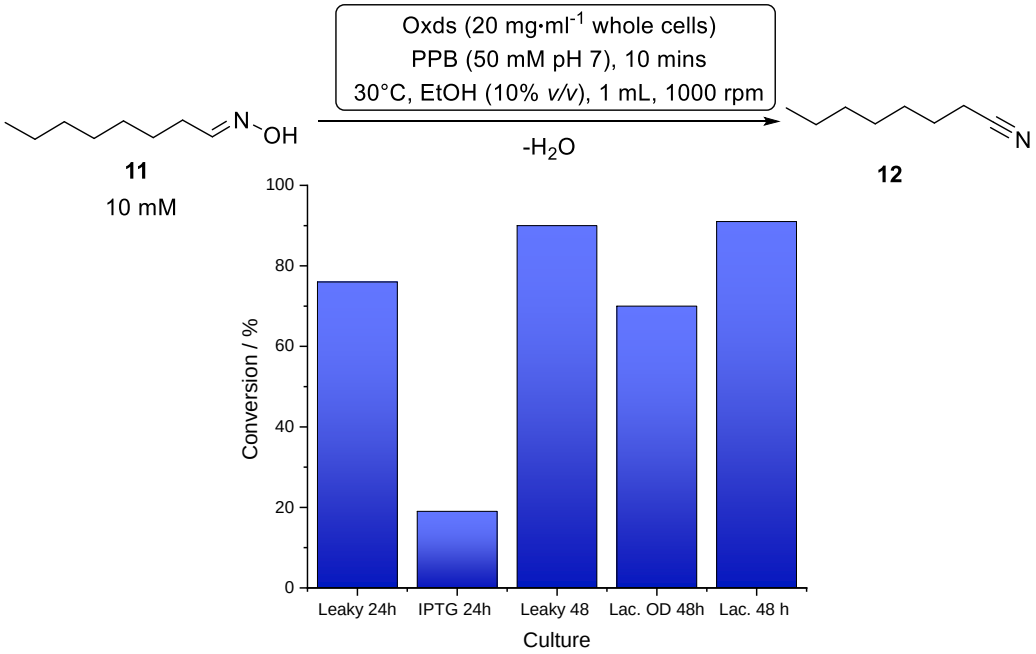

Scheme 25: Activity test of different expressed OxdRE-WT.

By comparing the 24 hours leaky expression with the 48 hours leaky expression, it seemed that for further optimization longer cultivation time were needed. Therefore, leaky expression for 72 hours with different cultivation temperature for OxdRE-WT and OxdRE-L145F were investigated (**Figure 26**). The SDS-PAGE shows well overexpressed target proteins at 20 °C cultivation temperature. It was also shown that the leaky expression is not suited for cultivation at 15 °C or 37 °C, indicated by the very low expression. For a direct comparison with the usual AI expression the standard activity test with octanal oxime (**11**) were performed (**Scheme 26**), which revealed that leaky expression tremendously increased the activity. For OxdRE-WT the activity was increased

about 20-fold, but the mutant L145F was 100 times more active than with the AI expression. Concluding that the slow basal expression leads to soluble proteins in high yield compared to the induced expression were accumulation of unfolded proteins lead to protein aggregates, reducing activity and stability of the biocatalyst.

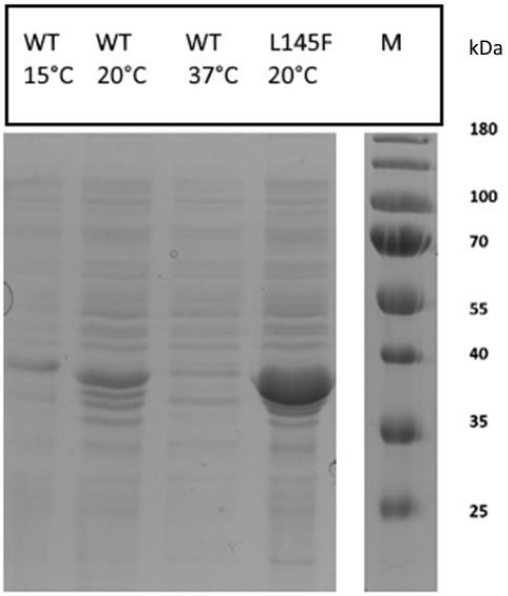

Figure 26: SDS-PAGE showing the crude extract of OxdRE-WT and OxdRE-L145F as leaky expression using different cultivation temperature. M: Marker (*PageRuler Prestained, thermo scientific*), Protein band located at 40 kDa.

In addition to the much better activity, the cultivation is particularly convenient since only one pre-culture has to be prepared and transferred to the main culture, which can then be harvested after 72 h. With the now optimized expression method, no further studies on expression were performed even though co-expression of chaperones would have offered a possible alternative.[125] With the completion of expression optimization, only one problem remained for the DDKR, and that was the selectivity of the enzyme.

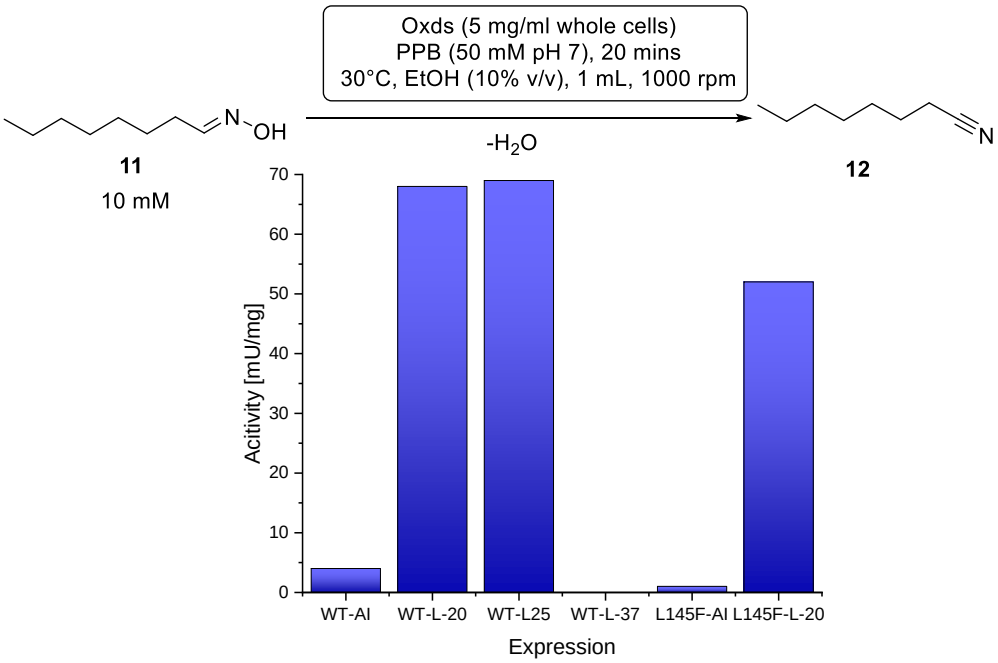

Scheme 26: Comparison of leaky expression at different temperature with AI-expression of OxdRE-WT and OxdRE-L145F

4.7 Rational designed mutations

Based on the rationalizing work in chapter 1 the L145F-mutant was identified as the variant of OxdRE with the highest selectivity. The investigation revealed that in the active site only the position L145 has a significant impact on the selectivity. However not excluding positions which could not be modified in a rational way such as backbone proteins. The mutant L145F led to higher selectivity due to smaller cavity, which gives the unpreferred conformations less space in the active site of the protein. Unfortunately, non-other amino acid were able to reduce the space just by the side chain size at this position. To overcome the problem of low selectivity, three different approaches were pursued. The first approach (i) was to determine whether polar amino acids could be used as geminate mutations at position 145, as these were considered promising in the *in silico* studies, even though the probability was very high that polar amino acids would deactivate the enzyme, due to their proximity to the catalytically active arginine and histidine. Another approach (ii) was to replace the enzyme instead of changing the mutation. This gave rise to the possibility that the mutation might have a much stronger effect on other aldoxime dehydratase. The last and most elaborate option (iii), but with the certainty of success, would be to screen saturated mutation libraries.

4.7.1 Investigation of mutation at position L145

As mentioned before position L145 is the most important site for modifying the selectivity, which is why this position was saturated *in silico*. It was shown that there are only very few possibilities to change this position with respect to the protein integrity and selectivity.

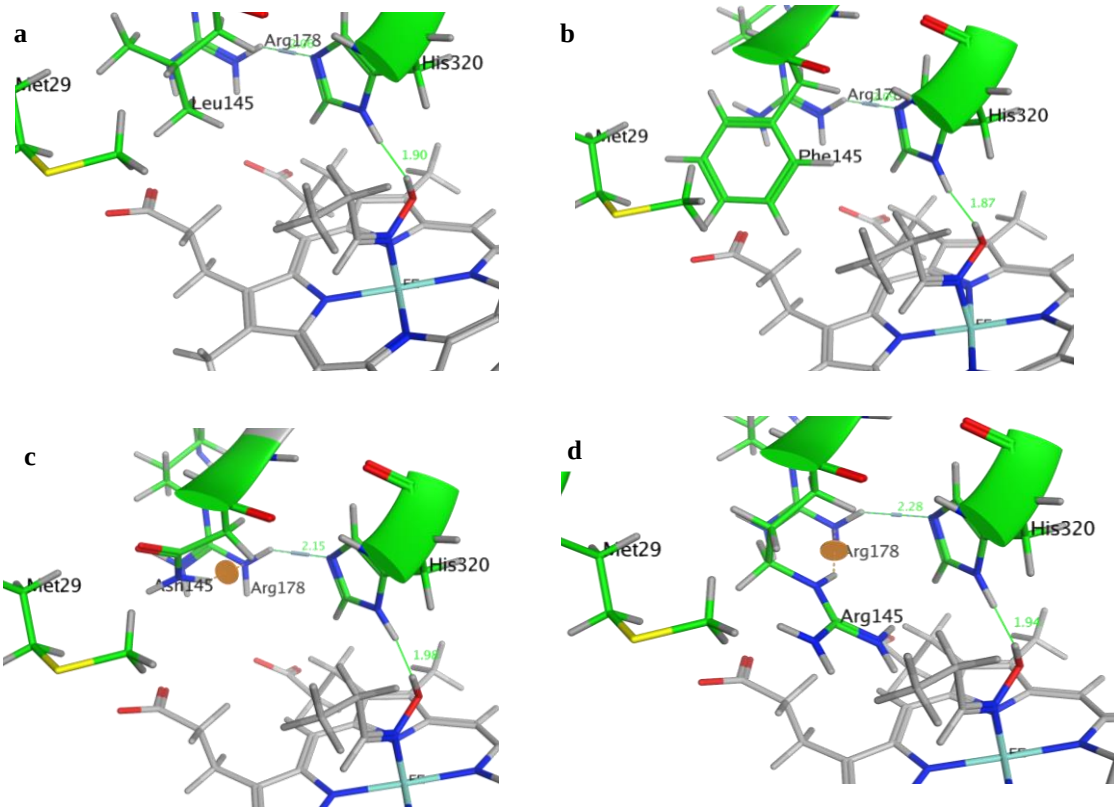

Figure 27: Comparison of OxdRE-L145 variants, showing suitability of the mutations. OxdRE-WT (a), OxdRE-L145F (b), OxdRE-L145N and OxdRE-L145R. Distance between R178 and H320 as well as H320 and the ligand are shown in Å.

While small amino acids, such as alanine and glycine, decrease the selectivity by an enlargement of the cavity size, larger amino acids can increase the selectivity by reducing the cavity space. From the possible larger amino acids only phenyl alanine and tyrosine remained available as tailored before in chapter 3. Moreover, polar amino acids could produce a similar effect by electrostatic repulsion (i). An example illustration of the suitability of an amino acid is shown in **Figure 27**. Comparing WT (a) with L145F (b) as rigid large amino acid and asparagine (c) as well as arginine (d) as polar amino acids examples. When comparing the wild type, with the L145F mutant the catalytic residues in proximity (R178, H320) do not change their position or distance to each other or to the ligand, moreover the model suggests a closer distance of histidine to the ligand (1.82 Å). This is different for the examples L145N and L145R. In both cases the model suggests increased distances between the H320 and R178 (2.15 Å and 2.28 Å) as well as with the ligand (1.98 Å and 1.94 Å). Besides the fact that arginine is also just too large for the cavity (**Figure 27**) both mutants (depending on the protonation state) could act as proton acceptor and therefore deactivate the enzyme. Thus, to validate the *in silico* studies, a set of mutants were designed *in vitro* via site directed mutagenesis and cultivated via leaky expression. Subsequently, the mutants were tested for their activity and selectivity using the standard substrate *rac*-(*E*/*Z*)**-8** (**Table 10**).

Table 10: Intial selectivity screening of rational designed Oxd-variants using *rac*-(*E/Z*)-PPOX (**8**) as standard substrate

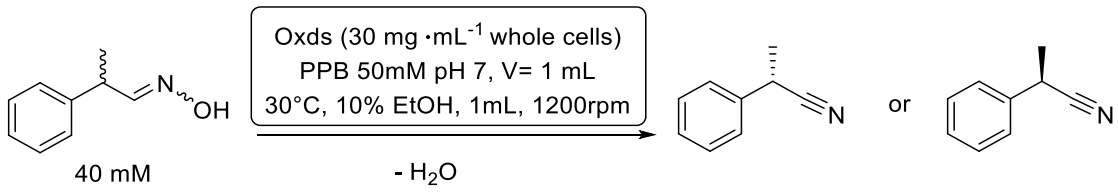

#	Enzyme	Expression / °C	conversion / %	*ee.* / %	Enantiomer
7	OxdRE-L145M	20	25	34.1	*S*
8	OxdRE-L145N	20	0	0.0	-
9	OxdRE-L145D	20	0	0.0	-
10	OxdRE-L145R	20	0	0.0	-
11	OxdRE-L145P	20	0	0.0	-
12	OxdRE-L145Del	20	0	0.0	-
13	OxdRE-L145S	20	21	37.8	*S*
14	OxdRE-L145Y	25	0	0	-
15	OxdRE-S219Y	20	0	0.0	-

The enzymes were well expressed as shown in the SDS-PAGE (**Figure 28**). Only L145P and L145Del were only found in the insoluble fraction (SDS-PAGE not shown). The polar amino acids, as predicted, showed no activity, although the proteins were very well expressed. Concluding that these mutations deactivate the catalytic triad of the enzyme, as predicted. Only L145M and L145S showed activity, but without a significant change in selectivity. The promising tyrosine mutant, which could have been an improved version of the phenyl alanine variant (L145F),

could not be stably expressed () as either OxdRE or OxdB variant and showed no significant activity. Concluding that, for OxdRE only the L145F mutant remains as selective variant for rational designed approach.

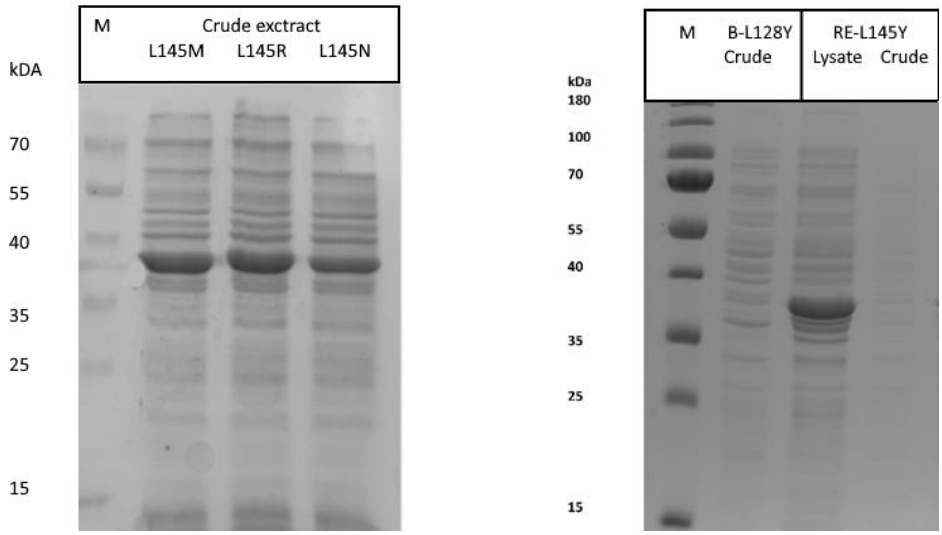

Figure 28: SDS-PAGE showing the expression of OxdRE-L145M, OxdRE-L145R and OxdRE-L145N as leaky expression (left). Expression of OxdB-128Y and OxdRE-L145Y are shown as leaky expression (right). M: Marker (*PageRuler Prestained, thermo scientific*), Protein band located at 40 kDa

4.7.2 Investigation of the L145F mutation in OxdA and OxdB

The mutant OxdRE-L145F was shown to be superior in terms of selectivity, therefore the same mutation in a different host enzyme could provide similar or better performance. Besides OxdRE[26] there are also 7 further known aldoxime dehydratase[18,21,22,25,27,126] from which OxdA[24] and OxdB[8,13] were chosen to investigate the same mutation as OxdRE-L145F.

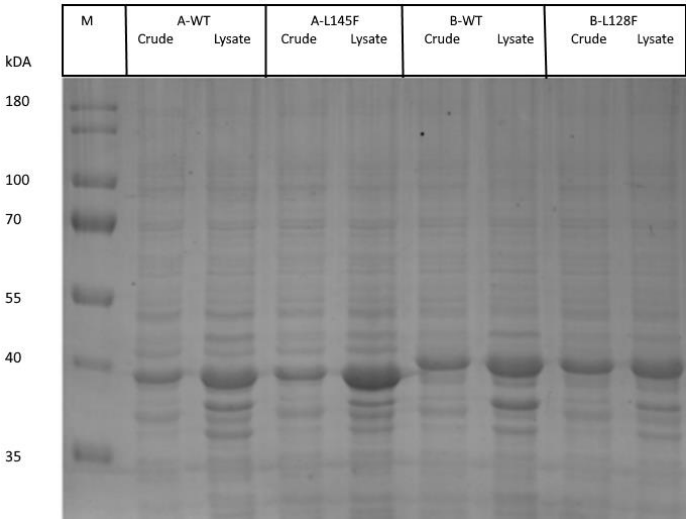

Figure 29: SDS-PAGE showing the expression of OxdA-WT, OxdA-L145F, OxdB-WT and OxdB-L128F as leaky expression using LB-media (72 h, 25 °C). M: Marker (*PageRuler Prestained, thermo scientific*), Protein band located at 40 kDa

The mutation L145F corresponds structurally to the exact same position in OxdA, in OxdB homologous mutation appeared to be the L128F. These two mutations were introduced into OxdB and OxdA *via* site directed mutagenesis. The enzymes were cultivated *via* leaky expression under optimized conditions (72 h, 25°C, 160 rpm) resulting in very good over expression of the target protein (**Figure 29**). The wild type and the phenyl alanine mutations were then screened with all available PPOX (**4**, **7**) substrates. This screening was intended to show whether there is a possible combination of enzyme and substrate that can achieve high selectivity for the corresponding nitrile without first separating the substrates into their isomers. The screening results are presented in **Figure 30**, showing the E-value of each reaction.

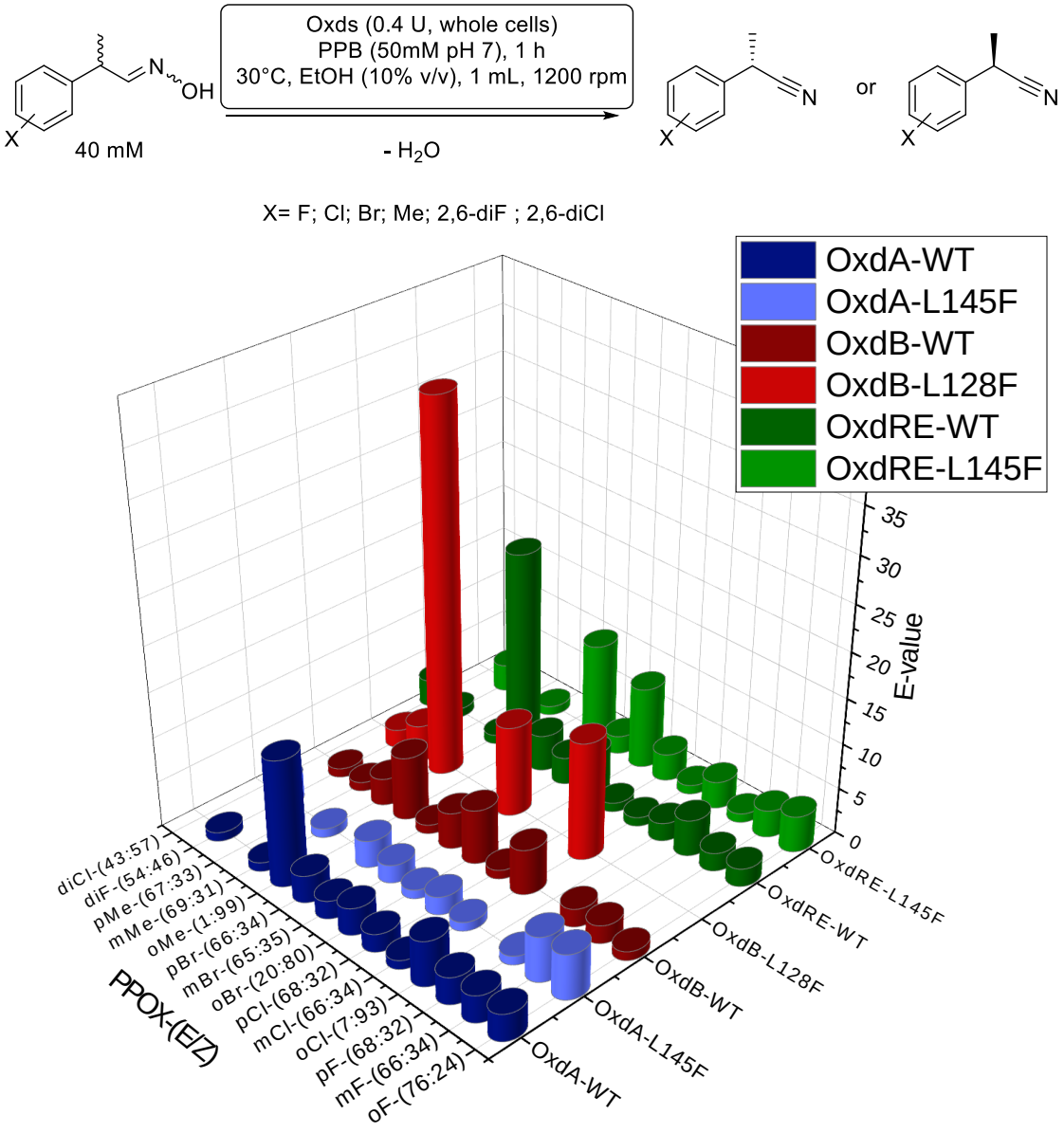

Figure 30: Screening results of OxdA, OxdB and OxdRE as wild types and L145/L128F mutants with 14 different PPOX derivatives

In general, the phenyl alanine mutants are more selective than the wild type enzymes, however the wild type enzymes show high selectivity for substrates which were not obtained as mixture, but more like pure isomers. The substrates *o*-Cl, and *o*-Me-PPOX are present as pure *Z*- isomers and *o*-Br-PPOX, respectively, in a ratio of 20:80 (*E*/*Z*), which is why the mutants show only a very low conversion under these reaction conditions and the wild-type enzymes achieve particularly high E-values (RE-WT, E=23). OxdA-WT and OxdA-L145F did not show any possible combination of substrate and enzyme set that achieved a sufficiently high E-value (minimum of 10). OxdB-L128F, seemed to be very promising on the first glance, showing that high E-values could be achieved with a small substrate scope. However, OxdB-L128F reached only for one substrate promising conversions for the other substrates the conversion did not exceed 5%, which makes the determined E-value unreliable. With *m*-Br-PPOX as substrate, an *ee*-value of 80% and 13% conversion could be achieved, corresponding to an E-value of 10. OxdRE-L145F was particularly interesting, since on the one hand *p*-Br-PPOX (70/30, E/Z) with an E-value of 11 was converted to the *R*-nitrile and on the other hand *o*-Br-PPOX to the *S*-nitrile with an E value of 9, although the *E*/*Z* ratio was 20/80. These two combinations are particularly promising since a selective conversion was achieved despite the fact that, the *E*/*Z* ratio was not favorable for the formed enantiomers. In detail, as described before if the isomers are separated and then used in a biocatalytic transformation the *E*-isomers is converted preferable to the *S*-nitrile and the *Z*-isomer preferable to *R*-nitrile, concluding that the least favored conformations are (*R*,*E*) and (*S*,*Z*) for the enzyme, which means the selectivity of a kinetic resolution for a mixture of all four conformations should depend on the affinity of (*S*,*E*) and (*R*,*Z*). If (*S*,*E*) and (*R*,*Z*) are both equal in terms of affinity, the selectivity would then only be dependent on the *E*/*Z*-ratio. In case of *p*-Br-PPOX the *E*/*Z* ratio is 66/34, which means 33% of the substrate is available as (*S*,*E*) and 17% (*R*,*Z*) and the reaction still reaches an E-Value of 11 for the *R*-nitrile and vice versa for the example of *o*-Br-PPOX with an *E*/*Z*-ratio of 20/80, which is illustrated in **Scheme 27**.

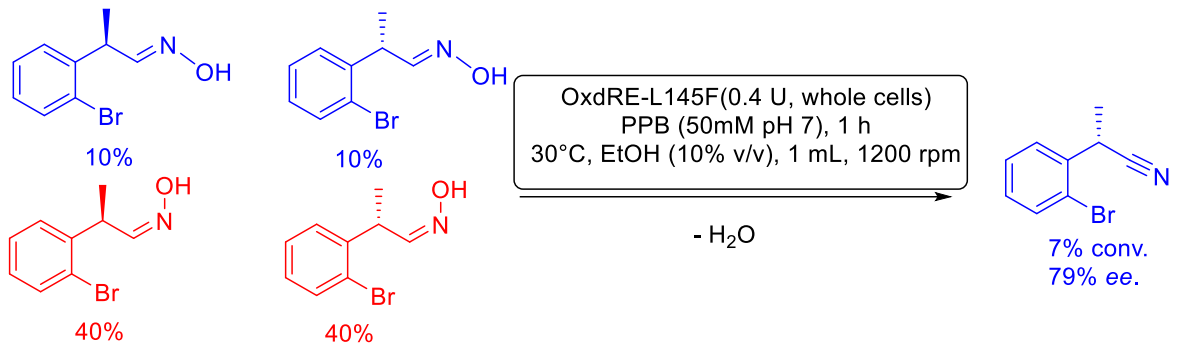

Scheme 27: Screening result for OxdRE-L145F with *o*-Br-PPOX as illustration for the increased affinity towards a low accessible substrate.

Thus, it can be concluded that this constellation of substrate and enzymes in the combination of the DDKR set up can only improve the selectivity, since the favored substrate is already present in the deficiency. Concluding that in total three possible combinations were found to perform a DDKR: OxdB-L128F with *m*-Br-PPOX, OxdRE-L145F with *p*-Br-PPOX and *o*-Br-PPOX. The fact that the DDKR could then only be presented as a proof of concept with a limited substrate spectrum, further investigation in terms of finding a more suitable biocatalyst were carried out.

4.8 Smart library screening to increase the selectivity of OxdRE-L145F

The rational approach of site-directed mutagenesis to increase the selectivity of aldoxime dehydratase proved to be limited, because the *in silico* designed variants may not necessarily represent the expressed enzyme (4.7). Furthermore, with the *in silico* approach only the active site of the enzyme can be investigated, since structural changes induced by mutations with greater distance to the active site are difficult to predict additionally the computational time is higher as well. In comparison with a randomized mutagenesis with a suitable screening method, which could cover a significantly higher mutation space (10^{10}-10^{12}-variants),[127] the in silico approach is very limited. However, a non-specific randomized mutagenesis such as ePCR[128] is not suitable to increase the selectivity especially for an already well-tailored enzymes.[129] Unlike stability, solubility or activity, selectivity is more likely to be influenced by a few positions in the protein.[130] The other protein properties can be improved very well by randomized mutagenesis as part of directed evolution.[131] Thus, only requiring a high-throughput screening method, which is usually provided by various color assays,[132] but the high effort is subsequently the bottleneck of directed evolution.[133,134] Alternatively, to the completely randomized directed evolution, a saturated mutagenesis can be performed for specific mutations (SM). The positions can be chosen via different rational approaches,[63,135] with the benefits of being more widely applicable and in general reducing the screening efforts. These rationally designed positions, which are chosen for saturation are called smart libraries.[78,136] These smart libraries reduce the number of mutants required for finding lead mutants and similar to directed evolution these achieved lead variants can then be used in repetitive cycles to amplify the properties, either by rescreening a new library, or by combining the lead structures in combinatorial mutations. The former one is a variation of the classical directed evolution the latter falls under the designation iterative saturated mutagenesis (ISM) (**Figure 31**).[64]

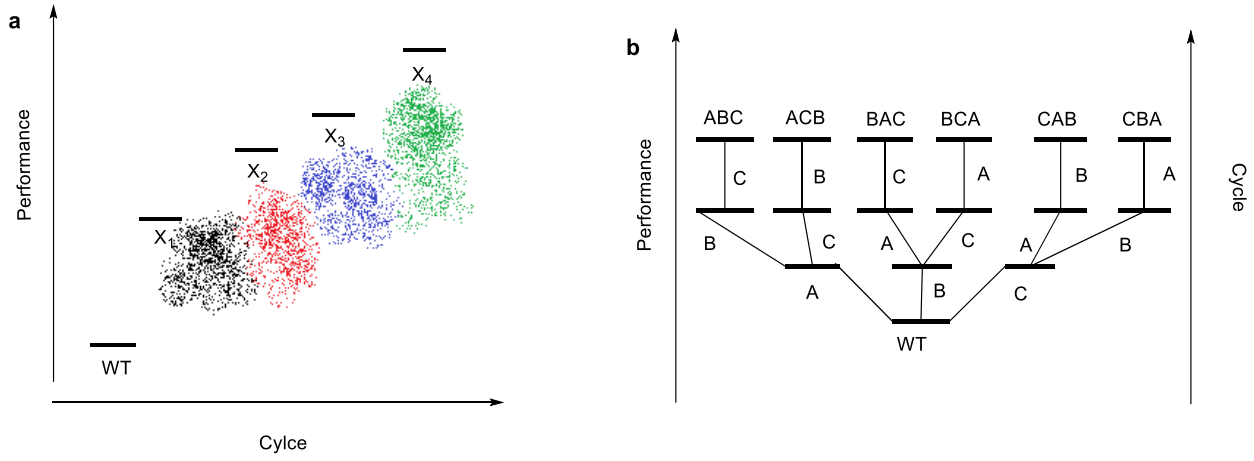

Figure 31: Illustration and comparison of directed evolution (**a**) and ISM (**b**).

Since, randomized mutagenesis mainly treats mutations distant from the active site and the improvement of enantioselectivity by mutation spatially close to the active pocket is more pronounced than mutation spatially distant from the active pocket, a (semi)-rational approach is clearly more useful to increase enantioselectivity.[130] The most promising and effective way to increase the enantioselectivity of an enzyme, while minimizing the effort, is to use smart libraries in an ISM. *Reetz et al*. described also specified version of ISM, which includes only amino acids in direct spatial distance to active site namely the Combinatorial Active-site Saturation Test (CAST).[137] The

CAST method has proven to be a valid method for improving the enantioselectivity of enzymes for many examples.[138] Thus, the following smart library was designed according to the CASTing method.

4.8.1 Generation of a smart library

The mutant library was commercially acquired from *Twist Bioscience*®, which had the advantage of dismissing bias in the libraries, because every mutant in one library is generated by a specific primer set. The mutants were generated on a semi-rational level for which MOE[94] was used as a tool. Positions were selected that were either close to the active pocket, in interaction with the active site, or at positions such as loops that could have a large influence on the positioning of the essential amino acids in the active site (**Figure 32**, **Figure 33**, **Figure 34**). OxdRE-L145F, with already increased enantioselectivity, was used as starting point.

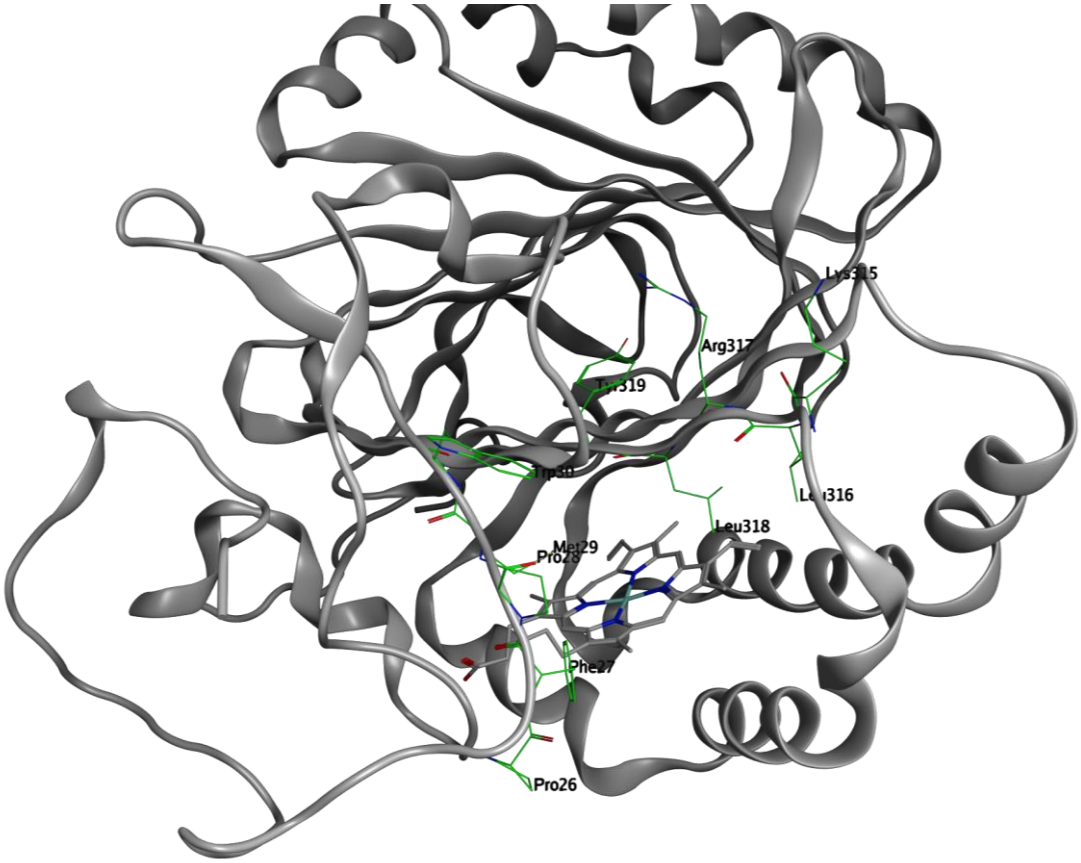

Figure 32: Library selection Set 1 of OxdRE-L145F with mutation sites spatial close to the active site highlighted in green.

In Set1 (**Figure 32**) all positions spatially close to the active site were chosen to be saturated. However, these positions are not promising, although they represent the closest amino acids to active pockets, they are very far from the selectivity determining cavity with the exception of Met29 and W30. Set 2 (**Figure 33**) is the most promising set, since the shown positions are on structural elements close to the F145, which was shown to have the highest impact on selectivity. Mutations in this area can have a direct influence on the orientation and positioning of the F145 or the entire structural element and thus also on the cavity. In **Figure 34**, Set 3 is shown,

consisting of positions far away from active pockets but localized at loops, which may also have an influence on activity and selectivity.

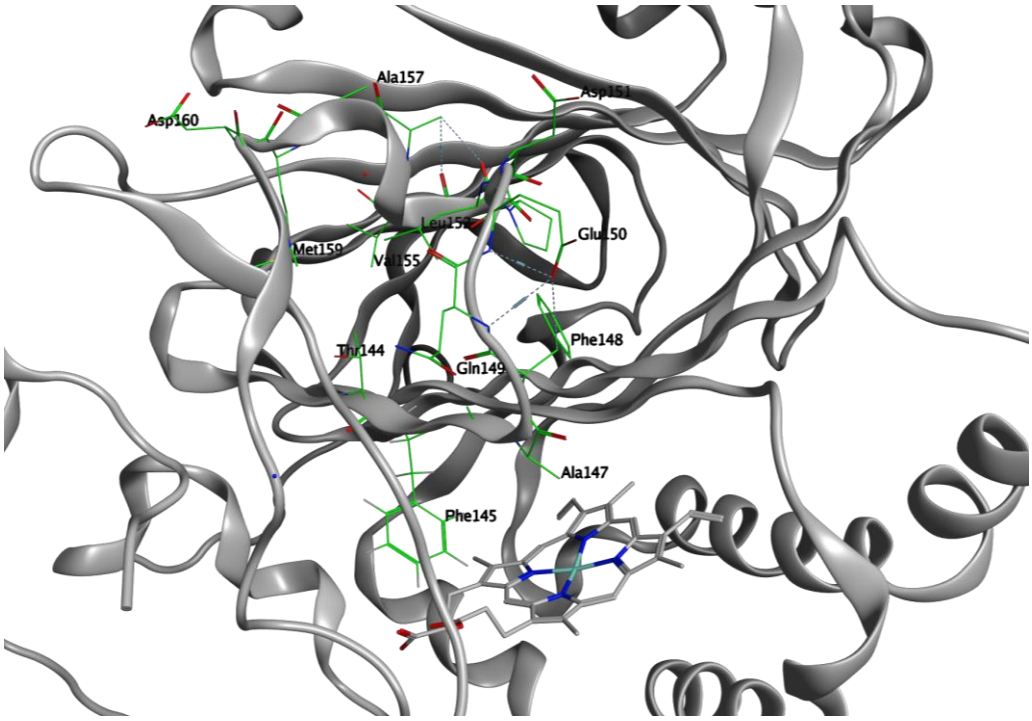

Figure 33: Library selection Set 2 of OxdRE-L145F with mutation sites on same β-strand as L145F highlighted in green.

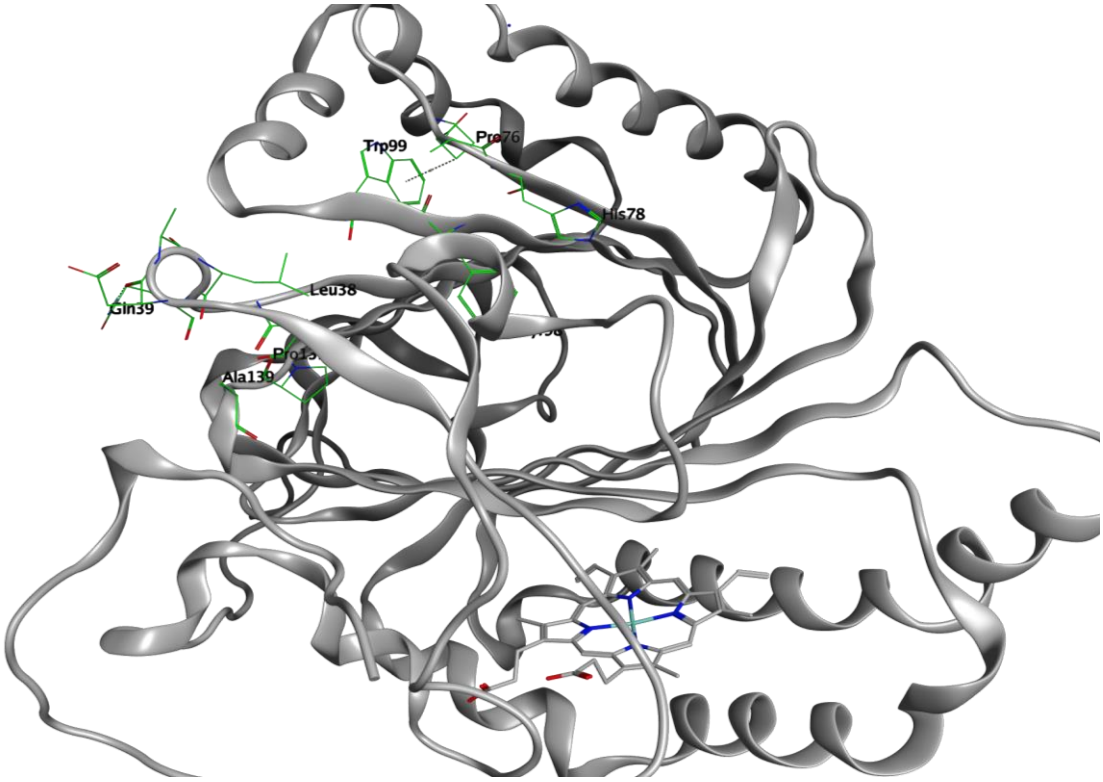

Figure 34: Library selection Set 3 of OxdRE-L145F with mutation sites on loops and turns far from the active highlighted in green.

4.8.1.1 Screening development and validation

A high throughput method for the screening of the smart libraries were developed. The standard analysis for PPOX derivates with HPLC (30 min) was not suitable. Therefore, a new method was developed for the substrate *o*-FPPOX (**4a**) with an analysis time of 5,5 min. 96-deep-well plates were selected to carry out the reaction and the work-up. The cultivation could also be carried out conveniently in the 96-deelwell plates, due to the preceding expression optimization. With the exception that after work up the samples had to be filled into glass vials, a high throughput method was developed.

The benchmark of the screening was carried out with OxdRE-WT, which was transformed in *E. coli*-BL21-Star strain using standard transformation protocol. For transformation 2 µL of the plasmid solution (200 ng·µL^{-1}) was used on 50 µL competent cell solution resulting in over 100 clones. The clones were transferred individually to a deep-well-plate with LB-Medium (1.8 mL) containing kanamycin (50 µg·mL^{-1}). Two different cultivation protocols were tested, to examine the most suitable. For the first cultivation method the picked clones were resuspended in the media and grown for 48 hours, thereby the temperature was reduced from 37 °C after 24 hours to 20 °C. For the second cultivation method, LB-Medium was inoculated with single colonies and cultivated for 24 h at 37 °C. The suspensions were used as preculture and were used to inoculate (50 uL) fresh media and then grown another 24 hours at 20 °C. The cells were then harvested via centrifugation (3500 rpm, 2 min) and resuspend in PPB (450 µL, 50 mM, pH 7). Then an ethanolic substrate solution of *rac*-2-FPPOX (**4a**, 20 mM, 50 µL) was added. The reaction was carried out for one hour in a shaker at 20 °C and 200 rpm. As workup cyclohexane (1 mL) was used to extract the reaction solution and then analyzed via HPLC. The results of the screening validation are shown in **Scheme 28**. In terms of conversion both cultivation method shows high fluctuations, but the preculture expression being slightly more stable with a standard deviation (SD) of 6.2 versus 9.9 the enantiomeric excess as well as the E-value are quite stable in both cultivation method. However, the clone expression shows again slightly better performance with a SD of 1.2 versus 2.3. Accordingly, clone expression was chosen for screening, as it not only had a lower standard deviation, but was also very easy to handle, with only the transfer of the clones into the deep-well plates. Based on the validation, the libraries were cultivated and screened with small adjustments (**Figure 35**). For transformation 10 µL of the plasmid solution (10 ng·µL^{-1}) was used instead of 2 µL. on the competent cells (50 µL) resulting in over 100 clones. The cultivation was carried out as clone expression.

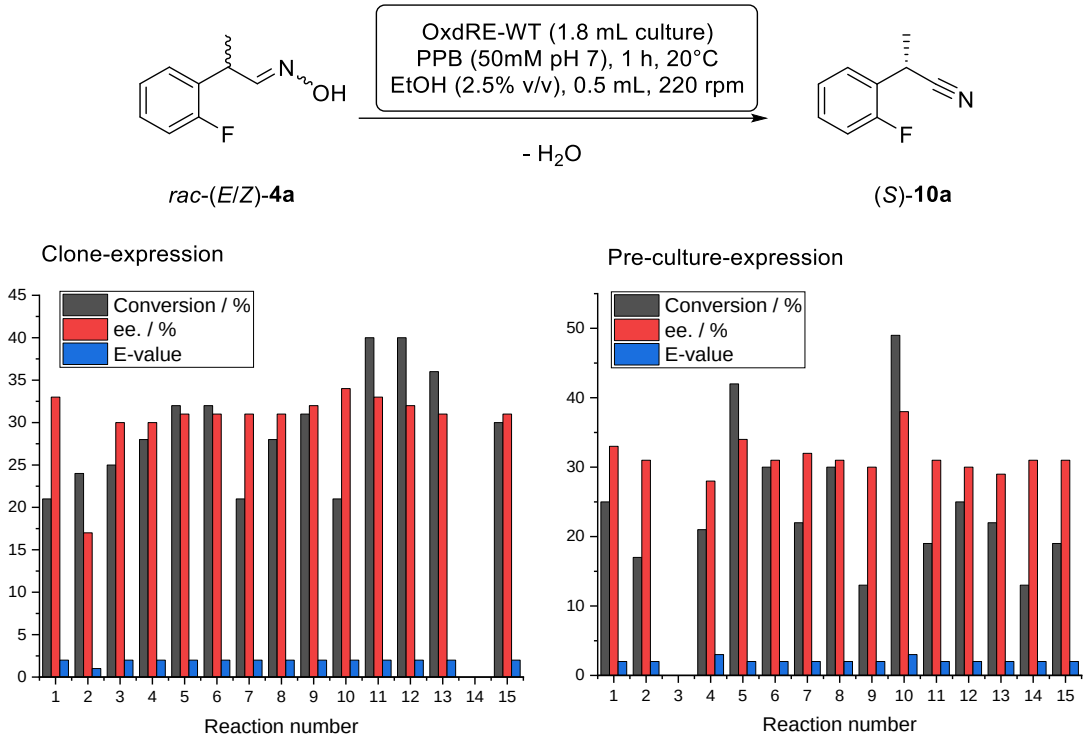

Scheme 28: Screening validation with OxdRE-WT and comparison of 96-well-plate leaky expression with and without preculture.

4.8.2 Screening results

The main culture volume as well as the substrate concentration was lowered to reduce the overall execution time and substrate consumption. Furthermore, one clone was used for two inoculations to have one culture as backup and one culture for the reaction. The backup was stored after harvesting at -20 °C.

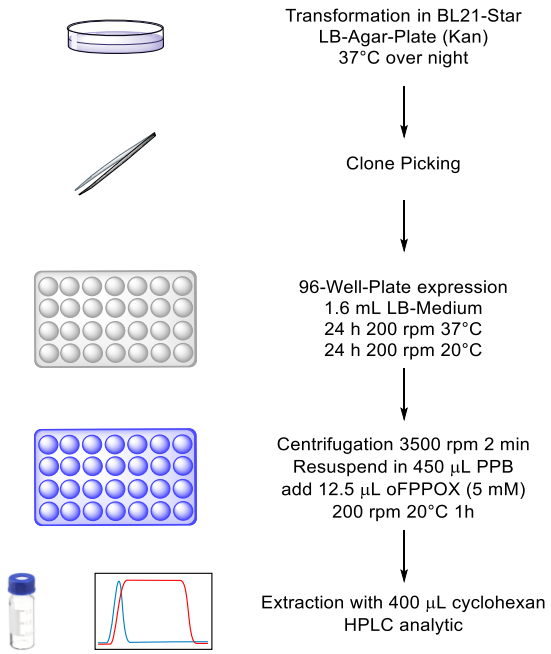

Figure 35: Schematic illustration of the screening method

The screening was carried out with 16 saturated positions mainly from Set 2 of the designed libraries leading to over 900 reactions. The measured conversions and enantiomeric excess are shown in experimental section (9.6.6.3). The corresponding E-values are displayed in **Scheme 29**.

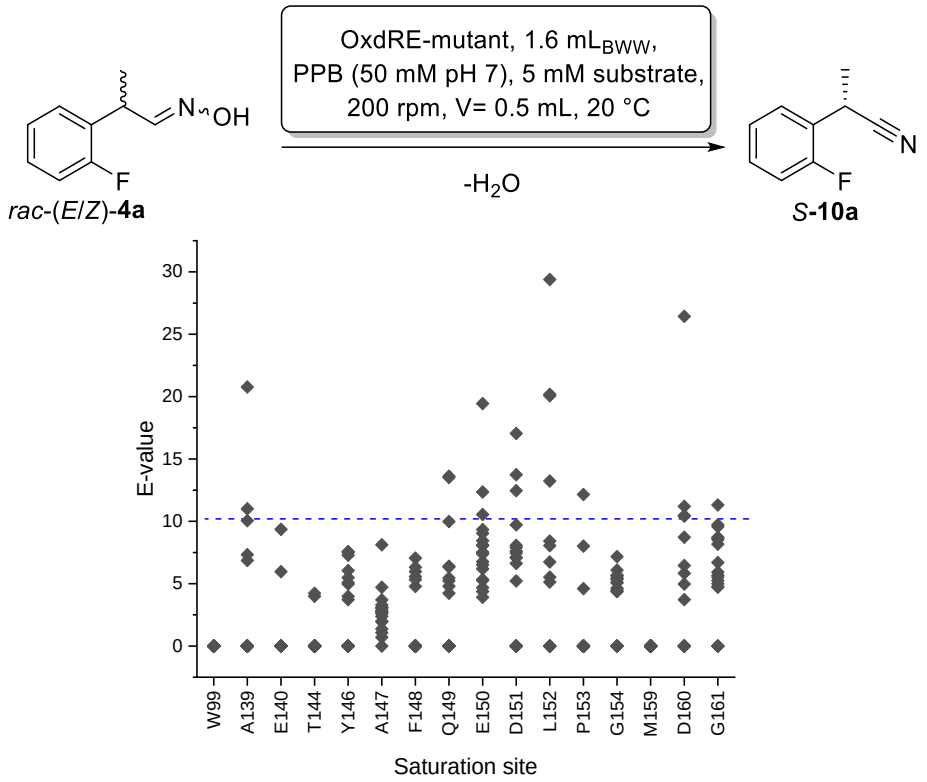

Scheme 29: Plot of all E-values from the screening of the 16 mutant libraries, for the reaction of *rac*-(*E*/*Z*)-**4a** to the product *S*-**10a.** The blue dotted line (E = 10) marks the minimal requirement for the hit identification.

The screening resulted also in E-values over 200, but those values were only reached, because the conversion were below 5% and therefore beyond the detection limit of the HPLC. Thus, these values were not included in the illustration and the results, as they were considered false positives. Set 2 proved to be extraordinarily successful, as almost every position showed a variant with improved E-values. Over 16 hits were found that have a higher E-value than 10. Positions W99 and M159 did not show conversion for any reactions, concluding that a systematic error must have occurred with a high probability in the production of the enzymes during the experiment. Nevertheless, a large number of variants with enhanced enantioselectivity were found. A small set of examples, with a minimum conversion of 10% were used to identify the mutation and further investigations (**Table 11**). Six mutants were cultivated in quantitative scaled and utilized in biotransformation. The chosen examples as well as the results of the biotransformation are shown in **Table 12**. The biotransformations revealed an overall much lower E-values than in the screening process. The cause for the discrepancy could be, that for the screening itself not the validated substrate concentration was used, but a much lower. The substrate concentration had to be lowered because of the high consumption of the substrate. The substrate access was limited and therefore a lower substrate loading was used. This lower substrate loading probably led to an inaccuracy in the E-value. However, the hits still showed improved E-values, but were not in the range to perform the DDKR.

Table 11: Promising hits of the screening that have been evaluated for their mutation. WT and L145F (blue) marking the starting point.

#	Clone	Mutation	E-Value
A	WT	-	2
B	L145F	-	4
1	4C-C8	Y146F	9
2	4D-C2	A147M	8
3	4E-F4	F148E	10
4	4F-D4	Q149D	13
5	4G-D4	G150W	12
6	4G-H2	E150C	19
7	4H-B2	D151E	17
8	4H-H5	D151L	12
9	6A-C3	D160C	26
10	6B-A3	G161R	9
11	6B-D1	G161D	10

Table 12: Results of OxdRE-L145F Library screening showing E-Values and mutation site. For comparison, the wild type and OxdRE-L145F also shown (blue).

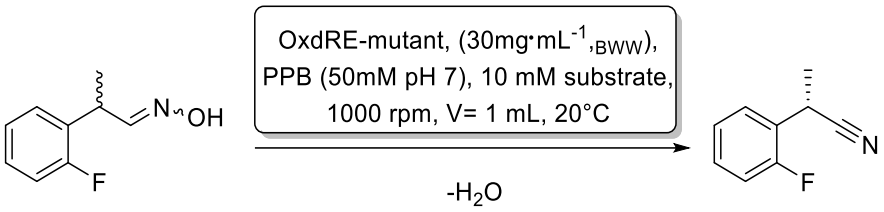

#	Clone	Site	E-Value
A	WT	-	2
B	L145F	-	4
1	6B-A3	G161R	7
2	6B-D1	G161D	8
3	6A-C3	D160C	9
4	4H-B2	D151E	10
5	4H-H5	D151L	5
6	4G-D4	G150W	6

Considering the WT as the initial enzyme, the L145F mutant represents phase 1 and the screening, phase 2 of this CASTing approach (**Scheme 30**). The next step (phase 3) would be to combine the mutations from phase 2 to create triple mutants with even higher selectivity. These triple mutants can then be formed into quadruple mutants in phase 4, this can be repeated until the desired enantioselectivity is reached, as already described and illustrated for a general ISM method (**Figure 31**).

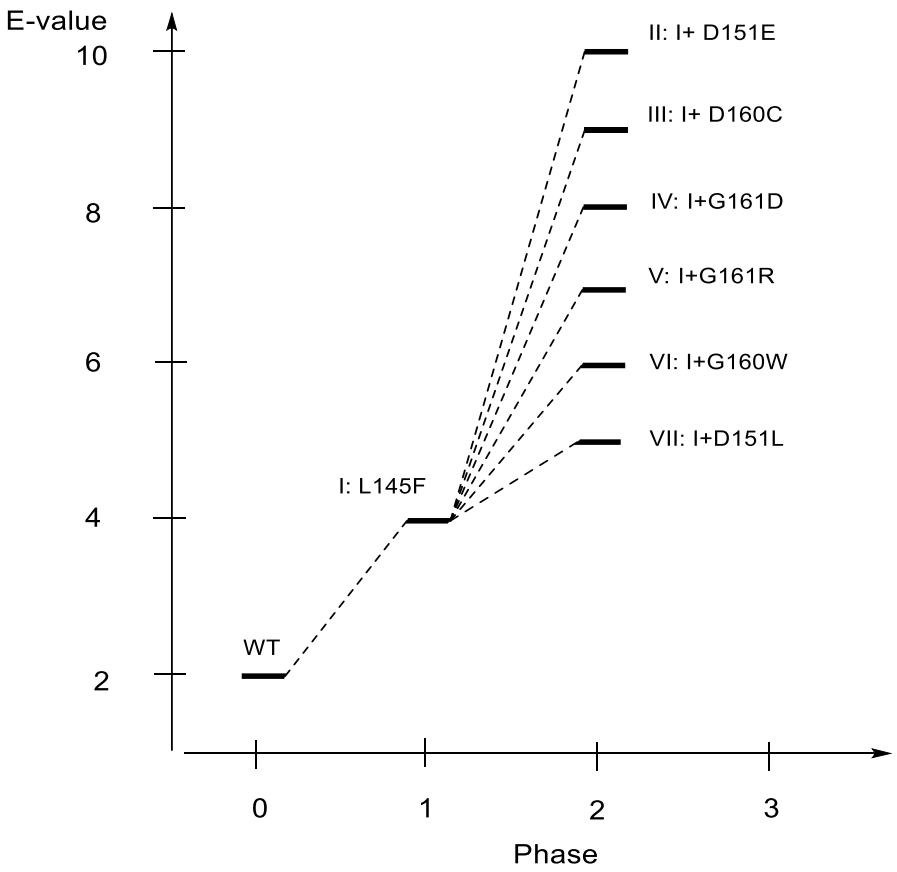

Scheme 30: Enantioselectivity of OxdRE as function of the ISM-phase

The mutants **II** (L145F, D151E), **III** (L145F, D160C) and **IV** (L145F, G161D) wich showed signifcant higher enantioselectivity, are part of the designed smart libaries from Set2. The positions are on close structure elemets to the active site and the cavity. By introducing mutations at this point, the structural properties can change. It was also attempted to rationlize the introduced mutations, which led to higher selectivity by perfomoring a MD-simluation for OxdRE-L145F and a combination of the mutants **II**, **III** and **IV**. Through preliminary rationalization with OxdRE-L145F, the model was already optimized and a MD-simulation showed no change in the protein structure. By introducing the new mutants and subsequent simulation for finding an optimal conformation (thermodynamical minimum), it was shown that the mutations contributed to a change in the orientation of the phenylalanine (**Figure 36**). However, no precise rational conclusion could be drawn on how these mutations led to this change. Only the D160C mutation did show a new hydrogen bond with L100. Nevertheless, the MD-simulation showed that mutations in library Set 2 can influence the cavitiy indirectly, as expected. Last, it can be concluded that the semirational screening led to an enzyme with higher selectivity, reaching an E-value of 10. With regard to the ISM, these variants may only need to be combined as suggested in the simualtion, to obtain a highly selective variant.

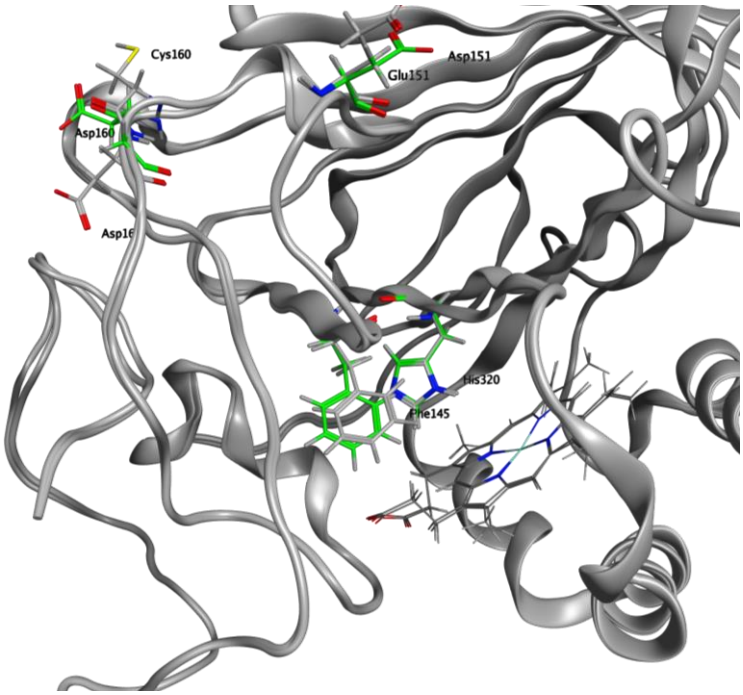

Figure 36: Conformational change of OxdRE-L145F (green) towards OxdRE-L145F/D151E/D160C/G161D (grey) using MD simulation for both enzymes.

4.9 Summary and Outlook for the chiral nitrile synthesis in a double dynamic kinetic resolution

This section focused on the development of an industrially relevant and academically first formulated double dynamic kinetic resolution, as tool to generate biocatalytically chiral nitriles. In this context, isomerization as well as racemization method for aldoximes were extensively studied and developed. The isomerization of aldoxime was achieved by thermal treatment and showed increased isomerization rates at higher substrate concentration, whereas the thermodynamic equilibrium (*E/Z*, 70/30) could be reached under three hours (**Scheme 31**).

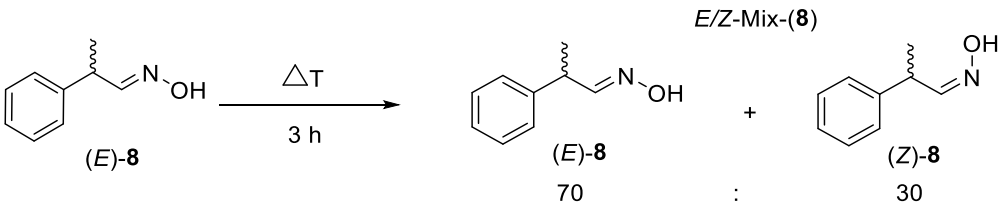

Scheme 31: Isomerization of (*E*)-PPOX (**8**, 89:11, *E/Z*) at 100°C at 240 mM substrate concentration reaching the thermodynamic equilibrium in 3 hours.

A racemization method for chiral aldoxime with PPOX derivates as examples could be developed and a possible mechanism was postulated (**Scheme 15**). Racemization was made possible with thiazoles, with thiamine hydrochloride as the best example. The enantiomeric excess of (*R,E*)-**8** was successfully reduced from 88% to 35% within 24 hours using thiamine hydrochloride (**Scheme 32**).

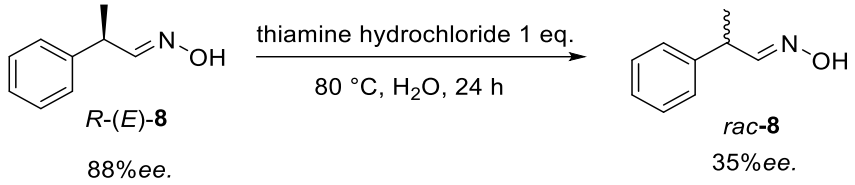

Scheme 32: Racemization of *(R,E)*-PPOX (**8**) with thiamine hydrochloride.

For the DDKR a flow set up was designed to perform the racemization and isomerization simultaneously with the enzymatic dehydration. The flow set-up consisted of a two-phase system (cyclohexane/water) with two reaction chambers. Cyclohexane was used as the mobile phase. The enzymatic reaction was carried out at room temperature while the racemization and isomerization were performed at 80 °C. The coupling of racemization and isomerization with enzymatic dehydration was successfully demonstrated in flow reaching 83% conversion and 36% *ee*, which showed the proof of concept for the first demonstrated DDKR (**Scheme 35**).

Since the reaction performs better at higher volume and substrate concentration, but the substrate access was limited, the substrate synthesis with only 10% isolated yield was optimized using hydroformylation of styrenes as key step with subsequent condensation of hydroxylamine. By using this alternative route, the substrates could be obtained conveniently and with high isolated yields reaching up to 98% (**Scheme 33**).

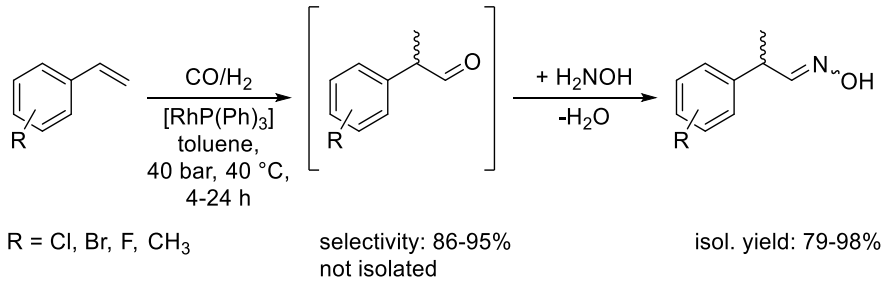

Scheme 33: General reaction overview of the synthesis of substituted phenylpropanal oximes.

The selectivity of OxdRE-WT was addressed via three different approaches. The biocatalyst production could also be optimized due to a new expression method (leaky expression), leading to a 100-fold higher activity for OxdRE-L145F. The fully rational site directed mutagenesis, led to the variant OxdRE-L145F with a twice higher enantioselectivity (E = 4) than the WT (E = 2). The introduction of the L145F mutant into other aldoxime dehydratases (OxdA and OxdB) was also successfully achieved, leading to increased selectivities for both aldoximes dehydratases compared to their wild type. As part of the approach, to introduce the mutant L145F into other aldoximes dehydratases, 16 different substrates were screened. The screening revealed a few combinations of Oxd-Variants and substrates with improved selectivities reaching E-values of up to 11. As last approach high throughput screening method as well as smart libraries were designed. The high-throughput screening was achieved utilizing expression and reactions in 96-deepwell plates with a subsequent fast analysis *via* HPLC-chromatography. As screening reaction *rac*-(*E/Z*)-2-FPPOX (**4a**) was used, for which a HPLC method of 5.5 mins could be designed. The 52 smart libraries were designed using MOE as visualization tool to define promising areas for mutation. The screening was conducted with over 900 clones from 16 smart libraries. Variants with 5 times higher selectivities than OxdRE-WT were identified. The best variant OxdRE-L145F/D151E showed an E-Value of 10 for the transformation of *rac*-(*E/Z*)-2-FPPOX (**4a**).

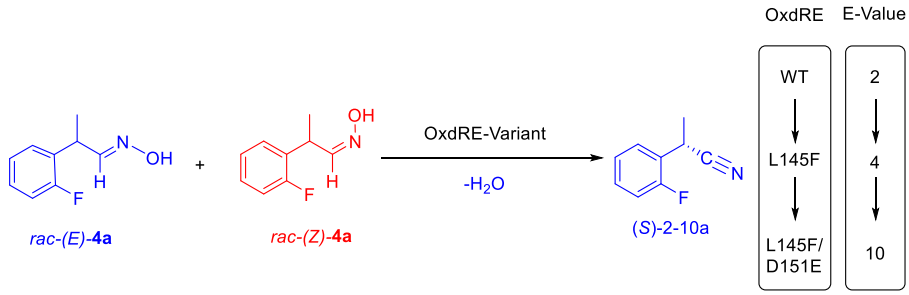

Scheme 34: Demonstration of the reaction with *rac*-(*E*/*Z*)-2-FPPOX and OxdRE variants.

Furthermore, MD-simulations were performed to show the influence of the new variants. The MD-simulation could illustrate structural changes in the active site induced by the identified mutations in the screening. As outlook those identified hits could be combined as part of the ISM to obtain a much more selective variant. With a highly selective variant the subsequent DDKR would need less optimization. Furthermore, the remaining unscreened libraries could be investigated before conducting ISM type combination of mutants. Alternatively the screening could also be conducted using citronellal oxime as citronellal is commercially available and presents an alternative chiral substrate with already established GC-methods.[139]

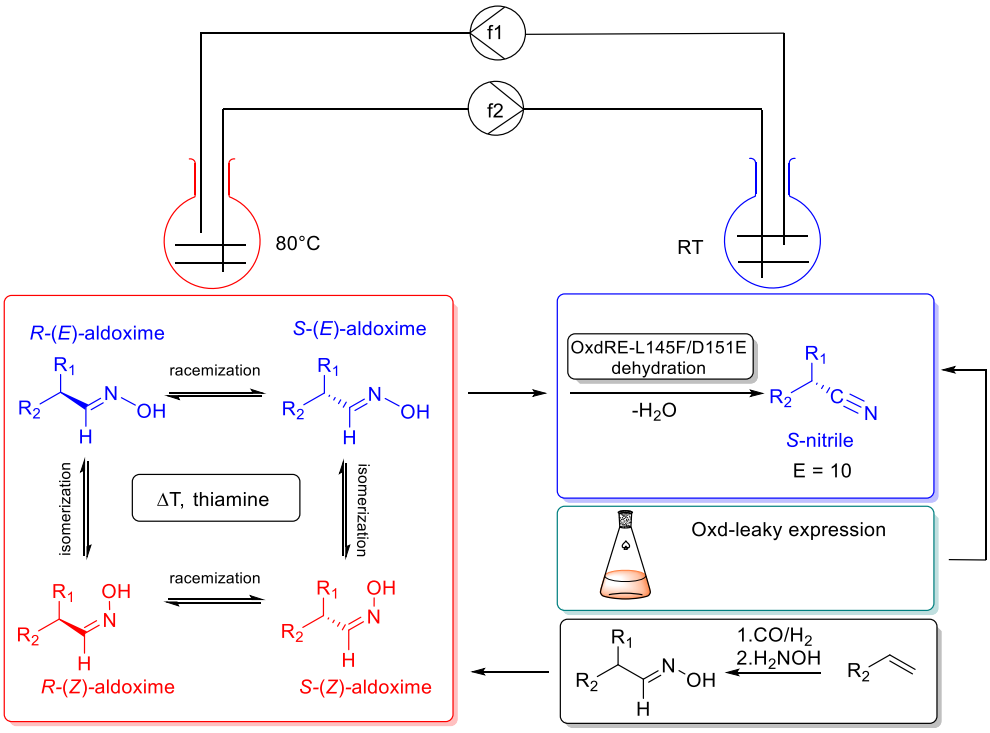

Scheme 35: Summary of the overall developed process in this work. Substrate preparation using hydroformylation (black), biocatalyst preparation (green), chemical racemization and isomerization (red) and nitrile synthesis with an engineered biocatalyst. Representation of DDKR as a flow process with enzymatic nitrile synthesis at room temperature and chemical racemization/isomerization at 80 °C.

Furthermore, if enzyme stability happen to be rate limiting for the developed process it is also thinkable option to switch from superabsorber/cyclohexane system towards alginate-beads in water.[139] *Hinzmann et al.* already demonstrated the compatibility of alginate beads with aldoximes dehydratase as encapsuling technique.[36] This method could provide higher stability for the enzyme while also the reaction temperature for the racemization/isomerization could be increased to 100 °C with water as solvent.

5 Improving the biocatalytic transformation of non-soluble fatty aldoximes by targeting activity and stability of OxdB

5.1 Motivation

Over the last years protein engineering gained significant interest in academia and industry.[57,91] With the latest achievements, enzymes can be optimized very effectively for their use as biocatalysts addressing either selectivity, activity or stability. The state of the art in protein engineering in terms of efficiency is the combination of directed evolution[58,140], high throughput screening (HTS) methods[141] and computational analysis[142,143]. Lately, machine learning was also incorporated showing future perspectives in terms of automatization and effectivity.[144] The only but crucial drawback of this methodology is its dependence on a screen able system[133,145]. If this cannot be realized *in silico* methods alone are also a viable tool to modify enzymes by direct identification of either mutation sites[79] or hot spots to generate smart libraries[78].

Aldoxime dehydratases proven to be interesting biocatalysts being capable of a cyanide free route for the synthesis of nitril compounds starting from an aldoxime. Beside their broad substrate scope[23,47], these heme b containing enzymes accept incredible substrate loading of 1.4 kg/L in case of octanal oxime and OxdB,[28] without the need of additional cofactors. Thus, they are clearly interesting for the bulk chemical sector. However, they were shown to be limited by the length of the substrate alkyl rest with respect to fatty aldoximes.[28] The longer the chain, the less conversion was observed. To clarify the reason behind the limitation of the enzyme for fatty aldoxime different aspects of the problem were targeted (**Figure 37**).

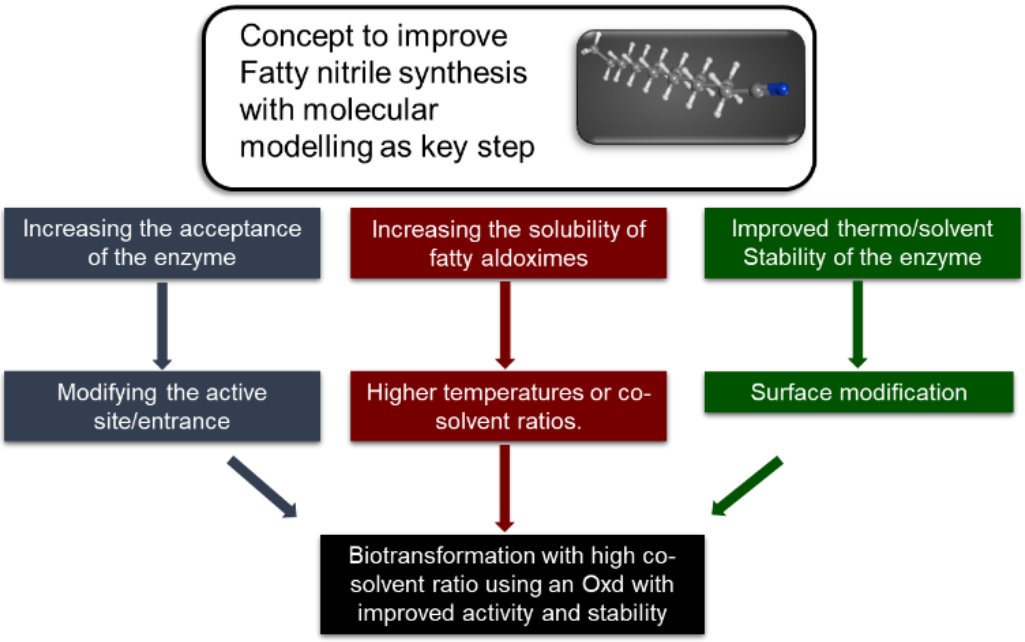

Figure 37: Concept to improve fatty nitrile synthesis with addressing three different problems to find a suited solution for the conversion of fatty nitriles

The acceptance of the fatty aldoximes and their solubility as well as the stability of the enzymes were investigated. Depending on what is identified as the bottleneck of the reaction, several approaches can be viable. The

identification can be done by first investigating the solubility of the substrates under certain reaction conditions and comparing these with kinetic data of the enzyme towards the substrate class. If for an instance the solubility would be the issue, increased reaction temperatures or cosolvent ratios could drastically increase the solubility. Temperature and co-solvent can only be increased if the enzyme is stable enough, which is why the enzyme itself or the biocatalyst formulation would need modification to withstand harsher conditions. Besides the protein engineering aspect, another option could be the incorporation of the enzyme in particles and use them in a two-phase system, where the fatty aldoxime are solved in the organic phase.[146,147] However, if the substrates are too large for the active site, these attempts would not be successful. Since, it is also possible, that the enzyme does not convert bulky substrates, because the enzyme-substrate-complex cannot be formed due to sterically hinderance, which can be investigated via molecular modeling. Therefore, molecular modeling studies including site directed mutagenesis were conducted to investigate the enzyme substrate complex of OxdB and long chain fatty aldoximes. The acceptance and activity were rationally modified using docking studies and homology modeling. The solubility of aldoximes were investigated using ACD/I-Lab and were targeted by increasing co-solvent ratios or the reaction temperature. To withstand increased reactions temperature and co-solvent ratios OxdB was modified in terms of stability. In the process, a new method for *in-silco* based enhancement of enzyme stability was developed.

5.2 Solubility and enzyme substrate complex of fatty aldoximes

To determine if the solubilities of the substrates were a problem, they were first calculated, which allowed a quantitative comparison. The calculation revealed the overall low solubility of the fatty aldoximes. As expected, the solubility drops dramatically with the growth of the chain length or in general the solubility is nearly halved per added alkyl rest. While heptanal oxime still had a relatively good solubility of 59 $\mu g \cdot ml^{-1}$, dodecanal oxime is practically insoluble with 6.20 $\mu g \cdot ml^{-1}$ (**Table 13**).

Table 13: Calculated solubilities of aldoximes in water at 25 °C by using the The ACD/I-Lab program.[148] The realibility of the calculation presented in colors (green = good, yellow = low).

Aldoxime	Solubility /$\mu g \cdot ml^{-1}$	LogSw	Reliability:	Conc. /µM
C7	59	-3.3	0.65	460
C8	39	-3.6	0.55	270
C9	24	-3.8	0.55	150
C10	18	-4.0	0.67	110
C11	11	-4.2	0.69	60
C12	6.2	-4.5	0.68	30
C13	2.9	-4.9	0.63	14
C14	0.37	-5.8	0.56	1.6
C15	0.17	-6.2	0.53	0.70
C16	0.10	-6.5	0.48	0.27
C17	0.02	-7.02	0.45	0.0007
C18	0.01	-7.29	0.45	0.0004

The K_M-values for OxdB (aldoxime dehydratase from *Bacillus sp.*) and fatty aldoxime are in the range of 4 mM.[13] Comparing the K_M-value with the solubility of the substrates, the obtained conversions reported by Hinzmann et al. are in agreement with the calculated data. The solubility of the substrates could also explain why such a high substrate loading is possible. While the aldoximes from hexanal oxime to decanal oxime are still soluble enough to be converted excellently, the solubility is at the same time probably low enough to cause no inhibition for the

enzyme. The higher fatty aldoximes, on the other hand, are even less soluble in water. The program did not allow to calculate solubilities at different temperatures or solvent ratios. In fact, the biotransformation proceeds in 10% ethanol, in which octanal oxime is soluble up to 100 mM and dodecanal oxime to approximately 5 mM (visual estimation). While substrates such as octanal oximes with a solubility higher than the K_M value of OxdB can easily be transformed to the nitrile, substrates with solubilities far below the K_M-values are converted poorly or not at all. To increase the overall conversion either the K_M-Value has to be lowered or the solubility of the substrates has to be increased. The former can be achieved by modifying the active pocket, the latter can be achieved by increasing the cosolvent content or the temperature. Since OxdB-WT is not stable enough to withstand higher reaction temperature or solvent ratios, the enzyme has to be engineered for both matters first.

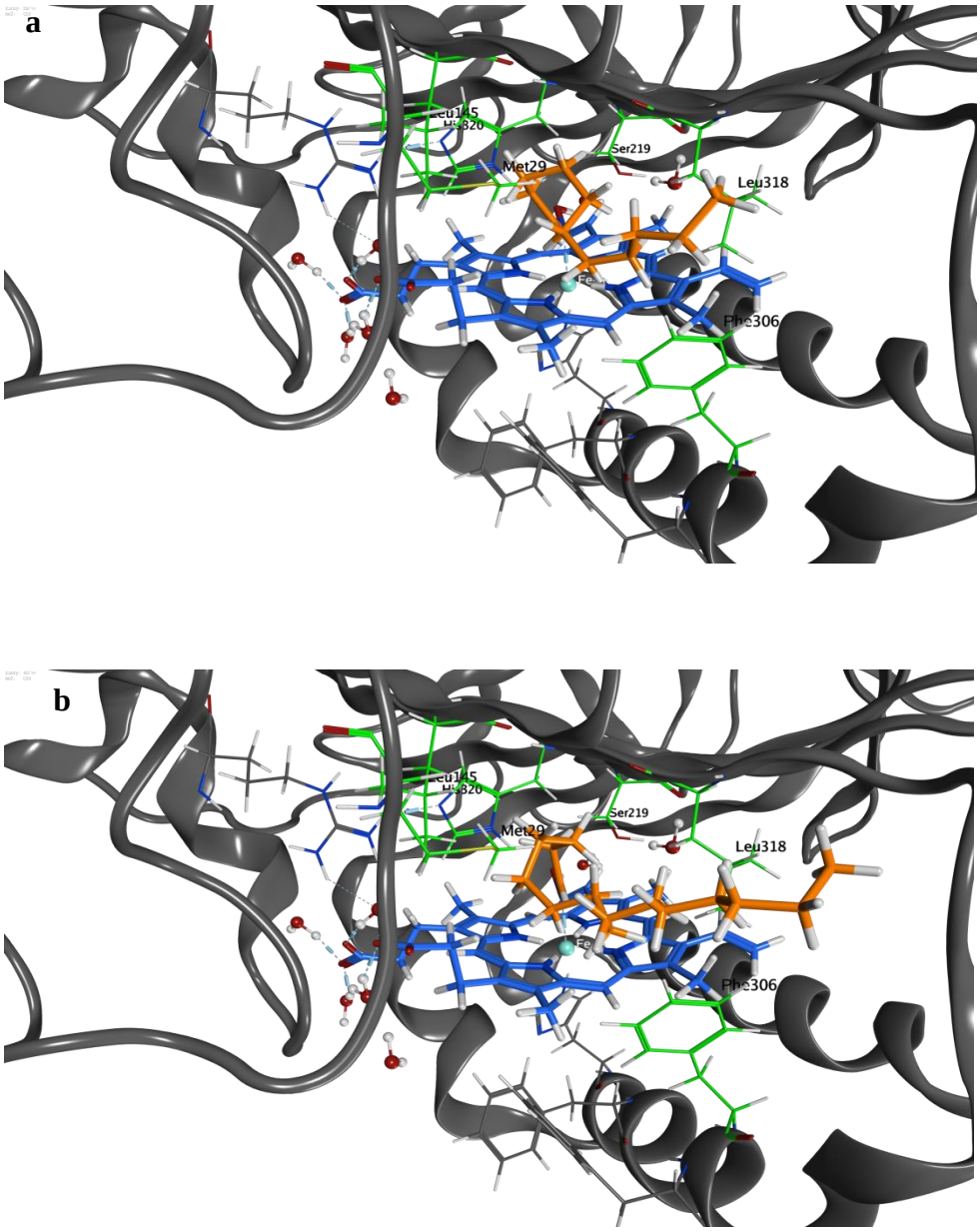

Figure 38: Molecular docking using MOE as software. Frame **a** shows dodecanal oxime inside the active site. Frame **b** showing hexadecanal oxime in the active site showing same pose as dodecanal oxime with only the alkyl rest merging further out.

5.3 Increasing protein stability and in silico method development

Protein stability prediction has been a challenge for decades. These approaches are either based on empirical forcefield, statistical potentials, sequence- and/or structural information. With the PoPMuSiC program being one of the earliest[149] a lot of powerful predictors with different approaches (FoldX, PoPMuSiC 2.1, I-Mutant2.0, I-Mutant3.0, HotSpotWizard 2.0) were developed.[150] Even though these methods represent very powerful tools, the overall accuracy is only moderate.[151] Besides intramolecular interactions and structural integrity protein stability depends on more than just the folded construct. When considering protein biosynthesis in a host cell, in which translation and folding have a major impact upon protein stability,[152] it is to be expected that these prediction tools provide only moderate accuracy. From the mentioned protein design applications HotSpotWizard2.0 has the advantage of using primer sequence and structural data as well as evolutionary information from three different databases to provide a combined prediction.[143] However, the tool does not predict specific mutations with a quantitative analysis, but instead it predicts hot spots for screening purposes. Therefore, the idea was to combine the advantages of both predictor types, using the information of database analysis and empirical forcefield calculation. For this purpose 3DM[153] and MOE[94] were used. 3DM creates large libraries, which are divided in subfamilies of specified enzyme class. Those libraries are generated by the structural identity of proteins using its own numbering scheme and automated access to protein structures and models. MOE (Molecular Operating Environment) is a multipurpose software and provides the stability calculation. The use of both tools combines structural and evolutionary information via 3DM and empirical force field calculation with MOE, which should lead to an increased accuracy of the prediction.

5.3.1 Design of a stable aldoxime dehydratase using OxdB as template

The aim of this project was to increase the stability of OxdB, which is the most stable aldoxime dehydratase known.[13,28,93] The structure of OxdB was only available as model, leading to a decrease in the prediction accuracy. However, due to a high structural homology with OxdA (3w08) it remained the best starting point. Using MOE, *in silico* saturated site directed mutagenesis can be performed to screen for mutants with increased stability, whereas the stability is calculated as Gibbs-Free-energy ($\Delta\Delta G = \Delta G_{(wildtype)} - \Delta G_{(mutant)}$) in an empirical forcefield based calculation. As starting point three different aldoxime dehydratases with known thermostabilities were compare to find structural differences. This comparison could provide information for possible mutation sites. Thereby OxdB represent the most stable, OxdA[16] second and OxdRE[14] the most instable protein. By comparing the *in silico* generated properties of the selected Oxds an interesting correlation (**Table 14**) were encountered.

Table 14: Comparison of calculated structure related properties of thermostable enzymes with three different aldoxime deydratases using MOE.

Enzyme (PDB-file)	K-D Hydrophobicity moment/ D	Dipole moment /D	Mobility /$cm^2 \cdot V.s^{-1}$	Dipole-/ Hydrophobicity moment	VdW Volume /$Å^3$	VdW Surface area /$Å^2$
Cal-A (2VEO)	1131	314	-4.9	0.28	42482	14389
Bc.st-ADH (1RJW)	791	615	-27	0.78	33628	14749
Lk-ADH (1ZK4)	329	364	7.3	1.1	24332	11353
Chol. Ox. (3JS8)	1136	442	15	0.39	53849	18600
P450-BM3 (4ZFA)	1575	990	-12	0.62	48282	19325
Cyp117 (1IO7)	1602	329	-2.9	0.20	39241	16339
OxdRE (3a17)	398	776	-75	1.95	35959	14432
OxdA (3w08)	497	607	-54	1.22	36401	14804
OxdB-WT	788	340	-17	0.43	30567	15613

The values of the hydrophobicity moment[154], the dipole moment and the mobility[155] of the enzymes showed a certain tendency in dependency to the enzyme stability. The most instable aldoxime dehydratase OxdRE among those three variants has the lowest hydrophobicity moment of 398 D and the highest dipole moment of 776 D, while the most stable aldoxime dehydratase OxdB has the highest hydrophobicity moment of 788 D and the lowest dipole moment of 340 D. A tendency can also be seen for the mobility (molecular shape and charge distribution) of the protein. Showing higher mobility for a more stable variant. To ensure that these findings were not just a coincidence, other thermostable and solvent-tolerant proteins were considered in the comparison. Therefore, (thermostability stated in °C) Cal-A (90 °C),[156] Bc-st-ADH (~70 °C),[157] Chol-Ox (85 °C),[158] CYP119 (91 °C)[159] and P450-BM3 (58 °C)[160] were chosen for the comparison. Those thermostable enzymes, including heme containing enzymes such as CYP119 and P450-BM3 also showed high hydrophobicity moments with smaller dipole moments. To complete the picture, a non-stable enzyme, namely LK-ADH[161] were included, which shows a low hydrophobicity moment. In order to validate the hypothesis about the utilizability of protein descriptors to enhance the thermostability of an enzyme, mutations with respect to the mentioned properties by choosing mutation sites on the surface randomly were screened.

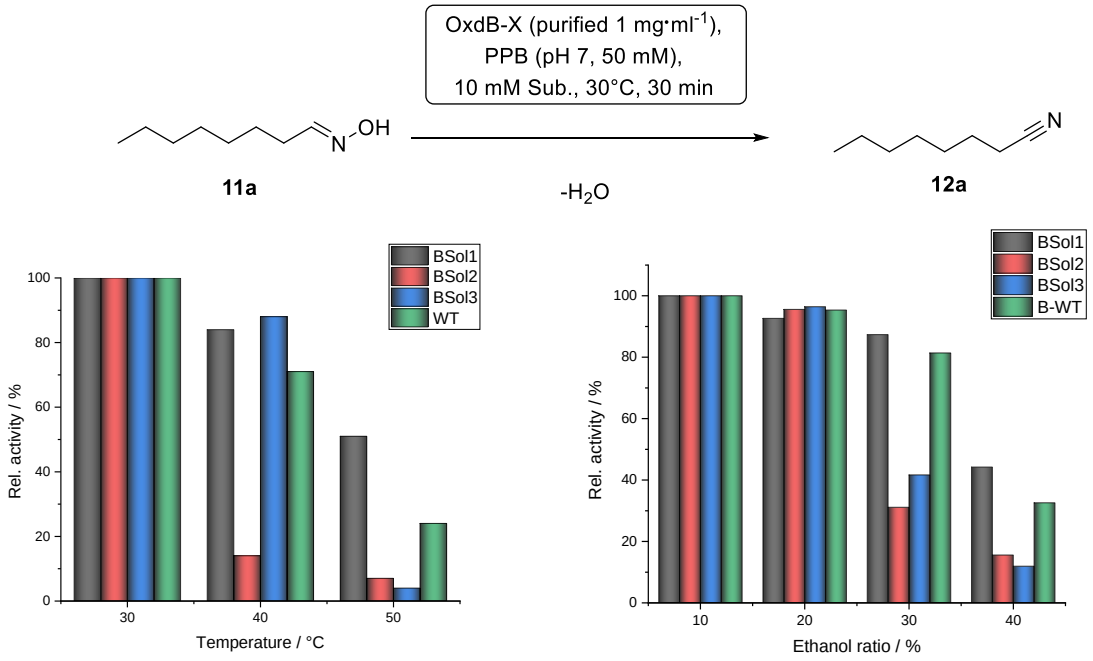

Scheme 36: Thermo and solvent stability investigation with OxdB-Sol derivatives and OxdB-WT. The thermostability investigation was carried out with 1 mg·mL^{-1} purified enzymes. The solvent tolerance study was carried out with 30 mg·mL^{-1} whole cell catalyst.

Initially, the mutants were divided depending on their position in secondary structure elements to investigate if these values can be improved randomly or not. From these mutants OxdB-Sol1 (M19L/P20R/P36R) with mutations on the loops showed enhanced properties in terms of stability and solvent tolerance (**Scheme 36**). The *in silico* determined hydrophobicity moment with these three mutations increased by 173 D and the dipole moment decreased by 189 D (**Table 15**). The thermostability was about twice as high at 50 °C compared to the wild type. The solvent tolerance could be stated as slightly improved with about 10% higher relative activity at 40% ethanol

ratio. This result indicates that the chosen methodology represents a good possibility to achieve a strong increase in the enzymes thermostability. However, the probability of introducing destabilizing mutations by randomly selecting the mutation sites is very high, since only one out of three variants showed improved stability. As that many mutations must be introduced to change the properties of the protein a reliable set of mutation sites has be to be obtained first.

Using database analysis promising mutation sites can be identified, which are not conserved or essential for the protein (ligand binding, ion- and intermolecular interactions). The identification can be achieved by using a primer sequence analysis[162], but the primer sequence has the disadvantages that its prediction reliability is depending on large library size and codon usage. With only eight known aldoxime dehydrases a primary sequence analysis is not a valid option. In comparison 3DM generates large libraries with its own numbering scheme by generating subfamilies of proteins based on their structural similarities and even integrates them into their evolutionary relationships. Those protein structures are either crystal structures or models generated by integrating metagenome databases.

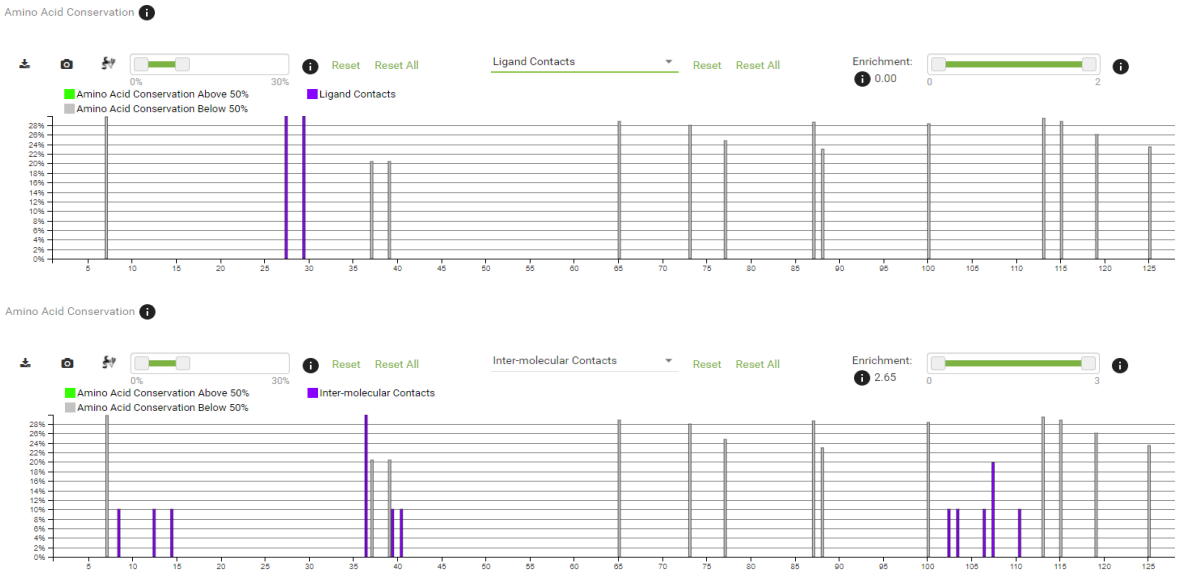

Figure 39: Illustrative example of 3DM-Sorting. Using structure-based subfamily alignment to identify conserved amino or essential amino acids. Grey bars are positions with conservation below 30%. Purple bars are essential amino acids which either interact with ligands, ions or intermolecular.

Using this alignment of 3DM, amino acids below 30% conservations were targeted with further refinements excluding sites, which had ligand-, ion- or intermolecular contacts. 34 mutation sites were obtained (**Figure 39**). In the section (**Figure 39**), some selected positions that are below the 30% limit (grey), as well as not included positions (purple) because of their ligand or intermolecular interactions, are shown. This selection should then result in possible mutations, which would not influence the function or structural integrity of the protein. In combination with MOE, these positions where then used for *in silico* saturated site directed mutagenesis screening for possible variants with respect to their properties of hydrophobic moment, dipole moment, mobility, and stability. The stability function (ΔG) was used to identify strong destabilizing variants. The mutation sites appeared to be only on the surface, which was expectable due to hydrophobicity and dipole moment screening but was not intended (**Figure 40**). The designed mutant OxdB-Set1 was a 10-fold mutant of OxdB-WT, but expecting that even with an high accuracy of over 90%, the probability that a 10-fold mutant would be correctly expressed and folded were too low, which in the end was the case and the designed mutant was only found in the insoluble

fraction (**Figure 41**). The prediction even showed that three mutations S340I, E348V and T350I would destabilize the protein.

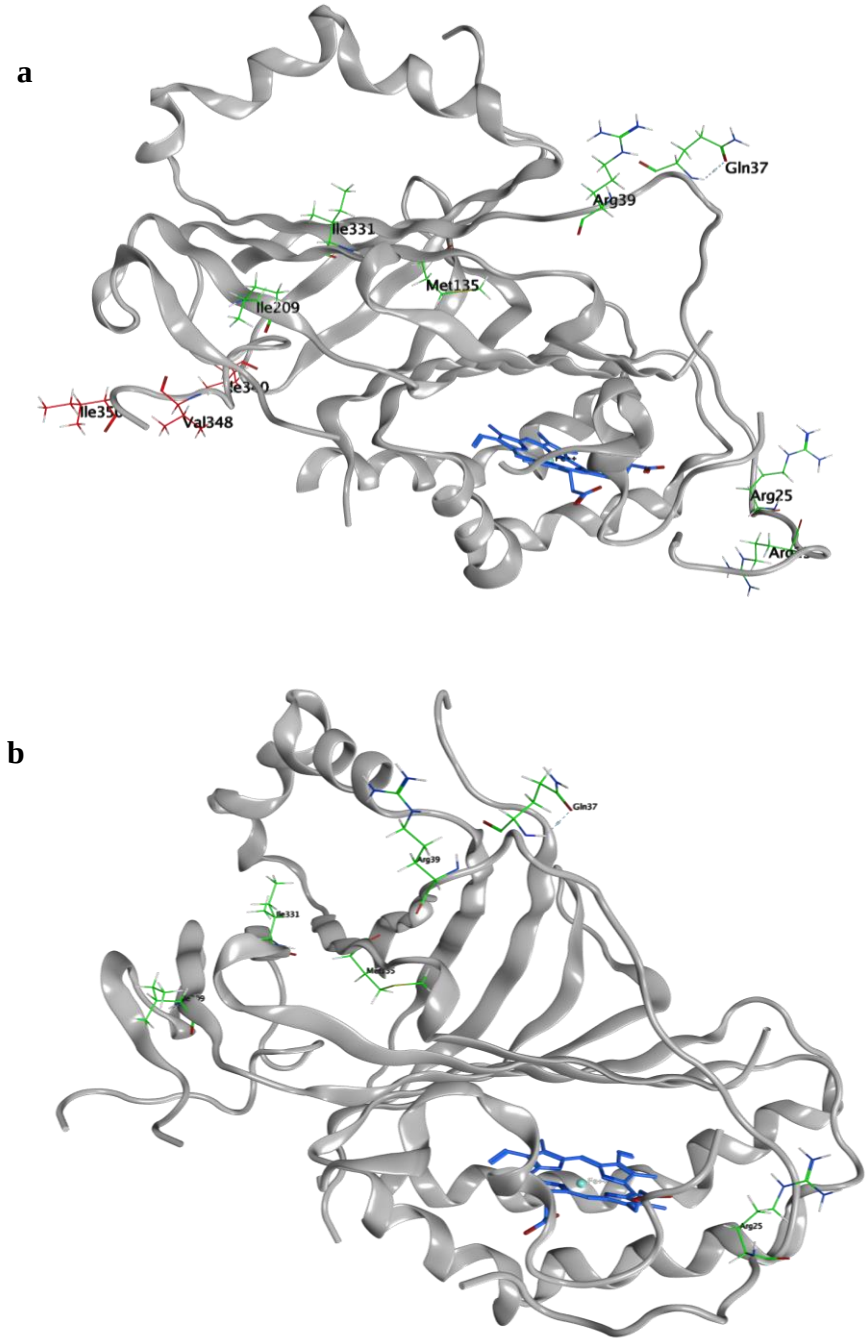

Figure 40: a) Model of OxdB-Set1(H23R/P25R/E37Q/S39R/T135M/T209I/E331I/S340I/E348V/T350I). b) model of OxdB-Set2 (P25R/E37Q/S39R/T135M/T209I/E331). Introduced mutations are highlighted in red (destabilizing mutations) and green (stabilizing mutations). Heme b highlighted in blue.

Therefore, Set1 was split into two different mutation sets (Set1a, Set1b). The splitting of the mutation sets showed that Set1b was also only found in the insoluble fraction (**Figure 41**), concluding that at least one mutation in Set1b was essential for OxdB.

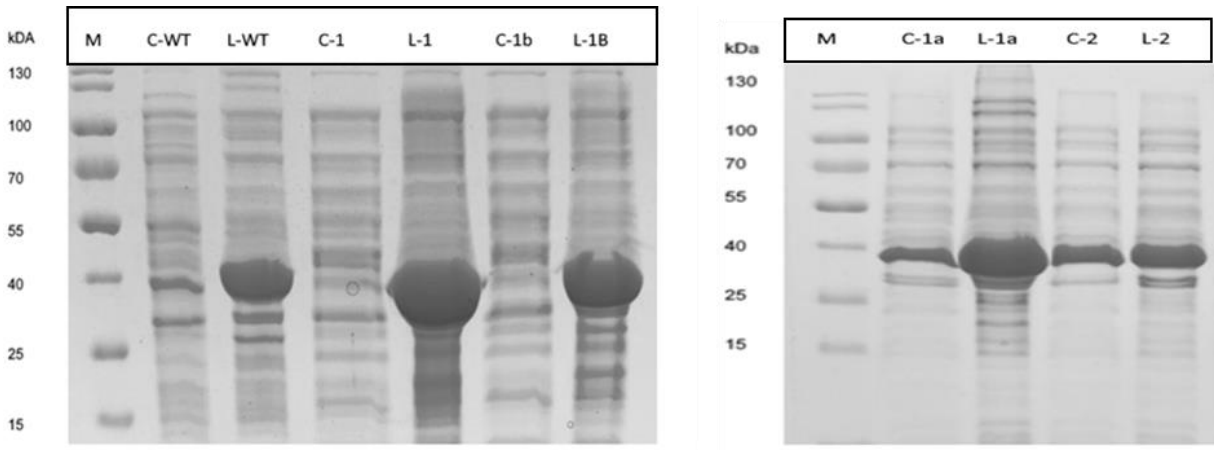

Figure 41: SDS-PAGE showing the expression of OxdB-WT (WT), OxdB-Set1 (1), OxdB-Set1a (1a), OxdB-Set1b (1b) and OxdB-Set2 (2) as crude extract (C) and lysate (L). M: Marker (*PageRuler Prestained, thermo scientific*), protein band located at 40 kDa.

As mentioned before the mutants were designed using the descriptors (hydrophobicity-, dipole moment and mobility) as sorting method showing that the difference in the Gibbs-free energy between mutant and wild type is not enough to predict a stabilization. OxdB-Sol1 is more stable than the wild type but from the change in ΔΔG-value the mutant would be less stable. This supports the formulated hypothesis that the descriptors correlate with the protein stability. Furthermore, the first sorting using 3DM to identify mutation sites is crucial showing that the *in silico* stability prediction is strongly dependent on the correct identification of non-conserved positions. Despites that it should have been possible to identify the mutation, which caused the destabilizing effect beforehand, the calculation showed a high increase in ΔΔG-value for T350F with 1.3 kcal $\cdot mol^{-1}$ (**Table 86**, experimental section). To be sure any of Set1b (S340, E348, T350) mutations were excluded for the final mutant OxdBSet2, leading to a well-expressed protein (**Figure 41**). A summary of all designed OxdB-variants, which were obtained using the developed method combining 3DM and MOE, in comparison to the initial variant OxdB-Sol1 are shown in **Table 15**. The hypothesis, that screening only for the Gibbs-free energy does not necessarily lead to a stabilized protein, could be proved wrong, as according to the Gibbs free energy values OxdB-Sol1 (+1.10 kcal$\cdot mol^{-1}$) would be less stable and OxdB-Set1 (-8.91 kcal$\cdot mol^{-1}$) would be much more stable compared to the wild type, which not the case.

Table 15: Cobinational site directed mutagenesis of constructed variants in comparison to the wild type. Showing stablilty, interaction and property changes. Symetric calculation from WT to Mutant.

Mutation	Variant	ΔΔG/ kcal$\cdot mol^{-1}$	Δ Mobility/ $cm^2 \cdot V \cdot s^{-1}$	Δ dipole/ D	Δ hydroph./ D
M19K. P20R, P36R	BSol1	+1.10	+8.61	-189.10	+173.73
H23R, P25R, E37Q, S39R, T135M, T209I, E331I, S340I, E348V, T350I	Set1	-8.91	+14.79	-139.75	+652.91
P25R, T135M, T209I, E331I	Set1a	-2.73	+4.46	-79.99	+255.48
S340I, E348V, T350I	Set1b	-1.54	+2.95	+45.55	+371.90
P25R, E37Q, S39R, T135M, T209I, E331I	Set2	-3.91	+10.45	-116.14	+259.79

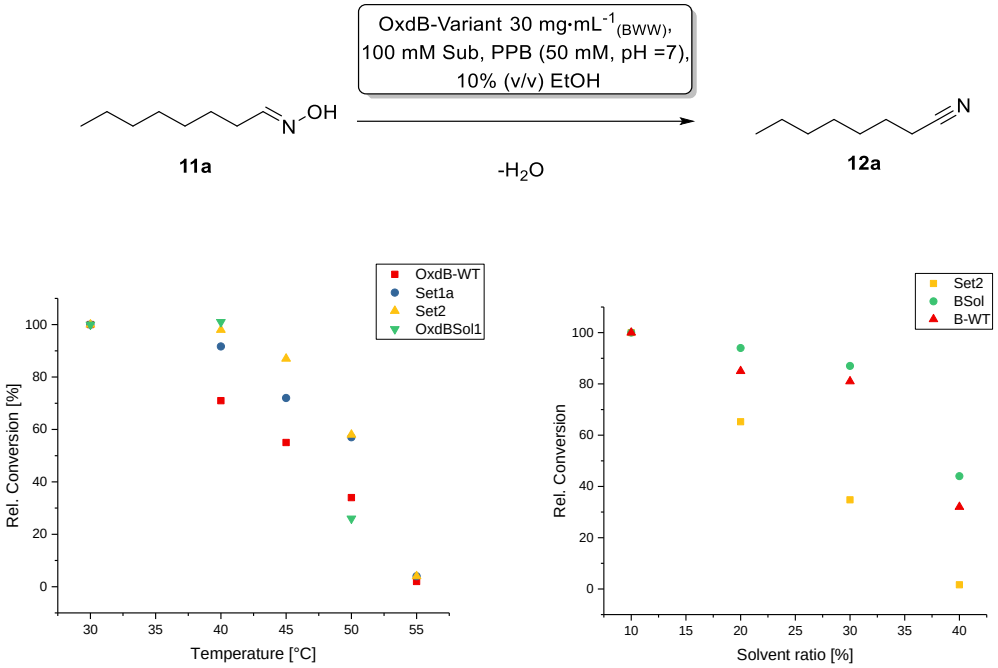

Figure 42: (a) Thermostability comparison of OxdB-WT, OxdB-Set1a, OxdB-Set2 and OxdBSol1. (b) Solvent tolerance of OxdB-Set2 in comparison with OxdB-WT. Rel. conversion relates to residual activity after an incubation period of 30 mins. The reactions were conducted for 15 mins at 30 °C with 100 mM substrate and 30 mg·ml^{-1} (BWW). OxdBSol-1 reaction parameters (Scheme 2)

The experimental stability was determined via biotransformations with 30 mins incubation time at the target temperature or solvent ratio. The reactions were started by the addition of octanal oxime (100 mM) at 30 °C for 15 mins. The resulting residual activity was plotted against temperature or against solvent content. DSF methods to determine melting temperatures were not conducted, due to the lack of an his-tag, which was avoided because of possible interference with the stability. The thermostability of OxdB-WT, OxdBSol1 and the 2 different OxdB-Sets are shown in **Figure 42**. OxdB-Set2 showed the highest thermostability with 90% residual activity at 45 °C, while the wild type has only 50% residual activity left, showing an enhance in thermal stability. The additional two mutations of Set1a towards Set2 increased the stability, showing 10% more residual activity at 45 °C. The solvent tolerance was also determined, but unfortunately OxdB-Set2 has decreased solvent resistance compared to the WT. The first initial variant OxdB-Sol1 did not show a loss in solvent tolerance, concluding that not the method itself led to the loss, but more likely that one of the mutations was crucial for the for the formation of a water shell or surface itself. From the observation of the findings and in the comparison of the mutants, it can be assumed that the mutation T209I or E331I cause the solvent lability. However, this issue was not investigated further. To avoid this problem in future calculations, a modifications of surface proteins from hydrophilic amino acids towards hydrophobic amino acids such as leucine, valine and isoleucine could be avoided and alternatively, other amino acids that also improve the protein properties could be used, even if the improvements are moderate.

5.3.2 Conclusion for the stability improvement method

Increasing the thermostability with the combination of protein descriptors and structural alignments has proven to be a possibility as an application for biocatalysis. The idea of combining structural database to identifying non conserved amino acids with force field calculations or in general other predictors can improve the prediction

ability. Also including further descriptors such as hydrophobicity moment and dipole moment could enhance to predictive power. Claiming that using protein descriptors the predicted mutations led to smaller, but more reliable changes and increasing the stability with the number of mutations adding up.

5.4 Increasing the activity of OxdB by rational design

In order to investigate the activity and acceptance of the substrates for the enzyme, docking studies were carried out with fatty aldoximes. As software MOE[94] was used, which has proven to be a powerful tool in several other works.[95,97] From the previous work[48] a suitable docking model was already available, which was used to perform a fatty aldoxime docking with OxdRE (aldoxime dehydratase from *Rhodococcus erythropolis*) and compared it then with the homology model of OxdB. The reason for using OxdB rather than OxdRE is that *Hinzmann et al.*[28] already showed the capabilities of this enzyme. Part of this work was to improve this enzyme further. Through the analysis of this data all fatty aldoximes fit in the active site with the alkyl chain oriented in direction of the entrance site (**Figure 43**). With increased chain length, the required space in the entrance is increasing. Thereby, the hypothesis was raised that the fatty aldoximes do not need to be fully incorporated in the active site. The fact that dodecanal oxime is already too large to be completely incorporated in the active site, but still being converted, indicates that the enzymes conformational change for a transformation does not include a fully closed entrance. In order to increase the activity, the entrance either has to be more hydrophobic or enlarged. Since the entrance is quite short and less tunnel shaped, hence it was decided to just enlarge it in order to increase the probability of the substrate finding the active site and decrease hindrance.

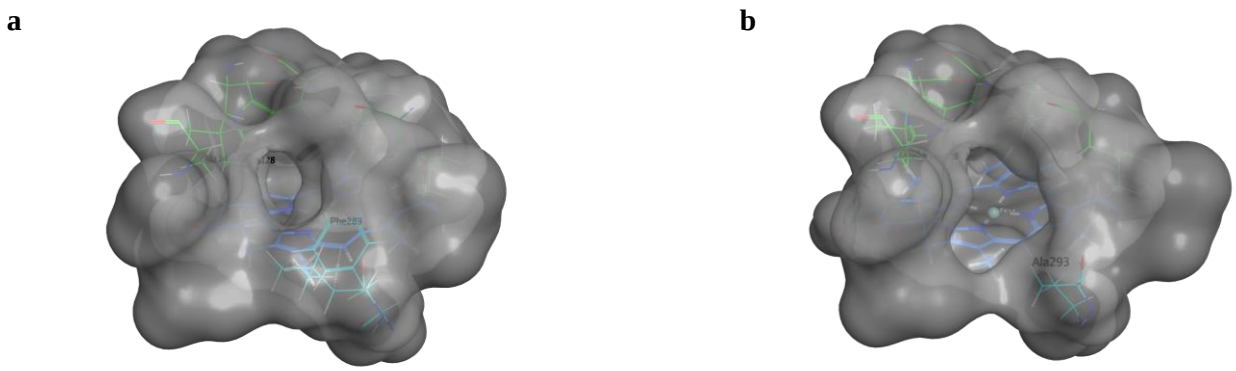

Figure 43: Modeled surface of OxdB-WT (Figure a) and OxdB5 (F289A/L293A) (Figure b). Showing enhanced entrance site for the mutant compared to the wild type.

In chapter **5.3** an *in silico* method to increase the thermostability of an enzyme using aldoxime dehydratase as example with 3DM[153] and MOE[94] as computational tool was introduced. For this work the thermostable enzyme (OxdB-Set2) and the wild type (OxdB-WT) were compared with the engineered protein (OxdB5, enhanced entrance site) in terms of activity and performance. The activities of these three enzymes were determined via biotransformation with octanal oxime as substrate (**Table 16**). The activities of OxdB-WT and Set2 are similar and in the range of 200 $mU \cdot mg^{-1}$. OxdB5 with the modified entrance site has 2.5-fold higher activity with 490 $mU \cdot mg^{-1}$ (**Table 16**).

Table 16: Activity of OxdB-WT, OxdB-Set2 (thermostable) and OxdB5 (increased entrance) with octanal oxime (100 mM) as substrate. The reaction was carried out at 30 °C with 11 mg·mL^{-1} Oxds as whole cells and 10 min reaction time.

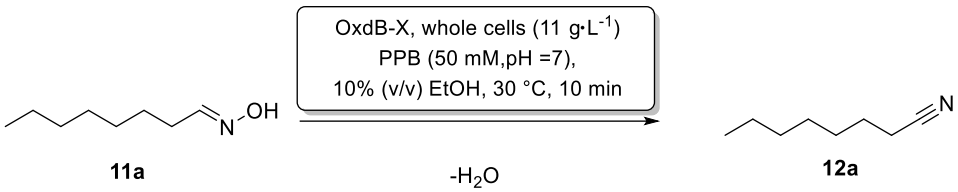

#	Enzyme	Substrate	Conversion / %	Activity / mU·mg^{-1}
1	OxdB-WT	C8	22	200
2	OxdB-Set2	C8	20	180
3	OxdB5	C8	54	490

To investigate the impact of an increased entrance site or a thermostable enzyme, biotransformation with a low soluble substrate (dodecanal oxime) were carried out at different reaction temperatures (**Table 17**). At 30 °C reaction temperature, OxdB5 showed the highest conversion with 6%, while OxdB-WT only showed 2% and OxdB-Set2 3% conversion. By increasing the reaction temperature to 40 °C the overall conversion can be increased. The thermostable mutant Set2 and the mutant with modified entrance site OxdB5 both reach 25% conversion, while the wild type only reached 15% conversion. At a reaction temperature of 50 °C OxdB-Set2 with the highest thermostability reached the highest conversion with 15%, while OxdB5 cannot operate at 50 °C. The WT still reached moderate conversion of 9%. For preparative syntheses with these enzymes, temperatures above 30 °C are still not suitable.

Table 17: Comparison of OxdB-WT with OxdB-Set2 (thermostable) and OxdB5 (increased entrance) in their perfomance for the conversion of dodecanal.

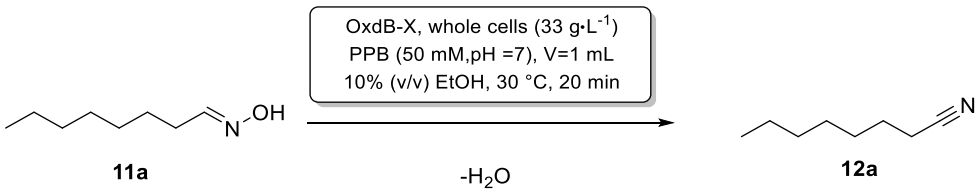

#	Enzyme	Substrate	Concentration / mM	temperature / °C	Conversion / %
1	WT	C12	100	30	2
2	Set2	C12	100	30	3
3	B5	C12	100	30	6
4	WT	C12	100	40	15
5	Set2	C12	100	40	25
6	B5	C12	100	40	25
7	WT	C12	100	50	9
8	Set2	C12	100	50	17
9	B5	C12	100	50	1

Even though the thermostable variant OxdB-Set2 and the OxdB5 showed the best performance at 40 °C with 25% conversion, it is important to mention here that these reactions were performed with 20 min reaction time and 100 mM substrate concentration. For preparative syntheses in 1 M range or higher, long reaction times are required. Therefore, a preparative synthesis of different fatty aldoximes with OxdB5 were conducted, which showed the

best performance at 30 °C. As substrates fatty aldoximes from dodecanal oxime up to hexadecanal oxime were used. To ensure comparability with the work of *Hinzmann et al.*[28] the same reaction setup was chosen for the preparative scale reaction of OxdB5 and OxdB-WT (**Table 18**).

Table 18: Biotransformation of OxdB-WT and OxdB5. Using long chain fatty aldoxime as substrates for preparative scale reactions. The reactions were performed by *Jianing Yang* in her master thesis.[163]

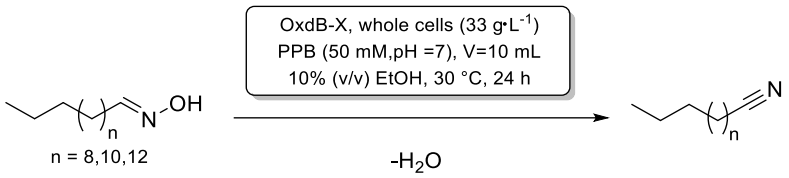

#	Enzyme	Substrate	Concentration / mM	BWW / mg·ml^{-1}	Conversion / %	Yield / g
1	B-WT	C12	1000	33	33	n.d
2	B-5	C12	1000	33	53	n.d
3	B-5	C12	1000	66	99	65%
4	B-5	C14	250	33	>99	89%
5	B-5	C16	250	33	54	n.d

n.d = not determined

In the reaction performed in preparative scale, it was possible to proof that the engineered variant of OxdB (OxdB5) is able to convert higher fatty aldoximes from dodecanal oxime up to hexadecanal oxime, surpassing its limitations and increasing the application range of these enzymes, by showing quantitative conversion and moderate yields up 89% (**Table 18**). The reaction speed could be further optimized by increasing the solubility of the fatty aldoximes. The solubility issue can be targeted with the combination of a thermostable variant and OxdB5 using higher reaction temperatures leading to more dissolved substate, an alternative approach using immobilization techniques to perform the reaction organic solvent was also attempted (chapter 6.3).

5.4.1 Conclusion of improved fatty nitrile synthesis using rationally engineered OxdBs

Higher fatty aldoximes appeared to be very inconvenient for biocatalytic reaction, due to their insolubility in water or solvents like dodecane. Therefore, it is difficult to find a suitable system, in which the enzyme and the substrate can interact with each other. The approach to increasing the thermostability of the enzyme proved to be good option to optimize the reaction. However, it turned out that the enzyme has to be even more stable than the variant that was generated in this work (OxdB-Set2). In fact, the best transformations were achieved by a rationally modified enzyme witch an increase entrance site (OxdB5). This variant showed increased conversions for lower fatty aldoximes and the successfull preparative transformation of higher fatty aldoximes with the best example of 250 mM tetradecanal aldoxime. For future perspective the two types of OxdB-Variants could be combined or the stability could be further increased in order to perform preparative scale reactions at higher temperatures. Another alternative could also bean encapsuling technique to perform the reaction in organic solvent, which will be discussed in chapter 6.

6 Compatibility of hydroxylamine and aldoxime dehydratase using Pickering emulsion in flow

6.1 State of the art and motivation

Performing multi-step cascade reactions in "one-pot" is one of the most difficult tasks and at the same time one of the most elegant ways to minimize the E-factor (mass efficiency) of a chemical process.[164] By minimizing the number of processing steps, the use of solvents can be reduced and the space-time yield increased. The cost-efficient use of solvents and production time plays especially in bulk chemical sector a big role. For bulk chemicals, which are in the high-volume low prize segment, an efficient chemical process is crucial in determining whether a product can be manufactured profitably. Another point when designing a new synthesis or optimizing an already applied method, is sustainability. With reference to our present situation of human interference with nature, even the small discoveries and minor improvements can have a significant impact towards ecological friendly synthesis. By using biocatalysts, the use of highly toxic substances can be avoided to a great extent or even completely, thus significantly increasing sustainability.[165]

A special class of bulk chemicals are the fatty nitriles with prominent examples hexane nitrile and nonane nitrile. The synthesis of these nitriles starting from aldoximes has already been demonstrated biocatalytically on a preparative scale. However, the direct conversion of the aldoxime after formation from aldehyde and hydroxylamine was not possible. Even a sequential synthesis after completion of the aldoxime formation could not be achieved, because excess of hydroxylamine deactivated the enzyme already in small amounts (1 mM), as *Carmen et al.*[39] could show in intensive studies. Alternatively, they also showed that a sequential approach is possible by heating the reaction solution. In this section, a method that allows the compatibility of the aldoxime formation with the biocatalytic nitrile synthesis in a simultaneous one-pot reaction will be discussed. This will involve the use of silica particles stabilized Pickering emulsions. *Bago Rodriguez et al.*[146] already showed that the enzymatic conversion of aldoxime in Pickering emulsion consisting of a water and dodecane phase is possible. In their investigations, they focused on the proof of concept and the physicochemical properties of the formed emulsions. By applying silica particles with different hydrophobicities the emulsion type (w/o or o/w) and properties could be changed.[166] With high silanol content (SiOH, >51%) oil in water emulsion are formed, while a low silanol ratio (SiOH, <51%) leads to water in oil emulsions. The encapsulation of the biocatalyst in the water in oil emulsions allows the reaction to proceed in pure organic solvent.

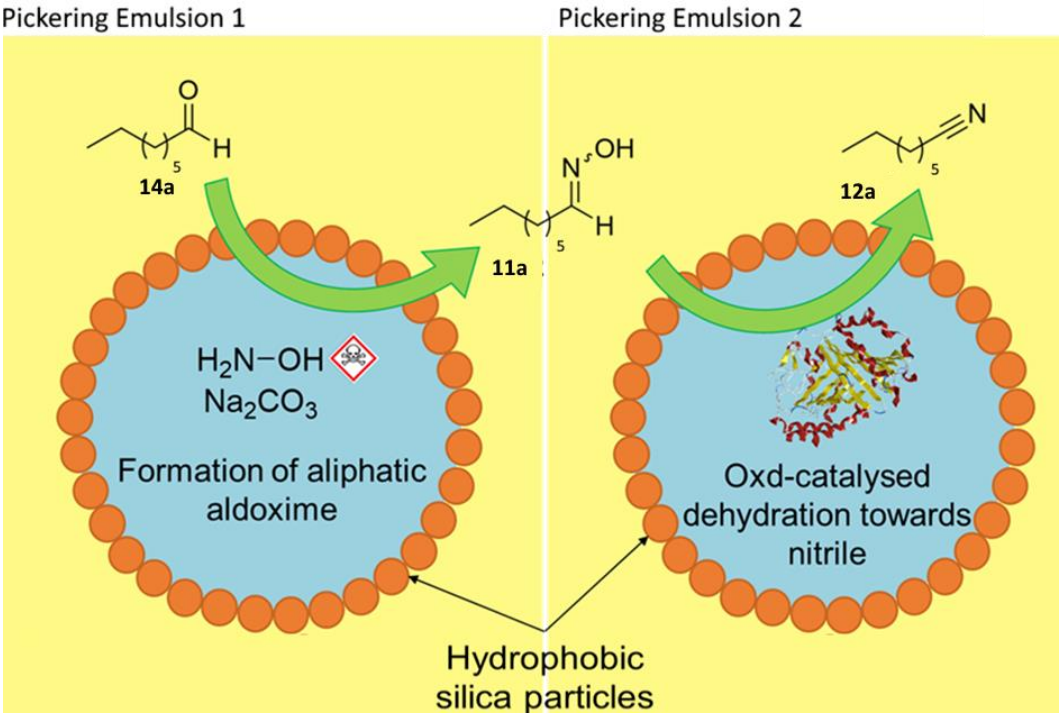

Figure 44: Envisioned concept for using Pickering emulsions to enable combination of aldoxime formation using hydroxylamine and subsequent dehydration towards *n*-octanenitrile (**12a**) and in a two-step one-pot cascade.[167]

The prerequisite of this concept is that two formed w/o emulsions can be mixed in a microreactor, without aggregation of the different aqueous droplets. Therefore, two different kind of Pickering emulsions with variable content can be used in one reaction. One emulsion (Pickering emulsion 1, PE1) contains the hydroxylamine in the aqueous phase and in the other emulsion (Pickering emulsion 2, PE2) the enzyme is present with the aldehyde as starting material (**Figure 44**). This concept of using two Pickering emulsion to enable the combination of aldoxime formation and subsequent dehydration was conceived by *Schober et al*.[167] While the aldehyde can diffuse in both emulsions, whereas in PE1 it can react with hydroxylamine to the aldoxime, the enzyme and hydroxylamine are trapped in the emulsions. The aldoxime, which is soluble in dodecane, can freely move through the organic phase into the enzymatic aqueous phase (PE2), where Oxd-B converts it to the nitrile. *Schober et al*.[167] showed that the combination of aldoxime formation and enzymatic dehydration performs well in batch, without any mixing. The mixing with a stirrer is restricted due to the shear forces, which would otherwise destroy the emulsions. Therefore, to further increase the performance investigation of the Pickering emulsion mediated reaction using an inverter and a flow set up (this work) as alternative mixing method, were performed.

6.2 Pickering emulsion enabled combination of aldoxime formation and biocatalytic nitril synthesis in flow

For the cascade reaction of octanal towards octane nitrile OxdB-Sol1, which is a good performing enzyme in terms of stability and activity, were used. The first flow reactions were carried out with 51% SiOH particle for both emulsions. The two emulsions were prepared separately, whereas Pickering emulsion 1 (PE1) contained hydroxylamine OxdB-Sol1 and octanal and Pickering emulsion 2 (PE2) contained OxdB-Sol1 and octanal (**14a**) (**Figure 45**). The two emulsions were mixed through a T-piece before entering the reactor with a volume of 3 mL, the overall flow rate of 1.5 mL·h^{-1} (0.75 mL·h^{-1} /syringe) lead to a residence time of 1 hour.

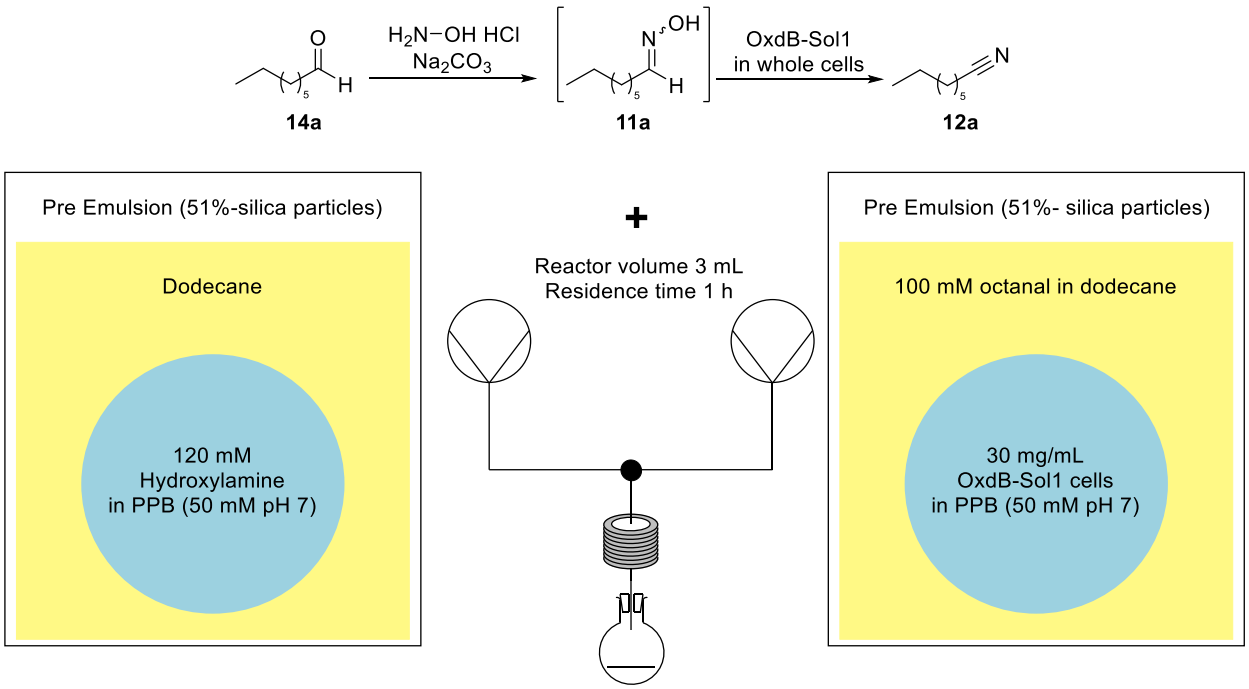

Figure 45: schematic composition of the two emulsions combined for the tandem process to obtain *n*-octanenitrile (**12a**) from octanal (**14a**) via *in-situ* aldoxime formation using hydroxylamine at different substrate and cell concentrations.

The reaction cascade did lead to a maximum conversion of 36%, However, there was a high fluctuation in the conversion, determined via samples taking at different times. The fluctuation could be explained by inhomogeneous flow caused by inclusion of air during filling and insertion of the syringes. Furthermore, it could be shown that only up to 40% of the aldehyde was consumed. Therefore, the aldoxime formation was observed separately and it was clarified that the performance of the reaction differs greatly from experiment to experiment. By closer examination of the workflow, the homogenizer was identified as origin of the problem. It was observed that, after a few emulsions the metal blade was already deformed and thus strongly impaired the quality and type (w/o or o/w) of the emulsion.

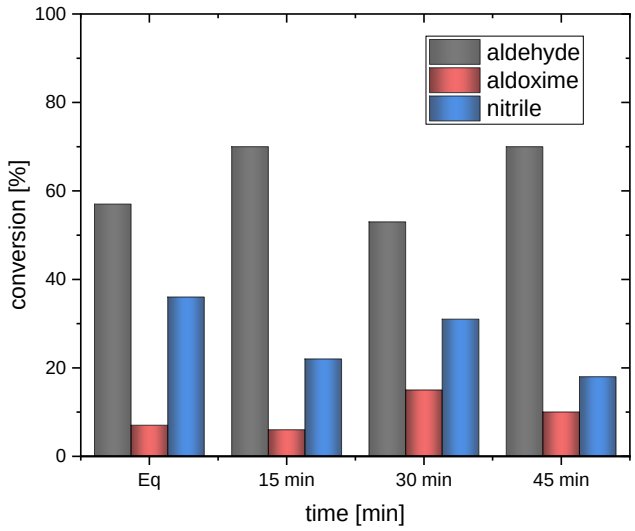

Figure 46: Conversion of the whole reaction cascade with hydroxylamine (120 mM) in PE1, OxdBSol1 (30 mg·mL^{-1}) and aldehyde (**11a**, 100 mM) in PE2 was performed with a flow rate of 1.5 mL·h^{1}, a reactor volume of 3 mL and a residence time of 60 minutes. Samples were taken every 15 mins.

When examining the aldoxime formation, it was found out that this step is not limiting as long as the emulsion was prepared correctly (**Figure 46**). The relatively low nitrile formation suggested that hydroxylamine may have leached from PE1. Therefore, the enzymatic reaction was also performed separately. For the reaction, octanal oxime was used instead of octanal in PE1 with different concentration of hydroxylamine. Hydroxylamine showed a strong decrease in conversion at the concentrations tested. The conversion dropped from an average 85% to an average of 20% when using 120 mM hydroxylamine and even at 300 mM hydroxylamine concentration nearly 10% conversion could be observed (**Figure 47**). Compared to the standard biotransformations without PE, 1 mM was already sufficient for complete deactivation.[39]

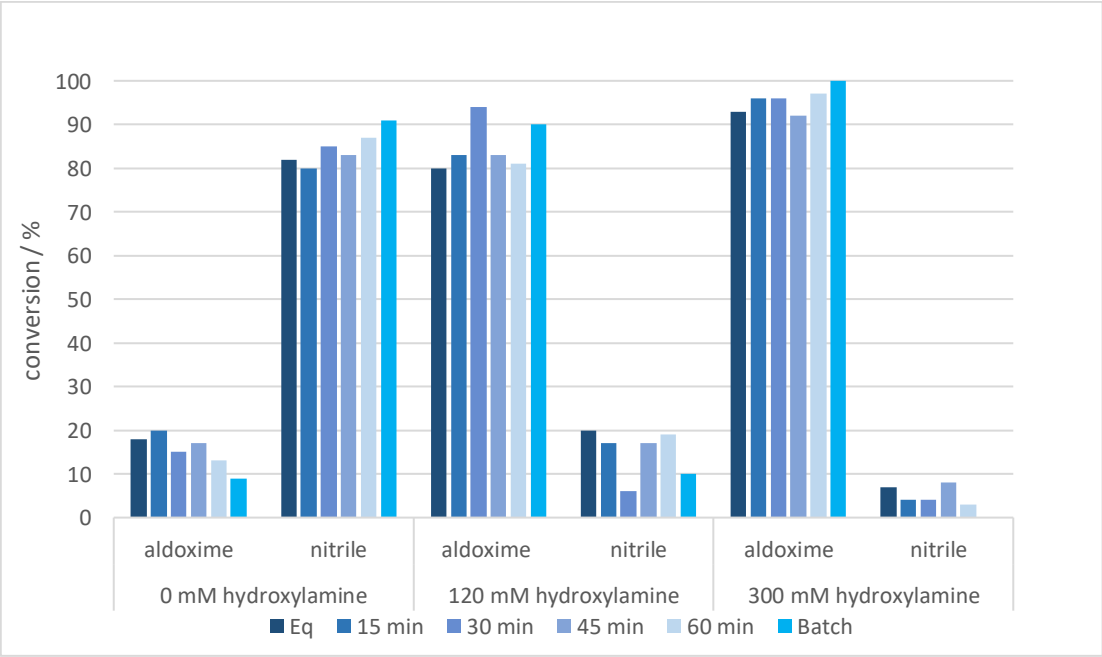

Figure 47: Pickering emulsion mediated biocatalytic nitril (14a) formation in flow. With aldoxime (**12a**, 100 mM) and hydroxyl amine (0-300 mM) encapsuled in PE1 and OxdBSol1 (30 mg·mL^{-1}) in PE2. The reaction was performed with a flow rate of 1.5 mL·h^{-1}, a reactor volume of 3 mL and a residence time of 60 minutes. Samples were taken every 15 mins.

Since 1 mM would be enough to inactivate the enzyme means that only a very small proportion in the range of >0.5% comes into contact with the enzyme.

In addition, the batch reaction showed significantly lower conversion and no conversion was observed at a hydroxylamine concentration of 300 mM. This shows the clear advantage of the flow reaction over the batch reaction. The comparison also revealed that the emulsions are not destroyed by the flow procedure, which would indicate higher conversion for the batch reaction. Therefore, hydroxylamine either leaches out of the emulsions or residual hydroxyl amine either by incomplete emulsifying or deformed emulsions are the cause for the inactivation of the enzyme.

To address this problem octanal and hydroxylamine were prepared in the same Pickering emulsion, whereby the aldoxime formation already proceeds during emulsion preparation and the total hydroxylamine concentration in the system is reduced. This modification led to an optimized reaction cascade of incompatible reaction steps in a two-step one-pot operating procedure. Thus, conversions of up to 56% could be achieved in one hour, compared with only 42% in the batch reaction. To achieve complete conversion, only the reaction time would have to be increased by enlarging the reactor volume or reducing the flow rate. Former option was due to the accessibility of particles not possible and latter couldn't be achieved with the used setup due to increased inhomogeneity in the reactor.

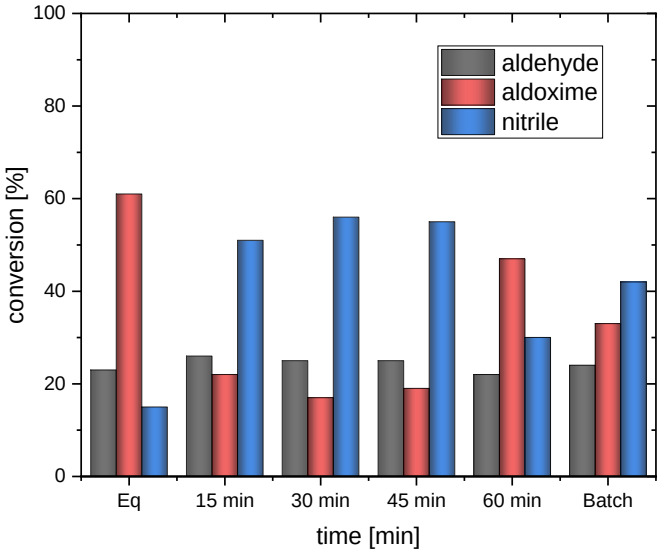

Figure 48: Conversion of the whole reaction cascade with the aldehyde (**11a**, 100 mM) and hydroxylamine (120 mM) in PE1 and OxdBSol1 (30 mg·mL^{-1}) in PE2 was performed with a flow rate of 1.5 mL·h^{1} a reactor volume of 3 mL and a residence time of 60 minutes. Samples were taken every 15 mins. The batch reaction was performed for one hour.

6.3 Addressing highly insoluble substrates with Pickering emulsions

In chapter 5 different approaches to increase the performance of aldoxime dehydratase catalyst dehydration of fatty aldoximes were discussed. In this section the high insolubility of fatty aldoximes were addressed by using PE (**Table 19**). The basic idea was that dodecane should be able to dissolve fatty aldoximes as it is highly hydrophobic and utilized as organic solvent for the PE. Thus, the phase transfer from the organic phase to the aqueous phase should be much faster than the transfer from solid into solution. Therefore, the overall conversion in PE would be higher than in a standard biotransformation in water.

Table 19: Biotransformation in Pickering emulsion as alternative for insolbule substrates with dodecanal- and tetradecanal oxime as substrate

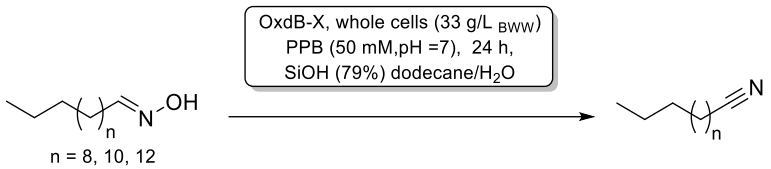

#	Enzyme	Substrate	Concentration / mM	BWW/ mg·ml^{-1}	Conversion / %
1	B-WT	C12	100	33	99
2	B-5	C12	100	33	99
3	B-WT	C14	100	33	19
4	B-5	C14	100	33	31

Contradicting the assumption, the fatty aldoximes starting from dodecanal oxime up to tetradecanal oxime were only poor or not soluble in dodecane, leading to unsatisfactory suspensions. Thus, the presented results show very low productivity compared to usual biotransformation with only 100 mM substrate loading (**Table 19**). Despite the low productivity, it shows the general possibility with this technology. Another two-phase system, with an organic solvent, which is on the one hand better able to solve fatty aldoximes and on the other hand suited for the Pickering emulsion could be an alternative to the standard biotransformation's in water and a thermostable enzyme would be redundant. Since the Pickering emulsion system with Oxds and aldoximes are only established for water-dodecane so far, further attempts were not performed at this stage.

6.4 Conclusion of Pickering emulsion mediated fatty nitrile synthesis

The use of Pickering emulsion as an alternative encapsuling technique to the superabsorbers,[38] for performing enzymatic reaction in pure organic solvent could be demonstrated. Picking emulsion have fluidic properties, while Superabsorber can be described as solidified aqueous phase. The fluidic properties enabled the possibility to use them in flow as mobile phase. Furthermore, the cascade reaction starting from aldehyde over the formation of the aldoxime with the use of the highly deactivating hydroxylamine and the enzymatic dehydration towards the nitrile could be performed as a one-pot reaction. Showing that Pickering emulsions also enables incompatible reaction system to be performed simultaneously by spatial distribution. The best result for the complete cascade reached 56% conversion with 100 mM aldehyde and 120 mM hydroxylamine as starting material. These results illustrate, the general possibilities with Pickering emulsion in organic chemistry as specially for incompatible systems.

Furthermore, the use of PE for insoluble substrate systems were also investigated, resulting in quantitative conversion with dodecanal oxime as substrate. Higher fatty aldoximes were not soluble in dodecane, leading to low conversion for tetradecanal oxime as example (31%). With a different organic solvent suitable for Pickering emulsion and simultaneously able to dissolve fatty aldoximes such as tetradecanal oxime, this system could present an alternative for biocatalytic synthesis of water insoluble products.

7 Summary and outlook

The work focused on the rationalization of the enantioselectivity of aldoxime dehydratases. These enzymes are able to form opposite enantiomers from one substrate depending on the isomeric form of the aldoxime used, which presents an extraordinary characteristic property for an enzyme (**Scheme 37**).

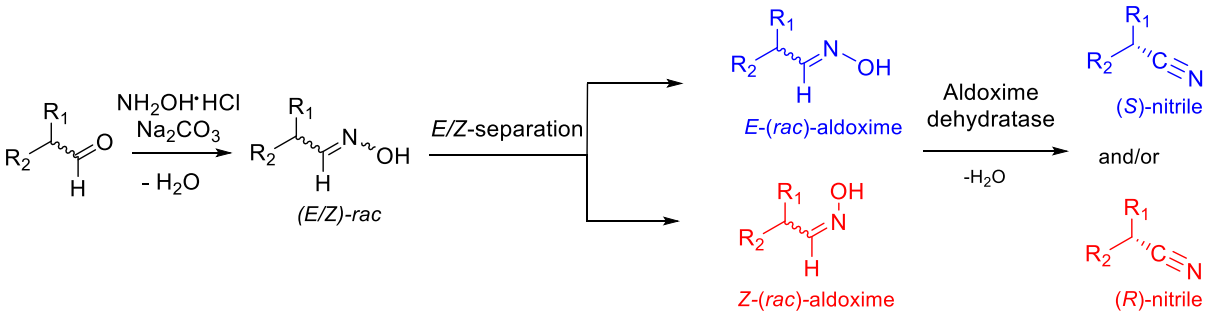

Scheme 37: Enantioselective dehydration of aldoximes towards nitriles with enabling opposite enantiomers depending on the isomer used for the reaction.

This rationalization was made possible by intensive studies *in silico* as well as *in vitro*. Therefore, a model was created to identify the correct enzyme-substrate complex, which in turn was used to calculate and thus predict the enantioselectivity. The special feature of the model was the automated recognition as well as the sortation of the criteria, which were necessary for the enzymatic reaction of a real protein-ligand structure and ensured reproducibility and predictive power (**Figure 49**).

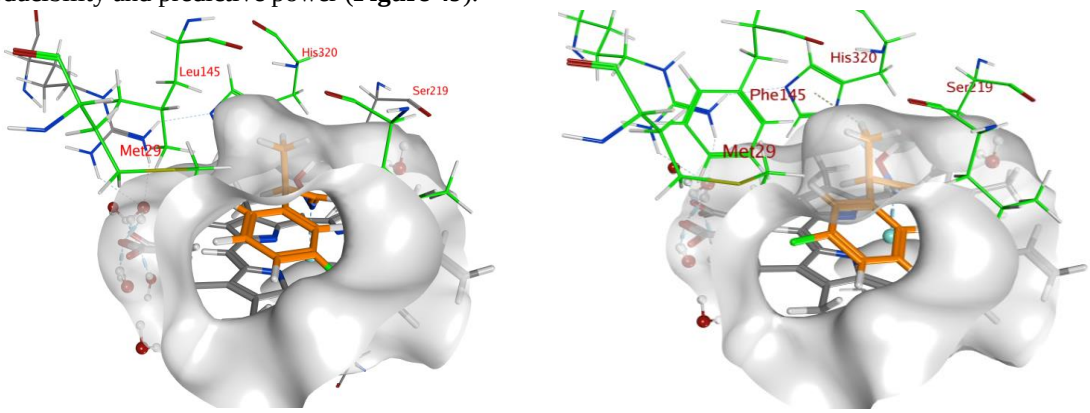

Figure 49: 3-(*Z*,*R*)-FPPOX bound in the catalytic center of OxdRE-WT (a) and L145F (b) with the methyl group in the cavity, which is formed by the amino acids M29, L145, A147 and H320. Showing a smaller cavity for OxdRE-L145F.

The rationalization study revealed that the positioning and orientation of the methyl group of the substrate in the cavity of the enzyme is the reason for the isomer dependent differentiation of the isomers. This hypothesis was proven *in silico* and experimentally. To proof the hypothesis *in silico* individual energy contributions for the binding of the ligand in the active pocket were provided. Furthermore, based on this finding a mutant (OxdRE-

L145F) was created. The variant OxdRE-L145F showed increased enantioselectivity *in silico* as well as experimentally, thus supporting the hypothesis. For example, in the reaction of *rac*-(*E*)-2-FPPOX (**4a**), an E-value of over 200 could be obtained. (**Scheme 38**).

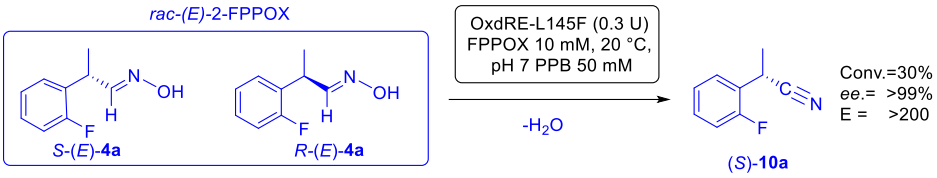

Scheme 38: Enantioselective synthesis of *S*-2-FPPN (**10a**) with *rac*-(*E*)-2-FPPOX (**4a**) as starting material and OxdRE-L145F as biocatalyst.

This model contributed significantly to a better understanding of this (so far rare) phenomenon as well as the enzymatic reaction of aldoxime dehydratases and thus provided the foundation for this work.

The preparation of chiral nitriles utilizing aldoxime dehydratases especially with the designed OxdRE-L145F variant, was possible with excellent selectivities. However, the reaction is strongly limited, firstly by the natural limitation of kinetic resolution and secondly by the necessary purification of the *E/Z* mixture. The purification of the isomers is however limited to similar structural motifs of the 2-phenylpropanal oxime (PPOX) derivatives. Thus, the direct utilization of the *E/Z* mixtures would be more elegant and enable the use of a wide variety of chiral aldoximes.

In order to extend the substrate scope and at the same time optimize the biocatalytic chiral nitrile synthesis, the first mentioned formal double dynamic kinetic resolution (DDKR) was developed. For this purpose, the isomerization as well as the racemization of aldoximes were investigated. The isomerization of aldoximes were achieved with thermal treatment, whereby the isomerization rate could be enhanced by increasing the substrate concentration. Racemization was made possible with thiazoles, with thiamine hydrochloride as the best racemization agent. The enantiomeric excess of (*R*,*E*)-**8** was successfully reduced from 88% to 35% after 24 hours using thiamine hydrochloride (**Scheme 39**).

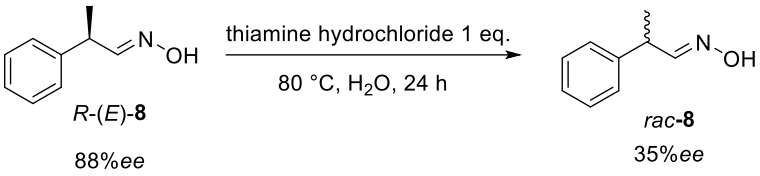

Scheme 39: Racemization of *(R,E)*-PPOX (**8**) with thiamine hydrochloride.

The most selective enzyme at this point OxdRE-L145F, showed an increase for the E-value from 2 (WT) to 4 in the reaction for the *E*/*Z*-mixture of *rac*-2-FPPOX. However, with an E-value of 4 OxdRE-L145F was not sufficiently selectivity for a DDKR and required further optimization (**Scheme 40**).

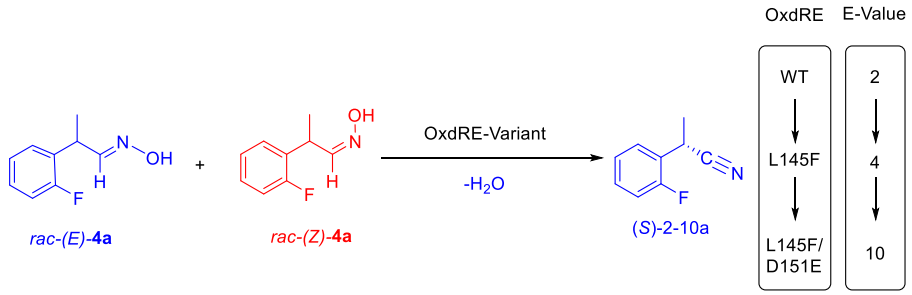

Scheme 40: Demonstration of the reaction with *rac*-(*E*/*Z*)-2-FPPOX and OxdRE variants.

An improved enantioselectivity was finally achieved by screening more than 900 variants as smart libraries, which led to some promising mutants. The best variant (OxdRE-L145F-D151E) even showed an E-value of 10. However, the use in the developed DDKR process as well as the further development of this variant in an iterative saturated mutagenesis (ISM) along with the other hits could not be accomplished in this work and offers an interesting topic for further research (**Scheme 41**). In connection with the process, the expression of the aldoxime dehydratases as well as the access to chiral aldoximes was investigated. An improved expression was achieved by "leaky" cultivation, whereby the activity of OxdRE-L145F as whole cell catalyst could be increased by factor of 100. The multistep substrate synthesis starting from benzaldehyde with only 10% isolated yield was replaced with the hydroformylation of styrenes and subsequent condensation with hydroxylamine. By using this alternative route, the substrates could be obtained conveniently and with high isolated yields reaching 98%.

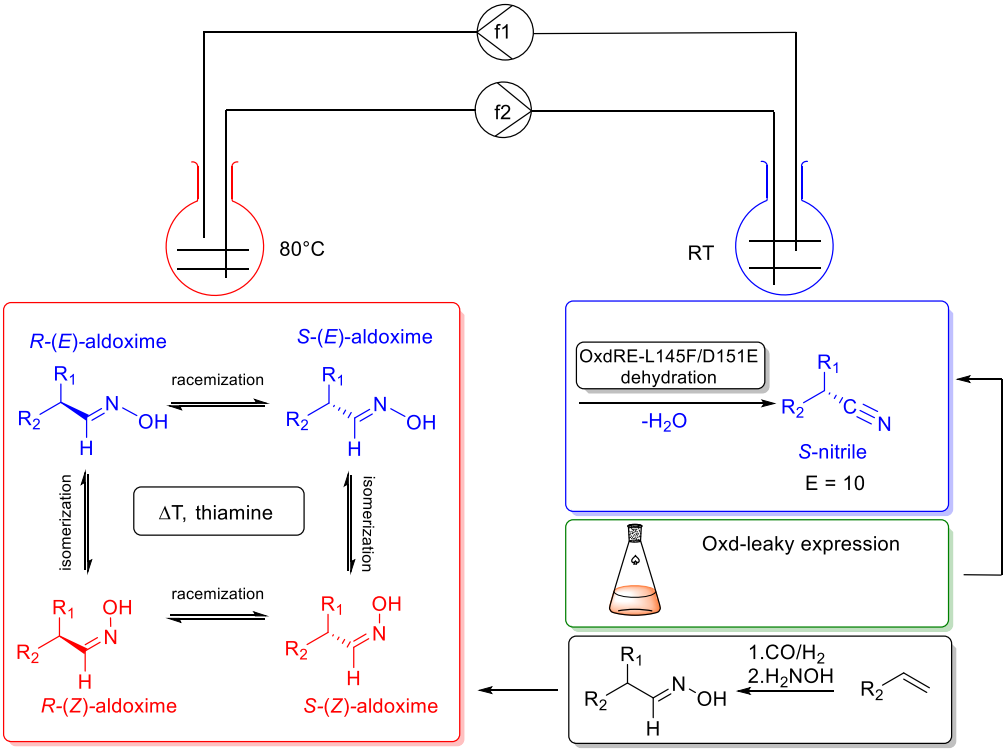

Scheme 41: Summary of the overall developed process in this work. Substrate preparation using hydroformylation (black), biocatalyst preparation (green), chemical racemization and isomerization (red) and nitrile synthesis with an engineered biocatalyst. Representation of DDKR as a flow process with enzymatic nitrile synthesis at room temperature and chemical racemization/isomerization at 80 °C.

In addition, this work dealt with the synthesis of long-chain aliphatic nitriles. In this context, the biocatalytic conversion of fatty nitriles with the largest example of C10 was extended to longer aliphatics substrates such as C12 and C14. For this purpose, the limitation was rationalized and tailored with different approaches. It was also possible to optimize the enzymatic conversion using molecular modeling. The previously developed docking method showed *via* visual analysis that the bound aldoximes such as dodecanal oxime are too large for the active pocket. As a consequence, the alkyl residue of these linear fatty aldoximes protrudes from the short but narrow entrance region. By enlarging the entrance to the catalytic center with OxdB5 (F288/L293A), the activity could be increased by 2.5 times, allowing the quantitative conversion of long aliphatic fatty nitriles for the first time. The poor solubility was identified as main problem for the enzymatic dehydration of aliphatic aldoximes. By raising the reaction temperature or the amount of cosolvent, the solubility of the long-chain aliphatic aldehydes in water can be increased. However, these conditions require as stable enzyme and aldoximes dehydratase are relatively unstable proteins in terms of solvent tolerance and thermostability.

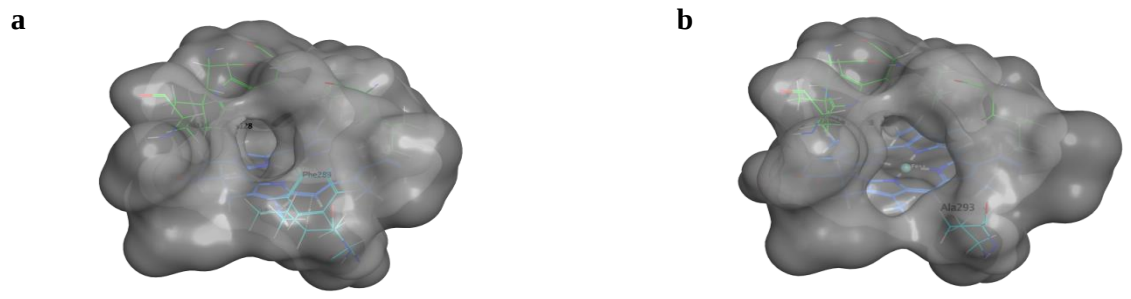

Figure 50: Modeled surface of OxdB-WT (**Frame a**) and OxdB5 (F290A-L294A) (**Frame b**). Showing enhanced entrance site for the mutant compared to the wild type.

In an attempt to increase the stability of the aldoxime dehydratase OxdB, a previously undefined correlation between protein descriptors (hydrophobicity moment, dipole moment, mobility) with stability (thermostability, solvent tolerance) was observed. High thermostability as well as solvent tolerance was found to be related to a high hydrophobicity moment, high mobility and a relatively low dipole moment. This described tendency was not only evident for aldoxime dehydratases, but for proteins in general. It could be shown that utilizing protein descriptors the thermostability of OxdB can be increased, using random mutation sites. The generated variant OxdB-Sol1 showed a doubled thermostability at 50 °C than the wild type. However, only one of three generated mutants showed the increased stability, suggesting that mutation site selection is necessary.

These values can only be significantly improved by multiple mutations. Therefore, a pre-selection of positions, which have little influence on the integrity of the protein was performed. 3DM-database was used to identify these positions, which led to the development of a method to modify proteins at non-essential positions and thus improve their stability. Using this method, a variant, namely OxdSet2 was developed, which showed 45% higher residual activity at 45 °C than the wild type. However, the stability to solvents decreased, so the method still needs to be optimized. The developed method for the prediction of mutations, which increase the stability of a protein, offers a new alternative in comparison to the present known calculation methods. Furthermore, this approach is also a possibility to extend the already existing stability predictions.

In this work, it was possible to improve the selectivity, activity and stability of aldoxime dehydratases using molecular modeling (**Figure 51**).

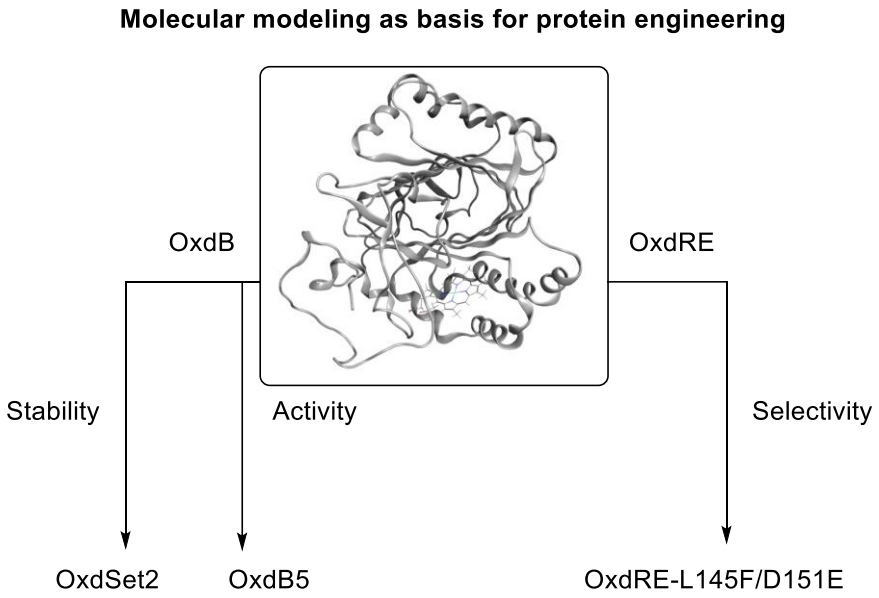

Figure 51: Overview of improved protein properties such as selectivity, activity and stability with molecular modeling as basis.

Furthermore, work was carried out on a method developed by *Lukas Schober*[167] for the compatibility of hydroxylamine with aldoxime dehydratase in a two-step one-pot synthesis of a nitrile starting from aldehyde using Pickering emulsions. The aim was to demonstrate that the Pickering emulsion[146] required for compatibility can also be used in a flow-system. The synthesis of octane nitrile from octanal within this system was successfully demonstrated. Within one hour retention time and 120 mM hydroxylamine present 56% conversion towards octanenitrile could be achieved, whereas in a standard biotransformation 1 mM hydroxylamine is sufficient enough to inactivate the enzyme.[39]

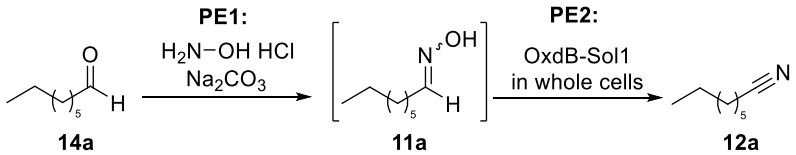

Scheme 42: Tandem process of *n*-octanenitrile synthesis in Pickering emulsions.

In connection with Pickering emulsions, which presents a two phase system (water/dodecane) attempts were made to address the problem of solubility of aliphatic aldoximes. The idea was that higher fatty aldoximes could be solved in dodecane and thereby becoming more accessible to the enzyme. Although the synthesis of dodecane nitrile with OxdB was successfully carried out in Pickering emulsion, longer aliphatics such as C14 did not dissolve in dodecane. A suitable choice of solvent that solves higher fatty aldoximes and forms Pickering emulsion could provide an alternative synthesis option for insoluble substrates.

8 Zusammenfassung und Ausblick

Die vorliegende Arbeit befasste sich mit der Rationalisierung der Enantioselektivität von Aldoximdehydratasen. Die Enzyme sind in der Lage aus einem Substrat gegensätzliche Enantiomere zu bilden und dies in der Abhängigkeit von der verwendeten isomeren Form des Aldoxims (**Schema 1**).

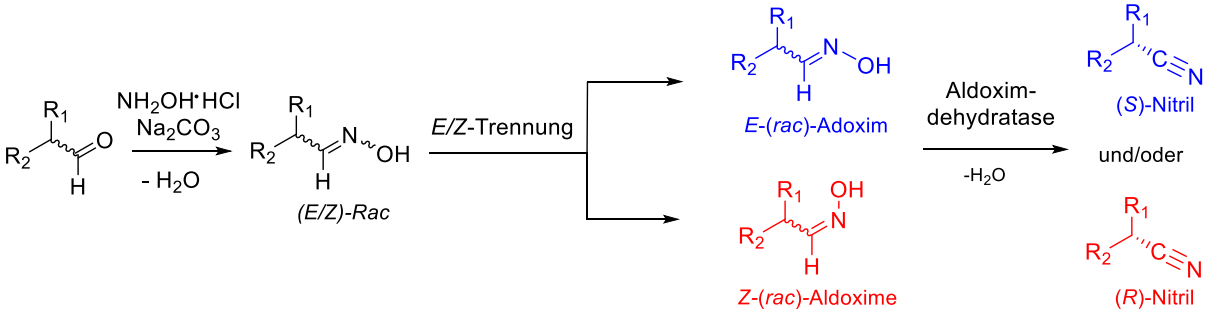

Schema 1: Enantioselektive Dehydratisierung von Aldoximen zu Nitrilen, wobei in Abhängigkeit des verwendeten Isomers entgegengesetzte Enantiomere ermöglicht werden.

Diese Rationalisierung wurde durch intensive Untersuchungen *in silico*, sowie *in vitro* ermöglicht. Dabei wurde zunächst ein Model zur Erkennung des korrekten Enzym-Substrat Komplexes erstellt, das wiederum zur Berechnung und damit zur Vorhersage der Enantioselektivität genutzt wurde. Die besondere Eigenschaft des Models war die automatisierte Erkennung sowie Sortierung der für die enzymatische Reaktion notwendigen Kriterien einer realen Protein-Ligand-Struktur, wodurch die Reproduzierbarkeit und Vorhersagekraft gewährleistet wurde (**Schema 2**).

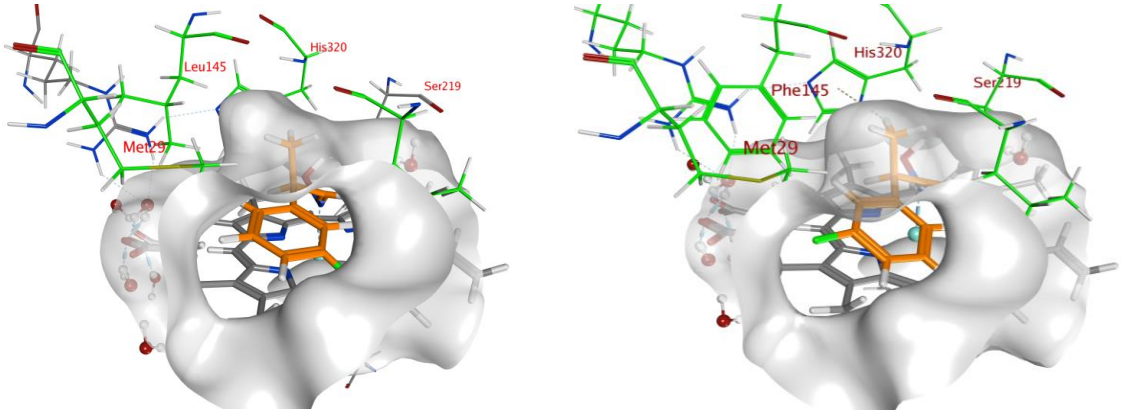

Schema 2: 3-(*Z*,*R*)-FPPOX gebunden im katalytischen Zentrum von OxdRE-WT (a) und OxdRE-L145F (b). Der Methylrest des Substrats befindet sich in der Furche die sich aus den Aminosäuren M29, L145, A147 und H320 formt. L145F zeigt hierbei die deutlich verkleinerte Furche.

Die Rationalisierungsstudie ergab, dass die Enantioselektivität von der Positionierung und Orientierung der Methylgruppe des Substrats in der Furche des Enzyms abhängig ist. Diese räumliche Orientierung unterscheidet sich vom jeweilig eingesetzten Isomer und ist der Grund für die Differenzierung. Bewiesen wurde die Hypothese *in silico* sowie experimentell. Der *in silco* Beweis konnte über die einzelnen Energiebeiträge für die Bindung des Liganden in der aktiven Tasche erbracht werden. Des Weiten wurde die Mutante OxdRE-L145F auf Basis dieser Hypothese erstellt, die durch Verkleinerung der Furche zur Erhöhung der Enantioselektivität *in silico* sowie experimentell geführt hat, wodurch die Hypothese untermauert wurde (**Schema 2**). So konnte beispielsweise für die Reaktion von *rac*-(*E*)-2-FPPOX (**4a**) mit OxdRE-L145F ein E-Wert von über 200 erzielt werden (**Schema 3**).

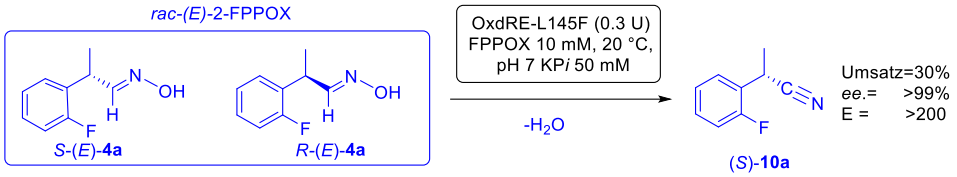

Schema 3: Enantioselektive Synthese von *S*-2-FPPN (**10a**) ausgehend von *rac*-(*E*)-2-FPPOX (**4a**) mit OxdRE-L145F.

Dieses Model trug maßgeblich dazu bei, dieses seltene Phänomen sowie die enzymatische Reaktion besser zu verstehen und legte damit die Basis der darauffolgenden Arbeiten.

Die Darstellung von chiralen Nitrilen wurde mit der OxdRE-L145F Mutante mit exzellenten Selektivitäten ermöglicht. Jedoch war diese Darstellung stark limitiert. Zum einen durch die natürliche Limitierung der kinetischen Racematspaltung und zum anderen durch die notwendige Aufreinigung der *E/Z*-gemisches. Außerdem setzt die Aufreinigung des E/Z-Gemisches voraus, dass die reinen Isomere stabil sind, was bislang nur für das Strukturmotiv der 2-Phenylpropanaloxime-(PPOX) Derivate gelang. Daher wäre die direkte Nutzung der *E/Z*-Gemische eleganter und würde den Einsatz einer Vielzahl von chiralen Aldoximen ermöglichen

Um die biokatalytische chirale Nitril-Synthese zu erweitern und gleichzeitig zu optimieren, wurde eine erstmals berichtete doppelte dynamisch kinetische Racematspaltung (DDKR) entwickelt. Zu diesem Zweck wurden sowohl die Isomerisierung als auch die Racemisierung von Aldoximen untersucht. Die Isomerisierung von Aldoximen wurde durch thermische Behandlung erreicht, wobei die Isomerisierungsrate durch Erhöhung der Substratkonzentration gesteigert werden konnte. Die Racemisierung wurde mit Thiazolen ermöglicht, mit Thiaminhydrochlorid als bestes Racemisierungsreagenz. Der Enantiomerenüberschuss von (*R*,*E*)-**8** wurde mit Thiaminhydrochlorid nach 24 Stunden erfolgreich von 88 % auf 35 % reduziert (**Schema 4**).

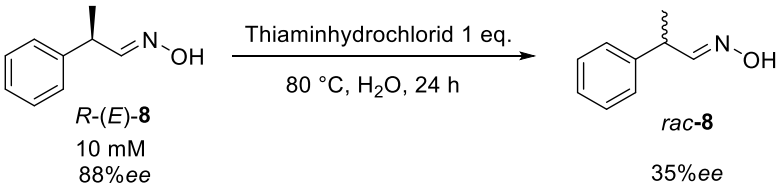

Schema 4: Racemisierung von (*R*,*E*)-PPOX (**8**) mittels Thiaminhydrochlorid.

Das bis dahin selektivste Enzym OxdRE-L145F, zeigte in der Reaktion für das Gemisch zwar eine Erhöhung des E-Werts von 2 (WT) auf 4, jedoch stellt ein E-Wert von 4 keine selektive Reaktion dar, weshalb das Enzym weiter optimiert werden sollte (**Schema 5**).

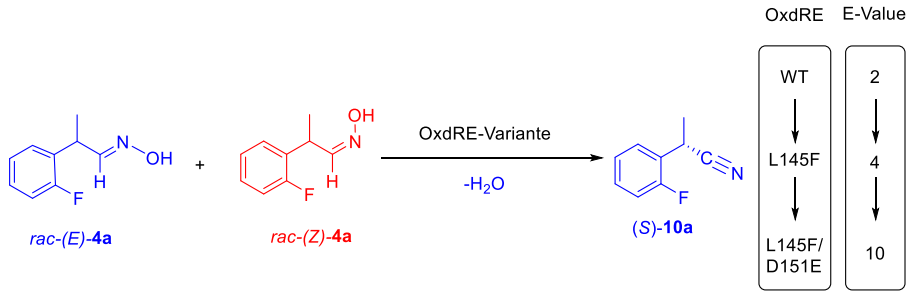

Schema 5: Darstellung der Reaktion von rac-2-FPPOX als E/Z-Gemisch mit OxdRE und optimierten Mutanten.

Dies wurde schließlich durch das Screening von mehr als 900 Varianten als „smart-libraries“ erreicht, was zu einigen vielversprechenden Mutanten führte. Eine Variante (OxdRE-L145F-D151E) zeigte sogar einen E-Wert von 10. Der Einsatz dieser Variante im entwickelten DDKR-Prozess sowie die Weiterentwicklung in einer iterativen gesättigten Mutagenese (ISM) konnte in dieser Arbeit jedoch nicht realisiert werden und bietet ein interessantes Thema für weitere Forschungsarbeiten (**Schema 6**). Im Zusammenhang mit dem Prozess wurde die Expression der Aldoximdehydratasen sowie der Zugang zu chiralen Aldoximen optimiert. Die optimierte Expression wurde durch "leaky" Kultivierung erreicht, wodurch die Aktivität des Enzyms als Ganzzellkatalysator am Beispiel der L145F-Mutante um das 100-fache gesteigert werden konnte. Die langwierige dreistufige Substratsynthese mit nur 10% isolierter Ausbeute wurde durch die Hydroformylierung von Styrolen und anschließender Kondensation mit Hydroxylamin ersetzt. Durch diese alternative Route konnten 16 verschiedene Substrate ohne großen Aufwand und mit hohen isolierten Ausbeuten von bis zu 98 % gewonnen werden.

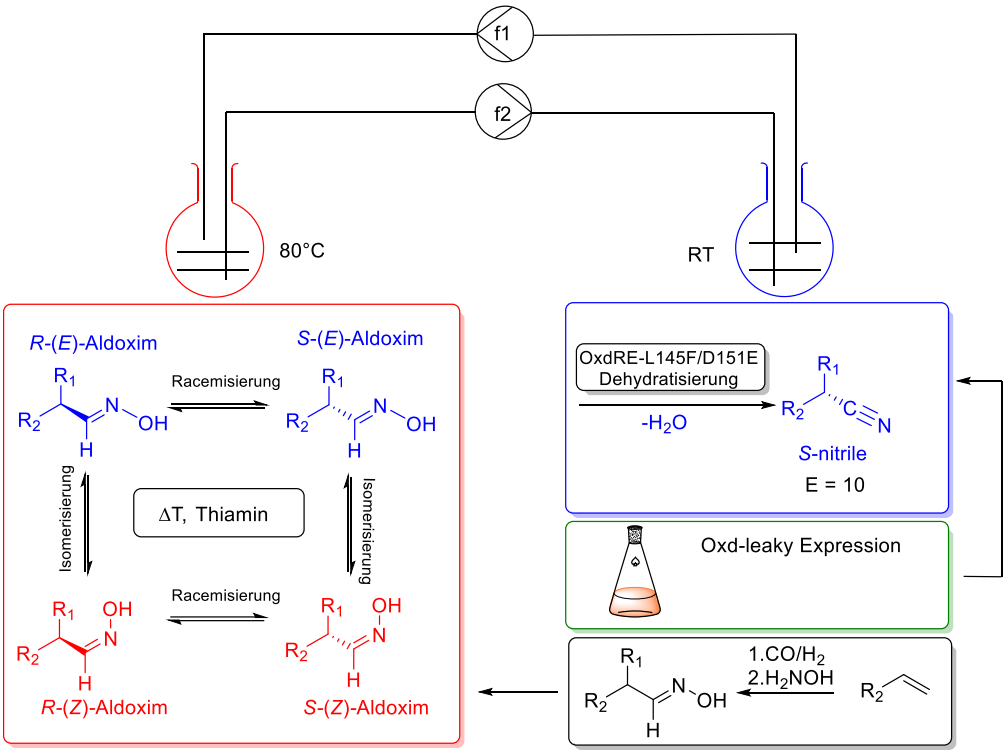

Schema 6: Momentaner Stand des gesamten entwickelten Prozesses in dieser Arbeit. Substratherstellung über Hydroformylierung (schwarz), Biokatalysatorherstellung (grün), chemische Racemisierung und Isomerisierung (rot) und Nitrilsynthese mit einem engineerten Biokatalysator. Darstellung der DDKR als Flow-Prozess mit der enzymatischen Nitrilsynthese bei Raumtemperatur und der chemischen Racemisierung/Isomerisierung bei 80 °C.

Darüber hinaus beschäftigte sich diese Arbeit mit der Synthese langkettiger aliphatischer Nitrile. Dabei sollte die biokatalytische Umsetzung von Fettnitrilen auf längere Aliphaten wie C12 und C14 hin erweitert werden. Hierzu wurde die Limitierung rationalisiert und über verschieden Ansätze erarbeitet. Die enzymatische Umsetzung konnte über molekulares Modeling optimiert werden. Die zuvor entwickelte Docking-Methode zeigte über eine visuelle Analyse, dass die gebundenen Aldoxime wie Dodecanaloxim zu groß für die aktiven Tasche sind und der Alkylrest aus dem kurzen jedoch schmalen Eingangsbereich herausragen. Durch die Vergrößerung des Eingangs zum katalytischen Zentrum mit OxdB5 (F288/L293A) konnte die Aktivität um das 2.5-fache erhöht werden und ermöglichte so die erstmalige quantitative Umsetzung von langen aliphatischen Fettnitrilen (**Abbildung 1**). Die Löslichkeit der langkettigen aliphatischen Aldoxime in Wasser kann sich durch die Steigerung der Reaktionstemperatur oder des Cosolventanteils erhöht werden. Dies ist wiederum nur möglich, wenn die veränderten Reaktionsparameter kompatibel mit dem Enzym sind.

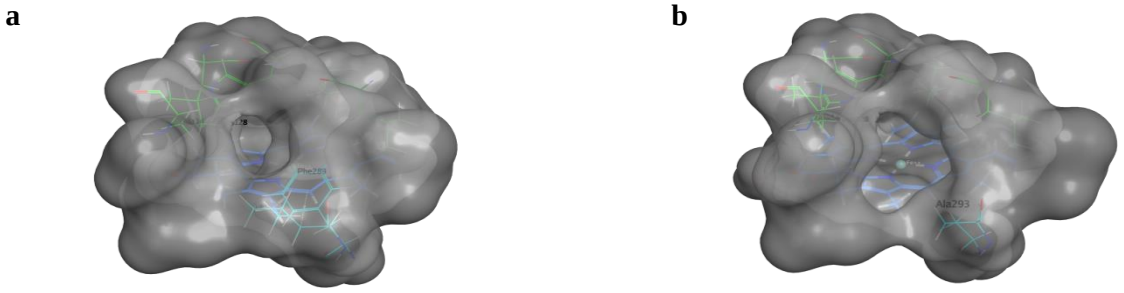

Abbildung 1: Modellierte Oberfläche von OxdB-WT (**Bild a**) und OxdB5 (F290A-L294A) (**Bild b**) im Vergleich. Die Abbildung zeigt die verbesserte Eintrittsstelle für die Mutante im Vergleich zum Wildtyp.

Beim Versuch die Stabilität der Aldoximdehydratase OxdB zu erhöhen, wurde eine bisher undefinierte Korrelation zwischen Protein-Deskriptoren (Hydrophobizitätsmoment, Dipolemoment, Mobility) mit der Stabilität (Thermostabilität, Solventtoleranz) beobachtet. Eine hohe Thermostabilität sowie Solventtoleranz stand im Zusammenhang mit einem hohen Hydrophobizitäts-Moment, einer hohen Mobilität und einem relativ niedrigen Dipolemoment. Dabei zeigte sich diese Tendenz nicht nur für Aldoximdehydratasen, sondern allgemein für Proteine. Es konnte gezeigt werden, dass OxdB bezogen auf diese Eigenschaften hin verändert werden kann, um die Stabilität zu erhöhen. Jedoch zeigte bei einer zufälligen Auswahl der Positionen nur eine von drei erstellten Varianten eine Steigerung der Stabilität. Diese Werte können nur durch viele Mutationen signifikant verbessert werden weshalb eine Vorauswahl von Positionen, die möglichst wenig Einfluss auf die Integrität des Proteins haben, entscheidend ist. An dieser Stelle wurde 3DM zu Identifikation dieser Stellen eingesetzt, wodurch eine Methode entwickelt wurde Proteine an nicht essentiellen Stellen zu verändern und somit ihre Stabilität zu verbessern. Die so entwickelte Variante OxdSet2 variante zeigte so 45% höhere Restaktivität bei 45°C als der Wildtyp. Jedoch sank die Stabilität gegenüber Lösungsmitteln, weshalb die Methode noch optimiert werden muss. Die erarbeitete Methode zur Vorhersage von Mutationen, die die Stabilität eins Proteins erhöhen, bietet in Vergleich zu den bisherigen bekannten Rechenmethoden eine neue alternative. Des Weiteren stellt diese Vorgehensweise auch eine Möglichkeit zu Erweiterung der bereits bestehenden Stabilitätsvorhersagen dar. Damit wurden in diese Arbeit die Selektivität, Aktivität und Stabilität von Aldoximdehydratasen über molekulares Modeln erfolgreich verbessert (**Schema 7**).

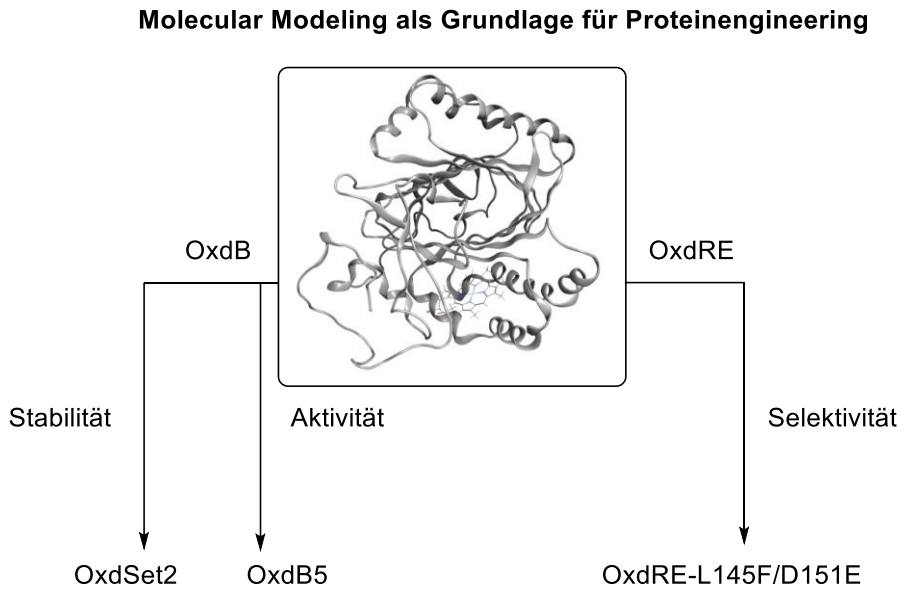

Schema 7: Überblick der veränderten Proteineigenschaften mithilfe von molekularem Modeling.

Des Weiteren wurde an der von *Lukas Schober* entwickelten Methode zur Kompatibilität von Hydroxylamin mit Aldoximdehydratasen gearbeitet. In seiner Arbeit zeigte er, dass unter der Nutzung von Pickering Emulsion Aldoximdehydratasen in Gegenwart von Hydroxylamin eingesetzt werden können. Diese Ergebnisse wurden in der vorliegenden Arbeit aufgegriffen und die für die Kompatibilität notwendigen Pickering Emulsion konnten erfolgreich in einem Flow-System etabliert werden. Dabei konnte erfolgreich die Synthese von Octannitril ausgehend von Octanal dargestellt werden (**Schema 8**).

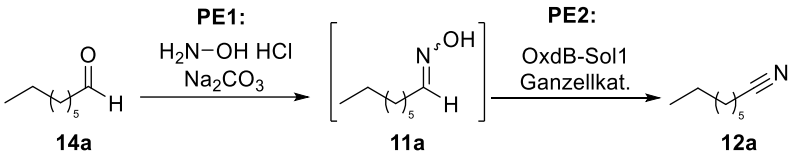

Schema 8: Tandem-Prozess der *n*-Octannitril-Synthese in Pickering emulsionen.

Im Zusammenhang mit Pickering Emulsionen wurden weiterhin versucht die Problematik der Löslichkeit von aliphatischen Aldoximen zu adressieren. Es konnte zwar erfolgreich mit quantitativen Umsätzen die Synthese von Dodecannitril mit OxdB in Pickering Emulsion dargestellt werden, jedoch lösten sich längere Aliphaten wie C14 nicht mehr in Dodecan, welches als Lösungsmittel für die Reaktion genutzt wurde. Über ein Lösungsmittels Screening könnte ein geeignetes Lösungsmittel identifiziert werden, welches zum Einen höhere Fettaldoxime und zum Anderen stabilere Pickering Emulsion formt.

9 Experimental section

9.1 Compounds

Unless otherwise stated, all compounds and solvents are commercially available from Acros Organics, Alfa Aesar, AppliChem GmbH, Carl Roth GmbH & Co. KG, J.T. Baker, Merck KGaA, Sigma-Aldrich, TCI Europe N.V. and VWR International GmbH in analytical or HPLC quality and used without further purification.

9.2 Chemical syntheses of substrates

9.2.1 General Procedure 1 (GP1): Nitroaldol condensation of fluorobenzaldehyde (1) with nitromethane

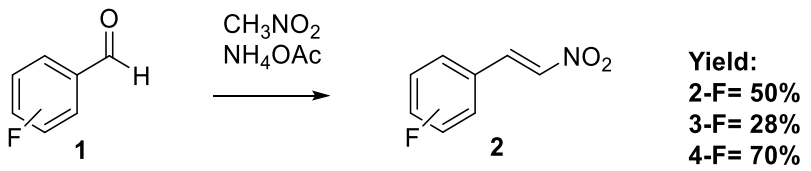

The synthesis was carried out in analogy to *Betke et al.*.[47] Fluorobenzaldehyde (1.0 eq.), ammonium acetate (0.1 eq.) and nitromethane (6.5 eq.) were dissolved in acetic acid. The solution was heated to reflux for 24 hours. The complete conversion was determined by means of TLC (cyclohexane/ethyl acetate, 6:1, *v/v*). Water (1:1, *v/v*) was added and the phases separated. The solid was filtered off and recrystallized from ethanol.

9.2.1.1 Synthesis of 2-fluoro-(*E*)-(2-nitrovinyl)-benzene (2a)

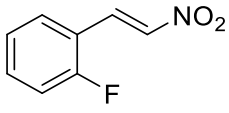

2a

$C_8H_6FNO_2$
MW: 167,14 g/mol

The synthesis was carried out according to GP1. 2-fluorobenzaldehyde (10 g, 80 mmol, 8.6 mL) was dissolved in acetic acid (30 mL) with nitromethane (21 mL, 400 mmol) and ammonium acetate (500 mg, 6.5 mmol) and heated to reflux. After workup, the product (**2a**) was obtained as an orange solid.

Yield: 7.6 g, 57%.

^{1}H NMR (500 MHz, Chloroform-*d*): δ [ppm] = 8.08 (d, ^3J = 13.7 Hz, 1H, C**H**=CH), 7.76 (d, ^3J = 13.8 Hz, 1H, C**H**=CH), 7.58 – 7.48 (m, 2H, Ar-**H**), 7.30 – 7.25 (m, 1H, Ar-**H**), 7.21 (dd, ^3J = 10.8, 8.3 Hz, 1H, Ar-**H**).

The ^{1}H-NMR-spectroscopy were compared with an analog compound from literature.[47]

9.2.1.2 Synthesis of 3-fluoro-(*E*)-(2-nitrovinyl)-benzene (2b)

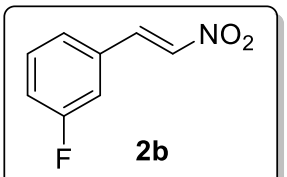

2b

$C_8H_6FNO_2$

Mw: 167.14 g/mol

The synthesis was carried out according to GP1. 3-fluorobenzaldehyde (20 g, 161 mmol) was dissolved in acetic acid (30 mL) with nitromethane (40 mL, 800 mmol) and ammonium acetate (500 mg, 6.5 mmol) and heated to reflux. After workup, the product (**2b**) was obtained as a yellow solid.

Yield: 7.6 g, 28%.

^{1}H NMR (500 MHz, Chloroform-*d*): δ [ppm] = 7.97 (d, ^3J = 13.7 Hz, 1H, CH=C**H**), 7.56 (d, ^3J = 13.7 Hz, 1H, CH=C**H**), 7.44 (td, ^3J = 8.1, 6.1 Hz, 1H, Ar-*H*), 7.34 (d, *J* = 7.6 Hz, 1H, Ar-**H**), 7.21 (ddd, *J* = 16.7, 7.9, 2.3 Hz, 2H, Ar-**H**)

The ^{1}H-NMR-spectroscopy were compared with an analog compound from literature.[47]

9.2.1.3 Synthesis of 4-fluoro-(*E*)-(2-nitrovinyl)-benzene (2c)

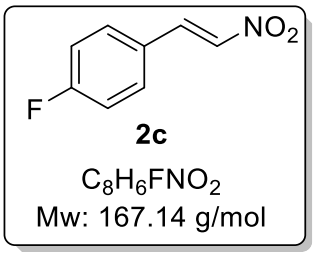

2c

$C_8H_6FNO_2$

Mw: 167.14 g/mol

The synthesis was carried out according to GP1. 4-fluorobenzaldehyde (10 g, 80 mmol, 8.55 mL) was dissolved in acetic acid (30 mL) with nitromethane (21 mL, 400 mmol) and ammonium acetate (500 mg, 6.5 mmol) and heated to reflux. After workup, the product (**2c**) was obtained as a yellow solid.

Yield: 8.85 g, 66 %.

^{1}H NMR (500 MHz, Chloroform-*d*): δ [ppm] = 7.98 (d, ^3J = 13.6 Hz, 1H, CH=C**H**), 7.58 – 7.51 (m, 3H, Ar-**H**, CH=C**H**), 7.19 – 7.12 (m, 2H, Ar-**H**).

The ^{1}H-NMR-spectroscopy were compared with an analog compound from literature.[47]

9.2.2 General procedure 2 (GP2): Michael-addition of fluoro-nitrovinyl benzenes with different Grignard reagents

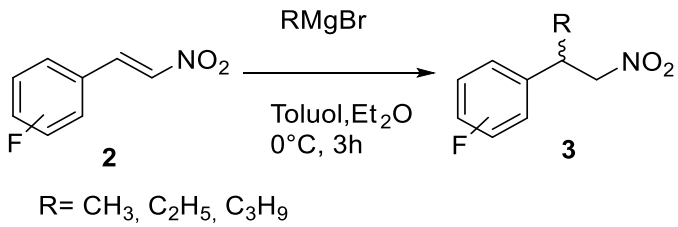

Yield:
3a= 41%
3b= 51%
3c= 52%
3d= 39%
3e= 64%
3f= 55%
3g= 48%

In analogy to *Betke et al.*,[47] the synthesis was carried out in a heat dried flask under argon atmosphere. Dry toluene was placed in the flask and cooled to 0 ° C. After addition of the fluoro-nitrovinyl benzene (1 eq.), a solution of alkyl magnesium bromide (1-3 M) in diethyl ether (1.5 eq.) was added dropwise under argon reflux and further stirring. After three hours of at 0 ° C conversion was controlled via TLC (cyclohexane/ethyl acetate, 6:1, *v/v*). The

reaction mixture was mixed with a saturated ammonium chloride solution (1:1, *v/v*). The phases were separated, and the aqueous phase was extracted three times with ethyl acetate (1:1, *v/v*). The combined organic phase was washed with saturated sodium chloride solution (1:3, *v/v*). The organic phase was dried over magnesium sulfate and the solvent was then evaporated *in vacuo*. The crude product was then purified by automated column chromatography (cyclohexane/ethyl acetate 6:1, *v/v*) to give the racemic nitroalkane as oils.

9.2.2.1 Synthesis of *rac*-2-fluoro-1-(1-nitropropan-2-yl) benzene (3a)

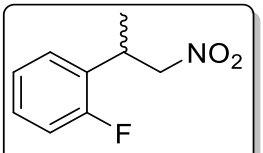

3a
$C_9H_{10}FNO_2$
Mw: 183.18 g/mol

The synthesis of the *rac*-2-fluoro-1-(1-nitropropan-2-yl) benzene was carried out according to GP2. 2-fluoro-(*E*)-(2-nitrovinyl) benzene (7.3 g, 43.3 mmol) was dissolved in toluene (150 mL) and then methyl magnesium bromide (15 mL, 45 mmol) was added dropwise. After work up, the product (**3a**) was obtained as pink oil.

Yield: 4.32 g, 53%.

^{1}H NMR (500 MHz, Chloroform-*d*): δ [ppm] = 7.29 – 7.20 (m, 2H, Ar-**H**), 7.12 (td, *J* = 7.6, 1.3 Hz, 1H, Ar-**H**), 7.06 (dd ^3J = 10.7, 8.3 Hz, 1H, Ar-**H**), 4.66 (dd, ^3J = 12.3, 7.0 Hz, 1H, C**H**$_2$), 4.55 (dd, ^3J = 12.3, 8.1 Hz, 1H, C**H**$_2$), 3.89 (h, ^3J = 7.3 Hz, 1H, C**H**-CH$_3$), 1.41 (d, ^3J = 7.1 Hz, 3H, C**H**$_3$).

The ^{1}H-NMR-spectroscopy were compared with an analog compound from literature.[47]

9.2.2.2 Synthesis of *rac*-3-fluoro-1-(1-nitropropan-2-yl) benzene (3b)

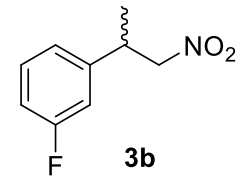

3b
$C_9H_{10}FNO_2$
Mw: 183.18 g/mol

The synthesis of the *rac*-3-fluoro-1-(1-nitropropan-2-yl) benzene was carried out according to GP2. 3-fluoro-(*E*)-(2-nitrovinyl) benzene (7.3 g, 42.6 mmol) was dissolved in toluene (150 mL) and methyl magnesium bromide (22.6 mL, 68 mmol) was then added dropwise. After work up, the product (**3b**) was obtained as an orange oil.

Yield: 0.44 g, 51 %.

^{1}H NMR (500 MHz, Chloroform-*d*): δ [ppm] = 7.24 – 7.15 (m, 2H, Ar-**H**), 7.03 (dd, ^3J = 8.6, 7.0 Hz, 2H, Ar-**H**), 4.57 – 4.40 (m, 2H, C**H**$_2$), 3.63 (h, ^3J = 7.3 Hz, 1H, C**H**-CH$_3$), 1.37 (dd, ^3J = 7.0, 1.2 Hz, 3H, C**H**$_3$).

The ^{1}H-NMR-spectroscopy were compared with an analog compound from literature.[47]

9.2.2.3 Synthesis of *rac*-4-fluoro-1- (1-nitropropan-2-yl) benzene (3c)

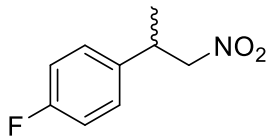

3c
$C_9H_{10}FNO_2$
Mw: 183.18 g/mol

The synthesis of the *rac*-4-fluoro-1-(1-nitropropan-2-yl) benzene was carried out according to GP2. 4-fluoro-(*E*)-(2-nitrovinyl) benzene (15.1 g, 101.7 mmol) was dissolved in toluene (150 mL) and methyl magnesium bromide (51 mL, 152 mmol) was then added dropwise. After work up, the product (**3c**) was obtained as yellow oil.

Yield: 9.7 g, 52%.

^{1}H NMR (500 MHz, Chloroform-*d*): δ [ppm] = 7.24 – 7.15 (m, 2H, Ar-**H**), 7.03 (dd, ^3J = 8.6, 7.0, 1.9 Hz, 2H, Ar-**H**), 4.57 – 4.40 (m, 2H, C**H**$_2$), 3.63 (h, ^3J = 7.3 Hz, 1H, C**H**-CH$_3$), 1.37 (dd, ^3J = 7.0, 1.2 Hz, 3H, C**H**-CH$_3$).

The ^{1}H-NMR-spectroscopy were compared with an analog compound from literature.[47]

9.2.2.4 Synthesis of *rac*-2-fluoro-1-(1-nitrobutan-2-yl) benzene (3d)

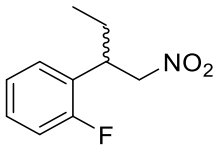

3d
$C_{10}H_{12}FNO_2$
Mw: 197.21 g/mol

The synthesis of the *rac*-2-fluoro-1-(1-nitropropan-2-yl) benzene was carried out according to GP2. 2-fluoro-(*E*)-(2-nitrovinyl) benzene (3.68 g, 22.2 mmol) was dissolved in toluene (100 mL) and then ethyl magnesium bromide (26 mL, 26 mmol) was added dropwise. After work up, the product (**3d**) was obtained as a brown oil.

Yield: 1.66 g, 39%.

^{1}H NMR (500 MHz, DMSO-d_6): δ [ppm] =7.48 (td, ^3J = 7.75, 7.63, ^2J= 1.88, 2H, Ar-**H**), 7.29 (td, *J* = 7.6, 1.3 Hz, 1H, Ar-**H**), 7.17 (dd, ^3J = 10.7, 8.3 Hz, 1H, Ar-**H**), 4.99 (dd, ^3J = 13.18, 6.12Hz, 1H, C**H**$_2$), 4.91 (dd, ^3J = 13.19, 9.52 Hz, 1H, C**H**$_2$), 3.69 (m, 1H, C**H**-CH$_2$), 1.7 (m (p), 1H, C**H**$_2$-CH$_3$), 1.58 (m (p), ^3J = 7.3 Hz, 1H, C**H**$_2$-CH$_3$), 0.75 (t, ^3J = 7.38 Hz, 3H, C**H**$_3$).

The ^{1}H-NMR-spectroscopy were compared with an analog compound from literature.[47]

9.2.2.5 Synthesis of *rac*-2-fluoro-1-(1-nitropentan-2-yl) benzene (3e)

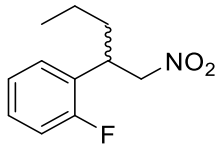

3e
$C_{11}H_{14}FNO_2$
Mw: 211.24 g/mol

The synthesis of the *rac*-2-fluoro-1-(1-nitropropan-2-yl) benzene was carried out according to GP2. 2-fluoro-(*E*)-(2-nitrovinyl) benzene (3.04 g, 18.2 mmol) was dissolved in toluene (100 mL) and then propyl magnesium bromide (11 mL, 22 mmol) was added dropwise. After work up, the product (**3e**) was obtained as a brown oil.

Yield: 2.44 g, 64%.

^{1}H NMR (500 MHz, DMSO-d_6): δ [ppm] = 7.53 (td, ^3J = 7.83, 7.67, ^2J= 1.88, 2H, Ar-**H**), 7.35 (td, ^3J = 7.6, Hz, 1H, Ar-**H**), 7.23 (dd ^3J = 10.7, 8.3 Hz, 1H, Ar-**H**), 4.99 (dd, ^3J = 13.15, 6.13 Hz, 1H, C**H**$_2$), 4.91 (dd, ^3J = 13.16, 9.52 Hz, 1H, C**H**$_2$), 3.7 (m, 1H, C**H**-CH$_2$), 1.66 (m, 2H, CH$_2$-C**H**$_2$CH$_3$), 1.22 (m, ^3J = 7.3 Hz, 2H, C**H**$_2$-CH$_3$), 0.88 (t, ^3J = 7.32 Hz, 3H, C**H**$_3$).

The ^{1}H-NMR-spectroscopy were compared with an analog compound from literature.[47]

9.2.2.6 Synthesis von *rac*-1-fluoro-4-(1-nitrobutan-2-yl) benzene (3f)

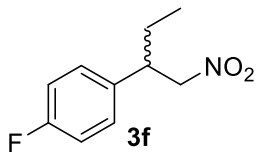

$C_{10}H_{12}FNO_2$
Mw 197.12 g/mol

The synthesis of the *rac*-1-fluoro-4-(1-nitrobutan-2-yl) benzene was carried out according to GP2. 4-fluoro-(*E*)-(2-nitrovinyl) benzene (2 g, 12.1 mmol) was dissolved in toluene (40 mL) and ethyl magnesium bromide (15 mL, 15 mmol) was then added dropwise. After work up, the product (**3f**) was obtained as a brown oil.

Yield: 1.29 g, 55%.

^{1}H NMR (500 MHz, Chloroform-*d*): δ [ppm] = 7.18 – 7.12 (m, 2H, Ar-**H**), 7.06 – 6.99 (m, 2H, Ar-**H**), 4.57 (dd, *J* = 12.2, 7.0 Hz, 1H, C**H**$_2$-NO$_2$), 4.50 (dd, ^{3}J = 12.2, 8.5 Hz, 1H, C**H**$_2$-NO2), 3.44 – 3.31 (m, 1H,-C**H**-CH$_2$-CH$_3$), 1.80 – 1.71 (m, 1H, CHC**H**$_2$CH$_3$), 1.66 (ddq, *J* = 14.2, 9.8, 7.3 Hz, 1H, -CH-C**H**$_2$CH$_3$), 00.84 (t, ^{3}J = 7.3 Hz, 3H, CH$_2$-C**H**$_3$).

The ^{1}H-NMR-spectroscopy were compared with an analog compound from literature.[47]

9.2.2.7 Synthesis of *rac*-1-fluoro-4-(3-methyl-1-nitrobutan-2-yl) benzene (3g)

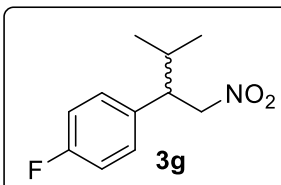

$C_{11}H_{14}FNO_2$
Mw: 211.24 g/mol

The synthesis of the *rac*-1-fluor-4-(3-methyl-1-nitrobutan-2-yl) benzene was carried out according to GP2. 4-fluoro-(*E*)-(2-nitrovinyl) benzene (2 g, 12.2 mmol) was dissolved in toluene (40 mL) and *i*-propyl magnesium bromide (11 mL, 14.3 mmol) was added dropwise. After work up, the product (**3g**) was obtained as a brown oil.

Yield: 1.23 g, 48%.

^{1}H NMR (500 MHz, Chloroform-*d*): δ [ppm] = 7.15 – 7.09 (m, 2H, Ar-**H**), 7.01 (t, *J* = 8.6 Hz, 2H, Ar-**H**), 4.75 (dd, *J* = 12.3, 5.5 Hz, 1H, C**H**$_2$-NO$_2$), 4.59 (m, CH**H**$_2$-NO$_2$), 3.22 (m, 1H, C**H**-CH$_2$), 1.98 – 1.87 (m, 1H, C**H**-(CH$_3$)$_2$), 1.01 (d, ^{3}J = 6.7 Hz, 3H, CH-(C**H**$_3$)$_2$), 0.80 (d, ^{3}J = 6.8 Hz, 3H, CH-(C**H**$_3$)$_2$).

The ^{1}H-NMR-spectroscopy were compared with an analog compound from literature.[47]

9.2.3 General procedure 3 (GP3): Disproportion of nitrile alkyl compound towards aldoximes using benzyl bromide

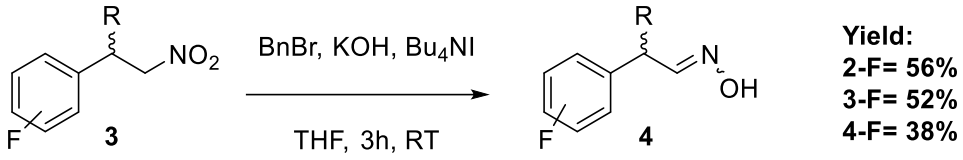

The synthesis was carried out in a heat dried flask under argon atmosphere. KOH (85 wt.% pellets, 1.05 eq.) was dissolved in dry THF, 4 Å molecular sieve were added, and the suspension was stirred for half an hour. Benzyl bromide (1.1 eq.) and tetrabutylammonium iodide (TBAI, 0.05 eq.) were added. The respective nitroalkane was then slowly added, dropwise. The suspension was stirred at room temperature for three hours. The conversion was controlled by means of TLC. Water (1:1 *v/v*) was added and the phases were separated. The aqueous phase was extracted three times with ethyl acetate (50 mL). The combined organic phases were washed with brine and dried over magnesium sulfate. The solvent was removed under reduced pressure and the crude product was obtained as an oil. *Rac*-(*E/Z*)-fluoro-phenylpropanal oximes were purified via automated column chromatography using the biotage system (cyclohexane/ethyl acetate), the mixture of *E*- and *Z*-isomers were obtained as colorless solids or as oils. The aggregate states were dependent on the *E*/*Z* ratios.

9.2.3.1 Synthesis of *rac*-(*E/Z*)-2-fluoro-2-phenylpropanal oxime (4a)

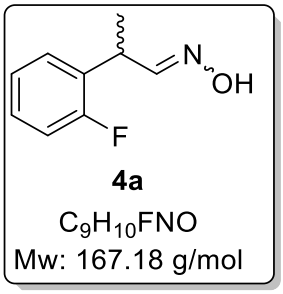

Synthesis of *rac*-(*E/Z*)-2-fluoro-phenyl-2-propanal oxime was performed according to GP 3. Potassium hydroxide pellets (1.3 g, 25 mmol), 4 Å molecular sieve (1 g) and THF (20 mL) were placed in the reaction flask (100 mL), then the mixture was stirred at room temperature for half an hour. Subsequently, benzyl bromide (2.5 mL, 21 mmol) and TBAI (360 mg, 1.1 mmol) were added to the reaction mixture and finally the rac-2-fluoro-1-(1-nitropropan-2-yl) benzene (4.2 g, 23 mmol) was added dropwise. The suspension was stirred at room temperature for three hours. Workup by means of automated chromatography (cyclohexane/ethyl acetate 6/1: *v/v*) led to a mixture of the *E*- and *Z*-diastereomers. The product (**4a**) was obtained as colorless oil.

Yield: 2.1 g, 56%, *E/Z*-ratio 80/20.

^{1}H NMR (500 MHz, DMSO-d_6): δ [ppm] = 10.94 (s, 1H, *Z*-NO*H*), 10.63 (s, 1H, *E*-NO**H**), 7.47 (d, ^3J = 5.7 Hz, 1H, *E*-C**H**=NOH), 7.43 – 7.07 (m, 4H, Ar-**H**), 6.86 (d, 1H, *Z*-C**H**=NOH), 4.44 (p, ^3J = 7.1 Hz, 1H, *E*-C**H**-CH_3), 3.89 (p, ^3J = 6.9 Hz, 1H, *E*-C**H**-CH_3), 3.33 (s, 1H, DMSO), 1.31 (d, ^3J = 7.2 Hz, 3H, C**H**$_3$).

^{13}C NMR (500 MHz, DMSO-d_6) δ [ppm]: 163.0, 161.0, 134.3, 129.4, 122.6, 116.3, 29.6, 21.0.

IR [cm^{-1}]: 3243 (υ, O-H), 2967 (υ, Ar-H), 2888 (υ, CH_3), 1594 (υ, C=C), 1489-1444 (δ, C-C-H), 1220 (υ, C-F).

HRMS (ESI, positive ions) m/z calculated for $C_9H_{10}FNOH^+$: 168.077 $[M+H]^+$, **found** 168.082.

9.2.3.2 Synthesis of *rac*-(*E/Z*)-3-fluoro-2-phenylpropanal oxime (4b)

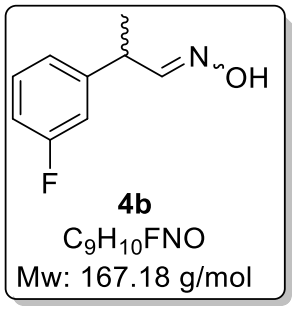

The Synthesis of the *rac*-(*E/Z*)-3-fluoro-2-phenylpropanal oxime was performed according to GP3. Potassium hydroxide pellets (1.2 g, 24 mmol), 4 Å molecular sieve (4 g) and THF (20 mL) were placed in the reaction flask (100 mL), then the mixture was stirred at RT for half an hour. Subsequently, benzyl bromide (3.5 mL, 28.8 mmol) and TBAI (300 mg, 1 mmol) were added to the reaction mixture and finally the rac-2-*rac*-3-fluoro-1-(1-nitropropan-2-yl) benzene (43.9 g, 20.8 mmol) was added dropwise. The suspension was stirred at RT for three hours. Workup by means of automated chromatography (cyclohexane/ethyl acetate 6/1, *v/v*) led to a mixture of the *E*- and *Z*-diastereomers. The product (**4b**) was obtained as colorless oil.

Yield: 1.9 g, 52 %, *E/Z*-ratio: 71/29.

^{1}H NMR (500 MHz, DMSO-d_6): δ [ppm] = 10.95 (s, 1H, *Z*-NO**H**), 10.6 (s, 1H, *E*-NO**H**), 7.41 (d, ^{3}J = 6.2 Hz, 1H, *E*-C**H**=NOH), 7.40 – 7.33 (m, 1H, Ar-**H**), 7.16 – 7.01 (m, 3H, Ar-**H**), 6.81 (d,^{3}J= 7.1 Hz, 1H, *Z*-C**H**=NOH), 3.65 (p, *J* = 7.1 Hz, 1H, *E*-C**H**-CH_3), 1.35 (d, *J* = 7.1 Hz, 3H, C**H**$_3$).

^{13}C NMR (500 MHz, DMSO-d_6) δ [ppm]: 163.3, 161.3, 152.0, 146.0, 130.4, 123.4, 114.0, 113.3, 19.1.

^{19}F NMR (500 MHz, DMSO-d6) δ [ppm]: -113.13, -113.28 (without standard)

IR [cm^{-1}]: 3239 (υ, O-H), 2971 (υ, Ar-H), 2888 (υ, CH_3), 1616-1607 (υ, C=C), 1462-1439 (δ, C-C-H),1284-1242 (υ, C-F).

HRMS (ESI, positive ions) m/z calculated for $C_9H_{10}FNOH^+$: 168.077 $[M+H]^+$, **found** 168.082.

9.2.3.3 Synthesis of *rac*-(*E/Z*)-4-fluoro-2-phenylpropanal oxime (4c)

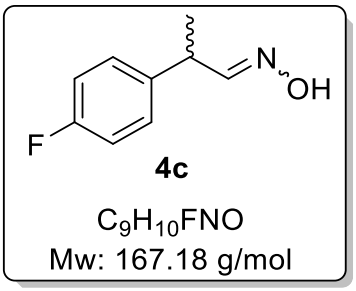

The synthesis of the *rac*-(*E/Z*)-4-fluoro-phenyl-2-propanal oxime was performed according to GP3. Potassium hydroxide pellets (2.9 g, 20.8 mmol), 4 Å molecular sieve (8 g) and THF (80 mL) were placed in the reaction flask (100 mL), then the mixture was stirred at room temperature for half an hour. Subsequently, benzyl bromide (6.2 mL, 0.5 mmol) and TBAI (900 mg, 2.4 mmol) were added to the reaction mixture and finally the *rac*-4-fluoro-1-(1-nitropropan-2-yl) benzene (9.5 g, 51 mmol) was added dropwise. The suspension was stirred at room temperature for three hours. Workup by means of automated chromatography (cyclohexane/ethyl acetate 6/1, *v/v*) led to a mixture of the *E*- and *Z*-diastereomers. The product (**4c**) was obtained as colorless oil.

Yield: 3.4 g, 40%, *E/Z*-ratio: 69/31

^{1}H NMR (500 MHz, DMSO-d_6): δ [ppm] = 10.91 (s, 1H, *Z*-NO**H**), 10.57 (s, 3H, *E*-NO**H**), 7.42 (d, ^3J = 6.1 Hz, 4H, *E*-C**H**=NOH), 7.30 (m, 2H, Ar-**H**), 7.19 – 7.06 (m, 2H, Ar-**H**), 6.78 (d, ^3J = 7.2 Hz, 1H, *Z*-C**H**=NOH), 4.19 (p, ^3J = 7.2 Hz, 1H, *E*-C**H**-CH_3) 3.65 (p, ^3J = 6.9 Hz, 1H, *Z*-C**H**-CH_3), 1.33 (d, ^3J = 7.1 Hz, 3H, C**H**$_3$).

The identity was confirmed via ^{1}H-NMR-spectroscopy.[47]

9.2.3.4 Synthesis of rac-(E/Z)-2-fluoro-2-phenylbutanal oxime (4d)

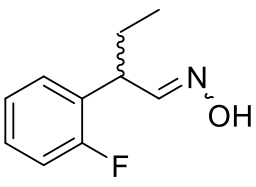

4d
$C_{10}H_{12}FNO$
Mw: 181.21 g/mol

The Synthesis of the *rac*-(*E/Z*)-2-fluoro-2-phenylbutanal oximes was performed according to GP 3. Potassium hydroxide pellets (0397 mg, 6.03 mmol), 4 Å molecular sieve (2.0 g) and THF (50 mL) were placed in the reaction flask (100 mL), then the mixture was stirred at RT for half an hour. Subsequently, benzyl bromide (85 mL, 5 mmol) and TBAI (172 mg, 0.5 mmol)) were added to the reaction mixture and finally the *rac*-4-fluoro-1-(1-nitropropan-2-yl) benzene (11 g, 5.3 mmol) was added dropwise. The suspension was stirred at RT for three hours. Workup by means of automated chromatography (cyclohexane/ethyl acetate 6/1: *v/v*) led to a mixture of the *E*- and *Z*-diastereomers. The product (**4d**) was obtained as a yellow oil.

Yield: 0.50 g, 54%. (*E/Z* ratio: 71/29)

^{1}H NMR (500 MHz, Chloroform-*d*): δ [ppm] = 7.56 (dd, ^3J = 6.86, ^2J = 1.19 Hz, 1H, *E*-C**H**=NOH), 7.24 – 7.00 (m, 4 H, Ar-**H**), 6.84 (d, ^3J = 7.34, ^2J = 1.99, 1H, *Z*-C**H**=NOH), 4.34 (q, ^3J = 7.63 Hz, 1H, *Z*-C**H**-CH_3), 3.70 (q, ^3J = 7.38, 7.36 Hz, 1H, *E*-C**H**-CH_2), 1.9-1.75 (m, 2H, C**H**$_2$-CH_3). 0.88 (t, ^3J = 7.39 Hz, 3H, C**H**$_3$).

The ^{1}H-NMR-spectroscopy were compared with an analog compound from literature.[47]

9.2.3.5 Synthesis of *rac*-(*E/Z*)-2-fluoro-2-phenylpentanal oxime (4e)

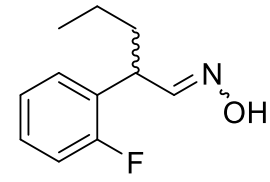

4e
$C_{11}H_{14}FNO$
Mw: 195.24 g/mol

The synthesis of the *rac*-(*E/Z*)-2-fluoro-phenyl-2-pentanal oxime was performed according to GP 3. Potassium hydroxide pellets (434 mg, 6.54 mmol), 4 Å molecular sieve (2.0 g) and THF (50 mL) were placed in the reaction flask (50 mL), then the mixture was stirred at room temperature for half an hour. Subsequently, benzyl bromide (0.81 mL, 6.59 mmol) and TBAI (234 mg, 0.64 mmol) were added to the reaction mixture and finally the rac-2-fluoro-1- (1-nitropropan-2-yl) benzene (**3e**, 1.44 g, 6.8 mmol) was added dropwise. The suspension was stirred at room temperature for three hours. Workup by means of automated chromatography (cyclohexane/ethyl acetate 6/1: *v/v*) led to a mixture of the *E*- and *Z*-diastereomers. The product (**4e**) was obtained as a yellow oil

Yield: 0.79 g, 59%, (*E/Z* ratio: 69/31).

^{1}H NMR (500 MHz, Chloroform-*d*): δ [ppm] = 7.54 (dd, ^3J = 6.86, ^2J = 1.19 Hz, 1H, *E*-C**H**=NOH), 7.25 – 7.07 (m, 4H, Ar-**H**), 6.94 (dd, ^3J = 6.86, ^2J = 1.19 Hz, 1H, *Z*-C**H**=NOH), 4.44 (q, ^3J = 7.63 Hz, 1H, *Z*-C**H**-CH_2), 3.62 (q, ^3J = 7.38 Hz, 1H, *E*-C**H**-CH_2), 1.65 (m, 2H, C**H**$_2$-CH_2-CH_3), 1.40-1.23 (m, 2H, C**H**$_2$-CH_3). 0.88 (t, ^3J = 7.42 Hz, 3H, C**H**$_3$)

The ^{1}H-NMR-spectroscopy were compared with an analog compound from literatue.[47]

9.2.3.6 Synthesis of *rac*-(*E*/*Z*)-2-(4-fluorophenyl)-butanal oxime (4f)

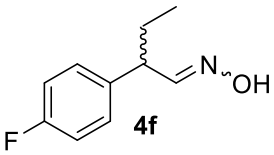

$C_{10}H_{12}FNO$
Mw: 181.10 g/mol

The synthesis of the *rac*-(*E*/*Z*)-2-(4-Fluorphenyl) butanal oxime was performed according to GP 3. Potassium hydroxide pellets (0.62 g, 9.4 mmol), 4 Å molecular sieve (1.5 g) and THF (30 mL) were placed in the reaction flask (100 mL), then the mixture was stirred at RT for half an hour. Subsequently, benzyl bromide (1.14 mL, 9.6 mmol) and TBAI (0.16 g, 0.4 mmol) were added to the reaction mixture and finally the *rac*-4-fluoro-1-(1-nitropropan-2-yl) benzene (1.29 g, 6.7 mmol) was added dropwise. The suspension was stirred at RT for three hours. Workup by means of automated chromatography (cyclohexane/ethyl acetate 6/1, *v/v*) led to a mixture of the *E*- and *Z*-diastereomers. The product (**4f**) was obtained as a colorless oil.

Yield: 510 mg, 40 %, (*E*/*Z* ratio = 68/32).

^{1}H NMR (500 MHz, DMSO-d_6): δ [ppm] = 10.83 (s, 1H, *Z*-CH=NO**H**), 10.54 (s, 1H, *E*-CH=NO**H**), 7.43 (d, ^3J = 7.1 Hz, 1H, *E*-C**H**=NOH), 7.29 (m, 2H, Ar-**H**), 7.19 – 7.08 (m, 2H, Ar-**H**), 6.81 (d, ^3J = 7.5 Hz, 1H, *Z*-C**H**=NOH), 4.07 (q, ^3J = 7.6 Hz, 1H, *Z*-C**H**-CH=NOH), 3.36 (q, ^3J = 7.5 Hz, 1H, *E*-C**H**-CH=NOH), 1.87 – 1.58 (m, 2H, C**H**$_2$-CH_3), 0.80 (t, ^3J = 7.3 Hz, 3H, C**H**$_3$).

^{13}C NMR (126 MHz, Chloroform-*d*): δ [ppm] 162.9, 160.9, 154.9, 137.6, 128.9, 115.6, 39.7, 34.3, 18.8.

ESI-MS m/z Calculated.: $[M+H]^+$: 182.097, $[M+Na]^+$: 204.079 m/z, $[M+K]^+$: 220.052.

Found: $[M+H]^+$: 181.996, $[M+Na]^+$: 203.999, $[M+K]^+$: 220.062.

9.2.3.7 Synthesis of *rac*-(*E*/*Z*)- 2-(4-fluorophenyl)-3-methylbutanal oxime (4g)

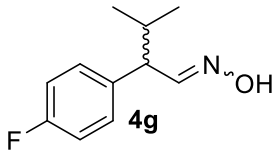

$C_{11}H_{14}FNO$
Mw: 195.237 g/mol

The synthesis of the *rac*-(*E*/*Z*)-2-(4-fluorophenyl)-3-methylbutanal oxime was performed according to GP 3. Potassium hydroxide pellets (0.60 g, 9.2 mmol), 4 Å molecular sieve (1.5 g) and THF (30 mL) were placed in the reaction flask (100 mL), then the mixture was stirred at room temperature for half an hour. Subsequently, benzyl bromide (1.14 mL, 9.6 mmol) and TBAI (0.16 g, 0.4 mmol) were added to the reaction mixture and finally the *rac*-4-fluoro-1-(1-nitropropan-2-yl) benzene (1.23 g, 5.8 mmol) was added dropwise. The suspension was stirred at room temperature for three hours. Workup by means of automated chromatography

(cyclohexane/ethyl acetate 6/1, *v/v*) led to a mixture of the *E*- and *Z*-diastereomers. The product (**4f**) was obtained as a yellow oil.

Yield: 450 mg, 40 %, (*E*/*Z* ratio = 63/37).

^{1}H NMR (500 MHz, DMSO-d_6): δ [ppm] = 10.74 (s, 1H, *Z*-CH=NO**H**), 10.49 (s, 1H, *E*-CH=NO**H**), 7.53 (d, ^3J = 8.4 Hz, 1H, *E*-C**H**=NOH), 7.31 – 7.23 (m, 2H, Ar-**H**), 7.17 – 7.09 (m, 2H, Ar-**H**), 6.93 (d, ^3J = 7.9 Hz, 1H, *Z*-C**H**=NOH), 3.86 (dd, ^3J = 9.6, 8.0 Hz, 1H, *Z*-C**H**-CH=NOH), 3.09 (t, ^3J = 8.9 Hz, 1H, *E*-C**H**-CH=NOH), 2.11 – 1.87 (m, 1H, CH-C**H**-(CH_3)$_2$), 0.92 (dd, ^3J = 6.6, 1.7 Hz, 3H, CH-(C**H**$_3$)$_2$), 0.69 (d, ^3J = 6.7 Hz, 3H, CH-(C**H**$_3$)$_2$).

^{13}C NMR (126 MHz, Chloroform-*d*): δ [ppm] = 162.7, 160.8, 153.9, 136.2, 129.7, 115.5, 53.1, 31.8, 21.0, 20.3.

ESI-MS m/z Calc: $[M+H]^+$: 196.113, $[M+Na]^+$: 218.095, $[M+K]^+$: 234.069.

Found: $[M+H]^+$: 196.023, $[M+Na]^+$: 218.022 m/z , $[M+K]^+$: 234.017.

9.2.4 General procedure 4 (GP4) (One-pot synthesis): Hydroformylation followed by aldoxime formation

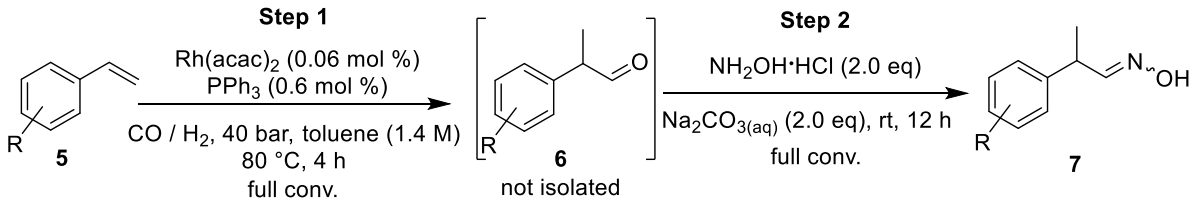

5a (R = *o*,Cl)	**6a** = 86% (*n* : *iso*)	**7a** = 7:93 (*E*/*Z*) 98% yield
5b (R = *m*,Cl)	**6b** = 94% (*n* : *iso*)	**7b** = 66:34 (*E*/*Z*) 86% yield
5c (R = *p*,Cl)	**6c** = 93% (*n* : *iso*)	**7c** = 68:32 (*E*/*Z*) 80% yield
5d (R = *o*,Br)	**6d** = 86% (*n* : *iso*)	**7d** = 20:80 (*E*/*Z*) 98% yield
5e (R = *m*,Br)	**6e** = 93% (*n* : *iso*)	**7e** = 65:35 (*E*/*Z*) 92% yield
5f (R = *p*,Br)	**6f** = 94% (*n* : *iso*)	**7f** = 66:34 (*E*/*Z*) 81% yield
5g (R = 1,4-Cl)	**6g** = 95% (*n* : *iso*)	**7g** = 43:57 (*E*/*Z*) 82% yield
5h (R = 1,4-F)	**6h** = 95% (*n* : *iso*)	**7h** = 54:46 (*E*/*Z*) 90% yield
5i (R = *o*, Me)	**6i** = 60% (*n* : *iso*)	**7i** = 1:99 (*E*/*Z*) 87% yield
5j (R = *m*, Me)	**6j** = 77% (*n* : *iso*)	**7j** = 69:31 (*E*/*Z*) 41% yield
5k (R = *p*, Me)	**6k** = 64% (*n* : *iso*)	**7k** = 67:33 (*E*/*Z*) 27% yield
5l (R = *o*, F)	**6l** = 64% (*n* : *iso*)	**4a** = 76:24 (*E*/*Z*) 79% yield
5m(R = *m*,F)	**6m**= 86% (*n* : *iso*)	**4b** = 66:34 (*E*/*Z*) 81% yield
5n (R = *p*, F)	**6n** = 94% (*n* : *iso*)	**4c** = 68:32 (*E*/*Z*) 89% yield

Scheme 2: Reaction scheme of a two-step one-pot aldoxime synthesis.

Step 1: Hydroformylation

Hydroformylation was conducted in a 50 mL steel autoclave using a magnetic stirrer. Dicarbonyl(acetylacetonato)rhodium(I) (Rh(acac)(CO)$_2$) (0.06 mol %), triphenyl phosphine (TPP) (0.6 mol %) and styrene derivative (5 g, 27.3 mmol, 1.0 eq.) were dissolved in toluene (25 mL). The reaction solution was purged three times with argon, nitrogen and syngas. The reaction was started using 40 bar syngas (CO/H_2:1:1) and heating to 80 °C. The conversion was controlled via inline manometer. After 4 hours the reaction was complete with a constant pressure of about ~25 bar.

Step 2: Aldoxime preparation

The aldehyde which is formed in step 1 (hydroformylation), was added to Hydroxylamine hydrochloride (2.0 eq.) $Na_2CO_{3(aq)}$ (2.0 eq) in water (20 mL) without removing the toluene. The reaction was stirred for 12 h at 600 rpm. As workup, the phases were separated, and the water phase was extracted with ethyl acetate (3x 50 mL). The solvent was removed under reduced pressure, and the product was purified via automated column chromatography (Biotage) using cyclohexane and ethyl acetate (6/1, *v/v*) as solvent.

9.2.4.1 Synthesis of *rac*-(*E/Z*)-2-Chloro-2-phenylpropanal oxime (7a)

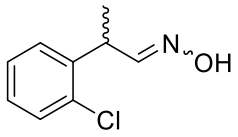

7a

$C_9H_{10}ClNO$

Mw: 183.63 g/mol

The synthesis was carried out according to GP4. **5a** (5.0 g, 36.2 mmol) was dissolved in dry toluene (25 mL) including dicarbonyl(acetylacetonato)rhodium(I) ($Rh(acac)(CO)_2$) (0.06 mol %.), triphenyl phosphine (TPP) (0.6 mol %). The reaction solution was purged three times with argon, nitrogen and syngas. The raction was carried out at 80 °C for 4 h and started by adding 40 bar syngas (CO/H_2:1:1).

The crude **7a** with toluene, was added to Hydroxylamine hydrochloride (2.0 eq.) $Na_2CO_{3(aq)}$ (2.0 eq) in water (20 mL). The reaction was stirred for 12 h and 600 rpm at RT. After work up the product **7a** was obtained as colorless solid.

Yield: 6.4 g, 98%, (*E*/*Z*-ratio = 3/97)

^{1}H NMR (500 MHz, DMSO-d_6) δ [ppm]: 10.96 (s, 1H, *Z*-NO**H**), 10.86 (s, 1H, *E*-NO**H**), 7.36 (m, 4H, Ar-**H**), 6.82 (d,^3J= 7.1 Hz, 1H, *Z*-C**H**=NOH), 4.57 (p, ^3J = 7.1 Hz, 1H, *Z*-C**H**-CH_3), 4.04 (p, ^3J = 6.9 Hz, 1H, *E*-C**H**-CH_3), 1.35 (d, ^3J = 7.1 Hz, 3H, *E*-C**H**$_3$), 1.31 (d, ^3J = 7.1 Hz, 3H, *E*-C**H**$_3$).

The identity was confirmed via ^{1}H-NMR-spectroscopy.[47]

9.2.4.2 Synthesis of *rac*-(*E/Z*)-3-Chloro-2-phenylpropanal oxime (7b)

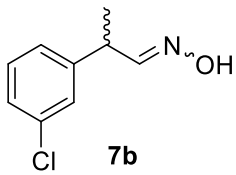

7b

$C_9H_{10}ClNO$

Mw: 183.63 g/mol

The synthesis was carried out according to GP4. **5b** (5.0 g, 36.2 mmol) was dissolved in dry toluene (25 mL) including dicarbonyl(acetylacetonato)rhodium(I) ($Rh(acac)(CO)_2$) (0.06 mol %.), triphenyl phosphine (TPP) (0.6 mol %). The reaction solution was purged three times with argon, nitrogen and syngas. The reaction was carried out at 80 °C for 4 h and started by adding 40 bar syngas (CO/H_2:1:1).

The crude **7b** with toluene, was added to Hydroxylamine hydrochloride (2.0 eq.) $Na_2CO_{3(aq)}$ (2.0 eq) in water (20 mL). The reaction was stirred for 12 and 600 rpm at RT. After work up the product **7b** was obtained as colorless solid.

Yield: 5.7 g, 86%, (*E*/*Z*-ratio = 66/34)

^{1}H NMR (500 MHz, DMSO-d_6) δ [ppm]: 10.96 (s, 1H, *Z*-NO**H**), 10.63 (s, 1H, *E*-NO**H**), 7.46 (d, ^3J = 6.2 Hz, 1H, *E*-C**H**=NOH), 7.29 (m, 4H, Ar-**H**), 6.82 (d,^3J= 7.1 Hz, 1H, *Z*-C**H**=NOH), 4.29 (p, ^3J = 7.1 Hz, 1H, *Z*-C**H**-CH_3), 3.67 (p, ^3J = 6.9 Hz, 1H, *E*-C**H**-CH_3), 1.33 (d, ^3J = 7.1 Hz, 3H, *E*-C**H**$_3$), 1.31 (d, ^3J = 7.1 Hz, 3H, *E*-C**H**$_3$).

The identity was confirmed via ^{1}H-NMR-spectroscopy.[47]

9.2.4.3 Synthesis of *rac*-(*E*/*Z*)-4-Chloro-2-phenylpropanal oxime (7c)

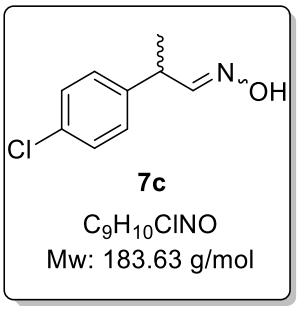

The synthesis was carried out according to GP4. **5c** (5.0 g, 36.2 mmol) was dissolved in dry toluene (25 mL) including dicarbonyl(acetylacetonato)rhodium(I) (Rh(acac)(CO)$_2$) (0.06 mol %.), triphenyl phosphine (TPP) (0.6 mol %). The reaction solution was purged three times with argon, nitrogen and syngas. The reaction was carried out at 80 °C for 4 h and started by adding 40 bar syngas (CO/H_2:1:1).

The crude mixture of **7c** with toluene, was added to Hydroxylamine hydrochloride (2.0 eq.) $Na_2CO_{3(aq)}$ (2.0 eq) in water (20 mL). The reaction was stirred for 12 h and 600 rpm at RT. After work up the product **7c** was obtained as yellow oil.

Yield: 5.3 g, 80%, (*E*/*Z* ratio = 68/32)

^{1}H NMR (500 MHz, DMSO-d_6) δ [ppm]: 10.95 (s, 1H, *Z*-NO**H**), 10.60 (s, 1H, *E*-NO**H**), 7.42 (d, ^3J = 6.1 Hz, 1H, *E*-C**H**=NOH), 7.29 (m, 4H, Ar-**H**), 6.78 (d,^3J= 7.1 Hz, 1H, *Z*-C**H**=NOH), 4.26 (p, ^3J = 7.2 Hz, 1H, *Z*-C**H**-CH_3), 3.65 (p, ^3J = 6.9 Hz, 1H, *E*-C**H**-CH_3), 1.33 (d, ^3J = 7.1 Hz, 3H, *E*-C**H**$_3$), 1.29 (d, ^3J = 7.1 Hz, 3H, *E*-C**H**$_3$).

The identity was confirmed via ^{1}H-NMR-spectroscopy.[47]

9.2.4.4 Synthesis of *rac*-(*E*/*Z*)-2-bromo-2-phenylpropanal oxime (7d)

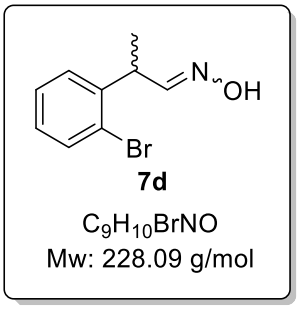

The synthesis was carried out according to GP4. **5d** (5.0 g, 27.3 mmol) was dissolved in dry toluene (25 mL) including dicarbonyl(acetylacetonato)rhodium(I) (Rh(acac)(CO)$_2$) (0.06 mol %.), triphenyl phosphine (TPP) (0.6 mol %). The reaction solution was purged three times with argon, nitrogen and syngas. The reaction was carried out at 80 °C for 4 h and started by adding 40 bar syngas (CO/H_2:1:1).

The crude **7d** with toluene, was added to Hydroxylamine hydrochloride (2.0 eq.) $Na_2CO_{3(aq)}$ (2.0 eq) in water (30 mL). The reaction was stirred for 12 h and 600 rpm at RT. After work up the product **7d** was obtained as yellow oil.

Yield: 6.1 g, 98%, (*E*/*Z* ratio = 20/80)

^{1}H NMR (500 MHz, DMSO-d_6) δ [ppm]: 10.95 (s, 1H, *Z*-NO**H**), 10.86 (s, 1H, *E*-NO**H**), 7.58 (d, ^3J = 6.2 Hz, 1H, *E*-C**H**=NOH), 7.30 (m, 4H, Ar-**H**), 6.81 (d,^3J= 6.6 Hz, 1H, *Z*-C**H**=NOH), 4.26 (p, ^3J = 6.8Hz, 1H, *Z*-C**H**-CH_3), 4.03 (p, ^3J = 7.1 Hz, 1H, *E*-C**H**-CH_3), 1.29 (d, ^3J = 7.2 Hz, 3H, C**H**$_3$).

The identity was confirmed via ^{1}H-NMR-spectroscopy.[47]

9.2.4.5 Synthesis of *rac*-(*E/Z*)-3-bromo-2-phenylpropanal oxime (7e)

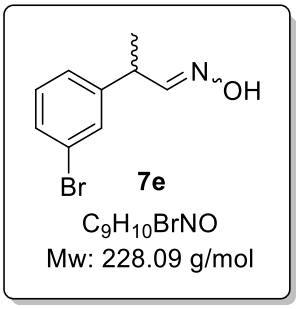

The synthesis was carried out according to GP4. **5e** (5.0 g, 27.0 mmol) was dissolved in dry toluene (25 mL) including dicarbonyl(acetylacetonato)rhodium(I) (Rh(acac)(CO)$_2$) (0.06 mol %.), triphenyl phosphine (TPP) (0.6 mol %). The reaction solution was purged three times with argon, nitrogen and syngas. The reaction was carried out at 80 °C for 4 h and started by adding 40 bar syngas (CO/H$_2$:1:1).

The crude **7e** with toluene, was added to Hydroxylamine hydrochloride (2.0 eq.) $Na_2CO_{3(aq)}$ (2.0 eq) in water (20 mL). The reaction was stirred for 12 h and 600 rpm at RT. After work up the product **7e** was obtained as yellow oil.

Yield: 5.7 g, 92%, (*E*/*Z* ratio = 65/35)

^{1}H NMR (500 MHz, DMSO-d_6) δ [ppm]: 10.96 (s, 1H, *Z*-NO**H**), 10.63 (s, 1H, *E*-NO**H**), 7.44 – 7.28 (m, 5H, Ar-**H,** *E*-C**H**=NOH), 6.81 (d,^3J= 7.1 Hz, 1H, *Z*-C**H**=NOH), 4.28 (p, ^3J = 7.1 Hz, 1H, *Z*-C**H**-CH_3), 3.66 (p, *J* = 7.1 Hz, 1H, *E*-C**H**-CH_3) 1.33 (d, ^3J = 7.1 Hz, 3H, *E*-C**H**$_3$), 1.30 (d, ^3J = 7.1 Hz, 3H, *Z*-C**H**$_3$).

The identity was confirmed via ^{1}H-NMR-spectroscopy.[47]

9.2.4.6 Synthesis of *rac*-(*E/Z*)-4-bromo-2-phenylpropanal oxime (7f)

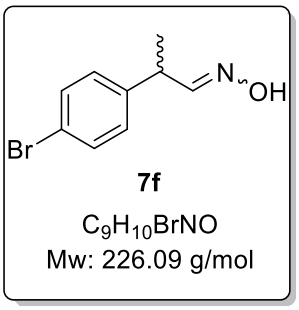

The synthesis was carried out according to GP4. **5f** (5.0 g, 27.3 mmol) was dissolved in dry toluene (25 mL) including dicarbonyl(acetylacetonato)rhodium(I) (Rh(acac)(CO)$_2$) (0.06 mol %.), triphenyl phosphine (TPP) (0.6 mol %). The reaction solution was purged three times with argon, nitrogen and syngas. The reaction was carried out at 80 °C for 4 h and started by adding 40 bar syngas (CO/H$_2$:1:1).

The crude **7f** with toluene, was added to Hydroxylamine hydrochloride (2.0 eq.) $Na_2CO_{3(aq)}$ (2.0 eq) in water (20 mL). The reaction was stirred 600 rpm 12 h in RT. After work up the product **7f** was obtained as yellow oil

Yield: 4.8 g, 80%, (*E*/*Z* -Ratio = 66/34)

^{1}H NMR (500 MHz, DMSO-d_6) δ [ppm]: 10.94 (s, 1H, *Z*-NO**H**), 10.60 (s, 1H, *E*-NO**H**), 7.51 – 7.23 (m, 4H, Ar-**H**), 6.78 (d, ^3J = 6.2 Hz, 1H, *E*-C**H**=NOH), 6.81 (d,^3J= 7.1 Hz, 1H, *Z*-C**H**=NOH), 4.26 (p, ^3J = 7.1 Hz, 1H, *Z*-C**H**-CH_3), 3.64 (p, ^3J = 7.1 Hz, 1H, *E*-C**H**-CH_3) 1.33 (d, *J* = 7.1 Hz, 3H, *E*-C**H**$_3$), 1.29 (d, ^3J = 7.1 Hz, 3H, *Z*-C**H**$_3$).

The identity was confirmed via ^{1}H-NMR-spectroscopy.[47]

9.2.4.7 Synthesis of *rac*-(*E*/*Z*)-2-(2,6-dichlorophenyl)-propanal oxime (7g)

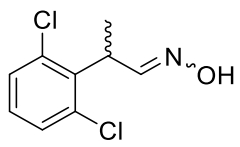

7g
$C_9H_9Cl_2NO$
Mw: 218.07 g/mol

The synthesis was carried out according to GP4. **5g** (2.5 g, 14.4 mmol) was dissolved in dry toluene (10.2 mL) including dicarbonyl(acetylacetonato)rhodium(I) (Rh(acac)(CO)$_2$) (0.06 mol %.), triphenyl phosphine (TPP) (0.6 mol %). The reaction solution was purged three times with argon, nitrogen and syngas. The reaction was carried out at 80 °C for 4 h and started by adding 40 bar syngas (CO/H_2:1:1).

The crude **7g** with toluene, was added to Hydroxylamine hydrochloride (2.0 eq.) $Na_2CO_{3(aq)}$ (2.0 eq) in water (10 mL). The reaction was stirred 600 rpm 12 h in RT. After work up the product **7g** was obtained as light-yellow oil.

Yield: 2.6 g, 82%, (*E*/*Z* ratio = 43/57)

^{1}H NMR (500 MHz, DMSO-d_6) δ [ppm]: δ 10.81 (s, 1H, *Z*-NO**H**), 10.66 (s, 1H, *E*-NO**H**), 7.60 (d, ^3J = 4.2 Hz, 1H, , *E*-C**H**=NOH), 7.47 (d, ^3J = 8.0 Hz, 1H, Ar-**H**), 7.41 (d, *J* = 8.0 Hz, 1H, Ar-**H**), 7.30 (t, ^3J = 8.0 Hz, 1H, Ar-**H**), 7.24 (t,^3J = 8.0 Hz, 1H, Ar-**H**), 7.06 (d, ^3J = 4.6 Hz, 1H, *Z*-C**H**=NOH), 4.72 (m, 1H, *E*-C**H**=NOH), 4.47 (m, 1H, *Z*-C**H**=NOH), 1.47 (d, ^3J = 7.2 Hz, 7H, *E*-C**H**$_3$), 1.38 (d, ^3J = 7.4 Hz, 3H, *Z*-C**H**$_3$)

HRMS (ESI): calcd for $C_9H_9Cl_2NONa$ *m/z* ([M+Na$^+$]) = 239.9950, found 239.9940

9.2.4.8 Synthesis of *rac*-(*E*/*Z*)-2-(2,6-difluorophenyl)-propanal oxime (7h)

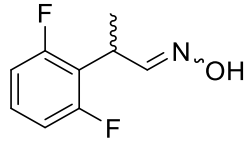

7h
$C_9H_9F_2NO$
Mw: 185,17 g/mol

The synthesis was carried out according to GP4. **5h** (1.0 g, 7.13 mmol) was dissolved in dry toluene (5.0 mL) and dicarbonyl(acetylacetonato)rhodium(I) (Rh(acac)(CO)$_2$) (0.06 mol %.), triphenyl phosphine (TPP) (0.6 mol %). The reaction solution was purged three times with argon, nitrogen and syngas. The reaction was carried out at 80 °C for 4 h and started by adding 40 bar syngas (CO/H_2:1:1).

The crude **7h** with toluene, was added to Hydroxylamine hydrochloride (2.0 eq.) $Na_2CO_{3(aq)}$ (2.0 eq) in water (4 mL). The reaction was stirred 600 rpm 12 h in RT. After work up the product **7h** was obtained as colorless oil.

Yield: 1.2 g, 90%, (*E*/*Z* ratio = 54/46)

^{1}H NMR (500 MHz, DMSO-d_6) δ [ppm]: 10.97 (s, 1H, *Z*-NO**H**), 10.66 (s, 1H, *E*-NO**H**), 7.50 (m, 1H, *E*-C**H**=NOH), 7.34 (m, 1H, Ar-**H**), 7.07 (m , 2H, Ar-**H**), 6.93 (m, 1H, *Z*-C**H**=NOH), 4.48 (m, 1H, *E*-C**H**=NOH), 4.01 (m, 1H, *Z*-C**H**=NOH), 1.41 (d, ^3J = 7.2 Hz, 3H, *E*-C**H**$_3$), 1.34 (d, ^3J = 7.3 Hz, 3H, *Z*-C**H**$_3$)

HRMS (ESI): calcd for $C_9H_9F_2NOH$ *m/z* ([M+H$^+$]) = 186.0720, found 186.0720

9.2.4.9 Synthesis of *rac*-2-(o-tolyl)-propanal oxime (7i)

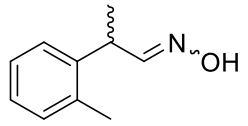

7i

$C_{10}H_{13}NO$

Mw: 163.22 g/mol

The synthesis was carried out according to GP4. **5i** (945.4 mg, 8.0 mmol) was dissolved in dry toluene (5 mL) including dicarbonyl(acetylacetonato)rhodium(I) (Rh(acac)(CO)$_2$) (1.3 mg, 5.0 nmol), triphenyl phosphine (TPP) (13.1 mg, 50.0 nmol). The reaction solution was purged three times with argon, nitrogen and syngas. The reaction was carried out at 80 °C for 4 h and started by adding 40 bar syngas (CO/H$_2$:1:1).

The crude **2i** with toluene, was added to Hydroxylamine hydrochloride (5.5g, 79.0 mmol) $Na_2CO_{3(aq)}$ (8.5 g, 80.0 mmol) in water (50 mL). The reaction was stirred 600 rpm 12 h in RT. Then, organic phase was extracted with ethyl acetate (3x 50 mL). After work up the product **7i** was obtained as white solid.

Yield: 1.15 g, 87 %, (*E*/*Z* ratio = 99/1)

^{1}H NMR (500 MHz, DMSO-d_6) δ [ppm]: 10.85 (s, 1H, *Z*-NO**H**), 10.52 (s, 1H, *E*-NO**H**), 7.40 (d, ^3J = 6.2 Hz, 2H, *E*-C**H**=NOH), 6.75 (d, ^3J = 7.3 Hz, 2H, Ar-**H**), 4.42 (p, ^3J = 7.3 Hz, 1H, *Z*-C**H**=NOH), 3.58 (p, ^3J = 6.9 Hz, 2H, *E*-C**H**-CH$_3$), 2.28 (s, 3H, Ar-C**H**$_3$), 1.32 (d, ^3J = 7.0 Hz, 3H, *E*-C**H**$_3$), 1.28 (d, ^3J = 7.1 Hz, 3H, *Z*-C**H**$_3$)

The identity was confirmed with a similar compound via ^{1}H-NMR-spectroscopy.[47]

9.2.4.10 Synthesis of *rac*-2-(*m*-tolyl)-propanal oxime (7j)

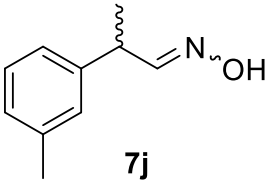

7j

$C_{10}H_{13}NO$

Mw: 163.22 g/mol

The synthesis was carried out according to GP4 under neat conditions. Styrene **5j** (5.0 g, 42.3 mmol) dicarbonyl(acetylacetonato)rhodium(I) (Rh(acac)(CO)$_2$) (5.3 g, 21.0 nmol) and triphenyl phosphine (TPP) (43.1 mg, 164.0 nmol) were placed in the reactor. The reaction solution was purged three times with argon, nitrogen and syngas. The reaction was carried out at 80 °C for 4 h and started by adding 40 bar syngas (CO/H$_2$:1:1).

The crude **7j**, was added to Hydroxylamine hydrochloride (5.5g, 79.0 mmol) $Na_2CO_{3(aq)}$ (8.5 g, 80.0 mmol) in water (50 mL). The reaction was stirred 600 rpm 12 h in RT After work up the product **7j** was obtained as colorless oil.

Yield: 42 %, 2.91 g, (*E*/*Z* ratio = 69/31)

^{1}H NMR (500 MHz, DMSO-d_6) δ [ppm]: 10.88 (s, 1H, *Z*-NO**H**), 10.54 (s, 1H, *E*-NO**H**), 7.42 (d, ^3J = 7.3 Hz, 1H, *E*-C**H**=NOH), 7,07 (m, 4H, Ar-**H**) 6.73 (d, ^3J = 7.1 Hz, 1H, *Z*-C**H**=NOH), 4.43 (p, ^3J = 7.1 Hz, 1H, , *Z*-C**H**-CH$_3$), 3.84 (p, ^3J = 6.8 Hz, 1H, *E*-C**H**-CH$_3$), 2.29 (s, 3H, Ar-C***H***$_3$), 1.33 (d, ^3J = 7.1 Hz, 3H, *E*-C**H**$_3$), 1.29 (d, ^3J = 7.1 Hz, 3H, *Z*-C**H**$_3$)

The identity was confirmed with a similar compound via ^{1}H-NMR-spectroscopy.[47]

Synthesis of *rac*-2-(*p*-tolyl)-propanal oxime (7k)

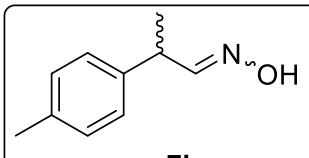

7k

$C_{10}H_{13}NO$

Mw: 163.22 g/mol

The synthesis was carried out according to GP4 under neat conditions. **5k** (5 g, 42.31 mmol) dicarbonyl(acetylacetonato)rhodium(I) ($Rh(acac)(CO)_2$) (5.3 g, 0.021 mmol) and triphenyl phosphine (TPP) (43.14 mg, 0.164 mmol) were placed in the reactor. The reaction solution was purged three times with argon, nitrogen and syngas. The reaction was carried out at 80 °C for 4 h and started by adding 40 bar syngas (CO/H_2:1:1).

The crude **7k**, was added to Hydroxylamine hydrochloride (5.5g, 79.0 mmol) $Na_2CO_{3(aq)}$ (8.5 g, 80.0 mmol) in water (50 mL). The reaction was stirred 600 rpm 12 h in RT. Then, organic phase was extracted with ethyl acetate (3x 50 mL). The organic phase was dried and purification was done by automated column chromatography to obtain the product **7k** as colorless oil.

Yield: 1.92 g, 27%, (*E*/*Z* ratio = 67/33)

^{1}H NMR (500 MHz, DMSO-d_6) δ [ppm]: 10.86 (s, 1H, *Z*-NO**H**), 10.54 (s, 1H, *E*-NO**H**), 7.39 (d, ^3J = 7.3 Hz, 1H, *E*-C**H**=NOH), 7,14 (m, 4H, Ar-H) 6,74 (d, ^3J = 7.3 Hz, 1H, *Z*-C**H**=NOH) 4.25 (p, *J* = 7.1 Hz, 1H, *Z*-C**H**-CH_3), 3.59 (p, ^3J = 6.9 Hz, 1H, *E*-C**H**-CH_3), 2.29 (s, 3H, Ar-C***H***$_3$), 1.33 (d, *J* = 7.1 Hz, 3H, *E*-C**H**$_3$), 1.29 (d, ^3J = 7.1 Hz, 3H, *Z*-C**H**$_3$)

The identity was confirmed with a similar compund via ^{1}H-NMR-spectroscopy.[47]

9.2.4.11 Synthesis of *rac*-2-(2-fluorophenyl)-propanal oxime (4a)

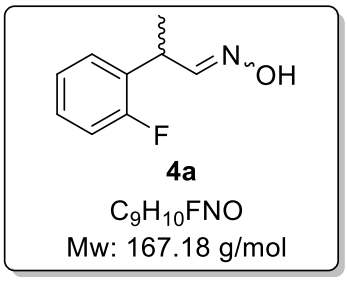

4a

$C_9H_{10}FNO$

Mw: 167.18 g/mol

The synthesis was carried out according to GP4. **5l** (5 g, 40.9 mmol) was dissolved in dry toluene (5.0 mL) and dicarbonyl(acetylacetonato)rhodium(I) ($Rh(acac)(CO)_2$) (12.9 mg, 0.05 mmol), triphenyl phosphine (TPP) (131.1 mg, 0.5 mmol). The reaction solution was purged three times with argon, nitrogen and syngas. The reaction was carried out at 80 °C for 4 h and started by adding 40 bar syngas (CO/H_2:1:1).

The crude **4a** with toluene, was added to Hydroxylamine hydrochloride (5.5g, 79.0 mmol) $Na_2CO_{3(aq)}$ (8.5 g, 80.0 mmol) in water (50 mL). The reaction was stirred 600 rpm 12 h in RT. The organic phase was dried and purification was done by automated column chromatography to obtain the product **4a** as colorless oil.

Yield: 3.15 g, 46%, (*E*/*Z* ratio = 76/24)

^{1}H NMR (500 MHz, DMSO-d_6) δ [ppm]: 10.95 (s, 1H, *Z*-NO**H**), 10.6 (s, 1H, *E*-NO**H**), 7.41 (d, ^3J = 6.2 Hz, 1H, *E*-C**H**=NOH), 7.40 – 7.33 (m, 1H, Ar-**H**), 7.16 – 7.01 (m, 3H, Ar-**H**), 6.81 (d,^3J= 7.1 Hz, 1H, *Z*-C**H**=NOH), 3.65 (p, ^3J = 7.1 Hz, 1H, *E*-C**H**-CH_3), 1.35 (d, ^3J = 7.1 Hz, 3H, C***H***$_3$).

9.2.4.12 Synthesis of *rac*-2-(3-fluorophenyl)-propanal oxime (4b)

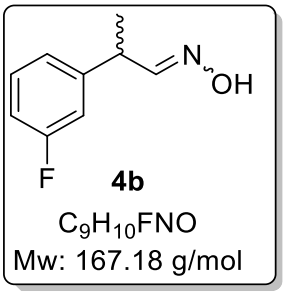

The synthesis was carried out according to GP4. **5m** (5 g, 40.9 mmol) was dissolved in dry toluene (5.0 mL) and dicarbonyl(acetylacetonato)rhodium(I) ($Rh(acac)(CO)_2$) (12.9 mg, 0.05 mmol), triphenyl phosphine (TPP) (131.14 mg, 0.5 mmol). The reaction solution was purged three times with argon, nitrogen and syngas. The reaction was carried out at 80 °C for 4 h and started by adding 40 bar syngas (CO/H_2:1:1).

The crude **4b** with toluene, was added to Hydroxylamine hydrochloride (5.5g, 79.0 mmol) $Na_2CO_{3(aq)}$ (8.5 g, 80.0 mmol) in water (50 mL). The reaction was stirred 600 rpm 12 h in RT. After work up the product **4b** was obtained as colorless oil.

Yield: 5.28 g, 77%, (*E*/*Z* ratio = 66/34)

^{1}H NMR (500 MHz, DMSO-d_6) δ [ppm]: 10.95 (s, 1H, *Z*-NO**H**), 10.6 (s, 1H, *E*-NO**H**), 7.41 (d, ^3J = 6.2 Hz, 1H, *E*-C**H**=NOH), 7.40 – 7.33 (m, 1H, Ar-**H**), 7.16 – 7.01 (m, 3H, Ar-**H**), 6.81 (d,^3J= 7.1 Hz, 1H, *Z*-C**H**=NOH), 3.65 (p, *J* = 7.1 Hz, 1H, *E*-C**H**-CH_3), 1.35 (d, *J* = 7.1 Hz, 3H, C**H**$_3$).

9.2.4.13 Synthesis of *rac*-2-(4-fluorophenyl)-propanal oxime (4c)

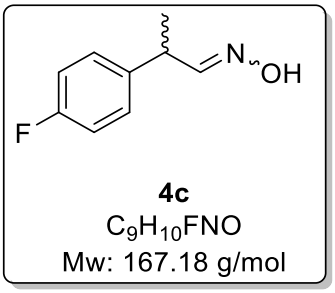

The synthesis was carried out according to GP4. **5n** (5 g, 42.31 mmol) was dissolved in dry toluene (5.0 mL) and dicarbonyl(acetylacetonato)rhodium(I) ($Rh(acac)(CO)_2$) (5.3 g, 0.021 mmol), triphenyl phosphine (TPP) (43.14 mg, 0.164 mmol). The reaction solution was purged three times with argon, nitrogen and syngas. The reaction was carried out at 80 °C for 4 h and started by adding 40 bar syngas (CO/H_2:1:1).

The crude **4c** with toluene, was added to Hydroxylamine hydrochloride (5.5g, 79.0 mmol) $Na_2CO_{3(aq)}$ (8.5 g, 80.0 mmol) in water (50 mL). The reaction was stirred 600 rpm 12 h in RT. The organic phase was dried and purification was done by auto column to afford the **4c** as colorless oil.

Yield: 5.80 g, 85%, (*E*/*Z* ratio = 68/32)

^{1}H NMR (500 MHz, DMSO-d_6) δ [ppm]: 10.91 (s, 1H, *Z*-NO**H**), 10.57 (s, 3H, *E*-NO**H**), 7.42 (d, ^3J = 6.1 Hz, 4H, *E*-C**H**=NOH), 7.30 (m, 2H, Ar-**H**), 7.19 – 7.06 (m, 2H, Ar-**H**), 6.78 (d, ^3J = 7.2 Hz, 1H, *Z*-C**H**=NOH), 4.19 (p, ^3J = 7.2 Hz, 1H, *E*-C**H**-CH_3) 3.65 (p, ^3J = 6.9 Hz, 1H, *Z*-C**H**-CH_3), 1.33 (d, *J* = 7.1 Hz, 3H, C**H**$_3$).

9.2.5 General procedure 5 (GP5): Synthesis of aldoximes via condensation using hydroxylamine

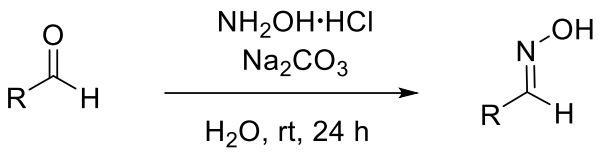

Hydroxylamine hydrochloride (2.5 eq.) and sodium carbonate (2.5 eq.) were dissolved in water. The aldehyde (1.0 eq.) was added, and the suspension was stirred at room temperature for 24 h. The suspension was extracted with ethyl acetate or cyclohexane. The combined organic phases were dried over magnesium sulfate and the solvent was removed under reduced pressure.

9.2.5.1 Synthesis of *rac*-(*E*/*Z*)-2-phenylpropanal oxime (8)

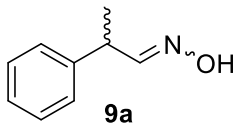

9a
$C_9H_{11}NO$
Mw: 149.14 g/mol

The synthesis of *rac*-(*E*/*Z*)-2-phenylpropanal oxime was carried out according to GP5. Hydroxylamine hydrochloride (13.0 g, 187 mmol) and sodium carbonate (19.8 g, 75 mmol) were dissolved in water. Then, *rac*-2-phenylpropanal (**8a**, 10 mL, 75 mmol,) was added. Workup led to the pure product as colorless oil.

Yield: 10.0 g, 90%, (*E*/*Z*-Ratio: 69/31).

^{1}H NMR (500 MHz, DMSO-d_6): δ [ppm] 10.88 (s, 1H, *Z*-NO**H**), 10.55 (s, 1H, *E*-NOH), 7.43 (d, ^3J = 6.2 Hz, 1H, *E*-C**H**=NOH), 7.35 – 7.19 (m, 5H, Ar-**H**), 6.79 (d, ^3J = 7.2 Hz, 1H, *Z*-C**H**=NOH), 4.29 (p, ^3J = 7.2 Hz, 1H, *Z*-C**H**-CH_3), 3.63 (p, ^3J = 6.9 Hz, 1H, *E*-C**H**-CH_3), 1.34 (d, ^3J = 7.1 Hz, 3H, *E*-C**H**$_3$), 1.33 (d, ^3J = 7.1 Hz, 3H, *Z*-C**H**$_3$).

9.2.6 General procedure 6 (GP6): Copper catalyzed nitrile synthesis

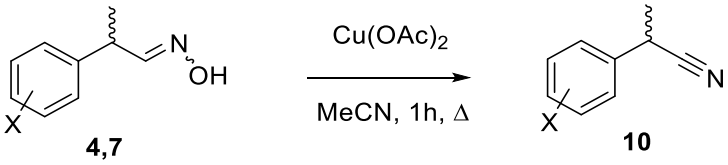

Copper(II)acetate (0.1 eq.) was dissolved in acetonitrile at room temperature. *Rac*-(*E/Z*)-fluoro-phenylpropanal oximes (1.0 eq.) were added and heated to reflux for 90 minutes. Conversion was controlled by means of TLC (cyclohexane/ethyl acetate, 6:1 *v/v*). The solvent was removed under reduced pressure to give the crude product. The crude product was dissolved in cyclohexane/ethyl acetate (8:1, *v/v*) and purified over silica gel (silica gel, 3 cm filling height). The pure products were obtained as oils.

9.2.6.1 Synthesis of the *rac*-2-(2-fluorophenyl)-propanenitrile (9)

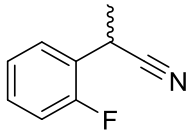

10a
C_9H_8FN
Mw: 149.17 g/mol

The synthesis of *rac*-2-(2-fluorophenyl)-propanenitrile was carried out according to GP6. Copper(II) acetate (8.2 mg, 45 µmol) was dissolved in acetonitrile (5 mL). The aldoxime (**7a**) (116.0 mg, 694.0 µmol) was then added. Workup by column chromatography (cyclohexane/ethyl acetate, 8:1 *v/v*) led to the product **9** as a colorless oil.

Yield: 65 mg, 63%.

^{1}H NMR (500 MHz, DMSO-d_6): δ [ppm] = 7.50 (td, ^3J = 7.7, 1.5 Hz, 1H, Ar-**H**), 7.47 – 7.39 (m, 1H, Ar-**H**), 7.32 – 7.22 (m, 2H, Ar-**H**), 4.46 (q, ^3J = 7.2 Hz, 1H, C**H**-CH_3), 1.54 (dd, ^3J = 11.2, 7.2 Hz, 3H, C**H**$_3$).

^{13}C NMR (500 MHz, DMSO-d_6): δ [ppm] = 163.31, 161.07, 134.3, 129.4, 122.65, 116.3, 29.6, 21.0.

IR [cm^{-1}]: 2999 (υ, Ar-H), 2933 (υ, CH_3), 2248 (υ, C=N) , 1603 (υ, C=C), 1509 (δ, C-C-H), 1201 (υ, C-F).

MS (ESI, positive ions) m/z calculated for $C_9H_8FNH^+$: 299.1 $[2M+H]^+$, found 301.2.

9.2.6.2 Synthesis of the *rac*-2-(3-fluorophenyl)-propanenitrile (10b)

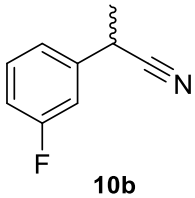

10b
C_9H_8FN
Mw: 149.17 g/mol

The synthesis of the *rac*-2-(3-fluorophenyl)-propanenitrile was carried out according to GP6. Copper(II)acetate (8.2 mg, 45 µmol) was dissolved in 5 mL acetonitrile. The aldoxime (60.0 mg, 359 µmol) was then added. After working up by column chromatography (cyclohexane/ethyl acetate, 8:1, *v/v*), product **10b** was obtained as colorless oil.

Yield: 50 mg, 92%.

^{1}H NMR (500 MHz, DMSO-d_6): δ [ppm] = 7.52 – 7.42 (m, 1H, Ar-**H**), 7.28 (dd, ^3J = 9.2, 2.7 Hz, 2H, Ar-**H**), 7.23 – 7.16 (m, 1H, Ar-**H**), 4.35 (q, ^3J = 7.2 Hz, 1H, C**H**-CH_3), 1.55 (dd,^3J = 7.3, 1.2 Hz, 3H, C**H**$_3$).

^{13}C NMR (500 MHz, DMSO-d_6): δ [ppm] = 163.7, 161.7, 140.7, 131.5, 123.4, 123.4, 122.3, 115.2, 114.4, 33.0, 20.7.

IR [cm^{-1}]: 2999 (υ, Ar-H), 2939 (υ, CH_3), 2242 (υ, C=N),1609-1600 (υ, C=C), 1484-1444 (δ, C-C-H), 1284-1239 (υ, C-F).

MS (ESI, positive ions) m/z calculated for $C_9H_8FNH^+$: 299.1 $[2M+H]^+$, found 301.2.

9.2.6.3 Synthesis of the *rac*-2-(4-fluorophenyl)-propanenitrile (10c)

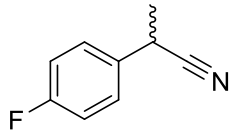

10c
C_9H_8FN
Mw: 149.17 g/mol

The synthesis of *rac*-2-(4-fluorophenyl)-propanenitrile was carried out according to GP6. Copper(II) acetate (8.2 mg, 45 µmol) was dissolved in acetonitrile (5 ml). The aldoxime (71.0 mg, 452.0 µmol) was then added. After working up by column chromatography (cyclohexane/ethyl acetate, 8:1, *v/v*), the product **10c** was obtained as a colorless oil.

Yield: 60 mg, 88%.

^{1}H NMR (500 MHz, DMSO-d_6) δ [ppm]: 7.46 (m, 2H, Ar-**H**), 7.25 (m, 2H, Ar-**H**), 4.32 (q, ^3J = 7.2 Hz, 1H, C**H**-CH_3), 1.53 (d, ^3J = 7.2 Hz, 3H, C**H**$_3$).

The identity was confirmed via ^{1}H-NMR-spectroscopy.[47]

9.2.6.4 Synthesis of the *rac*-2-(2,6-dichlorophenyl)-propanenitrile (10d)

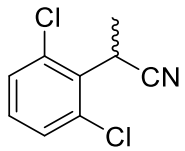

10d
$C_9H_7Cl_2N$
Mw: 200.06 g/mol

The synthesis was carried out according to GP6. Copper(II) acetate (9.8 mg, 10 mol%) was dissolved in acetonitrile (2.7 mL) allow to stir for 10 min. Subsequently, aldoxime **7h** (100 mg, 0.54 mmol) was added and kept for two hours in reflux condition. The full conversion was monitored by TLC. To quench and purification, filtration over silica resulted in **10d** as a brown oil.

Yield: quant., brown oil.

^{1}H NMR (500 MHz, Chloroform-*d*): δ [ppm] = 7.38 (dd, *J* = 8.1, 1.6 Hz, 2H, Ar-*H*), 7.27 – 7.21 (m, 1H, Ar-H), 4.86 (dd, *J* = 7.2, 1.5 Hz, 1H, C**H**-CH_3), 1.72 (dd, *J* = 7.3, 1.6 Hz, 3H, C**H**$_3$).

^{13}C NMR (126 MHz, Chloroform-*d*) δ [ppm] = 134.7, 131.9, 129.8, 129.4, 27.1, 16.7 (one carbon overlappes).

HRMS (ESI) m/z calculated for $C_9H_7Cl_2NH$: 200.0030 [M+H$^+$], found 200.0000.

9.2.6.5 Synthesis of the *rac*-2-(2,6-difluorophenyl)-propanenitrile 4h:

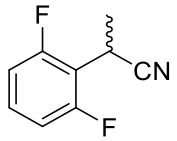

10h
$C_9H_7F_2N$
Mw: 167.05 g/mol

The synthesis was carried out according to GP5. CuOAc (9.8 mg, 0.1 eq) was dissolved in acetonitrile (2.7 mL) allow to stir for 10 min. Subsequently, aldoxime **7g** (100 mg, 0.5 mmol) was added and kept for two hours in reflux condition. The full conversion was monitored by TLC. To quench and purification, filtration over silica resulted in **10h** as a brown oil

Yield: quant., brown oil.

^{13}C NMR (126 MHz, Chloroform-*d*) δ [ppm]: 161.4, 161.3, 159.4, 159.3, 130.2, 130.1, 130.1, 113.2, 112.0, 112.0, 111.9, 111.9, 77.2, 77.0, 76.7, 20.0, 20.0, 20.0, 18.6.

HRMS (ESI): m/z calculated for $C_9H_7F_2NH$: [M+H$^+$] = 168.0620, found 168.1000.

9.2.6.6 Synthesis of *rac*-2-(*o*-tolyl)-propionitrile (10f)

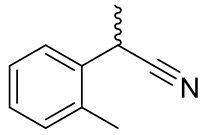

10i
$C_{10}H_{11}N$
Mw: 145.21 g/mol

The synthesis was carried out according to GP5. Cupper(II) acetate (16.3 mg, 0.09mmol) was dissolved in 20 mL acetonitrile. *Rac*-(*E*/*Z*)-2-methyl-phenylpropanal oxime (150 mg, 0.9 mmol) was added. Acetonitrile was removed and the product **10f** was obtained after automated column chromatography as colorless oil.

Yield: 79 mg, 58%.

^{1}H NMR (500 MHz, DMSO-d_6): δ [ppm] = 7.21 – 7.01 (m, 4H, Ar-**H**) 4.38 (m, 1H, C**H**), 2.34 (s, 3H, Ar-C**H**$_3$), 1.52 (d, ^3J = 7.2 Hz, 3H, C**H**$_3$)

9.2.6.7 Synthesis of *rac*-2-(*m*-tolyl)-propionitrile (10g)

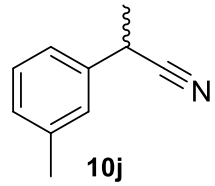

10j
$C_{10}H_{11}N$
Mw: 145.21 g/mol

The synthesis was carried out according to GP5. Cupper(II) acetate (16.3 mg, 0.09 mmol) was dissolved in 20 mL acetonitrile. *Rac*-(*E*/*Z*)-3-methyl-phenylpropanal oxime (150 mg, 0.9 mmol) were added. Acetonitrile was removed and the product was obtained after automated column chromatography as colorless oil.

Yield: 51 mg, 36%.

^{1}H NMR (500 MHz, DMSO-d_6): δ [ppm] = 7.21 – 6.97 (m, 4H, Ar-**H**) 4.25 (m, 1H, C**H**), 2.33 (s, 3H, Ar-C**H**$_3$), 1.53 (d, ^3J = 7.2 Hz, 3H, C**H**$_3$)

9.2.6.8 Synthesis of *rac*-2-(*p*-tolyl)-propionitrile (10h)

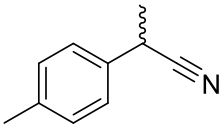

10k
$C_{10}H_{11}N$
Mw: 145.21 g/mol

The synthesis was carried out according to GP6. Cupper(II) acetate (16.3 mg, 0.09 mmol) was dissolved in 20 mL acetonitrile. *Rac*-(*E*/*Z*)-3-methyl-phenylpropanal oxime (150 mg, 0.9 mmol) were added. Acetonitrile was removed and the product was obtained after automated column chromatography as colorless.

Yield: 26 mg, 19%.

^{1}H NMR (500 MHz, DMSO-d_6): δ [ppm] = 7.23 – 6.99 (m, 4H, Ar-**H**) 4.24 (q, ^3J = 7.2 Hz, 1H, C**H**), 2.30 (s, 3H, Ar-C**H**$_3$), 1.52 (d, ^3J = 7.2 Hz, 3H, C**H**$_3$)

9.2.6.9 Synthesis of *rac*-2-(4-Fluorphenyl)-butanenitrile (10l)

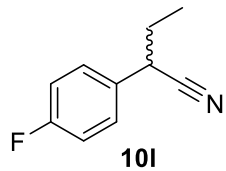

10l
$C_{10}H_{10}FN$
Mw: 163.19 g/mol

The synthesis was carried out according to GP6. Cupper(II)acetate (6.3 mg, 0.034 mmol) was dissolved in acetonitrile (3.5 mL). *Rac*-(*E*/*Z*)-2-(4-fluorophenyl)butanal oxime (61.5 mg, 0.34 mmol) were added. Acetonitrile was removed and the product **10l** was obtained after automated column chromatography as yellow oil.

Yield: 19 mg, 34%.

^{1}H NMR (500 MHz, Chloroform-*d*): δ [ppm] = 7.34 – 7.27 (m, 2H, Ar-**H**), 7.07 (m, 2H, Ar-**H**), 3.72 (t, ^3J = 7.2 Hz, 1H, C**H**-CH_2-), 1.93 (pd, *J* = 6.9, 2.4 Hz, 2H, C**H**$_2$-CH_3), 1.07 (t, *J* = 7.4 Hz, 3H, CH_2-C**H**$_3$).

9.2.6.10 Synthesis of *rac*-2-(4-fluorophenyl)-3-methylbutanenitrile (10m)

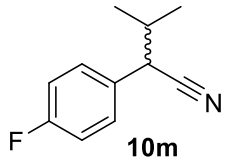

10m

$C_{11}H_{12}FN$
Mw: 177.22 g/mol

The synthesis was carried out according to GP6. Cupper(II) acetate (7.2 mg, 0.04 mmol) was dissolved in acetonitrile (3.5 mL). *rac*-(*E*/*Z*)- 2-(4-fluorophenyl)-3-methylbutanal oxime (75.4 mg, 0.39 mmol) were added. Acetonitrile was removed and the product **10m** was obtained after automated column chromatography as a yellow oil.

Yield: 19 mg, 27%.

^{1}H NMR (500 MHz, Chloroform-*d*): δ [ppm] = 7.31 – 7.25 (m, 2H, Ar-**H**), 7.07 (t, *J* = 8.6 Hz, 2H, Ar-**H**), 3.64 (d, *J* = 6.3 Hz, 1H, C**H**-CH-(CH_3)$_2$), 2.10 (h, *J* = 6.6 Hz, 1H, CH-C**H**-(C*H*$_3$)$_2$), 1.04 (dd, *J* = 8.8, 6.7 Hz, 6H, -CH-CH-(C**H**$_3$)$_2$).

9.3 Biochemical and molecular biological methods

9.3.1 Buffers and Solutions

Table 20: Buffers and composition.

Solution	Composition
Potassium phosphate buffer (100 mM, pH 8)	6.42 g potassium dihydrogen phosphate 0.52 g dipotassium hydrogen phosphate In 500 mL dH_2O
Potassium phosphate buffer (100 mM, pH 7)	6.81 g potassium dihydrogen phosphate 8.71 g dipotassium hydrogen phosphate in 500 mL dH_2O
Tris-HCl-Buffer (100 mM, pH 6)	12.1 g tris(hydroxymethyl)-aminomethane calibration pH with HCl-Solution (100 mM) in 1 L dH_2O
HEPES-Buffer (100 mM, pH 6.8-8.4)	23.8 g 4-(2-hydroxyethyl)-1-piperazine-ethanesulfonic acid) pH with NaOH-Solution (100 mM) in 1 L dH_2O
Citric acid-Buffer (100 mM, pH 6)	2.41 g citric acid monohydrate 25.88 g trisodium citrate dihydrate in 1 L dH_2O

Table 21: Buffers for Ni-NTA column chromatography.

Solution	Composition
Lysis buffer	50 mM PPB, pH 8
	300 mM sodium chloride
	10 mM imidazole
	pH 8 in 250 mL H_2O
Washing buffer A	50 mM PPB, pH 8
	300 mM sodium chloride
	20 mM imidazole
	pH 8 in 250 mL H_2O
Washing buffer B	50 mM PPB, pH 8
	300 mM sodium chloride
	40 mM imidazole
	pH 8 in 250 mL H_2O
Washing buffer C	50 mM PPB, pH 8
	300 mM sodium chloride
	60 mM imidazole
	pH 8 in 250 mL H_2O
Elution buffer	50 mM PPB, pH 8
	300 mM sodium chloride
	250 mM imidazole
	pH 8 in 250 mL H_2O

Table 22: Media, solitions and their composition.

Solution	Composition
LB-Medium	10 g·L^{-1} tryptone
	5 g·L^{-1} yeast extract
	10 g L^{-1} sodium chloride
LB-Agar	LB-Medium
	15 g·L^{-1} Agar
TB-Medium	12 g·L^{-1} tryptone
	24 g·L^{-1} yeast extract
	5 g·L^{-1} glycerol
	90 mM potassium phosphate buffer, pH 7.4
Ampicillin	stock solution 100 mg·mL^{-1}
	end concentration 100 µg·mL^{-1}
Kanamycin	stock solution 50 mg·mL^{-1}
	end concentration 50 µg·mL^{-1}
Chloramphenicol	stock solution 34 mg·mL^{-1}
	end concentration 34 µg·mL^{-1}
IPTG	stock solution 1 mol·L^{-1}
	end concentration 100 mmol·L^{-1}

Table 23: SDS-gel solutions and compositions.

Solution	Composition
Collector gel (4%)	2.97 mL dH_2O
	1.25 mL 0.5 M Tris-HCl (pH 6.8)
	50 µL SDS (10%)
	0.67 mL Acrylamide
	0.05 mL APS
	5 µL TEMED
Separation gel (15%)	2.2 mL dH_2O
	5 mL acrylamide (10%)
	2.6 mL 1.5 M Tris (pH8.8)
	100 µL SDS (10%)
	100 µL APS
	10 µL TEMED
Staining solution	acetic acid (10%)
	ethanol (30%)
	dH_2O (60 %)
	1 g·L^{-1} coomassie
Destaining solution	acetic acid (10%)
	ethanol (30%)
	dH_2O (60 %)

9.3.2 Plasmids and Strains

Table 24: Genes and their corresponding vectors.

Gene	Origin	Plasmid
OxdRE	*Rhodococcss erythropolis*	pET28(+)a, *lac*I, Kan$_R$, pBR322 origin, t7
OxdA	*Pseudomonas chlororaphis*	pET28(+)a, *lac*I, Kan$_R$, pBR322 origin, t7
OxdB	*Bacillus sp.*	pET28(+)a, *lac*I, Kan$_R$, pBR322 origin, t7
OxdB	*Bacillus sp.*	pUC18, *lac*I, CM$_R$, pBR322 origin, lac-promotor

Table 25: *E.coli* strains that were used for expression or plasmid amplification.

Strain	Application
BL21-(DE3)	Expression
BL21-(DE3)-STAR	Expression
BL21-(DE3)-RIL	Expression
DH5α	Plasmid amplification, cloning

9.3.3 Site directed mutagenesis via Quick-Change PCR

The site directed mutagenesis was carried out with a template plasmid and a set of designed primer. The primers were designed according to the Quick-Change-protocol. The Quick-Change PCR was done with the following program in **Table 27** and the composition in **Table 26**.

Table 26: Component mixture for PCR-Reaction.

Component	Volume/ µL
HF-Buffer	5
dNTP (10 mM)	0.5
Fw-Primer (10 µM)	0.5
Rw-Primer (10 µM)	0.5
Phusion-Polymerase (0.02 U/µL)	0.5
Template (50 ng/µL)	2.0
DMSO	1
dH_2O	15.0

Table 27: QC-PCR-program.

PCR-Steps	Temperature/ °C	Time/ s	Cycle
Initial denaturation	98	120	1
Denaturation	98	30	25
Annealing	58-64	30s	25
Elongation	72	64	25
Final elongation	72	300	1
Storage	4	∞	1

9.3.4 Aldoxime dehydratase variants and constructs

Table 28: List of Oxds and variants with their vector construct and mutation.

Oxd-Variants	Mutation	Plasmid
OxdRE-1	WT	pET28a-(+)-(n-His)
OxdRE-2	M29G	pET28a-(+)-(n-His)
OxdRE-3	L145A	pET28a-(+)-(n-His)
OxdRE-4	A147G	pET28a-(+)-(n-His)
OxdRE-5	M28	pET28a-(+)-(n-His)
OxdRE-6	L145F	pET28a-(+)-(n-His)
OxdRE-7	L318A	pET28a-(+)-(n-His)
OxdRE-8	L145G	pET28a-(+)-(n-His)
OxdRE-9	L145F/L318A	pET28a-(+)-(n-His)
OxdRE-10	M28/L145A/A147G	pET28a-(+)-(n-His)
OxdRE-11	M29G/L145G/A147G/L318G	pET28a-(+)-(n-His)
OxdRE-12	M29G/L145A/A147G/L318G	pET28a-(+)-(n-His)
OxdRE-13	F306A	pET28a-(+)-(n-His)
OxdRE-14	L145M	pET28a-(+)-(n-His)
OxdRE-15	L145R	pET28a-(+)-(n-His)
OxdRE-16	S218Y	pET28a-(+)-(n-His)
OxdRE-17	L145S	pET28a-(+)-(n-His)
OxdRE-18	L318A/F306A	pET28a-(+)-(n-His)
OxdRE-19	L145F/M29G	pET28a-(+)-(n-His)
OxdRE-20	L145N	pET28a-(+)-(n-His)
OxdRE-21	L217K	pET28a-(+)-(n-His)
OxdRE-22	L145D	pET28a-(+)-(n-His)
OxdRE-23	M29G/A147G	pET28a-(+)-(n-His)
OxdRE-24	M29G/L318G	pET28a-(+)-(n-His)
OxdRE-25	M29G/L145G/A147G	pET28a-(+)-(n-His)
OxdRE-26	M29G/L145A	pET28a-(+)-(n-His)
OxdRE-27	M28/A147G	pET28a-(+)-(n-His)
OxdRE-28	L145Del	pET28a-(+)-(n-His)
OxdRE-29	H299C	pET28a-(+)-(n-His)
OxdRE-30	L318N	pET28a-(+)-(n-His)
OxdRE-31	L145Y	pET28a-(+)-(n-His)
OxdRE-32	L145P	pET28a-(+)-(n-His)
OxdB-1	WT	pUC18
OxdB-2	F288	pUC18
OxdB-3	L304G	pUC18

Oxd-Variants	Mutation	Plasmid
OxdB-4	L288/L293A/K294G	pUC18
OxdB-5	F288/L293A	pET28a
OxdB-6(Sol1)	(M19L/P20R/P36R)	pET28a-(+)-(n-His)
OxdB-7(Sol2)	(K79E/I116E/L235E/L237R/Y303R)	pET28a-(+)-(n-His)
OxdB-8(Sol3)	(M19L/P20R/P36R/K79E/I116E/L235R/Y303R)	pET28a-(+)-(n-His)
OxdB-9	L128F	pUC18
OxdB-10	L128Y	pUC18
OxdA-1	WT	pET28a-(+)-(n-His)
OxdA-2	L145F	pET28a-(+)-(n-His)
OxdRE-3DM-Set1	H23R/P25R/E37Q/S39R/T135M/T209I/E331I/S340I/E348V/ T350I	pET28a
OxdRE-3DM-Set1a	P25R/T135M/T209I/E331I	pET28a
OxdRE-3DM-Set1b	S340I/E348V/T350I	pET28a
OxdRE-3DM-Set2	P25R/E37Q/S39R/T135M/T209I/E331	pET28a

9.3.5 DPN1 -Treatment, Ligation and Transformation

The PCR-product was treated with *DPN1* for 1 hour at 37 degrees. After the *DPN1* treatment the PCR-Product was treated with T4-ligase, which is not a necessary step, but recommended one to ligate the PCR-product to a closed Vector. This closed Vector was then transformed to competent *E. coli* Cells.

For the Transformation the competent cells, which are stored at -80 °C, are placed in a tubes with ice. Then the ligation solution or the plasmid of choice is added to the competent cells and incubated for 30 minutes. Afterwards the cells are heat shock treated for 90 seconds at 42 °C. Then 700 µL LB-Medium is added and the cell solution is incubated for 3 hours at 37 °C and 1200 rpm. The suspension was then centrifuged at 11.000 g and 600 µL of LB-Medium was discarded. The cell pellet was then resuspended again in the left 100 µL medium. The cell suspension of 100 µL was then poured over an LB-agar-plate and incubated over night at 37 °C

9.3.6 Agar plate preparation

The agar plates were prepared by dissolving 10 g of LB-medium, 6 g of agar in 400 mL of water. The solution is then sterilized using an autoclave. The thick solution of agar is cooled down until ~60 °C, before adding the respective antibiotics (100 $\mu g \cdot ml^{-1}$ final concentration). Afterwards the solution is poured into sterile plates.

9.3.7 Preculture

The preliminary cultures were prepared in test tubes. 5 ml of LB-medium and the desired antibiotic with a concentration of 50 $\mu g \cdot ml^{-1}$ were transferred to the sterile test tubes. The colonies were removed from the plate with a toothpick and then used to inoculate the precultures.

9.3.8 Main culture

IPTG-Expression

For the main culture, sterilized 2 L-Flask with 1800 mL TB- or LB-Medium and the respective antibiotics (**Table 22**) were used. The cultivating started by adding 5 ml of the preculture. The main culture was incubated at 20-30 °C, 120 rpm for 12 hours till the OD_{600} has reached 0.5-0.7. The expression was started by adding 2 mL of IPTG (1 mM). After 24 hours, the cells were harvested.

Auto-Induction-Expression

For auto induction medium, sterilized 2-L-Flask with TB-Medium (1.7 L, pH 7.2) Glucose (20 mL, $20 g \cdot L^{-1}$), Lactose (180 mL, $20 g \cdot L^{-1}$) and the respective antibiotics (**Table 22**). The cultivating started by adding 5 ml of the preculture. For the cell growth the culture was first incubated at 37 °C for two hours then at 15 °C for 72 °C hours, for expression.

Leaky-Expression

For the main culture, sterilized 500 mL-Flask with LB-Medium (400 mL) and Kanamycin ($50 \mu g \cdot mL^{-1}$) were used. The cultivating started by adding 5 ml of the preculture. The main culture was incubated at 20°C, 155 rpm for 72 hours.

9.3.9 Cell free extract

The cells being resuspended in 75% wt potassium phosphate buffer (PPB, 10 mM, pH 8). For cell destruction, the cells were sonicated 2 times with 10% energy 50% pulse time and 3 min duration. The Suspension was centrifuged at 5000 g for 15 mins. The supernatant was centrifuged at 21.000 g for 20 mins. As result in the first pellet, the cell parts are to be found, in the second pellet the inclusion bodies and in the supernatant the proteins.

9.3.10 Purification via Ni-NTA column chromatography

The harvested cell was resuspended with 25 % (w/v) of lysis buffer and sonicated 2x 15 mins with 10% energy and 50% cycles. The suspension was centrifugated 20 mins with 20.000 g. The cell pellet was discarded, and the supernatant was used fort the purification. The Ni-NTA column was first washed with water (5 CV). Then the column was equilibrated with Lysis buffer (5 CV). After equilibration, the supernatant was loaded to the column. The column was washed with washing buffer **A** (10 CV), washing buffer **B** (5 CV) and with washing buffer **C** (5 CV). The protein was then eluted with elution buffer (2 CV) The column was regenerated by washing with washing buffer **C**, 1 M NaOH and dH_2O each step using 5 CV. The column or the Ni-NTA was stored in 20% ethanol.

9.3.11 Desalting and Buffer exchange

Buffer was changed by either using a prepacked PD-10 sephadex G-25 gel filtration column or washing with target buffer using centrifugal filters. To apply the protein on PD10, the column was washed with 5 CV water and 5CV

of target buffer for equilibration. The Protein solution was concentrated to final volume of 2.5 mL. The protein solution was applied onto the column. And eluted with 3.8 mL of target buffer.

For desalting or buffer exchange with centrifugal filters the protein solution was concentrated from 15 mL volume to 500 µL by centrifuging at 5000 g for 45 mins. As washing step, the target buffer was added to the protein solution to a final volume of 15 mL and centrifuged again to 500 µL final volume. The washing step was repeated five times.

9.3.12 Determination of protein concentration (Bradford-Assay)

The protein concentration was determined via standard Bradford-Assay[168]. In a microtiter plate, bovine serum albumin as a calibration series and the protein solutions that need to be investigated are placed. Bradford reagent is then added, and the solutions are incubated at 25 °C for 15 min. The measured absorbance at 595 nm is then used to calculate the protein concentration in triplicate.

9.3.13 Sodium dodecyl sulfate polyacrylamide gel electrophoresis (SDS-PAGE)

The gel was prepared according to **Table 23** and loaded with 10 µL of 1 $mg \cdot mL^{-1}$ protein solutions. The protein concentrations were measured via standard Bradford assay, using Bradford reagent and protocol from Sigma Aldrich. The samples were prepared by mixing 6 µL of loading buffer with the protein solution. The samples were mixed with 6 µL of loading buffer and filled the rest with water to a total volume of 30 µL and an end concentration of 1 $mg \cdot mL^{-1}$. A voltage of 80 V was set for the collecting gel. When the separation gel was reached, the voltage was increased to 120 V, the maximum current reached was 15 mA.

9.4 Modeling with MOE (Molecular Operating Environment)

9.4.1 General procedure for docking with MOE

The docking was performed with MOE (Molecular Operating Environment) (**Table 29**).[94] First the protein was prepared, therefore the co-crystal of OxdRE (PDB 3A16) was used. The preparation included protonation, adding missing atoms, preparing the heme structure, and minimizing the protein energy in the corresponding force-field (MMFF94). The ligands were prepared using MOE to design the ligands and minimize within the force-field of interest. Over many optimization steps regarding the placement and scoring, also including reaction mechanism and experimental data, a final docking method was developed to find realistic protein ligand structures. These protein ligand structures (pose) were then used for general rationalizing of the enzyme's selectivity. In the following part procedure for a successful docking is tailored.

Table 29: General molecular docking flow chart

Sequence	Step	Description
1	Protein structure	Homology model, or crystal structure of target protein
2	Protein preparation	Protonation, adding atoms, structural correction, energy minimization
3	Ligand	Load or generate ligands of interest
4	Ligand preparation	Prepare ligand, restriction, conformers, energy minimization
5	Initial docking	First insight and visualization
6	Refine	Mechanism and/or data driven optimization of parameters
7	Automate/ advance techniques	Pharmacophores, sorting, covalent docking, flexible docking
8	Final score	Final results, comparison, evaluation, MD-sims

9.4.2 Initial docking

The PDB data 3A16 contained the crystal structure of OxdRE as co-crystal with propanal oxime as ligand was loaded into the software MOE (molecular operating environment). Using the co-crystal and the postulated mechanism for aldoxime dehydratase to tailor the binding motif of the ligand.

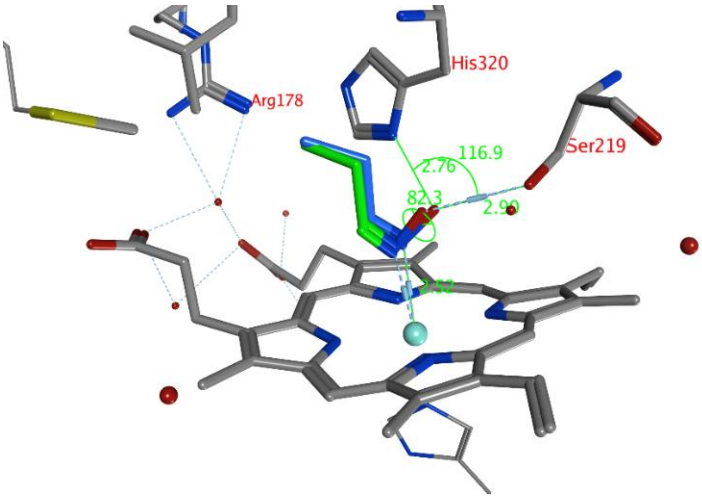

Figure 52: Propanal oxime as Co-crystal and docked structure in OxdRE-WT. Showing distances, angles and dihedrals of the correct pose. Green ligand (docked) blue ligand (co-cystal).

According to the mechanism the aldoxime has to bind the heme iron(II) and need to be coordinated via serine and histidine. The serine is here the hydrogen acceptor and the histidine the hydrogen donor. The co-crystal does only show the serine and the heme interaction towards the aldoxime as ligand (**Figure 52**). Even though the hydrogen donation towards the aldoxime is not recognized, the oxygen π- electrons show towards the histidine, which indicates the right ligand binding. Furthermore, the binding motif itself was then quantified in binding distances, angles and dihedrals. Afterwards the same ligand (propanal oxime) was redocked into the active site. The redocked structure gave us the variance of these quantified values, which then could be used as "cut-off" values for other ligands (**Scheme 43**).

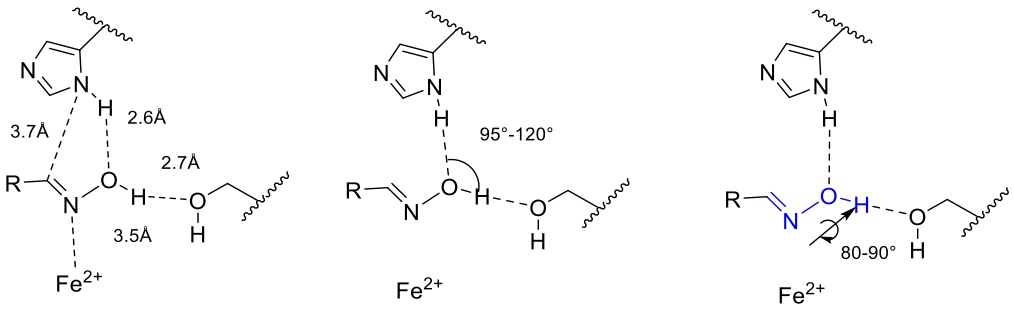

Scheme 43: Schematic representation of the bond angles, distances and dihedrals as 2D structure.

9.4.3 Docking with ligands of interest phenylpropanal oxime derivatives

First of all, for each substrate with two enantiomers and two isomers in total 4 ligands for the docking study had to be generated. The ligand had to be minimized and their movement needed to be restricted to the chosen conformers. The ligands were then docked inside the active site using GDP 1 (general docking procedure 1). The results gave a hint how the ligand could fit inside the pocket (active site) of the enzyme.

9.4.4 Placement

Triangle matcher: Poses are generated by aligning ligand triplets of atoms on triplets of alpha spheres in a more systematic way than in the Alpha Triangle method.

Pharmacophore: Information from the pharmacophore is directly used to place the ligand in the binding site. This is the preferred method when a pharmacophore is present but will not work if there is no pharmacophore.

9.4.5 Pharmacophore generation

The pharmacophore docking describes a placement method where the ligand is forced into specified areas for indicated interaction patterns, such as hydrogen bonds, metal ligation and hydrophobic or aromatic interaction. In **Figure 53** the generated pharmacophore is shown.

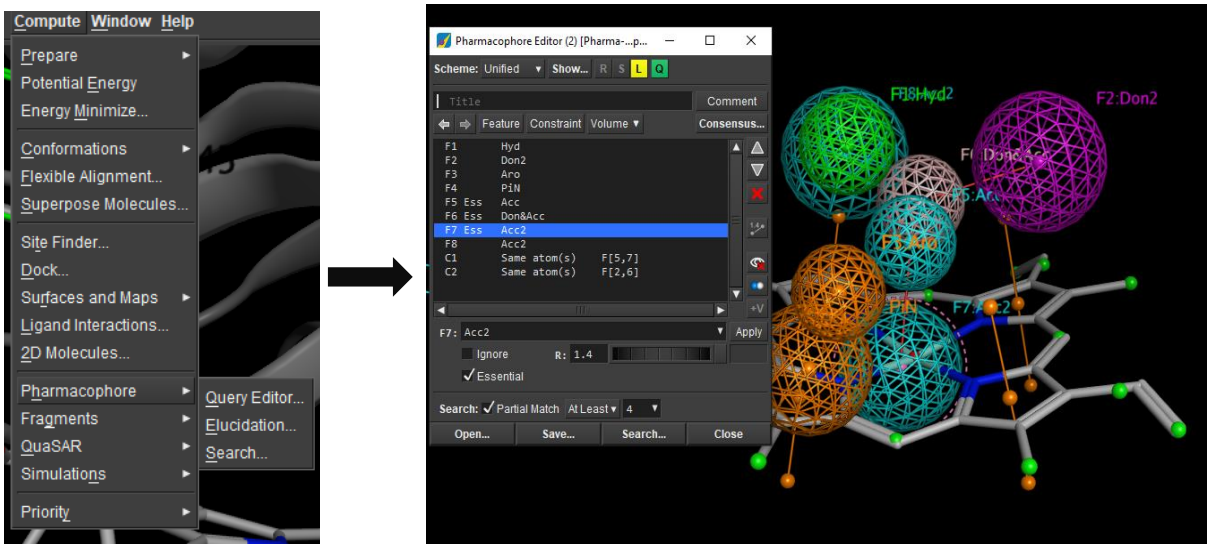

Figure 53: Pharmacophore generation with MOE.

By using the pharmacophore editor, a different visualization of the molecule appears. The lined dots are interaction vectors, which can represent a projection of certain interaction towards a specified location, while dots alone represent a certain property of the area. For an instance the cavity is marked by a green dot, which represents a hydrophobic area, while blue lined dot from the nitrogen towards the iron is a H-Bond acceptor projection. Those dots can be selected to be featured in the pharmacophore query. The dots appear now as spheres, which define the area of the interaction. The size and position of the sphere can be modified manually. The interaction of the aldoxime functionality was defined to be essential. Furthermore, the pharmacophore constraints were defined for

the oxygen, whereas the positioning as well as the projection for H-bond interaction would be restricted to the oxygen.

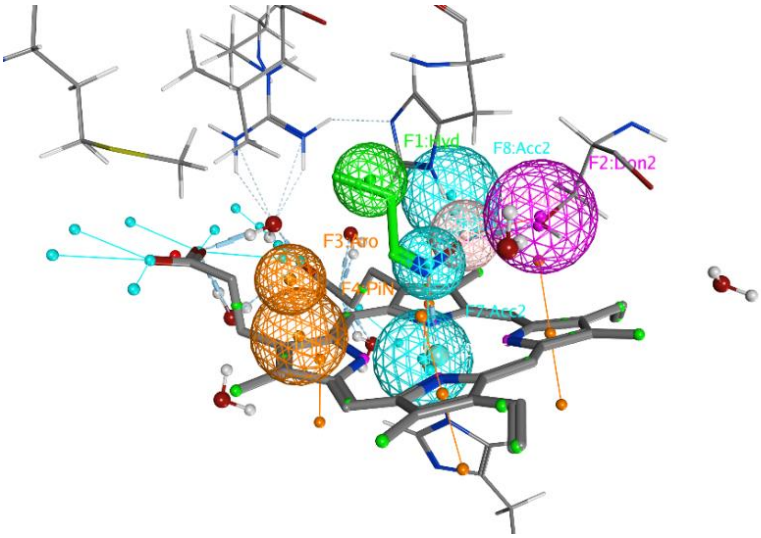

Figure 54: Pharmacophore generated with propanal oxime as ligand.

The orange sphere describes an aromatic and the green sphere hydrophobic interaction. Both of these pharmacophores are not essential just giving a possible position for either an aromatic or a hydrophobic part of the ligand. The nitrogen is a hydrogen acceptor (blue sphere) with the right angle the electron pair need to show in the direction of the iron(II), which is why the bigger blue sphere (hydrogen acceptor projection) is around the iron(II). The hydroxyl group is hydrogen acceptor as well as a donator. Therefore, the sphere for the hydroxyl group has also two different projection spheres one for hydrogen acceptor projection (towards histidine) and one for hydrogen donator projection (towards serine). This projection spheres are created according to the co-crystal and the mechanism behind the aldoxime dehydration. The position and the projections are determined with the measured angles, dihedrals and distances. The pharmacophore as such is the result of the correct binding distances, angles and dihedrals (**Figure 54**).

A well-defined and adjusted pharmacophore leads then to a proper ligand interaction pattern. With defined energy contributions and projections (**Figure 55**).

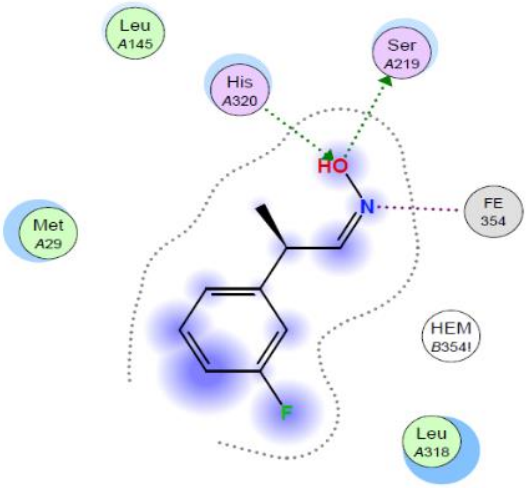

Figure 55: Ligand interaction pattern with (*Z*,*R*)-3FPPOX as example bound in the active site of OxdRE-WT

9.4.6 Set up and parameters

Forcefield and parameter set up: MMFF94 is well parametrized for nitrogen interactions. Docking was performed with the MMF94 force field. In the following the potential set up with MOE is shown. Enabled all potential energy terms for bonded, van der Waals and electrostatic interaction and restraints. The cut off for non-bonded interaction with 8 to 10 was not changed. As solvation the reaction field model was used. The threads value indicates the number of processors, which were used for the calculation (**Figure 56**).

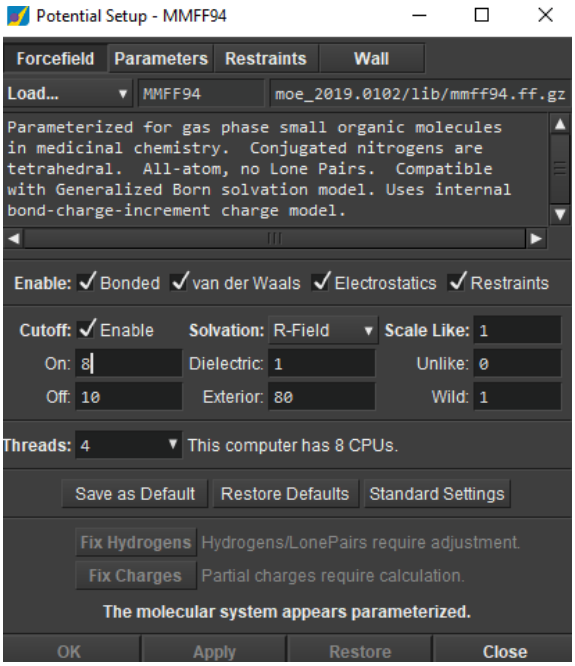

Figure 56: Forcefield and parameter set up. The figure shows the adjustable panel in MOE.

In the following the docking panel (**Figure 57**)in MOE is shown.

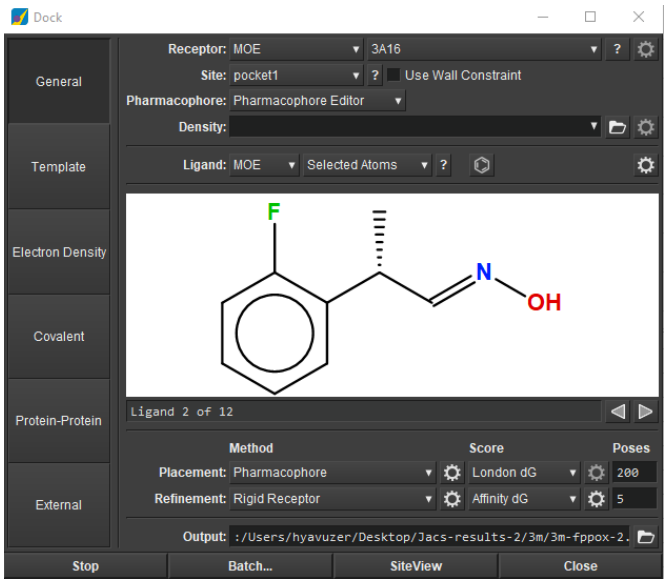

Figure 57: Screenshot of the docking panel, showing adjustable parameters: Placement, refinement, scoring function.

Affinity dG Scoring: This function estimates the enthalpic contribution to the free energy of binding using a linear function:

$$G = C_{hb}f_{hb} + C_{ion}f_{ion} + C_{mlig}f_{mlig} + C_{hh}f_{hh} + C_{hp}f_{hp} + C_{aa}f_{aa}$$

where the f terms fractionally count atomic contacts of specific types and the C's are coefficients that weight the term contributions to the affinity estimate. The individual terms are:[94]

Table 30: Terms and description of the affinity dG scoring function.

Term	Description
hb	Interactions between hydrogen bond donor-acceptor pairs. An optimistic view is taken; for example, two hydroxyl groups are assumed to interact in the most favorable way.
ion	Ionic interactions. A Coulomb-like term is used to evaluate the interactions between charged groups. This can contribute to or detract from binding affinity.
mlig	Metal ligation. Interactions between Nitrogens/Sulfurs and transition metals are assumed to be metal ligation interactions.
hh	Hydrophobic interactions, for example, between alkane carbons. These interactions are generally favorable.
hp	Interactions between hydrophobic and polar atoms. These interactions are generally unfavorable.
aa	An interaction between any two atoms. This interaction is weak and generally favorable.

London dG Scoring (default): The London dG scoring function estimates the free energy of binding of the ligand from a given pose. The functional form is a sum of terms:

$$\Delta G = c + E_{flex} + \sum_{h-bond} C_{HB} f_{HB} + \sum_{m-lig} C_M f_M + \sum_{atoms\ i} \Delta D_i$$

in which c represents the average gain/loss of rotational and translational entropy; E_{flex} is the energy due to the loss of flexibility of the ligand (calculated from ligand topology only); f_{HB} measures geometric imperfections of hydrogen bonds and takes a value in [0,1]; c_{HB} is the energy of an ideal hydrogen bond; f_M measures geometric imperfections of metal ligations and takes a value in [0,1]; c_M is the energy of an ideal metal ligation; and Di is the desolvation energy of atom i. The difference in desolvation energies is calculated according to the formula

$$\Delta D_i = c_i R^3{}_i \left\{ \iiint_{u \notin A \cup B} |u|^{-6}\, du - \iiint_{u \notin B} |u|^{-6}\, du \right\}$$

in which A and B are the protein and/or ligand volumes with atom i belonging to volume B; R_i is the solvation radius of atom *i* (taken as the OPLS-AA van der Waals sigma parameter plus 0.5 Angstrom); and c_i is the desolvation coefficient of atom *i*. The coefficients {c, c_{HB}, c_M, c_i} were fitted from ~400 x-ray crystal structures of protein-ligand complexes with available experimental pK_i data. Atoms are categorized into ~12 atom types for the assignment of the c_i coefficients. The triple integrals are approximated using Generalized Born integral formulas.[94]

9.4.7 Energy adjustment

After finding the right placement method, the scoring of these poses had to be adjusted. The weighting of the parameters for hydrogen bond, metal ligation, hydrophobic contact and hydrophobic-polar interaction were increased. The adjustment in parameters led to improved protein-ligand-structure and also the associated energy values. These values and structures would then describe the best approximation of reality (**Table 31**).

Table 31: Energy adjustment for docking with PPOX-derivatives using affinity dG as final scoring function.

Energy scoring												
	weighting						Scoring / kcal · mol^{-1}					
#	Atom-atom	Hydrophob-polar	Hydrop.-contact	Metal-ligation	Ionic interaction	Hydrog.-bond	ER/	ES/	ZR/	ZS/	diff E/	diff Z/
1	-0.00834	0.02497	-0.01235	-1.0	1.0	-1.0	7.13	7.42	6.49	6.07	-0.29	0.42
2	-0.00834	0.02497	-0.01235	-1.0	1.0	-2.0	10.3	10.85	8.82	8.03	-0.55	0.79
3	-0.00834	0.02497	-0.01235	-1.0	1.5	-2.0	10.3	10.85	8.82	8.03	-0.55	0.79
4	-0.00834	0.02497	-0.01235	-2.0	1.0	-2.0	10.49	11.23	9.55	8.64	-0.74	0.91
5	-0.00834	0.02497	-0.0247	-2.0	1.0	-2.0	14.1	14.81	13.12	12.22	-0.71	0.9
6	-0.00834	0.05	-0.01235	-2.0	1.0	-2.0	5.92	6.75	5.36	4.31	-0.83	1.05
7	-0.02	0.05	-0.01235	-2.0	1.0	-2.0	13.49	14.2	12.58	11.61	-0.71	0.97
8	-0.00834	0.05	-0.01235	-3.0	1.0	-3.0	9.29	10.56	8.41	6.83	-1.27	1.58
9	-0.00834	0.05	-0.01235	-3.5	1.0	-3.5	10.97	12.46	9.94	8.81	-1.49	1.13
10	-0.00834	0.06	-0.01235	-3.5	1.0	-3.5	9.14	10.67	8.27	6.44	-1.53	1.83
11	-0.00834	0.07	-0.01235	-3.5	1.0	-3.5	7.32	8.89	6.6	4.47	-1.57	2.13
12	-0.00834	0.07	-0.0247	-3.5	1.0	-3.5	10.5	12.47	9.49	8.25	-1.97	1.24

9.4.8 General docking procedure 1 (GDP1)

Receptor is set to 3A16 including the protein, the solvent and the heme as receptor. Docking site was the complete active site including all amino acids next to the heme group. No walls of constraints were used. Pharmacophore was set to none. No electron density file. The ligand was set to MOE selected atoms, which includes all selected ligands for the calculation. As placement the triangle matcher and as refinement the rigid receptor option was used. The scoring functions for initial score was London dG and for final score affinity dG. Number of placement poses were set to 200 and the number of shown poses to 20.

9.4.9 General docking procedure 2 (GDP2)

Receptor is set to 3A16 including the protein the solvent and the heme as receptor. Docking site was the complete active site including all amino acids next to the heme group. No walls of constraints were used. The designed pharmacophore file was chosen for the pharmacophore set up. No electron density file. The ligand was set to MOE selected atoms, which includes all selected ligands for the calculation. As placement the pharmacophore search were chosen and as refinement the rigid receptor option was used. The scoring functions for initial score was London dG and for final score affinity dG. Number of placement poses were set to 200 and the number of shown poses to 5.

9.5 Rationalizing the unprecedented stereochemistry of resolutions with aldoxime dehydratases via molecular modeling

9.5.1 Docking results with wild type OxdRE

Docking of PPOX derivatives for OxdRE-WT was performed according to GDP2. Also, the partial energy contribution of the aldoxime function was determined (**Table 32**).

Table 32: Docking results with OxdRE-WT and all mono substituted chloro-, bromo- and fluoro- PPOX derivatives (as for the ΔΔGvalues, the absolute values are given (without sign); for each specific E- or Z-aldoxime, these values were calculated from the ΔGvalues of the two related enantiomers of this aldoxime). Red number indicates low docking quality

#	PPOX	ΔG/ kcal·mol^{-1}	ΔΔG/ kcal·mol^{-1}	Enantiomer	OH-Ser/ kcal·mol^{-1}	Fe-N/ kcal·mol^{-1}	His-OH/ kcal·mol^{-1}	Sum-energies/ kcal·mol^{-1}	Δ-sum energies/ kcal·mol^{-1}
1	ER	-7.22	2.14	*S*	-2.4	-0.7		-3.1	-0.6
2	ES	-9.37			-0.5	-2		-2.5	
3	ZR	-5.92	1.23	*R*	-0.6	-2.4	-1.8	-4.8	-0.6
4	ZS	-4.69			-0.5	-2	-1.7	-4.2	
5	2FER	-7.30	1.87	*S*	-2.4	-0.7		-3.1	-0.6
6	2FES	-9.17			-0.5	-2		-2.5	
7	2FZR	-6.24	1.63	*R*	-0.9	-2.6	-2	-5.5	-1.2
8	2FZS	-4.60			-0.6	-2	-1.7	-4.3	
9	3FER	-7.68	1.98	*S*	-2.5	-0.5		-3	-0.5
10	3FES	-9.66			-0.5	-2		-2.5	
11	3FZR	-6.28	1.51	*R*	-0.7	-2.3	-1.7	-4.7	-0.4
12	3FZS	-4.77			-0.6	-2	-1.7	-4.3	
13	4FER	-7.07	2.65	*S*	-2.7	-0.9		-3.6	-0.9
14	4FES	-9.72			-1.3	-1.4		-2.7	
15	4FZR	-5.88	0.93	*R*	-0.6	-2.4	-1.8	-4.8	-0.5
16	4FZS	-4.96			-0.6	-2	-1.7	-4.3	
17	2BrER	-7.18	1.01	*S*	-2.6	-1		-3.6	0.2
18	2BrES	-8.19			-2.8	-1		-3.8	
19	2BrZR	-8.26	0.73	*R*	-1.6	-2.4	-1.7	-5.7	-1.5
20	2BrZS	-7.53			-0.7	-2.3	-1.2	-4.2	
21	3BrER	-6.06	2.41	*S*	-2.1	-0.8		-2.9	0.6
22	3BrES	-8.47			-2.8	-0.7		-3.5	
23	3BrZR	-7.00	0.75	*S*	-1.3	-2.6	-0.5	-4.4	1.2
24	3BrZS	-7.75			-1.6	-2.4	-1.6	-5.6	
25	4BrER	-5.20	4.31	*S*	-1.4	-1.1		-2.5	0
26	4BrES	-9.51			-0.5	-2		-2.5	
27	4BrZR	-6.18	0.84	*R*	-0.7	-2.4	-1.8	-4.9	-0.4
28	4BrZS	-5.34			-0.7	-2.1	-1.7	-4.5	
29	2ClER	-6.47	1.55	*S*	-2.7	-1.2		-3.9	-0.9
30	2ClES	-8.02			-2.4	-0.6		-3	
31	2ClZR	-7.78	2.89	*R*	-1.4	-2.5	-1.6	-5.5	-3.5
32	2ClZS	-4.89				-2		-2	
33	3ClER	-7.48	2.32	*S*	-2.5	-0.8		-3.3	-0.7
34	3ClES	-9.80			-1.3	-1.3		-2.6	
35	3ClZR	-10.05	5.05	*R*	-1.1	-2.4		-3.5	1

#	PPOX	ΔG/ kcal·mol^{-1}	ΔΔG/ kcal·mol^{-1}	Enantiomer	OH-Ser/ kcal·mol^{-1}	Fe-N/ kcal·mol^{-1}	His-OH/ kcal·mol^{-1}	Sum-energies/ kcal·mol^{-1}	Δ-sum energies/ kcal·mol^{-1}
36	3ClZS	-5.01			-0.7	-1.7	-2.1	-4.5	
37	4ClER	-5.27	4.79	*S*	-2	-1.5		-3.5	-0.4
38	4ClES	-10.06			-1	-2.1		-3.1	
39	4ClZR	-6.36	1.20	*R*	-0.8	-2.4	-1.8	-5	-0.8
40	4ClZS	-5.16			-0.6	-1.6	-2	-4.2	

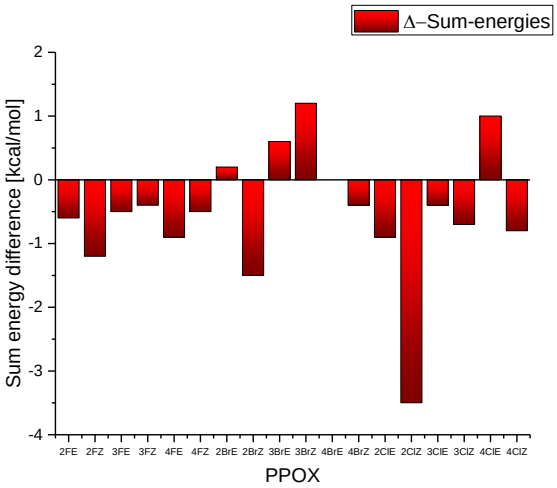

Figure 58: Energy contribution of the aldoxime function in dependency of the enantiomer formed.

The energy contribution of the aldoxime function is random (**Figure 58**) there is no dependency between the enantioselectivity and the interaction pattern of the functional group. **Figure 58** shows the sum of energy contributions of the functional group in dependency of the formed enantiomer. For example, when taking the value obtained from the ΔG-value for the S-enantiomer of a specific E- or Z aldoxime minus the ΔG-value for the R-enantiomer of this E- or Z-aldoxime, 2FE has a ΔΔG-value of 1.87 kcal mol-1 , which is positive and predicts the S-enantiomer (2FER-2FES, -7.36 kcal mol-1 -(-9.31 kcal · mol-1)), therefore the Δ-sum-energy has to be also positive, but in fact it is not. A dependency with the enantioselectivity would be indicated with an alternating graph.

9.5.2 Docking results with OxdRE-L145F

Docking of PPOX derivatives for the L145F mutant of OxdRE was performed according to GDP2. The partial energy contribution was not determined (**Table 33**).

Table 33: Docking results with OxdRE-L145F and all mono substituted chloro-, bromo- and fluoro-PPOX derivatives (as for the ΔΔGvalues, the absolute values are given (without sign); for each specific *E*- or *Z*-aldoxime, these values were calculated from the ΔGvalues of the two related enantiomers of this aldoxime). Red number indicates low docking quality.

#	PPOX	ΔG/ kcal·mol^{-1}	ΔΔG/ kcal·mol^{-1}	Enantiomer
1	2FER	-7.20	3.65	*S*
2	2FES	-10.85		
3	2FZR	-8.74	2.33	*R*
4	2FZS	-6.41		
5	3FER	-7.52	2.91	*S*
6	3FES	-10.43		
7	3FZR	-5.69	0.06	-
8	3FZS	-5.75		
9	4FER	-7.19	3.85	*S*
10	4FES	-11.04		
11	4FZR	-7.84	1.36	*R*
12	4FZS	-6.48		
13	2BrER	-7.32	1.43	*S*
14	2BrES	-8.75		
15	2BrZR	-7.47	0.12	*R*
16	2BrZS	-7.35		
17	3BrER	-7.49	3.73	*S*
18	3BrES	-11.22		
19	3BrZR	-7.75	0.56	*R*
20	3BrZS	-7.19		
21	4BrER	-7.04	3.13	*S*
22	4BrES	-10.17		
23	4BrZR	-6.92	0.42	*R*
24	4BrZS	-6.50		
25	2ClER	-7.17	4.03	*S*
26	2ClES	-11.20		
27	2ClZR	-7.12	3.98	*R*
28	2ClZS	-3.14		
29	3ClER	-6.20	5.29	*S*
30	3ClES	-11.49		
31	3ClZR	-5.10	1.79	*S*
32	3ClZS	-6.89		
33	4ClER	-6.27	3.76	*S*
34	4ClES	-10.03		
35	4ClZR	-7.44	0.04	-
36	4ClZS	-7.40		

9.5.3 Docking results with OxdRE-M28-L145A-A147G

Docking of PPOX derivatives for the triple point mutant of OxdRE was performed according to GDP2. The partial energy contribution was not determined (**Table 34**).

Table 34: Docking result with OxdRE-3-M and all mono substituted chloro-, bromo- and fluoro-PPOX derivatives (as for the ΔΔG-values, the absolute values are given (without sign); for each specific E- or Z-aldoxime, these values were calculated from the ΔG-values of the two related enantiomers of this aldoxime). Red number indicates low docking quality.

#	PPOX	ΔG/ kcal·mol^{-1}	ΔΔG/ kcal·mol^{-1}	Enantiomer
1	2FER	-6.55	1.77	*S*
2	2FES	-8.32		
3	2FZR	-3.13	0.20	*R*
4	2FZS	-2.93		
5	3FER	-6.82	1.87	*S*
6	3FES	-8.69		
7	3FZR	-2.53	1.00	*S*
8	3FZS	-3.53		
9	4FER	-7.12	1.54	*S*
10	4FES	-8.66		
11	4FZR	-2.43	1.40	*S*
12	4FZS	-3.83		
13	2BrER	-2.76	2.34	*S*
14	2BrES	-5.10		
15	2BrZR	-9.55	6.77	*R*
16	2BrZS	-2.78		
17	3BrER	-5.40	1.84	*S*
18	3BrES	-7.24		
19	3BrZR	-8.16	1.66	*R*
20	3BrZS	-6.50		
21	4BrER	-4.99	0.24	*S*
22	4BrES	-5.23		
23	4BrZR	-7.37	4.79	*R*
24	4BrZS	-2.58		
25	2ClER	-3.82	1.09	*S*
26	2ClES	-4.91		
27	2ClZR	-9.74	9.89	*R*
28	2ClZS	0.15		
29	3ClER	-3.64	6.62	*S*
30	3ClES	-10.26		
31	3ClZR	-6.60	1.47	*R*
32	3ClZS	-5.13		
33	4ClER	-2.16	6.24	*S*
34	4ClES	-8.40		
35	4ClZR	-4.12	1.69	*R*
36	4ClZS	-2.43		

9.5.4 Correlation of Enantioselectivity and ΔΔG-values

The energy values, which were determined via molecular modeling were used to calculate the E-value. The resulting E-values from the biotransformation were also transformed into the corresponding ΔΔG-values. **Table 35** shows the calculated E-values from the energy values (ΔΔG) determined during docking experiments. **Table 36** shows the energy values (ΔΔG) that were determined on the basis of the E-values of the biotransformations

Table 35: Calculation of E-values from the determined energy values resulting from the *in silico* experiments.

	WT		**L145F**		**3M**	
	ΔΔG/ kcal·mol^{-1}	E-value	ΔΔG/ kcal·mol^{-1}	E-value	ΔΔG/ kcal·mol^{-1}	E-value
2FE	1870	28	3640	696	1730	22
2FZ	1630	19	2320	65	190	1
3FE	1980	35	2900	184	1870	29
3FZ	1510	15	70	1	1000	6
4FE	2650	117	3850	1016	1540	15
4FZ	930	5	1350	11	1340	11

Table 36: Calculation of energy values from the determined E-values resulting from the biotransformations.

	WT		**L145F**		**3M**	
	E-value	ΔΔG/ kcal·mol^{-1}	E-value	ΔΔG/ kcal·mol^{-1}	E-value	ΔΔG/ kcal·mol^{-1}
2FE	112	2623	302	3175	75	2401
2FZ	9	1222	20	1666	4	771
3FE	146	2771	309	3188	16	1542
3FZ	9	1222	8	1156	2	385
4FE	44	2104	64	2312	22	1719
4FZ	4	771	11	1333	1	0

9.5.5 Biotransformation

9.5.5.1 Activity assay

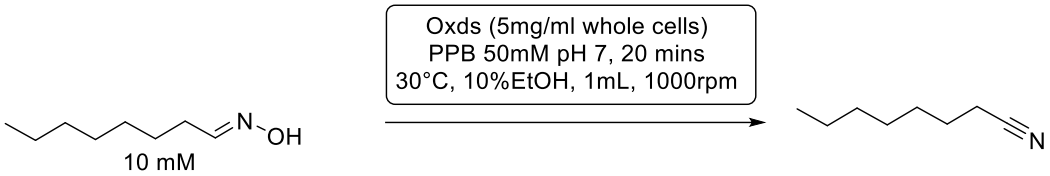

The activity assay was performed with whole cells of Oxd-variants in 5 mg·mL^{-1} solution. First the buffer (800 µL, PPB 50 mM, pH 7) was placed into a 2 mL Eppendorf tubes. Then the substrate solution of octanal oxime in ethanol (100 µL, 100 mM) was added to the buffer to an end concentration of 10 mM octanal oxime and 10% ethanol. The temperature was set to 30 °C. Afterwards the enzyme as whole cell solution was added to the reaction mixture. The reaction mixture was stirred for 20 min at 1000 rpm. The reaction was quenched and extracted with ethyl acetate (800 µL). The organic phase was analyzed via GC.

Entry	Enzyme	Conversion / %	Activity/ mU ·mg^{-1}
1	OxdRE-WT	68	68
2	OxdRE-L145F	52	52
3	OxdRE-10-(3M) M28/L145A/A147G	5	5
4	OxdRE-10-(3G) M29G/L145G/A147G	0	0

9.5.6 Biocatalytic chiral nitrile synthesis

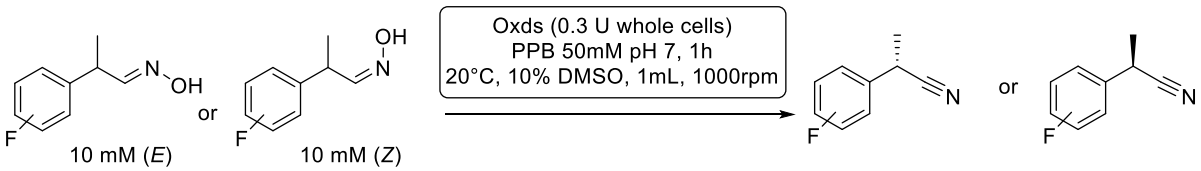

The biotransformation was performed with whole cells of Oxd -variants. First the buffer (PPB 50 mM, pH 7) was placed into a 2 mL Eppendorf tubes. Then the substrate solution, containing a FPPOX derivate in DMSO (100 µL, 100 mM), was added to the buffer to an end concentration of 10 mM FPPOX and 10% DMSO. The temperature was arranged to 20 °C. Afterwards the enzyme as whole cell solution was added to the reaction mixture (0.3 U). The reaction solution was stirred for 1h min at 1000 rpm. The reaction was quenched and extracted with cyclohexane (800 µL). The organic phase was analyzed via HPLC (**Table 37**).

Table 37: Biotransfromation of OxdRE-WT, OxdRE-L145F and OxdRE-3M with FPPOX derivatives as isolated isomers. Double point measurement and mean values. The E-value was calculated with the mean values.

OxdRE	**PPOX**	**Conv.1 /%**	**Conv.2 /%**	**Conv. Mean /%**	***ee*1 / %**	***ee*2 / %**	***ee* mw/ %**	**E-value**
WT	2FE (99/1)	43	47	45	96	96	96	112
WT	2FZ (1/99)	52	47	50	65	65	65	9
WT	3FE (99/1)	48	49	48	96	97	96	146
WT	3FZ (10/90)	52	51	52	64	65	64	9
WT	4FE (98/2)	35	34	34	93	93	93	44
WT	4FZ (3/97)	38	26	32	55	54	54	4
L145F	2FE (99/1)	28	31	29	>99	>99	>99	302
L145F	2FZ (1/99)	46	45	46	83	83	83	20
L145F	3FE (99/1)	33	29	31	>99	>99	>99	309
L145F	3FZ (10/90)	28	34	31	69	70	70	8
L145F	4FE (98/2)	19	25	22	97	95	96	64
L145F	4FZ (3/97)	18	26	22	81	80	80	11
3M	2FE (99/1)	45	46	45	94	95	94	75
3M	2FZ (1/99)	53	54	54	39	42	40	4
3M	3FE (99/1)	25	24	25	83	87	85	16
3M	3FZ (10/90)	45	50	48	66	32	17	2
3M	4FE (98/2)	40	39	39	84	86	85	22
3M	4FZ (3/97)	50	51	50	11	08	10	1

9.6 Chiral nitrile synthesis and formal double dynamic kinetic resolution

9.6.1 General procedure (GP7): Isomerization of *rac-E-* and *Z-* PPOX (8)

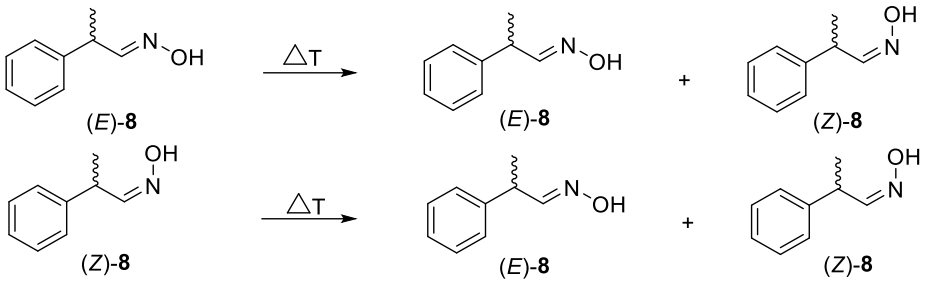

To characterize the isomerization of this specific aldoxime class, *rac*-PPOX was first separated into its pure isomers via automated column chromatography. The isomerization rate was investigated from opposite starting points. To determine the time course of the isomerization of PPOX (**8**), stock solutions (0.1-1 M) in ethanol and DMSO-d_6 were made. D_2O/ethanol or D_2O/ DMSO-d_6 mixture, stock solutions were first prepared in ethanol or DMSO-d_6, respectively. These were then diluted to the desired final concentration with water and, in some cases, further ethanol or DMSO-d_6. In addition, the desired solvent ratio was thereby adjusted. The reaction was carried out in 10 mL glass vials on a magnetic stirrer. Reaction volume was set to 5 mL and 600 µL sample were taken in regular intervals for the analysis. The (*E*/*Z*)-ratio was determined via ^{1}H-NMR-spectroscopy.

9.6.1.1 Initial screening with time and temperature dependency of *E-* and *Z-* PPOX (8) isomerization rate

The isomerization of *rac*-(**8**) was carried out according to GP7, with 40 °C and 90 °C reaction temperature and different DMSO-d_6 ratios. The reaction was started with *rac-E*-(**8**) (86%, 10 mM) and *rac-Z*-(**8**) (94%, 10 mM). The analyzed samples at different reaction times are shown in **Table 38**.

Table 38: Isomerization of *rac*-(**8**) with different DMSO-ratios at 40 and 90 °C showing *E*- and *Z*-isomer ratios at specified reaction times.

	***E*- and *Z*-ratio of *rac*-PPOX (8)**									
solvent	0 h		2 h 40 °C		6 h 40 °C		24 h 40 °C		18 h 90 °C	
D_2O: DMSO-d_6	(*E*)	(*Z*)	(*E*)	(*Z*)	(*E*)	(*Z*)	(*E*)	(*Z*)	(*E*)	(*Z*)
1:0	0.06	**0.94**	0.05	0.95	0.08	0.92	0.11	0.89	0.70	0.30
9:1	0.04	**0.96**	0.04	0.96	0.05	0.95	0.08	0.92	0.71	0.29
8:2	0.04	**0.96**	0.05	0.95	0.05	0.95	0.09	0.91	0.40	0.60
0:1	0.06	**0.94**	0.06	0.94	0.06	0.94	0.05	0.95	0.07	0.94
1:0	**0.86**	0.14	0.85	0.15	0.86	0.15	0.85	0.15	0.70	0.30
9:1	**0.85**	0.15	0.85	0.15	0.85	0.15	0.85	0.15	0.71	0.29
8:2	**0.83**	0.17	0.85	0.15	0.85	0.15	0.84	0.16	0.73	0.28
0:1	**0.85**	0.15	0.84	0.16	0.85	0.15	0.85	0.15	0.85	0.15

9.6.1.2 Temperature dependency of *E*- and *Z*- PPOX (8) isomerization rate

The isomerization of *rac*-(**8**) at different temperatures was carried out according to GP7, with the difference of using Eppendorf-tubess (2 mL) and a reaction volume of 600 uL. The reaction was started with *rac*-*E*-(**8**) (10 mM) and *rac*-*Z*-(**8**) (10 mM). The total reaction volume was used for work up and analyzed via ^{1}H-NMR (**Table 39**) For each individual measured value, a reaction was performed.

Table 39: Isomerization of *rac*-(**8**) with different at different reaction temperatures showing *E*- and *Z*-isomer ratios at specified reaction times.

	***E*- and *Z*-ratio of *rac*-PPOX (8)**											
	0 h		0.5 h		1 h		3 h		6 h		16 h	
T / °C	(*E*)	(*Z*)	(*E*)	(*Z*)	(*E*)	(*Z*)	(*E*)	(*Z*)	(*E*)	(*Z*)	(*E*)	(*Z*)
60	0.17	**0.83**	0.16	0.84	0.19	0.81	0.18	0.82	0.18	0.82	0.21	0.79
80	0.17	**0.83**	0.17	0.83	0.18	0.82	0.19	0.81	0.22	0.78	0.43	0.57
100	0.17	**0.83**	0.19	0.81	0.19	0.81	0.24	0.76	0.45	0.55	0.70	0.30
60	**0.89**	0.11	0.90	0.10	0.90	0.10	0.89	0.11	0.90	0.10	0.89	0.12
80	**0.89**	0.11	-	-	0.90	0.10	0.90	0.10	0.89	0.12	0.75	0.25
100	**0.89**	0.11	0.90	0.10	0.90	0.10	0.88	0.12	0.75	0.25	0.73	0.28

9.6.1.3 Concentration dependency of *rac*-*E*-PPOX (8) isomerization rate

The isomerization of *rac*-(**8**) at substrate concentrations was carried out according to GP7 with DMSO-d_6 (10%, *v/v*) as cosolvent and a reaction temperature of 100 °C. The reaction was started with *rac*-*E*-(**8**) (10-320 mM). The analyzed samples at different reaction times are shown in **Table 40** and **Table 41**.

Table 40: Isomerization of *rac*-(**8**) with different at different substrate concentration showing *E*- and *Z*-isomer ratios at specified reaction times.

	***E*- and *Z*-ratio of *rac*-PPOX (8)**											
	0 h		**1 h**		**3 h**		**6 h**		**16 h**		**24 h**	
c / mM	(*E*)	(*Z*)	(*E*)	(*Z*)	(*E*)	(*Z*)	(*E*)	(*Z*)	(*E*)	(*Z*)	(*E*)	(*Z*)
10	**0.96**	0.04	0.95	0.05	0.93	0.07	0.81	0.19	0.71	0.29	0.69	0.31
40	**0.97**	0.03	0.96	0.04	0.93	0.07	0.84	0.16	0.70	0.30	0.73	0.27
80	**0.95**	0.05	0.94	0.07	0.88	0.12	0.79	0.21	-	-	0.73	0.28
160	**0.95**	0.05	0.88	0.12	0.75	0.25	0.73	0.28	0.71	0.29	-	-
240	**0.89**	0.12	0.78	0.22	0.72	0.28	0.74	0.26	0.71	0.29	-	-
10	**0.89**	0.12	0.89	0.12	0.88	0.12	0.80	0.20	0.68	0.32	0.70	0.30
40	**0.89**	0.12	0.89	0.12	0.87	0.13	0.85	0.15	0.80	0.20	0.70	0.30
80	**0.91**	0.09	0.87	0.13	0.77	0.23	0.75	0.25	-	-	0.71	0.29
160	**0.89**	0.11	0.86	0.14	0.77	0.23	0.74	0.27	0.71	0.29	-	-
240	**0.89**	0.11	0.83	0.17	0.75	0.25	0.74	0.26	0.74	0.27	-	-
	***E*/*Z*-ratio of *rac*-PPOX (8)** **Mean value**											
10	**0.92**	0.08	0.92	0.08	0.90	0.10	0.80	0.20	0.70	0.31	0.70	0.31
40	**0.93**	0.07	0.92	0.08	0.90	0.10	0.84	0.16	0.75	0.25	0.72	0.29
80	**0.93**	0.07	0.90	0.10	0.82	0.18	0.77	0.23	-	-	0.72	0.28
160	**0.92**	0.08	0.87	0.13	0.76	0.24	0.73	0.27	0.71	0.29	-	-
240	**0.89**	0.11	0.80	0.20	0.74	0.27	0.74	0.26	0.72	0.28	-	-

Table 41: Isomerization of *rac*-(**8**, 320 mM) in short sample intervals showing *E*- and *Z*-isomer ratios at specified reaction times.

	***E*- and *Z*-ratio of *rac*-PPOX (8)**									
c / mM	**0 h**		**0.25 h**		**0.5 h**		**0.75 h**		**1 h**	
	(*E*)	(*Z*)	(*E*)	(*Z*)	(*E*)	(*Z*)	(*E*)	(*Z*)	(*E*)	(*Z*)
320	**0.89**	0.11	0.86	0.15	0.85	0.15	0.78	0.23	0.83	0.17
320	**0.91**	0.09	0.89	0.12	0.86	0.15	0.81	0.19	0.83	0.17
	***E* and *Z*-ratio of *rac*-PPOX (8)** **Mean value**									
320	**0.90**	0.10	0.87	0.13	0.85	0.15	0.79	0.21	0.83	0.17

9.6.1.4 Solvent influence towards the isomerization rate of *rac*-E-PPOX (8)

The isomerization of *rac*-(**8**) at different solvent ratios using ethanol as cosolvent was carried out according to GP7, with the difference of using Eppendorf-tubess (2 mL) and a reaction volume of 600 µL. The reaction was started with *rac*-*E*-(**8**) (10 mM) and *rac*-*Z*-(**8**) (10 mM). The total reaction volume was used for work up and analyzed via ^{1}H-NMR (**Table 42**). For each individual measured value, a reaction was performed.

Table 42: Isomerization of *rac*-(**8**, 10 mM) at 100 °C and different D_2O/EtOH ratios, showing *E*- and *Z*-isomer ratios at specified reaction times.

D_2O: Et-OH	***E*- and *Z*-ratio of *rac*-PPOX (8)**											
	0 h		**1 h**		**3 h**		**6 h**		**16 h**		**24 h**	
	(*E*)	(*Z*)	(*E*)	(*Z*)	(*E*)	(*Z*)	(*E*)	(*Z*)	(*E*)	(*Z*)	(*E*)	(*Z*)
9:1	0.22	**0.78**	0.23	0.78	0.39	0.61	0.62	0.38	0.68	0.32	0.72	0.28
8:2	0.22	**0.78**	0.23	0.78	0.34	0.66	0.60	0.40	0.70	0.30	0.73	0.28
7:3	0.22	**0.78**	0.23	0.78	0.30	0.70	0.43	0.57	0.69	0.32	0.70	0.30
9:1	**0.96**	0.04	0.95	0.05	0.90	0.10	0.76	0.24	0.69	0.32	0.72	0.28
8:2	**0.96**	0.04	0.98	0.02	0.89	0.11	0.78	0.22	0.72	0.28	0.77	0.23
7:3	**0.96**	0.04	0.97	0.03	0.92	0.08	0.85	0.15	0.75	0.25	0.70	0.30
9:1	0.06	**0.94**	0.07	0.94	0.10	0.90	0.21	0.79	0.67	0.33	0.71	0.29
8:2	0.06	**0.94**	0.06	0.94	0.08	0.92	0.23	0.78	0.67	0.33	0.67	0.33
7:3	0.06	**0.94**	0.06	0.94	0.08	0.92	0.24	0.76	0.69	0.32	0.70	0.30
9:1	**0.96**	0.04	0.94	0.06	0.90	0.10	0.77	0.23	0.69	0.31	0.71	0.29
8:2	**0.96**	0.04	0.94	0.06	0.93	0.07	0.79	0.21	0.69	0.31	0.72	0.28
7:3	**0.96**	0.04	0.96	0.04	0.94	0.07	0.85	0.15	0.71	0.29	0.70	0.30
	***E*- and *Z*-ratio of *rac*-PPOX (8)**											
	Mean value											
9:1	0.14	**0.86**	0.15	0.86	0.24	0.76	0.41	0.59	0.68	0.33	0.71	0.29
8:2	0.14	**0.86**	0.14	0.86	0.21	0.79	0.41	0.59	0.68	0.32	0.70	0.30
7:3	0.14	**0.86**	0.14	0.86	0.19	0.81	0.33	0.67	0.69	0.32	0.70	0.30
9:1	**0.96**	0.04	0.95	0.05	0.90	0.10	0.76	0.24	0.69	0.31	0.72	0.28
8:2	**0.96**	0.04	0.96	0.04	0.91	0.09	0.78	0.22	0.71	0.29	0.74	0.26
7:3	**0.96**	0.04	0.97	0.03	0.93	0.07	0.85	0.15	0.73	0.27	0.70	0.30

9.6.1.5 Isomerization rate of *rac*-*E*-4-FPPOX (4c)

The isomerization of *rac*-(**4c**) was carried out according to GP7 with DMSO-d_6 (10%, *v/v*) as cosolvent and a reaction temperature of 100 °C. The reaction was started with *rac*-*E*-(**4c**) (10 mM). The analyzed samples at different reaction times are shown in **Table 43**.

Table 43: Isomerization of *rac*-(**4c**, 10 mM) at 100 °C showing *E*- and *Z*-isomer ratios at specified reaction times.

	***E*- and *Z*-ratio of *rac*-PPOX (8)**											
	0 h		**1 h**		**3 h**		**6 h**		**16 h**		**24 h**	
c / mM	(*E*)	(*Z*)	(*E*)	(*Z*)	(*E*)	(*Z*)	(*E*)	(*Z*)	(*E*)	(*Z*)	(*E*)	(*Z*)
10	**0.81**	0.19	0.83	0.17	0.81	0.19	0.79	0.21	0.71	0.29	0.74	0.27
10	**0.75**	0.25	0.76	0.24	0.74	0.26	0.75	0.25	0.71	0.29	0.66	0.34
	Mean value											
10	**0.78**	0.22	0.80	0.21	0.78	0.22	0.77	0.23	0.71	0.29	0.70	0.78

9.6.1.6 Isomerization rate of *rac-E*-PPOX (8) in cyclohexane

The reaction was carried out according to GP7. As solvent cyclohexane was used with 320 mM substrate concentration. Isomerization in cyclohexane was performed in 5 mL glass vials with a reaction volume of 2.5 mL and reaction temperature of 80 °C. Samples (300 µL) were taken at regular intervals and at the start of isomerization reaction. Methyl alcohol d_4 (300 µL) was added to the samples for 1H NMR measurement. The analyzed samples at different reaction times are shown in **Table 44**.

Table 44: Isomerization of *rac*-(**8**, 320 mM) at 80 °C in cyclohexan showing *E*- and *Z*-isomer ratios at specified reaction times.

	***E*- and *Z*-ratio of *rac*-PPOX (8)**									
	0 h		**0.5 h**		**1 h**		**3 h**		**6 h**	
Solvent	(*E*)	(*Z*)	(*E*)	(*Z*)	(*E*)	(*Z*)	(*E*)	(*Z*)	(*E*)	(*Z*)
Cyclohexane	0.88	0.12	0.86	0.15	0.83	0.17	0.78	0.23	0.72	0.28

9.6.2 General procedure (GP8): Investigating the racemization of (*R*,*E*)-PPOX (8) and (*S*)-PPN (9)

Stock solution of *(R,E)*-PPOX (**8**, 250 mM, in ethanol), *S*-PPN (**9**, 250 mM, in ethanol) and Thiazole (25 mM, in water) were prepared. For the reaction, the investigated substrate (5 mM) and thiazole (0.13 mM- 20 mM) were dissolved in water. The reaction was carried out in a 5 mL glass vial at 80 °C and 600 rpm. For the extraction of the aqueous phase MTBE (1:1, *v/v*) was used, the phases were separated via centrifugation at 150 rpm. The organic phase was then analyzed via HPLC.

9.6.2.1 Thiazole screening for the racemization of (*R*,*E*)-PPOX (8)

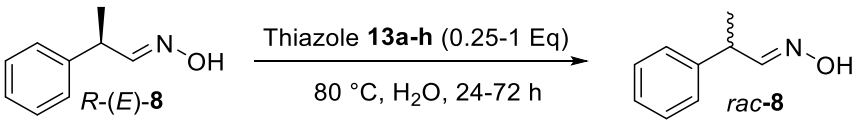

The screening was performed according to GP8 with a reaction volume of 1 mL. Water (930 µL) was first placed into a glass vial adding *(R,E)*-PPOX (20 µL, 5 mM, 68% *ee*) and the respective thiazole (50 µL, 1.3 mM). The reaction solution was stirred for 24 h at 80°C. After work up the remaining enantiomeric excess was determined via HPLC (**Table 45**).

Table 45*:* Racemization screening of *(R,E)*-PPOX with eight different thiazole derivatives (**13a-13h**). Showing remainging *ee*-values after 24 hours.

#	Thiazole	*ee* / %
13a	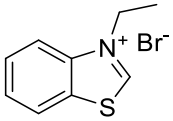 3-ethylbenzothiazolium bromide	68
13b	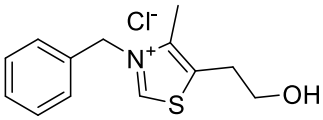 3-benzyl-5-(2-hydroxyethyl)-4-methylthiazol-3-ium chloride	60
13c	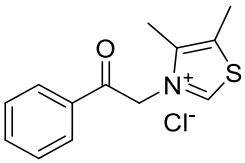 Alagebrium chloride	60
13d	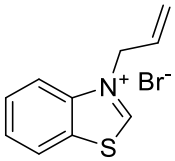 N-Allylbenzothiazolium bromide	40
13e	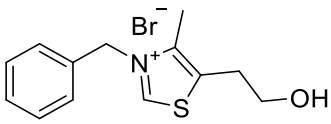 3-benzyl-5-(2-hydroxyethyl)-4-methylthiazol-3-ium bromide	60
13f	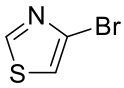 4-bromothiazole	60
13g	 Thiazole	54
13h	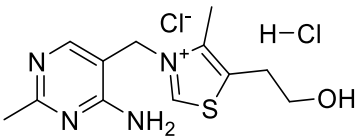 Thiamine hydrochloride	48

9.6.2.2 Racemization of (*R*,*E*)-PPOX with N-allylbenzothiazolium bromide (13d)

The reaction was carried out according to GP8. (*R*,*E*)-PPOX (20 µL, 5 mM, 88% *ee*,) was dissolved in water (1 mL) The N-allybenzothiazolium bromide (**13d**) concentration was adjusted with a stock solution (25, 6.5 mg, 25 µmol). The volume of N-allybenzothiazolium bromide (**13d**) and water was adjusted to the investigated concentration. After work up the remaining enantiomeric excess was determined via HPLC (**Table 46**).

Table 46: Concentration and time dependency for the racemization of (R,E)-PPOX (**8**) with N-allybenzothiazolium bromide (**13d**).

Thiazole	Eq.	V_{stock} / µL	V_{water} / mL	t / h	*ee* / %
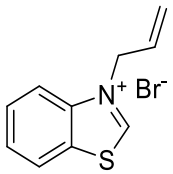 **13d**	0.25	50	930	24	n.a.
	0.5	100	880	24	n.a.
	1	200	780	24	30
	0.25	50	930	72	21
	0.5	100	880	72	14
	1	200	780	72	13

9.6.2.3 Racemization of (*R*,*E*)-PPOX with thiazole (13g)

The reaction was carried out according to GP8. (*R*,*E*)-PPOX (20 µL, 5 mM, 88% *ee*) was dissolved in water (1 mL) The thiazole (**13g**) concentration was adjusted with a stock solution (25 mM, 6.5 mg, 25 µmol). The volume of thiazole and water was adjusted to the investigated concentration (**Table 47**).

Table 47: Concentration and time dependency for the racemization of (*R*,*E*)-PPOX (**8**) with thiazole (**13g**).

Thiazole	Eq.	V_{stock} / µL	V_{water} / mL	t / h	*ee* / %
13g	0.25	50	930	24	65
	0.5	100	880	24	63
	1	200	780	24	65
	0.25	50	930	72	44
	0.5	100	880	72	37
	1	200	780	72	41

9.6.2.4 Racemization of *(R,E)*-PPOX with thiamine hydrochloride (13h)

The reaction was carried out according to GP8. *(R,E)*-PPOX (20 µL, 5 mM, 88% *ee*) was dissolved in water (1 mL). The thiamine hydrochloride concentration was adjusted with a stock solution (250 mM, 8.9 mg, 26 µmol). The volume of thiamine hydrochloride **13h** and water was adjusted to the investigated concentration. After work up the remaining enantiomeric excess was determined via HPLC (**Table 48**).

Table 48: Concentration and time dependency for the racemization of (*R,E*)-PPOX (**8**) with thiamine hydrochloride (**13h**).

Thiazole	Eq.	V_{stock} / µL	V_{water} / mL	t / h	*ee* / %
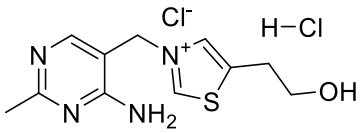 **13h**	0.25	50	930	24	n.a.
	0.5	100	880	24	40
	1	200	780	24	35
	0.25	50	930	72	23
	0.5	100	880	72	13
	1	200	780	72	12

9.6.2.5 Investigating the inhibitory effect of thiazole towards aldoxime dehydratases

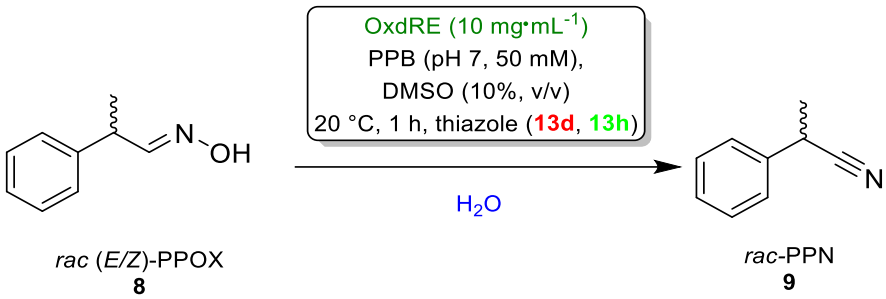

The biotransformation was performed with whole cells of OxdRE. First the buffer (PPB 50 mM, pH 7, 800 µL) with different amounts of thiazoles (**13d**, **13h**, 0.06-1 eq.) were placed into a 2 mL Eppendorf tubes. Then the enzyme as whole cell suspension was added (100 µL, 10 mg·mL^{-1}). The reaction was started by the addition of the substate solution containing *rac*-(*E*/*Z*)-**8** in DMSO (100 µL, 10 mM). The reaction was carried out at 20 °C and 1000 rpm. After 1-4 hours the reaction was quenched and extracted with 800 µL of $CDCl_3$. The organic phase was analyzed via ^{1}H-NMR-spectroscopy (**Table 49**).

Table 49: Influence of Thiazoles 13d and 13h upon the Oxd catalyzed dehydration of *rac*-(*E*/*Z*)-**8**.

Thiazole	Eq	Time / h	Conversion / %
Control	-	1	50
	-	4	47
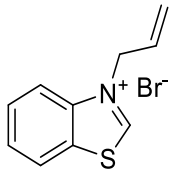 **13d**	0.06	1	21
	0.06	4	19
	0.25	1	15
	0.25	4	10
	1.0	1	13
	1.0	4	11
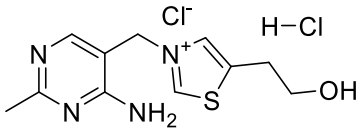 **13h**	0.06	1	48
	0.06	4	45
	0.25	1	11
	0.25	4	49
	1.0	1	7
	1.0	4	46

9.6.2.6 Racemization of (*S*)-PPN with N-allylbenzothiazolium bromide (13d)

The reaction was carried out according to GP8. (*S*)-PPN (20 µL, 5 mM, 80% *ee*) was dissolved in water (1 mL). The N-allybenzothiazolium bromide (**13d**) concentration was adjusted with a stock solution (25 mM, 19.5 mg, 76 µmol). The volume of N-allybenzothiazolium bromide (**13d**) and water was adjusted to the investigated concentration. Additionally, the pH-dependency was also investigated using PPB (50 mM, pH 6-7). After work up the remaining enantiomeric excess was determined via HPLC (**Table 50**).

Table 50: Investigating the racemization of (*S*)-PPN with N-allylbenzothiazolium bromide (**13d**)

Thiazole	Eq.	pH	Time / h	*ee* / %
Control	0	7	0	80 (*S*)
	0	7	24	81 (*S*)
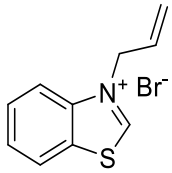 **13d**	1	7	24	81 (*S*)
	4	7	72	14 (*S*)
	4	6	72	23 (*S*)

9.6.2.7 Racemization of (*S*)-PPN with thiamine hydrochloride (13h)

The reaction was carried out according to GP8. (*S*)-PPN (20 µL, 5 mM, 80% *ee*) was dissolved in water (1 mL). The thiamine hydrochloride (**13h**) concentration was adjusted with a stock solution (25 mM, 25.5 mg, 75 µmol). The volume of thiamine hydrochloride (**13h**) and water was adjusted to the investigated concentration. Additionally, the pH-dependency was also investigated using PPB (50 mM, pH 6-7). After work up the remaining enantiomeric excess was determined via HPLC (**Table 51**).

Table 51: Investigating the racemization of (*S*)-PPN with thiamine hydrochloride (**13h**).

Thiazole	Eq.	pH	Time / h	*ee* / %
Control	0	7	0	80 (*S*)
	0	7	24	81 (*S*)
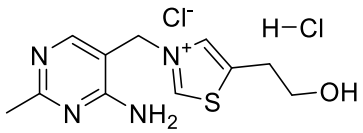 **13h**	1	7	24	83 (*S*)
	1	7	48	12 (*S*)
	1	6	48	24 (*S*)
	2	7	48	42 (*S*)
	2	6	48	38 (*S*)
	4	7	48	45 (*S*)
	4	6	48	77 (*S*)
	4	7	72	17 (*S*)
	4	6	72	36 (*S*)

9.6.3 Flow reaction and set up

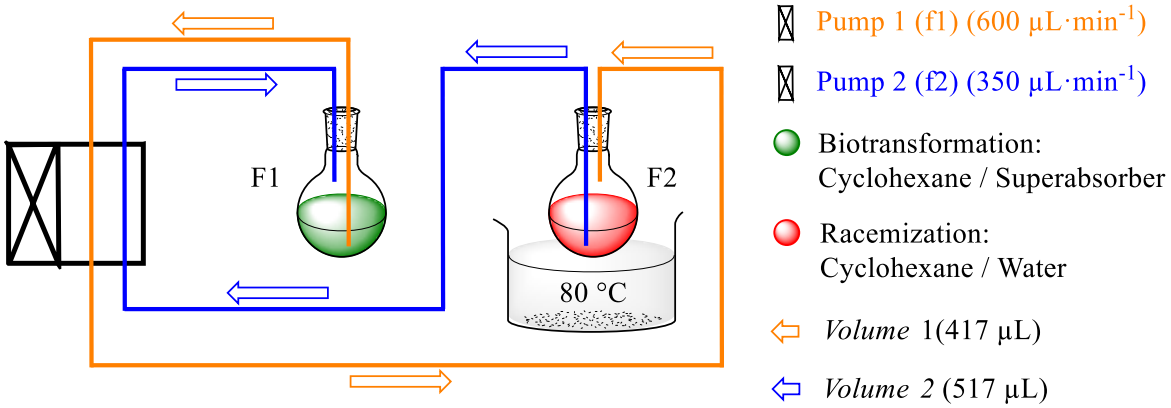

Scheme 44: Visualization of the flow set up for the DDKR.

The Double dynamic kinetic resolution was preformed according to **Scheme 44**. For the biotransformation in a 10 mL round flask 600 mg of $OxdRE_{BWW}$ in PPB (5 mL, 50 mM, pH 7) was immobilized with superabsorber (~100 mg). For the racemization a 25 mL round flask with 5 mL water containing thiamin hydrochloride (5-15 mM) and 20 mL cyclohexane with the substrate (10 mM) were prepared. The whole system then contained about 30 mL (pipes not included). Given concentration refer for simplicity to the total volume of 30 mL. The flasks were closed with rubber plungers with holes inside for the pipes. The temperature for the racemization was set up

to 80 °C. The flow rate (f1) from the biotransformation flask **F1** to the isomerization flask **F2** was set to 600 µL·min^{-1} and the flow rate (f2) from the F2-flask to the F1-flask was set to 350 µL·min^{-1}. With the height of the pipe in F1 the volume was kept constant (~3 mL). The conversion and the *ee*-value were determined via SFC-HPLC (**Table 52**, **Table 53**, **Table 54**).

Table 52: Biotransformation of OxdRE with PPOX derivates in the double dynamic kinetic resolution.

#	Substrate	Enzyme	Volume /ml	Thiamin	Flow (f1/f2) /ml·min^{-1}	Bww/ mg·ml^{-1}	Sub. /mM	Conv. /%	ee %
1	PPOX	WT	30	0.5 eq.	0.6/0.35	20	10	87	Rac
2	PPOX	WT	30	1.5 eq.	0.6/0.35	20	10	100	Rac
3	4FPPOX	WT	30	1.5 eq.	0.6/0.35	20	10	92	15
4	4FPPOX	WT	30	1.0 eq.	0.6/0.35	20	10	83	36
5	3FPPOX	L145F	30	1.0 eq.	0.6/0.35	20	10	-	-
6	4FPPOX	WT	30	1.0 eq.	1.5/1	20	10	43	33
7	4FPPOX	WT	10	0.4 eq	1.5/1	60	230	41	39

Table 53: Time course comparison of the double dynamic kinetic resolution and the kinetic resolution of OxdRE with 4-FPPOX.

	Double dynamic kinetic resolution (flow)			Kinetic resolution in (batch)		
#	Time /h	Conv. /%	ee. /%	Time /h	Conv. /%	ee. /%
1	1	14	68	1	19	70
2	2	48	53	2	41	63
3	3	56	51	3	44	63
4	5	71	45	5	47	63
5	6	78	43	6	47	63
6	7	78	39	7	51	63
7	17	82	36	17	49	61

Table 54: Flow reaction results with reduced volume using tubes instead of flask for the reaction separation.

Entry	Substrate	Enzyme	Volume /ml	Thiamin / eq.	Flow (f1/f2) /ml·min^{-1}	Bww/ mg·ml^{-1}	Sub. /mM	Conv. /%	ee %
1	PPOX	RE-WT	7	1	0.7/0.2	115	25	14	6 (*rac*)
2	4FPPOX	RE-WT	8	2.5	0.7/0.2	100	10	40	18
3	4FPPOX	RE-WT	8	2.5	0.7/0.2	100	10	47	17

9.6.4 Expression optimization comparison of leaky vs AI

The enzymes were expressed as described in 9.3.8, using auto induction-, IPTG induced- and leaky expression with first different cultivation- and induction time (**Table 55**), then different expression temperatures (**Table 56**). The activities were determined using a standard activity assay with octanal oxime.

9.6.4.1 General procedure 9 (GP9): Activity assay with octanal oxime

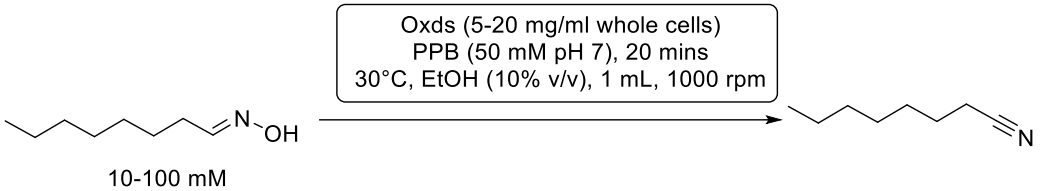

The activity assay was performed with whole cells of Oxd-variants in 5-20 mg·mL^{-1} solution. First the buffer (800 µL, PPB 50 mM, pH 7) was placed into a 2 mL Eppendorf tubes. Then the substrate solution of octanal oxime in ethanol (100 µL, 100-1000 mM) was added to the buffer to an end concentration of 10-100 mM octanal oxime and 10% ethanol. The temperature was arranged to 30 °C. Afterwards the enzyme as whole cell solution was added to the reaction mixture. The reaction solution was stirred for 20 min at 1000 rpm. The reaction was quenched and extracted with 800 µL of ethyl acetate. The organic phase was analyzed via GC.

Table 55: Dertermined activities of the expressions optimization including induction time and agent with 10 min reaction time 10 mM octanal oxime and 20 mg·mL^{-1} whole cell biocatalyst.

Entry	Cultivation time / h	Induction time	Induction with	Conversion / %	Activity / mU ·mg^{-1}	Harvested cell mass / g
1	24	-	-	76	38	2.2
2	24	OD600	IPTG	19	1	1.5
3	48	-	-	90	45	2.4
4	48	OD600	Lac.	70	35	2.3
5	48	24h	Lac.	91	45	2.3

Table 56: Dertermined activities of the expressions optimization regarding leaky expression and different temperatures, with 20 min reaction time 10 mM octanal oxime and 5 mg·mL^{-1} whole cell catalyst.

#	Enzyme	Expression	Expression temp. / °C	Conv. / %	Activity / mU·mg^{-1}
1	RE-WT	AI	15	4.0	4
2	RE-WT	Leaky	20	68	68
3	RE-WT	Leaky	25	68	69
4	RE-WT	Leaky	37	0.4	0
5	L145F	AI	15	0.5	1
6	L145F	Leaky	20	52	52

9.6.5 Rational designed mutants to increase selectivity

9.6.5.1 Activity of rational designed mutants

The activities of Oxd-variants were investigated according to GP9. Oxds as whole cells (5 mg·mL^{-1}) were placed into a 2 mL Eppendorf tubes along with PPB (800 µL, 50 mM, pH 7). The reaction was started by adding octanal oxime (100 µL, 100 mM) to an end concentration of 10 mM and 10% (*v/v*) ethanol. After work up the conversion were determined via GC (**Table 57**).

Table 57: Activity screening of Oxd variants using standard activity assay with octanal oxime as substrate. The enyzmes were obtained using leaky expression.

#	Enzyme	Expression temperature / °C	Conv. /%	Activity / mU·mg^{-1}
1	OxdRE10	20	4	4
2	OxdRE-L145Y	20	0	0
3	OxdRE-L145S	20	0	0
4	OxdRE-S219Y	20	0	0
5	OxdRE-L145G	20	2	2
6	OxdRE-RE25	20	0	0
7	OxdRE-L145M	20	53	53
8	OxdRE-L145N	20	0	0
9	OxdRE-L145D	20	0	0
10	OxdRE-L145R	20	0	0
11	OxdRE-L145P	20	0	0
12	OxdA-WT	20	70	70
13	OxdA-L145F	20	76	76
14	OxdB-WT	30	59	59
15	OxdB-L128F	30	3	3
16	OxdB-L128Y	30	1	1

9.6.5.2 Selectivity screening using PPOX as standard substrate

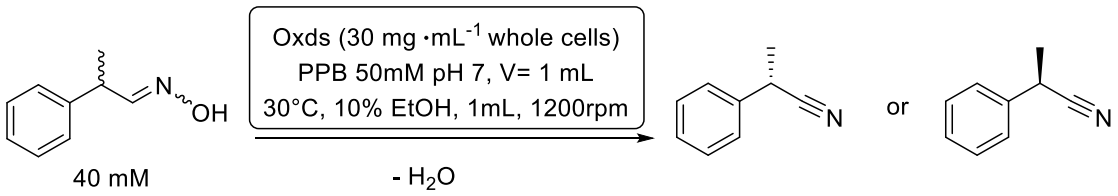

The selectivity investigation was carried similar to GP9. Oxds as whole cells (100 µL, 30 mg·mL^{-1}) were placed into a 2 mL Eppendorf tubes along with PPB (800 µL, 50 mM, pH 7). The reaction was started by adding a PPOX solution (100 µL, 40 mM, 10% *v/v* ethanol). After 19 hours at 10 °C the reaction was extracted with cyclohexane (800 µL). The conversion and the ee-value were determined via SFC-HPLC (**Table 58**).

Table 58: Intial selectivity screening of rational designed Oxd-variants using *rac*-(*E*/*Z*)-PPOX (**8**) as standard substrate

#	Enzyme	Expression/ °C	conversion / %	*ee.* / %	Enatiomer
1	OxdA-WT	20	46	12.4	*S*
2	OxdRE-WT	25	63	11.9	*S*
3	OxdB-WT	25	51	20.2	*S*
4	OxdA-L145F	25	29	41.3	*S*
5	OxdB-L128F	25	8	64.4	*R*
6	OxdB-L128Y	25	1	20.5	*R*
7	OxdRE-L145M	20	25	34.1	*S*
8	OxdRE-L145N	20	0	0.0	-
9	OxdRE-L145D	20	0	0.0	-
10	OxdRE-L145R	20	0	0.0	-
11	OxdRE-L145P	20	0	0.0	-
12	OxdRE-L145Del	20	0	0.0	-
13	OxdRE-L145S	20	21	37.8	*S*
14	OxdRE-L145Y	25	1	17.2	*R*
15	OxdRE-S219Y	20	0	0.0	-

9.6.5.3 Investigation of different the phenyl alanine mutation in different Oxds with a set of PPOX derivatives

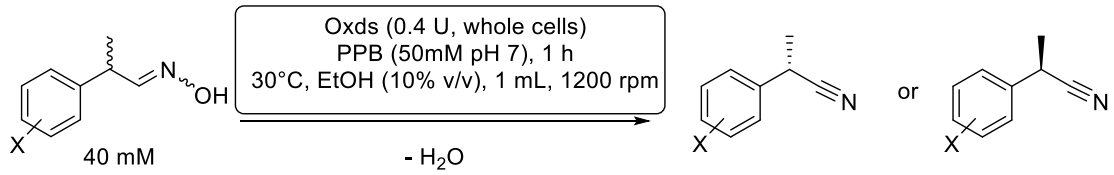

X= F; Cl; Br; Me; 2,6-diF ; 2,6-diCl

The selectivity investigation was carried similar to GP9. Oxds as whole cells (200-400 mU) were placed into a 2 mL Eppendorf tubes along with PPB (, 50 mM, pH 7). The reaction was started by adding a PPOX solution (100 µL, 40 mM, 10% *v/v* ethanol). After 1 hours at 30 °C the reaction was extracted with $CDCl_3$ (1 mL). The conversion was determined via ^{1}H-NMR. Afterwards the solvent of the ^{1}H-NMR-samples were removed and the residue absorbed in cyclohexane (800 µL). the new samples were then used to determine the ee-value SFC-HPLC (**Table 59**).

Table 59: Selectivity screening with 14 different PPOX derivatives. Using OxdA-WT and OxdA-L145F.

#	Enzyme	Substrate	E/Z ratio	Activity /mU	Conv. / %	*ee.* / %	Enatio-mer	E
1	OxdA-L145F	oF	76/24	200	21	63	*S*	5
2	OxdA-L145F	mF	66/34	200	12	63	*S*	5
3	OxdA-L145F	pF	68/32	200	8	7	*S*	1
4	OxdA-L145F	oCl	3/97	200	n.d.	n.d.	-	-
5	OxdA-L145F	mCl	66/34	200	23	11	*S*	1
6	OxdA-L145F	pCl	64/36	200	6	40	*R*	2
7	OxdA-L145F	oBr	20/80	200	3	0	-	1
8	OxdA-L145F	mBr	65/35	200	13	27	*R*	2
9	OxdA-L145F	pBr	66/34	200	18	50	*R*	3
10	OxdA-L145F	oMe	0/100	200	0	0	-	-
11	OxdA-L145F	mMe	69/31	200	10	3	-	1
12	OxdA-L145F	pMe	67/33	200	n.d.	n.d.	-	-
13	OxdA-L145F	diF	54/46	200	4	50	*S*	3
14	OxdA-L145F	diCl	43/57	200	0	0	-	-
15	OxdA-WT	oF	76/24	400	38	39	*S*	3
16	OxdA-WT	mF	66/34	400	44	43	*S*	3
17	OxdA-WT	pF	68/32	400	17	41	*S*	3
18	OxdA-WT	oCl	3/97	400	43	57	*R*	5
19	OxdA-WT	mCl	66/34	400	15	1	*R*	1
20	OxdA-WT	pCl	64/36	400	3	40	*R*	2
21	OxdA-WT	oBr	20/80	400	22	49	*S*	3
22	OxdA-WT	mBr	65/35	400	5	28	*R*	2
23	OxdA-WT	pBr	66/34	400	2	46	*R*	3
24	OxdA-WT	oMe	0/100	400	5	86	*R*	14
25	OxdA-WT	mMe	69/31	400	21	16	*S*	1
26	OxdA-WT	pMe	67/33	400	n.d.	n.d.	-	-
27	OxdA-WT	diF	54/46	400	35	15	*S*	1
28	OxdA-WT	diCl	43/57	400	2	18	*S*	1

Table 60: Selectivity screening with 14 different PPOX derivatives. Using OxdB-WT and OxdB-L128F.

#	Enzyme	Substrate	E/Z ratio	Activity /mU	Conv. / %	*ee* / %	Enatio-mer	E
1	OxdB-L128F	oF	76/24	200	0	0	-	-
2	OxdB-L128F	mF	66/34	200	2	99	*R*	-
3	OxdB-L128F	pF	68/32	200	0	0	-	-
4	OxdB-L128F	oCl	3/97	200	0	0	-	-
5	OxdB-L128F	mCl	66/34	200	4	85	*R*	13
6	OxdB-L128F	pCl	64/36	200	0	0	-	-
7	OxdB-L128F	oBr	20/80	200	0	0	-	-
8	OxdB-L128F	mBr	65/35	200	13	80	*R*	10
9	OxdB-L128F	pBr	66/34	200	n.d.	n.d.	-	-
10	OxdB-L128F	oMe	0/100	200	0	0	-	-
11	OxdB-L128F	mMe	69/31	200	4	95	*R*	41
12	OxdB-L128F	pMe	67/33	200	3	60	*R*	4
13	OxdB-L128F	diF	54/46	200	2	38	*R*	2
14	OxdB-L128F	diCl	43/57	200	0	0	-	-
15	OxdB-WT	oF	76/24	400	22	4	*R*	1
16	OxdB-WT	mF	66/34	400	18	20	*R*	2
17	OxdB-WT	pF	68/32	400	34	21	*S*	2
18	OxdB-WT	oCl	3/97	400	n.d.	n.d.	-	-
19	OxdB-WT	mCl	66/34	400	8	63	*R*	5
20	OxdB-WT	pCl	64/36	400	16	7	*S*	1
21	OxdB-WT	oBr	20/80	400	5	70	*R*	6
22	OxdB-WT	mBr	65/35	400	8	56	*R*	4
23	OxdB-WT	pBr	66/34	400	7	12	*R*	1
24	OxdB-WT	oMe	0/100	400	2	76	*R*	7
25	OxdB-WT	mMe	69/31	400	18	46	*R*	3
26	OxdB-WT	pMe	67/33	400	21	7	*S*	1
27	OxdB-WT	diF	54/46	400	24	3	*R*	1
28	OxdB-WT	diCl	43/57	400	0	0	-	-

Table 61: Selectivity screening with 14 different PPOX derivatives. OxdRE as wild type and L145F mutant.

#	Enzyme	Substrate	E/Z ratio	Activity /mU	Conv. / %	*ee* / %	Enatio-mer	E
1	OxdRE-L145F	oF	76/24	200	3	60	*S*	4
2	OxdRE-L145F	mF	66/34	200	3	47	-	3
3	OxdRE-L145F	pF	68/32	200	2	8	-	1
4	OxdRE-L145F	oCl	3/97	200	3	48	-	3
5	OxdRE-L145F	mCl	66/34	200	11	16	*S*	1
6	OxdRE-L145F	pCl	64/36	200	5	50	*R*	3
7	OxdRE-L145F	oBr	20/80	200	7	79	*S*	9
8	OxdRE-L145F	mBr	65/35	200	13	34	*R*	2
9	OxdRE-L145F	pBr	66/34	200	10	82	*R*	11
10	OxdRE-L145F	oMe	0/100	200	0	0	-	-
11	OxdRE-L145F	mMe	69/31	200	5	14	*R*	1
12	OxdRE-L145F	pMe	67/33	200	0	0	-	-
13	OxdRE-L145F	diF	54/46	200	5	42	*S*	3
14	OxdRE-L145F	diCl	43/57	200	0	0	-	-
15	OxdRE-WT	oF	76/24	400	45	26	*S*	2
16	OxdRE-WT	mF	66/34	400	54	26	*S*	2
17	OxdRE-WT	pF	68/32	400	11	54	*S*	4
18	OxdRE-WT	oCl	3/97	400	29	30	*R*	2
19	OxdRE-WT	mCl	66/34	400	25	0	-	1
20	OxdRE-WT	pCl	64/36	400	2	18	-	1
21	OxdRE-WT	oBr	20/80	400	19	62	*S*	5
22	OxdRE-WT	mBr	65/35	400	9	51	*R*	3
23	OxdRE-WT	pBr	66/34	400	1	58	-	4
24	OxdRE-WT	oMe	0/100	400	7	91	*R*	23
25	OxdRE-WT	mMe	69/31	400	31	11	*S*	1
26	OxdRE-WT	pMe	67/33	400	n.d.	n.d.	-	-
27	OxdRE-WT	diF	54/46	400	42	4	*S*	1
28	OxdRE-WT	diCl	43/57	400	3	47	*S*	3

9.6.5.4 Investigation of different the tyrosine mutation in OxdB and OxdRE with a set of PPOX derivatives

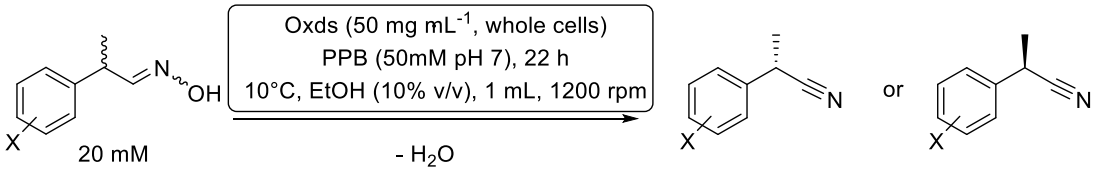

X= F; Cl; Br; Me; 2,6-diF ; 2,6-diCl

The selectivity investigation of OxdB-L128Y and OxdRE L145Y was carried similar to GP9. Oxds as whole cells (50 mg·mL^{-1}) were placed into a 2 mL Eppendorf tubes along with PPB (50 mM, pH 7). The reaction was started by adding a PPOX solution (100 µL, 20 mM, 10% *v/v* ethanol). After 22 hours at 10 °C the reaction was extracted with $CDCl_3$ (1 mL). The conversion was determined via ^{1}H-NMR. Afterwards the solvent of the ^{1}H-NMR-samples were removed and the residue absorbed in cyclohexane (800 µL). the new samples were then used to determine the *ee*-value SFC-HPLC (**Table 62**).

Table 62: Selectivity screening with 14 different PPOX derivatives. OxdB-L128Y and OxdRE-L145Y mutants

Enzyme	Substrate	E/Z-ratio	conversion / %	*ee* / %	Enantiomer
OxdB-L128Y	oF	76/24	5	22	*S*
OxdB-L128Y	mF	66/34	0	15	-
OxdB-L128Y	pF	68/32	0	0	-
OxdB-L128Y	oCl	3/97	14	94	*R*
OxdB-L128Y	mCl	66/34	0	0	-
OxdB-L128Y	pCl	64/36	2	59	-
OxdB-L128Y	oBr	20/80	2	38	-
OxdB-L128Y	mBr	65/35	0	0	-
OxdB-L128Y	pBr	66/34	0	0	-
OxdB-L128Y	oMe	0/100	0	0	-
OxdB-L128Y	mMe	69/31	1	16	*S*
OxdB-L128Y	pMe	67/33	1	21	*S*
OxdB-L128Y	diF	54/46	0	0	-
OxdB-L128Y	diCl	43/57	0	0	-
OxdRE-L145Y	oF	76/24	0	53	*S*
OxdRE-L145Y	mF	66/34	0	26	*S*
OxdRE-L145Y	pF	68/32	0	0	-
OxdRE-L145Y	oCl	3/97	11	94	*R*
OxdRE-L145Y	mCl	66/34	0		-
OxdRE-L145Y	pCl	64/36	1	46	-
OxdRE-L145Y	oBr	20/80	18	94	*R*
OxdRE-L145Y	mBr	65/35	0	0	-

9.6.6 OxdRE-L145F-library

The mutant library was commercially acquired from *Twist Bioscience*®. The mutants were generated on a semi-rational level for which MOE was used as a tool. Positions were selected that were

either close to the active pocket, in interaction with the active site, or at positions such as loops that could have a large influence on the positioning of the essential amino acids in the active site (**Table 63**).

Table 63: Summary of existing mutation libraries and their positions on the plate.

	1	2	3	4	5	6	7
A	P 26	L 37	W 99	T 144	L 152	D 160	L 316
B	F 27	Q 38	K 100	F 145	P 153	G 161	R 317
C	P 28	P 39	A 136	Y 146	G 154	I 162	L 318
D	M 29	A 76	P 137	A 147	V 155	S 163	Y 319
E	W 30	H 77	R 138	F 148	G 156	G 164	
F	A 34	H 78	A 139	Q 149	A 157	E 165	
G	D 35	Y 79	E 140	E 150	V 158	I 166	
H	D 36	W 98	Q 141	D 151	M 159	K 315	

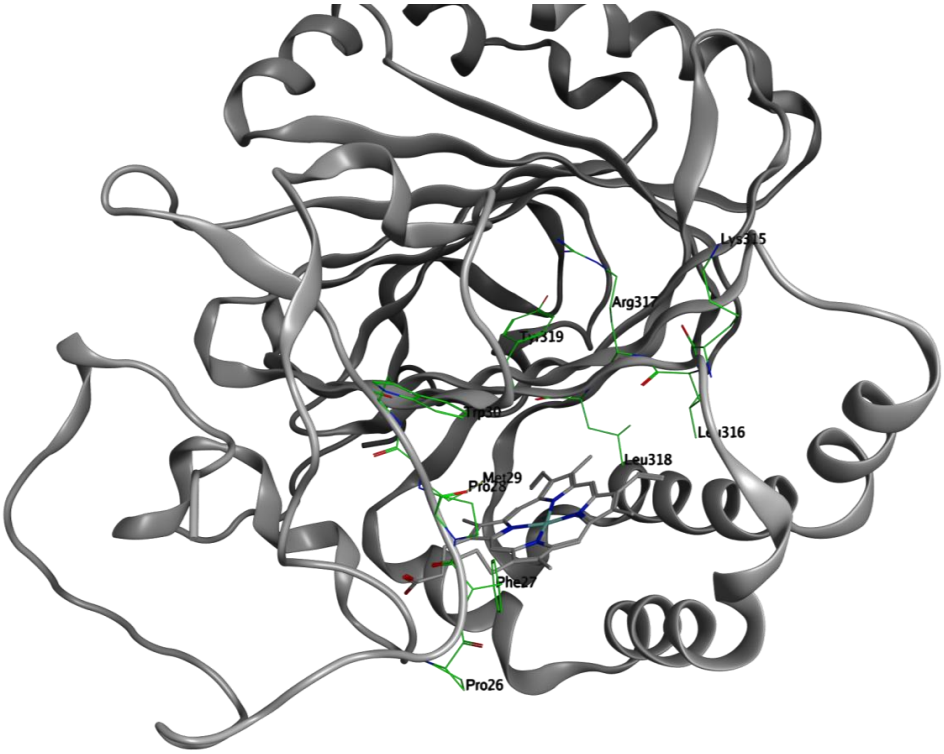

Figure 59: Library selection Set 1 of OxdRE-L145F with mutation sites spatial close to the active site are highlighted in green.

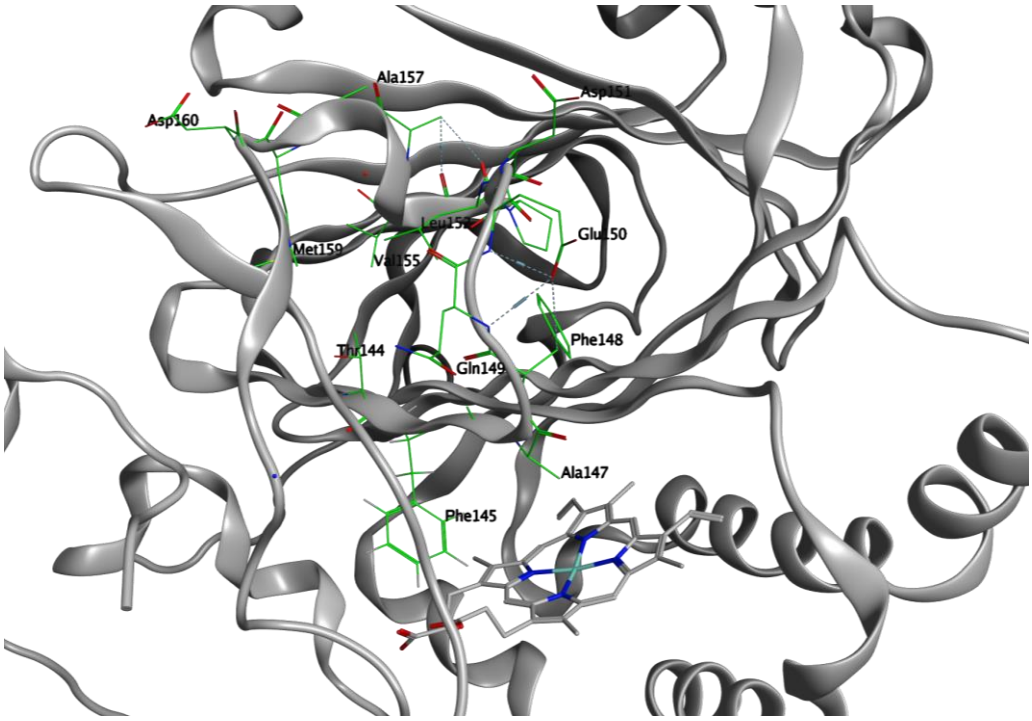

Figure 60: Library selection Set 2 of OxdRE-L145F with mutation sites on the same β-strand of as L145F highlighted in green.

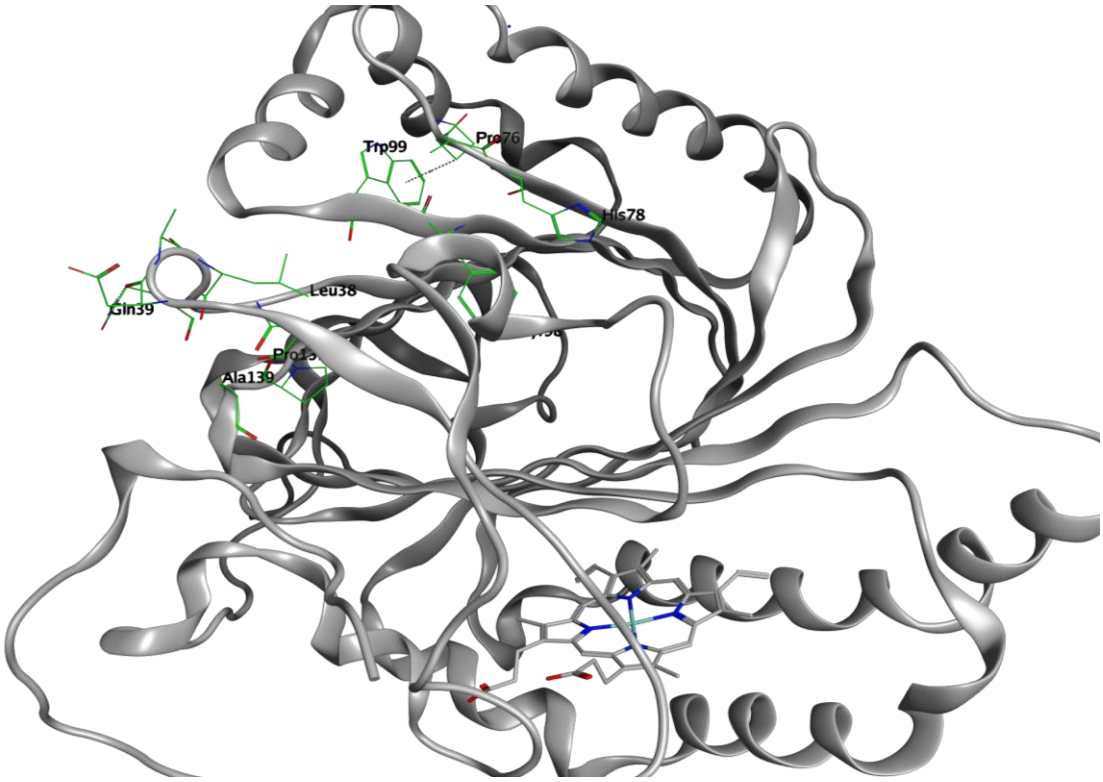

Figure 61: Library selection Set 3 of OxdRE-L145F with mutation sites located on loops and turns far from the active site highlighted in green.

9.6.6.1 Screening development and validation

OxdRE-WT was transformed in BL21(DE3)-Star strain using standard transformation protocol (9.3.5). For transformation 2 µL of the plasmid solution (200 ng·µL) was used on the competent cell solution (50 µL) resulting in over 100 clones. The clones were transferred individually to a deep-well-plate with LB-Medium (1.8mL) containing kanamycin. Two different cultivation protocols were tested, to examine the most suitable. For the first cultivation method the picked clones were resuspended in the media and grown for 48 hours, thereby the temperature was reduced from 37 °C after 24 hours to 20 °C. For the second cultivation method, LB-Medium was inoculated with single colonies and cultivated for 24 h at 37 °C. The suspensions were used as preculture and were used to inoculate (50 µL) fresh media and then grown another 24 hours at 20 °C. The cells were then harvested via centrifugation (3500 rpm, 2 min) and resuspend in PPB (450 µL, 50 mM, pH 7). Then an ethanolic substrate solution of *rac*-2-FPPOX (**4a**, 10 mM, 50 µL) was added. The reaction was carried out for one hour in a shaker at 20 °C and 200 rpm. As workup cyclohexane (1 mL) was used to extract the reaction solution and then analyzed via HPLC.

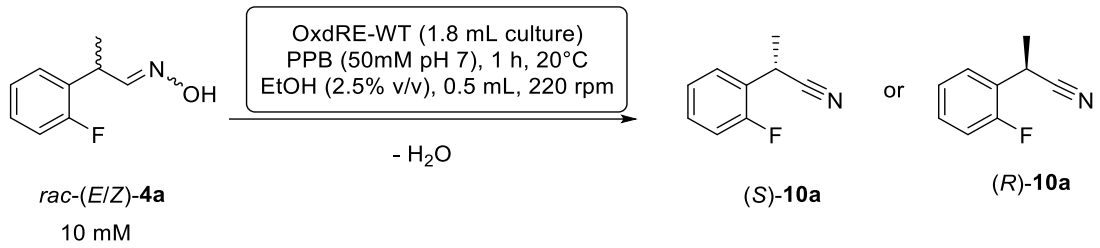

Table 64: Validation with OxdRE-WT expression and reaction in 96 deep-well plates directly using the picked clones for the expression.

			Clone-Expression				
#	**Nitril/ mM**	**Ox. / mM**	**Total/ mM**	**Conv./ %**	**Recovery/ %**	***ee.* / %**	**E**
1	1.7	6.2	7.9	21	79	33	2
2	1.8	5.6	7.3	24	73	17	1
3	1.8	5.5	7.3	25	73	30	2
4	2.2	5.6	7.8	28	78	30	2
5	2.5	5.3	7.8	32	78	31	2
6	2.6	5.4	7.9	32	79	31	2
7	1.7	6.7	8.5	21	85	31	2
8	1.9	5.0	6.9	28	69	31	2
9	2.2	5.0	7.2	31	72	32	2
10	1.5	5.9	7.4	21	74	34	2
11	3.1	4.6	7.7	40	77	33	2
12	3.1	4.7	7.7	40	77	32	2
13	2.8	5.0	7.8	36	78	31	2
14	0.0	7.0	7.0	0	70		
15	2.4	5.7	8.1	30	81	31	2

Table 65: Validation with OxdRE-WT expression and reaction in 96 deep-well plates with precultures before expression.

			Preculture-Expression				
#	**Nitril / mM**	**Ox. / mM**	**Total / mM**	**Conv./ %**	**Recovery/ %**	***ee.* / %**	**E**
1	2.0	5.8	7.7	25	77	33	2
2	1.4	6.7	8.2	17	82	31	2
3	0.0	0.0	0.0	0	0	0	
4	1.8	6.8	8.6	21	86	28	3
5	2.9	3.9	6.8	42	68	34	2
6	2.3	5.3	7.6	30	76	31	2
7	1.9	6.7	8.6	22	86	32	2
8	2.6	6.0	8.7	30	87	31	2
9	1.2	7.8	9.0	13	90	30	2
10	1.9	2.0	4.0	49	40	38	3
11	1.6	7.1	8.7	19	87	31	2
12	2.0	6.0	8.0	25	80	30	2
13	2.0	7.1	9.1	22	91	29	2
14	1.2	8.3	9.5	13	95	31	2
15	1.9	8.3	10.2	19	102	31	2

9.6.6.2 General Screening method (GSM)

The library was transformed in *E. coli* BL21-Star strain using standard transformation protocol. For transformation 10 µL of the plasmid solution was used on the competent cell solution (50 µL) resulting in over 100 clones. The clones were transferred individually to a deep-well-plate with LB-Medium (1.6 mL) containing kanamycin, one clone was used for two inoculations. One backup culture one reaction culture. Cultures were first grown at 37 °C for 24 hours then another 24 hors at 20 °C (leaky expression). The cells were harvested via centrifugation (3500 rpm, 2 min). The reaction cultures are resuspended in buffer (PPB, pH 7, 50 mM) and used for the reaction, which also takes place in the deep-well plates. An ethanolic substrate solution of *rac*-2-FPPOX (5 mM, 12.5 µL) was added. The reaction was carried out in the deep well plates using a shaker at 20 °C and 200 rpm for one hour. As workup cyclohexane (400 µL) was used to extract the reaction solution and then analyzed via HPLC. The backup cultures are stored in the freezer at -20°C.

9.6.6.3 Library screening results

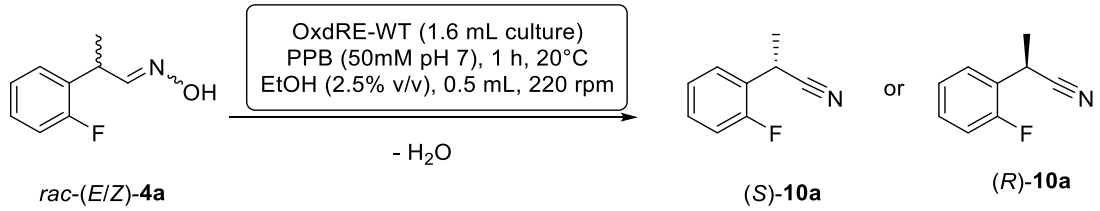

rac-(*E*/*Z*)-**4a** (*S*)-**10a** (*R*)-**10a**

The screening was carried out as described in the general screening method (GSM). The determined *ee*-values and conversions are listed in the following tables for each mutation site and position in the deep-well plates.

Table 66: Screening results of position 4A (mutation site T144).

T144	Enantiomeric excess / %								
4A	1	2	3	4	5	6	7	8	9
A	0	0	0	0	0	0	57	41	0
B	0	0	0	0	0	0	0	0	0
C	0	0	0	0	0	0	0	0	
D	0	0	0	0	0	0	0	0	
	Conversion / %								
4A	1	2	3	4	5	6	7	8	9
A	0	0	0	0	0	0	21	57	0
B	0	0	0	0	0	0	0	0	0
C	0	0	0	0	0	0	0	0	0
D	0	0	0	0	0	0	0	0	0

Table 67: Screening results of position 4C (mutation site Y146).

Y146	Enantiomeric excess / %								
4C	1	2	3	4	5	6	7	8	9
A	0	0	0	0	0	0	0	0	0
B	0	75	73	0	0	0	0	0	0
C	0	0	0	0	0	0	0	75	0
D	0	0	0	0	0	0	0	0	0
E	0	0	0	0	0	0	0	0	0
F	59	0	47	43	0	0	0	0	0
G	0	0	57	0	0	0	0	0	0
H	65	0	0	0	61	0	0	0	0
	Conversion / %								
4C	1	2	3	4	5	6	7	8	9
A	0	0	0	0	0	0	0	0	0
B	0	10	15	0	0	0	0	0	0
C	0	0	0	0	0	0	0	9	0
D	0	0	0	0	0	0	0	0	0
E	0	0	0	0	0	0	0	0	0
F	32	0	45	50	0	0	0	0	0
G	0	0	36	0	0	0	0	0	0
H	29	0	0	0	33	0	0	0	0

Table 68: Screening results of position 4D (mutation site A147)

A147	Enantiomeric excess / %								
4D	1	2	3	4	5	6	7	8	9
A	15	31	0	0	9	0	25	11	0
B	29	0	0	0	0	-17	43	3	0
C	0	70	0	0	0	0	42	29	38
D	38	0	0	0	0	0	64	40	0
E	38	43	0	0	0	0	0	0	0
F	0	0	0	0	0	0	31	31	37
G	0	0	0	0	0	43	41	0	0
H	55	73	39	0	0	0	0	37	0
	Conversion / %								
4D	1	2	3	4	5	6	7	8	9
A	8	13	0	0	18	0	19	0	0
B	33	0	0	0	0	7	34	6	0
C	0	32	0	0	0	0	27	18	30
D	49	0	0	0	0	0	31	33	0
E	59	14	0	0	0	0	0	0	0
F	0	0	0	0	0	0	19	0	19
G	0	0	0	0	0	19	38	0	0
H	38	25	45	0	0	0	0	55	0

Table 69: Screening results of position 4E (mutation site F148)

F148	Enantiomeric excess / %								
4E	1	2	3	4	5	6	7	8	9
A	0	0	0	0	0	0	0	0	0
B	0	57	0	0	63	0	0	0	0
C	0	67	0	0	0	0	0	0	0
D	0	0	0	0	0	0	0	0	67
E	0	0	0	0	0	63	0	0	0
F	0	0	0	67	0	0	0	0	0
G	0	0	0	0	0	0	0	0	0
H	0	0	0	0	0	0	0	0	0
148	Conversion / %								
4E	1	2	3	4	5	6	7	8	9
A	0	0	0	0	0	0	0	0	0
B	0	33	0	0	24	0	0	0	0
C	0	26	0	0	0	0	0	0	0
D	0	0	0	0	0	0	0	0	20
E	0	0	0	0	0	28	0	0	0
F	0	0	0	34	0	0	0	0	0
G	0	0	0	0	0	0	0	0	0
H	0	0	0	0	0	0	0	0	0

Table 70: Screening results of position 4F (mutation site Q149).

Q149	Enantiomeric excess / %								
4F	1	2	3	4	5	6	7	8	9
A	0	0	0	68	69	0	0	0	0
B	0	0	0	0	0	0	0	0	0
C	0	0	0	0	0	0	75	0	51
D	59	0	0	85	0	73	0	85	63
E	0	0	0	0	0	0	0	0	0
F	0	0	0	0	0	0	0	59	0
G	0	0	0	0	0	0	0	0	0
H	0	0	0	0	99	99	0	57	0
	Conversion / %								
4F	1	2	3	4	5	6	7	8	9
A	0	0	0	23	18	0	0	0	0
B	0	0	0	0	0	0	0	0	0
C	0	0	0	0	0	0	33	0	40
D	27	0	0	10	0	16	0	11	26
E	0	0	0	0	0	0	0	0	0
F	0	0	0	0	0	0	0	31	0
G	0	0	0	0	0	0	0	0	0
H	0	0	0	0	7	0	0	40	0

Table 71: Screening results of position 4G (mutation site E150).

E150	Enantiomeric excess / %					
4G	1	2	3	4	5	6
A	63	67	0	61	0	0
B	65	63	77	55	0	0
C	65	69	79	0	0	0
D	0	46	59	75	73	0
E	0	45	49	51	47	0
F	0	59	0	57	0	0
G	99	59	0	0	75	0
H	75	80	70	65	43	0
	Conversion / %					
4G	1	2	3	4	5	6
A	36	42	0	46	0	0
B	0	0	0	0	0	0
C	48	31	22	0	0	0
D	0	46	48	43	18	0
E	0	54	55	46	0	0
F	0	50	0	0	0	0
G	16	0	0	0	16	0
H	26	48	42	16	0	0

Table 72: Screening results of position 4H (mutation site D151).

D151	Enantiomeric excess / %					
4H	1	2	3	4	5	6
A	0	51	65	65	51	0
B	49	87	55	59	40	0
C	55	0	99	77	0	57
D	0	79	69	70	40	0
E	47	0	0	0	0	0
F	0	0	0	49	33	0
G	0	0	0	37	0	33
H	73	79	60	65	70	59
	Conversion / %					
4H	1	2	3	4	5	6
A	0	0	45	43	0	0
B	0	17	0	0	0	0
C	0	0	17	0	0	0
D	0	0	23	25	0	0
E	58	0	0	0	0	0
F	0	0	0	0	0	0
G	0	0	0	0	0	0
H	37	38	54	42	52	51

Table 73: Screening results of position 3A (mutation site W99).

W99	Enantiomeric excess / %					
3A	1	2	3	4	5	6
A	0	0	0	0	0	0
B	0	0	0	0	0	0
C	0	0	0	0	0	0
D	0	0	0	0	0	0
E	0	0	0	0	0	0
F	0	0	0	0	0	0
G	0	0	0	0	0	0
H	0	0	0	0	0	0
	Conversion / %					
3A	1	2	3	4	5	6
A	0	0	0	0	0	0
B	0	0	0	0	0	0
C	0	0	0	0	0	0
D	0	0	0	0	0	0
E	0	0	0	0	0	0
F	0	0	0	0	0	0
G	0	0	0	0	0	0
H	0	0	0	0	0	0

Table 74: Screening results of position 3G (mutation site E140).

E140	Enantiomeric excess / %					
3G	1	2	3	4	5	6
A	0	0	0	0	0	80
B	0	0	0	99	0	0
C	0	0	99	0	0	0
D	0	0	0	0	0	0
E	0	0	0	0	0	0
F	0	0	63	0	0	70
G	0	0	0	0	0	0
H	0	0	0	0	0	0
	Conversion / %					
3G	1	2	3	4	5	6
A	0	0	0	0	0	5
B	0	0	0	4	0	0
C	0	0	5	0	0	0
D	0	0	0	0	0	0
E	0	0	0	0	0	0
F	0	0	0	0	0	7
G	0	0	0	0	0	0
H	0	0	0	0	0	0

Table 75: Screening results of position 3F (mutation site A139).

A139	Enantiomeric excess / %					
3F	1	2	3	4	5	6
A	0	0	0	0	0	0
B	0	0	0	0	0	0
C	0	0	0	0	0	0
D	0	0	0	0	0	0
E	0	0	0	75	0	0
F	99	0	0	0	0	0
G	0	0	73	0	0	0
H	0	0	0	81	90	83
	Conversion / %					
3F	1	2	3	4	5	6
A	0	0	0	0	0	0
B	0	0	0	0	0	0
C	0	0	0	0	0	0
D	0	0	0	0	0	0
E	0	0	0	6	0	0
F	6	0	0	0	0	0
G	0	0	9	0	0	0
H	0	0	0	6	9	3

Table 76: Screening results of position 5A (mutation site L152).

L152	Enantiomeric excess / %					
5A	1	2	3	4	5	6
A	0	0	0	85	65	99
B	77	0	99	0	0	0
C	0	0	0	0	0	0
D	0	90	0	0	93	0
E	0	0	99	0	0	0
F	0	99	90	0	67	77
G	0	0	0	0	99	0
H	0	0	0	0	73	0
	Conversion / %					
5A	1	2	3	4	5	6
A	0	0	0	8	12	3
B	6	0	3	0	0	0
C	0	0	0	0	0	0
D	0	6	0	0	6	0
E	0	0	5	0	0	0
F	0	6	6	0	12	11
G	0	0	0	0	7	0
H	0	0	0	0	7	0

Table 77: Screening results of position 5B (mutation site P153).

P153	Enantiomeric excess / %					
5B	1	2	3	4	5	6
A	0	0	0	0	0	0
B	0	0	0	0	0	0
C	0	63	0	0	0	0
D	0	0	0	0	0	0
E	0	0	0	0	0	0
F	0	0	0	0	0	0
G	0	0	0	0	99	0
H	84	99	0	0	77	0
	Conversion / %					
5B	1	2	3	4	5	6
A	0	0	0	0	0	0
B	0	0	0	0	0	0
C	0	6	0	0	0	0
D	0	0	0	0	0	0
E	0	0	0	0	0	0
F	0	0	0	0	0	0
G	0	0	0	0	5	0
H	6	6	0	0	5	0

Table 78: Screening results of position 5C (mutation site G154).

G154	Enantiomeric excess / %					
5C	1	2	3	4	5	6
A	0	47	65	0	0	0
B	0	60	60	0	0	0
C	0	53	0	0	0	0
D	60	55	0	0	0	0
E	0	0	0	0	0	0
F	0	67	70	0	0	0
G	50	53	0	0	0	0
H	52	50	0	0	0	0
	Conversion / %					
5C	1	2	3	4	5	6
A	0	54	23	0	0	0
B	0	34	38	0	0	0
C	0	31	0	0	0	0
D	29	31	0	0	0	0
E	0	0	0	0	0	0
F	0	35	0	0	0	0
G	54	55	0	0	0	0
H	42	56	0	0	0	0

Table 79: Screening results of position 5H (mutation site M159).

M159	Enantiomeric excess / %					
5H	1	2	3	4	5	6
A	0	0	0	0	0	0
B	0	0	0	0	0	0
C	0	0	0	0	0	0
D	0	0	0	0	0	0
E	0	0	0	0	0	0
F	0	0	0	0	0	0
G	0	0	0	0	0	0
H	0	0	0	0	0	0
	Conversion / %					
5H	1	2	3	4	5	6
A	0	0	0	0	0	0
B	0	0	0	0	0	0
C	0	0	0	0	0	0
D	0	0	0	0	0	0
E	0	0	0	0	0	0
F	0	0	0	0	0	0
G	0	0	0	0	0	0
H	0	0	0	0	0	0

Table 80: Screening results of position 6A (mutation site D160).

D160	Enantiomeric excess / %					
6A	1	2	3	4	5	6
A	57	0	67	99	0	0
B	0	81	0	0	0	0
C	0	0	91	99	0	0
D	43	0	0	0	0	0
E	43	60	0	0	70	70
F	79	0	0	0	0	0
G	99	77	0	0	0	82
H	0	0	0	0	0	0
	Conversion / %					
6A	1	2	3	4	5	6
A	46	0	27	5	0	0
B	0	10	0	4	0	0
C	0	0	20	5	0	0
D	50	0	0	0	0	0
E	50	27	0	10	14	0
F	26	0	0	0	0	0
G	6	14	0	0	0	4
H	0	0	0	0	0	0

Table 81: Screening results of position 6B (mutation site G161).

G161	Enantiomeric excess / %					
6B	1	2	3	4	5	6
A	51	75	73	71	0	0
B	61	59	0	0	0	0
C	99	0	75	0	57	0
D	70	57	0	0	99	0
E	60	77	81	0	0	0
F	0	0	0	77	0	0
G	0	52	53	59	0	0
H	59	0	0	0	0	0
	Conversion / %					
6B	1	2	3	4	5	6
A	54	17	30	15	0	0
B	24	26	0	0	0	0
C	5	0	21	0	47	0
D	44	40	0	0	7	0
E	38	23	18	0	0	0
F	0	0	0	14	0	0
G	0	0	43	43	44	0
H	35	0	0	0	0	0

9.6.6.4 Biotransformation with selected hits from library screening

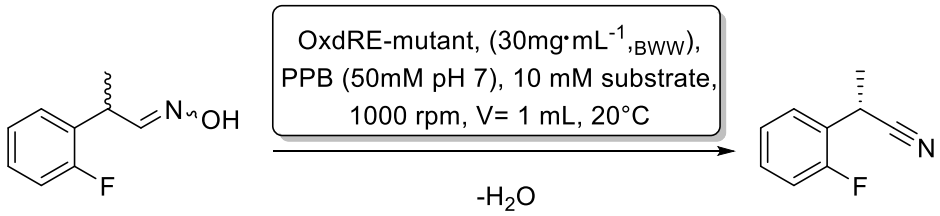

Oxds as whole cells (30 mg·mL^{-1}, $_{BWW}$) were placed into a 2 mL Eppendorf tubes along with PPB (800 µL, 50 mM, pH 7). The reaction was started by adding *rac*-(*E/Z*)-2FPPOX (**4a**, 50 µL, 200 mM) to an end concentration of 10 mM and 5% (*v/v*) ethanol. After work up the conversion were determined via HPLC (**Table 57**).

Table 82: Biotransformations of identified hits in the screening using *rac*-(*E/Z*)-2FPPOX (**4a**) as substrate.

#	Clone	Site	Conv. / %	Ee / %	E-Value
A	WT	-	15	31	2
B	L145F	-	28	48	4
1	6B-A3	G161R	55	55	7
2	6B-D1	G161D	49	60	8
3	6A-C3	D160C	35	71	9
4	4H-B2	D151E	67	47	10
5	4H-H5	D151L	70	33	5
6	4G-D4	G150W	45	57	6

9.7 In silico method to increase thermostability of enzymes

9.7.1 Discovery of an undefined correlation

The modeling software MOE[94] provides an inhouse tool to calculate protein properties. The tool was used to compare protein properties of different aldoxime dehydratase (OxdRE, OxdA and OxdB), with literature know thermostable enzymes (**Table 83**). The crystal structures of the compared proteins were accessed via PDB-Database. For OxdB-WT a homology model was used.

Table 83: Comparison of calculated structure related properties of thermostable enzymes with three different aldoxime deydratases using MOE.

Enzyme (PDB-file)	K-D Hydrophobicity moment/ D	Dipole moment / D	Mobility / cm^2·V.s^{-1}	Dipole-/ Hydrophobicity moment	VdW Volume / Å^3	VdW Surface area / Å^2
Cal-A (2VEO)	1131	314	-4.9	0.28	42482	14389
Bc.st-ADH (1RJW)	791	615	-27	0.78	33628	14749
Lk-ADH (1ZK4)	329	364	7.3		24332	11353
Chol. Ox. (3JS8)	1136	442	15	0.39	53849	18600
P450-BM3 (4ZFA)	1575	990	-12		48282	19325
Cyp117 (1IO7)	1602	329	-2.9	0.20	39241	16339
OxdRE (3a17)	398	776	-75	1.95	35959	14432
OxdA (3w08)	497	607	-54	1.22	36401	14804
OxdB-WT	788	340	-17	0.43	30567	15613

9.7.2 3DM-Sorting (Stage 1)

The sorting method to define mutation sites, which would appear to not have a negative impact upon modification were carried out by using the structure database 3DM. 3DM is a matrix-based structure alignment and classifies protein structures into subfamilies. This database can show conserved amino acids and the ratio of conservation. Based on that, amino acids below 30% conservation were chosen. To further refine amino acids which had ligand, ion or inter molecular interaction were removed from the selection. This resulted to 36 mutation sites (**Table 84**). The selection was used for the saturated site directed mutagenesis.

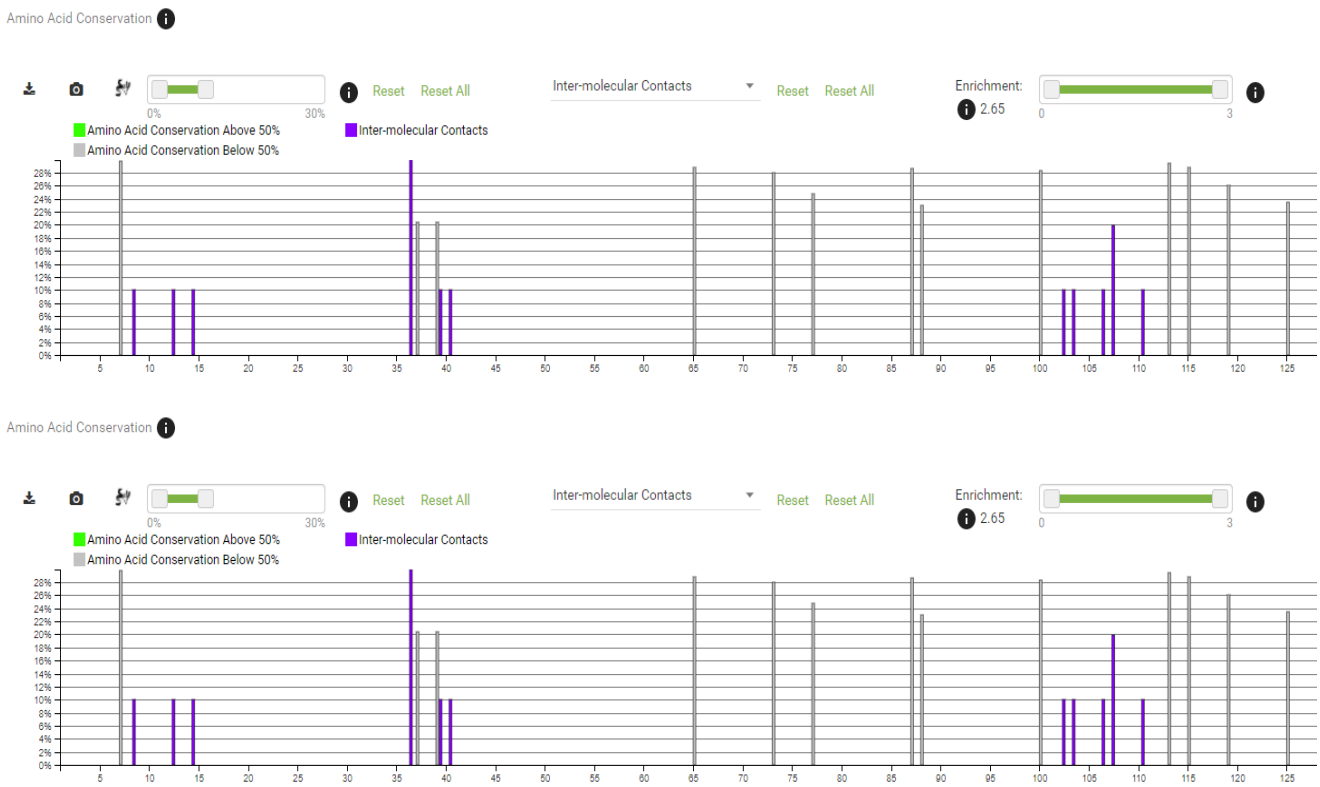

Figure 62: Image section from the mutation site selection with positions below 30% conversion and without intermolecular contacts.

Table 84: Mutation site chosen from 3DM-Sorting

7	23	25	37
39	61	65	73
77	87	88	100
113	115	119	125
135	149	151	162
188	190	252	254
252	254	255	273
311	314	329	331
340	348	349	350

9.7.3 MOE-protein design- and sorting Site directed mutagenesis *in silico* screening (Stage 2)

9.7.3.1 General procedure 9 (GP9): Site directed mutagenesis application

The screening was performed using AMBER10:EHT force field with Born-solvation model a dielectric constant of 1 and an exterior constant of 80. The cut-off for non-bonded interaction were set to 8-10 Å. The mutation sites were picked and only the target mutation was chosen. The mutants were refined with a RMSD-gradient of 0.5 and an environmental repack with a 4.5 Å cut off. The mutation site was varied. If not mentioned all experiments were done with this set up.

In stage 2, the mentioned mutation sites in **Table 84** were used to perform saturated site directed mutagenesis for each position (**Table 85**).

Table 85: Saturated site directed mutagenesis results of every position showing also the property changes for each mutant.

#	Mutation	Stability/ kcal·mol^{-1}	ΔΔG/ kcal·mol^{-1}	Mobility/ cm^2·V·s^{-1}	Δ dipole/ D	Δ hydroph/ D
1	H23H	303285.1	0.0	0.0	0.0	0.0
2	H23A	303286.1	1.1	-0.6	16.7	-89.2
3	H23R	303284.6	-0.4	2.8	-72.6	24.4
4	H23N	303286.0	0.9	-0.6	15.5	7.7
5	H23D	303286.2	1.2	-3.6	145.7	7.5
6	H23C	303286.0	0.9	-0.7	16.1	-102.8
7	H23Q	303285.5	0.4	-0.6	19.3	6.8
8	H23E	303285.7	0.6	-3.4	141.4	6.0
9	H23G	303286.8	1.8	-0.6	15.7	-49.1
10	H23I	303284.6	-0.5	-0.4	29.7	-133.6
11	H23L	303284.8	-0.2	-0.6	22.8	-123.1
12	H23K	303285.3	0.2	2.8	-72.2	14.7
13	H23M	303285.1	0.0	-0.6	21.2	-94.4
14	H23F	303284.3	-0.8	-0.6	14.7	-110.2
15	H23P	303286.7	1.6	-0.6	42.1	-26.8
16	H23S	303286.4	1.3	-0.7	23.6	-43.1
17	H23T	303285.6	0.6	-0.4	26.1	-46.0
18	H23W	303284.7	-0.4	-0.6	13.8	-48.3
19	H23Y	303284.2	-0.9	-0.6	40.0	-38.9
20	H23V	303284.9	-0.1	-0.6	28.1	-128.4
21	P25P	303280.3	0.0	0.0	0.0	0.0
22	P25A	303281.1	0.8	-0.1	-19.5	-66.8
23	P25R	303280.2	-0.1	2.5	-109.2	55.1
24	P25N	303281.1	0.8	0.4	-19.5	38.1
25	P25D	303281.6	1.3	-2.7	99.2	38.1
26	P25C	303281.1	0.8	-1.0	24.3	-83.3
27	P25Q	303281.2	0.9	0.7	-30.5	36.7
28	P25E	303281.2	0.9	-3.2	101.5	36.6
29	P25G	303282.0	1.7	0.2	-18.4	-21.5
30	P25H	303281.2	0.9	0.5	-43.3	31.0
31	P25I	303282.0	1.7	-0.2	12.7	-122.0
32	P25L	303280.4	0.1	0.7	-36.5	-107.3
33	P25K	303280.5	0.2	2.8	-119.3	45.1
34	P25M	303280.3	0.0	0.2	-16.9	-73.9
35	P25F	303280.7	0.4	0.4	-32.7	-91.5

#	Mutation	Stability/ kcal·mol^{-1}	ΔΔG/ kcal·mol^{-1}	Mobility/ cm^2·V·s^{-1}	Δ dipole/ D	Δ hydroph/ D
36	P25S	303281.3	1.0	0.0	-13.0	-15.8
37	P25T	303280.5	0.2	-0.1	-10.3	-18.9
38	P25W	303282.0	1.7	0.4	-31.1	-21.2
39	P25Y	303281.0	0.7	0.5	-28.8	-11.2
40	P25V	303281.7	1.4	-0.4	15.1	-115.4
41	E37E	558386.08	0.00	0.00	0.00	0.00
42	E37A	558385.91	-0.17	2.80	-54.56	-24.52
43	E37R	558386.10	0.02	5.37	-55.26	5.10
44	E37N	558386.23	0.15	2.85	-55.08	0.54
45	E37D	558386.65	0.56	-0.29	-5.37	0.55
46	E37C	558385.96	-0.12	2.73	-54.09	-27.10
47	E37Q	558386.28	0.20	2.38	-54.77	0.57
48	E37G	558386.05	-0.04	2.78	-54.29	-15.48
49	E37H	558386.75	0.67	2.87	-58.17	-2.42
50	E37I	558385.77	-0.32	2.85	-54.98	-30.75
51	E37L	558385.76	-0.33	2.89	-55.02	-29.94
52	E37K	558386.57	0.49	5.32	-45.01	2.47
53	E37M	558386.10	0.02	2.85	-55.22	-26.16
54	E37F	558385.66	-0.42	2.75	-54.82	-27.82
55	E37P	558393.69	7.60	2.79	-51.97	-10.49
56	E37S	558386.02	-0.07	2.79	-54.74	-14.31
57	E37T	558385.95	-0.13	2.81	-54.91	-15.18
58	E37W	558385.85	-0.24	2.74	-55.02	-15.85
59	E37Y	558385.98	-0.11	2.42	-54.76	-12.85
60	E37V	558385.62	-0.46	2.81	-54.82	-30.29
61	S39S	558378.34	0.00	0.00	0.00	0.00
62	S38	558378.42	0.08	0.01	0.25	-4.37
63	S39R	558378.49	0.15	3.07	-30.27	11.19
64	S39N	558378.14	-0.20	0.53	-0.91	7.50
65	S39D	558379.93	1.59	-2.61	63.20	7.55
66	S39C	558379.20	0.86	-0.14	2.60	-5.05
67	S39Q	558378.81	0.48	0.54	-1.06	7.49
68	S39E	558380.04	1.71	-2.46	62.16	7.59
69	S39G	558376.98	-1.35	0.02	0.78	-0.70
70	S39H	558379.76	1.42	0.92	-11.64	6.08
71	S39I	237340429.34	236782051.00	0.53	-0.70	-5.22
72	S39L	558377.66	-0.68	0.54	-0.91	-5.52
73	S39K	558379.34	1.00	3.03	-39.87	8.80
74	S39M	558378.36	0.02	0.56	-1.37	-4.54
75	S39F	558378.60	0.27	0.53	-1.82	-5.36
76	S39P	558428.57	50.24	0.01	2.08	1.89
77	S39T	558386.10	7.76	0.00	-0.28	-0.26
78	S39W	558378.50	0.17	0.52	-2.94	-1.06
79	S39Y	558377.96	-0.38	0.54	-2.17	0.09
80	S39V	558383.89	5.55	0.01	-0.40	-5.45
81	G47G	558377.84	0.00	0.00	0.00	0.00
82	G47A	558499.73	121.90	0.50	0.66	18.67
83	G47R	568903.13	10525.29	1.17	19.37	-28.83
84	G47N	558915.65	537.81	0.40	2.08	-22.70
85	G47D	565042.30	6664.47	-2.25	-45.67	-22.67
86	G47C	558627.50	249.67	0.47	1.33	25.60

#	Mutation	Stability/ kcal·mol⁻¹	ΔΔG/ kcal·mol⁻¹	Mobility/ cm²·V·s⁻¹	Δ dipole/ D	Δ hydroph/ D
87	G47Q	625727.45	67349.61	0.28	2.45	-22.40
88	G47E	566659.18	8281.34	-1.45	-26.81	-22.36
89	G47H	635691.10	77313.26	0.32	2.48	-19.94
90	G47I	25207614.66	24649236.82	0.41	2.09	43.22
91	G47L	3972642.56	3414264.72	0.39	2.09	36.98
92	G47K	615892.13	57514.30	0.55	6.01	-25.13
93	G47M	611803.32	53425.49	0.32	2.43	21.21
94	G47F	1108441.94	550064.10	0.57	3.09	29.39
95	G47P	562416.32	4038.48	0.44	-2.72	-8.22
96	G47S	558553.32	175.48	0.47	1.18	-2.21
97	G47T	11483084.51	10924706.67	0.44	1.68	-0.91
98	G47W	9317750972.64	9317192594.81	0.50	4.06	-0.46
99	G47Y	726830.93	168453.09	0.10	3.27	-3.94
100	G47V	16608860.24	16050482.40	0.45	1.66	40.20
101	I48I	558376.01	0.00	0.00	0.00	0.00
102	I48A	558376.87	0.86	0.06	-1.90	-26.49
103	I48R	558376.57	0.56	2.98	84.33	-74.33
104	I48N	558377.19	1.18	0.00	0.01	-68.22
105	I48D	558377.64	1.63	-2.49	-71.26	-68.28
106	I48C	558376.76	0.75	0.03	-1.10	-19.02
107	I48Q	558377.06	1.06	0.50	0.60	-67.94
108	I48E	558377.31	1.30	-2.58	-75.64	-67.90
109	I48G	558377.47	1.46	0.08	-2.64	-45.79
110	I48H	558377.13	1.12	0.21	0.69	-65.22
111	I48L	558376.17	0.16	0.00	-0.03	-6.71
112	I48K	558376.78	0.77	3.02	85.86	-70.81
113	I48M	558376.59	0.58	0.00	0.68	-23.53
114	I48F	558376.12	0.12	0.45	1.58	-14.55
115	I48P	558380.33	4.32	0.01	-4.57	-54.29
116	I48S	558377.01	1.00	0.04	-1.21	-48.05
117	I48T	558377.26	1.25	0.02	-0.61	-46.86
118	I48W	558376.62	0.62	0.40	3.53	-45.32
119	I48Y	558376.39	0.38	0.42	2.02	-49.42
120	I48V	558376.51	0.51	0.02	-0.59	-3.35
121	Q49Q	558379.58	0.00	0.00	0.00	0.00
122	Q48	558380.21	0.63	-0.04	-2.88	58.18
123	Q49R	558383.36	3.78	2.26	82.26	-8.83
124	Q49N	558379.16	-0.42	0.26	-0.68	-0.80
125	Q49D	558379.41	-0.17	0.56	-10.03	-0.78
126	Q49C	558379.12	-0.46	-0.12	-6.03	68.51
127	Q49E	558380.33	0.75	1.84	38.19	-0.06
128	Q49G	558379.23	-0.35	0.08	-3.81	31.24
129	Q49H	558380.76	1.18	0.26	0.09	3.89
130	Q49I	558386.24	6.66	0.26	-0.26	94.01
131	Q49L	558380.75	1.17	0.26	-0.82	85.15
132	Q49K	558381.35	1.77	1.38	43.59	-4.19
133	Q49M	558379.61	0.03	0.37	0.00	63.01
134	Q49F	558383.11	3.53	0.34	1.03	75.04
135	Q49P	614474.83	56095.25	-0.09	-7.86	19.49
136	Q49S	558380.52	0.94	0.29	-2.32	28.15
137	Q49T	558386.32	6.74	0.32	-1.65	30.11

#	Mutation	Stability/ kcal·mol^{-1}	ΔΔG/ kcal·mol^{-1}	Mobility/ cm^2·V·s^{-1}	Δ dipole/ D	Δ hydroph/ D
138	Q49W	558384.18	4.60	0.19	3.21	33.29
139	Q49Y	558390.19	10.61	0.32	1.31	27.29
140	Q49V	558385.95	6.37	0.37	-0.95	89.43
141	Q91Q	558379.69	0.00	0.00	0.00	0.00
142	Q91A	558380.13	0.44	0.04	-2.94	42.29
143	Q91R	558380.09	0.40	3.02	90.03	-7.21
144	Q91N	558380.51	0.83	0.01	-0.88	-0.79
145	Q91D	558380.77	1.09	-2.48	-78.38	-0.88
146	Q91C	558380.08	0.40	-0.04	-3.79	49.97
147	Q91E	558380.95	1.27	-2.33	-84.60	-0.39
148	Q91G	558380.57	0.89	0.06	-3.65	22.36
149	Q91H	558380.87	1.19	0.70	9.83	2.18
150	Q91I	558380.64	0.96	0.00	-0.89	69.77
151	Q91L	558379.55	-0.13	0.01	-0.90	62.80
152	Q91K	558380.61	0.93	3.05	91.56	-3.45
153	Q91M	558380.34	0.65	0.04	0.05	45.74
154	Q91F	558379.74	0.05	0.54	0.90	54.61
155	Q91P	558434.26	54.57	0.01	-8.66	13.86
156	Q91S	558380.54	0.85	0.02	-2.16	20.06
157	Q91T	558381.02	1.34	0.02	-1.50	21.36
158	Q91W	558380.57	0.88	0.50	2.27	21.75
159	Q91Y	558380.18	0.49	0.52	0.97	18.15
160	Q91V	558380.42	0.74	0.02	-1.59	66.23
161	D92D	558382.76	0.00	0.00	0.00	0.00
162	D92A	558385.23	2.47	2.73	66.43	37.42
163	D92R	558381.75	-1.01	5.40	126.37	-5.10
164	D92N	558382.32	-0.44	2.74	68.08	0.01
165	D92C	558381.55	-1.21	0.04	0.46	44.26
166	D92Q	558381.75	-1.00	2.80	68.59	0.52
167	D92E	558382.68	-0.08	0.05	7.39	0.48
168	D92G	558382.06	-0.70	2.74	65.56	20.09
169	D92H	558384.25	1.49	2.80	68.66	2.87
170	D92I	559984.66	1601.90	2.73	68.02	61.03
171	D92L	558381.98	-0.78	2.75	68.07	55.26
172	D92K	558385.18	2.42	3.17	70.82	-2.27
173	D92M	558381.21	-1.55	2.74	68.44	40.53
174	D92F	558395.79	13.03	2.82	69.41	48.37
175	D92P	559063.67	680.91	2.73	63.37	12.57
176	D92S	558382.09	-0.66	2.74	67.04	18.14
177	D92T	558389.01	6.25	2.74	67.54	19.24
178	D92W	558383.51	0.75	2.82	70.40	21.30
179	D92Y	558389.39	6.63	2.84	69.82	17.53
180	D92V	560034.92	1652.16	2.74	67.47	57.90
181	V109V	558375.31	0.00	0.00	0.00	0.00
182	V108	558376.48	1.17	0.04	-0.60	-24.16
183	V109R	558375.05	-0.26	2.79	56.80	-68.79
184	V109N	558376.66	1.36	0.49	0.33	-64.05
185	V109D	558377.25	1.94	0.12	-12.36	-63.98
186	V109C	558376.63	1.32	0.01	-0.01	-16.23
187	V109Q	558376.14	0.84	0.46	1.17	-63.71
188	V109E	558376.58	1.27	-1.14	-27.10	-63.61

#	Mutation	Stability/ kcal·mol^{-1}	ΔΔG/ kcal·mol^{-1}	Mobility/ cm^2·V·s^{-1}	Δ dipole/ D	Δ hydroph/ D
189	V109G	558377.15	1.85	0.06	-1.15	-43.48
190	V109H	558376.83	1.53	0.23	1.98	-61.01
191	V109I	558376.28	0.97	0.48	0.48	3.65
192	V109L	558375.36	0.06	0.47	0.63	-3.29
193	V109K	558375.61	0.31	2.70	55.41	-66.07
194	V109M	558375.51	0.21	0.48	1.12	-20.68
195	V109F	558375.21	-0.10	0.43	3.17	-11.10
196	V109P	594025.77	35650.47	0.01	-1.22	-51.58
197	V109S	558376.60	1.30	0.01	-0.31	-45.67
198	V109T	558376.41	1.11	0.51	-0.03	-44.31
199	V109W	558374.72	-0.59	0.39	4.25	-41.79
200	V109Y	558375.35	0.05	0.45	1.42	-45.81
201	A19	558377.51	0.00	0.00	0.00	0.00
202	A110R	558378.15	0.64	3.03	73.15	-64.84
203	A110N	558378.36	0.85	0.48	0.97	-58.09
204	A110D	558379.48	1.97	-2.35	-26.91	-57.98
205	A110C	558378.05	0.54	0.45	-0.33	10.92
206	A110Q	558378.23	0.72	0.47	1.41	-57.20
207	A110E	558378.61	1.09	-2.67	-30.59	-57.20
208	A110G	558378.51	1.00	0.00	-0.63	-27.63
209	A110H	558379.32	1.81	0.75	7.97	-53.58
210	A110I	558377.68	0.17	0.51	0.99	39.05
211	A110L	558377.40	-0.12	0.48	0.93	29.23
212	A19	558378.36	0.85	3.09	52.28	-61.18
213	A110M	558378.11	0.60	0.48	1.36	4.96
214	A110F	558378.51	1.00	0.58	2.08	18.32
215	A110P	561259.66	2882.15	0.49	-1.14	-39.38
216	A110S	558378.24	0.73	0.51	0.31	-30.71
217	A110T	558377.88	0.37	0.51	0.61	-28.93
218	A110W	558379.20	1.69	0.55	3.27	-25.21
219	A110Y	558378.83	1.32	0.57	2.25	-31.42
220	A110V	558377.82	0.31	0.52	0.64	33.87
221	Q115Q	558379.93	0.00	0.00	0.00	0.00
222	Q115A	558380.50	0.58	0.02	-2.09	80.41
223	Q115R	558380.68	0.75	3.09	79.65	-12.51
224	Q115N	558380.79	0.86	0.00	-0.54	-0.89
225	Q115D	558381.31	1.38	-2.37	-54.19	-0.86
226	Q115C	558380.60	0.67	-0.06	-2.86	94.82
227	Q115E	558380.96	1.03	-2.43	-53.06	-0.02
228	Q115G	558380.92	0.99	0.03	-2.87	43.09
229	Q115H	558381.14	1.21	0.70	8.18	5.34
230	Q115I	558380.13	0.20	0.00	-0.63	130.35
231	Q115L	558379.85	-0.08	0.01	-0.63	118.09
232	Q115K	558380.77	0.85	3.07	80.57	-5.68
233	Q115M	558380.71	0.78	0.02	0.00	86.81
234	Q115F	558380.28	0.35	0.52	0.63	103.51
235	Q115P	604091.74	45711.81	0.00	-5.13	26.56
236	Q115S	558380.64	0.71	0.01	-1.52	38.82
237	Q115T	558382.57	2.64	0.01	-1.08	41.31
238	Q115W	558380.93	1.01	0.52	2.38	45.43
239	Q115Y	558380.66	0.73	0.51	0.91	36.93

#	Mutation	Stability/ kcal·mol^{-1}	ΔΔG/ kcal·mol^{-1}	Mobility/ cm^2·V·s^{-1}	Δ dipole/ D	Δ hydroph/ D
240	Q115V	558379.98	0.05	0.00	-1.08	124.04
241	K116K	558382.80	0.00	0.00	0.00	0.00
242	K116A	558382.87	0.07	-2.72	-73.90	101.08
243	K116R	558382.96	0.16	-0.02	-5.51	-8.51
244	K116N	558383.43	0.63	-2.73	-72.99	5.95
245	K116D	558383.74	0.94	-5.26	-72.73	5.93
246	K116C	558382.91	0.11	-2.80	-74.30	117.85
247	K116Q	558383.39	0.60	-2.72	-72.77	7.01
248	K116E	558383.45	0.65	-5.25	-72.92	7.32
249	K116G	558382.79	0.00	-2.73	-74.26	57.49
250	K116H	558383.55	0.75	-2.39	-67.01	13.15
251	K116I	558382.67	-0.12	-2.73	-73.20	159.45
252	K116L	558382.74	-0.06	-2.71	-73.04	145.16
253	K116M	558383.24	0.44	-2.73	-72.56	108.69
254	K116F	558382.79	-0.01	-2.72	-72.09	128.20
255	K116P	560026.80	1644.00	-2.74	-74.14	38.19
256	K116S	558382.98	0.18	-2.73	-73.58	52.43
257	K116T	558383.17	0.38	-2.73	-73.38	55.42
258	K116W	558382.84	0.04	-2.72	-70.99	59.32
259	K116Y	558382.93	0.13	-2.72	-71.92	50.09
260	K116V	558382.83	0.03	-2.73	-73.40	152.00
261	W118W	558376.03	0.00	0.00	0.00	0.00
262	W118A	558378.92	2.90	0.18	-4.94	37.23
263	W118R	558377.46	1.43	3.08	72.73	-55.03
264	W118N	558378.55	2.53	0.14	-3.04	-42.92
265	W118D	558379.09	3.06	-2.52	-68.06	-42.90
266	W118C	558378.67	2.64	0.16	-4.50	50.70
267	W118Q	558378.22	2.19	0.14	-2.68	-42.71
268	W118E	558378.54	2.51	-2.59	-71.89	-42.16
269	W118G	558379.26	3.23	0.19	-6.08	0.86
270	W118H	558378.81	2.78	0.12	-2.22	-37.04
271	W118I	558377.31	1.28	0.15	-3.15	85.21
272	W118L	558377.07	1.04	0.14	-3.11	73.36
273	W118K	558377.83	1.80	2.83	64.72	-47.91
274	W118M	558377.57	1.55	0.12	-2.40	42.66
275	W118F	558376.99	0.96	0.07	-1.60	58.71
276	W118P	558699.26	323.23	0.19	-8.32	-15.34
277	W118S	558379.06	3.04	0.18	-4.24	-3.51
278	W118T	558378.37	2.35	0.17	-3.63	-1.16
279	W118Y	558377.05	1.03	0.04	-1.08	-6.77
280	W118V	558377.89	1.86	0.17	-3.70	79.28
281	S119S	558377.74	0.00	0.00	0.00	0.00
282	S118	558378.40	0.66	0.00	-0.76	49.96
283	S119R	558377.58	-0.16	3.01	87.51	-63.76
284	S119N	558378.75	1.01	0.52	1.13	-48.83
285	S119D	558378.98	1.24	-2.35	-65.07	-48.81
286	S119C	558378.37	0.64	-0.06	-1.28	66.71
287	S119Q	558378.36	0.62	0.52	1.92	-47.54
288	S119E	558378.75	1.01	-2.43	-66.64	-47.63
289	S119G	558378.64	0.90	0.00	-1.82	5.28
290	S119H	558379.09	1.35	0.65	8.18	-41.63

#	Mutation	Stability/ kcal·mol^{-1}	ΔΔG/ kcal·mol^{-1}	Mobility/ cm^2·V·s^{-1}	Δ dipole/ D	Δ hydroph/ D
291	S119I	558378.09	0.35	0.52	1.21	108.92
292	S119L	558378.23	0.49	0.52	1.22	94.52
293	S119K	558378.61	0.87	3.03	79.79	-55.03
294	S119M	558378.30	0.56	0.52	1.85	56.91
295	S119F	558378.24	0.51	0.52	2.58	76.42
296	S119P	560698.16	2320.43	0.00	-5.16	-14.70
297	S119T	558378.62	0.88	0.00	0.65	3.10
298	S119W	558378.95	1.21	0.53	5.07	7.77
299	S119Y	558378.43	0.70	0.50	2.73	-3.64
300	S119V	558378.14	0.41	0.00	0.64	101.43
301	D124D	558383.63	0.00	0.00	0.00	0.00
302	D124A	558384.04	0.41	2.86	118.27	115.44
303	D124R	558383.03	-0.60	5.66	263.88	-16.53
304	D124N	558383.89	0.26	2.86	120.94	0.01
305	D124C	558383.88	0.25	2.78	116.83	134.95
306	D124Q	558383.62	-0.01	2.86	121.94	1.73
307	D124E	558383.89	0.26	0.23	-4.35	1.71
308	D124G	558384.63	1.00	2.86	117.18	63.48
309	D124H	558384.30	0.67	3.01	145.55	9.22
310	D124I	558382.85	-0.78	2.86	120.97	183.15
311	D124L	558382.56	-1.07	2.86	120.91	166.52
312	D124K	558383.56	-0.07	5.65	252.98	-6.82
313	D124M	558383.15	-0.48	2.85	121.98	124.03
314	D124F	558383.35	-0.28	2.87	123.45	146.95
315	D124P	560952.58	2568.96	2.85	110.92	40.33
316	D124S	558384.16	0.53	2.85	119.27	57.42
317	D124T	558383.87	0.24	2.85	120.20	61.14
318	D124W	558383.92	0.29	2.88	126.36	66.49
319	D124Y	558383.95	0.32	2.87	123.92	54.59
320	D124V	558383.12	-0.51	2.85	120.08	174.59
321	E125E	558385.87	0.00	0.00	0.00	0.00
322	E125A	558385.90	0.03	2.91	144.14	117.38
323	E125R	558385.79	-0.08	5.29	303.06	-18.66
324	E125N	558386.14	0.28	2.91	147.28	-1.61
325	E125D	558386.57	0.71	0.12	0.32	-1.61
326	E125C	558385.65	-0.22	2.70	135.26	137.67
327	E125Q	558386.14	0.28	2.92	148.32	0.02
328	E125G	558385.91	0.04	2.90	143.03	63.37
329	E125H	558386.39	0.52	2.92	165.45	7.56
330	E125I	558385.40	-0.47	2.92	147.13	188.41
331	E125L	558385.66	-0.21	2.93	147.19	171.20
332	E125K	558386.16	0.29	5.28	302.20	-8.84
333	E125M	558385.83	-0.04	2.93	148.39	126.58
334	E125F	558385.53	-0.34	2.94	149.57	150.47
335	E125P	558400.20	14.34	2.91	137.44	39.50
336	E125S	558386.02	0.15	2.91	145.27	57.03
337	E125T	558385.88	0.01	2.92	146.29	60.89
338	E125W	558385.66	-0.21	2.91	152.20	65.99
339	E125Y	558385.51	-0.36	2.91	150.17	54.16
340	E125V	558385.52	-0.34	2.92	146.17	179.43
341	Y130Y	558376.63	0.00	0.00	0.00	0.00

#	Mutation	Stability/ kcal·mol^{-1}	ΔΔG/ kcal·mol^{-1}	Mobility/ cm^2·V·s^{-1}	Δ dipole/ D	Δ hydroph/ D
342	Y130A	558379.16	2.53	0.17	-3.42	36.51
343	Y130R	558378.05	1.41	3.11	102.53	-42.15
344	Y130N	558378.95	2.31	0.11	-1.17	-32.08
345	Y130D	558379.51	2.88	-2.48	-88.23	-32.07
346	Y130C	558378.99	2.35	0.14	-2.60	48.15
347	Y130Q	558378.34	1.71	0.09	-0.29	-30.90
348	Y130E	558379.09	2.45	-2.19	-95.29	-30.99
349	Y130G	558379.93	3.29	0.20	-4.24	5.59
350	Y130H	558378.75	2.11	0.35	-0.32	-26.76
351	Y130I	558377.83	1.20	0.11	-1.28	77.06
352	Y130L	558377.96	1.32	0.11	-1.23	67.05
353	Y130K	558378.17	1.54	3.12	104.75	-36.03
354	Y130M	558377.93	1.30	0.11	-0.29	41.80
355	Y130F	558376.92	0.29	0.05	0.73	55.19
356	Y130P	558501.69	125.05	0.13	-8.68	-7.92
357	Y130S	558379.23	2.60	0.15	-2.61	1.97
358	Y130T	558378.91	2.27	0.13	-1.89	4.22
359	Y130W	558378.22	1.59	0.53	2.80	6.74
360	Y130V	558378.94	2.30	0.13	-2.02	71.83
361	F202F	558377.44	0.00	0.00	0.00	0.00
362	F202A	558377.91	0.47	-0.13	-5.21	-34.46
363	F202R	558378.33	0.88	3.01	131.64	-179.08
364	F202N	558378.38	0.94	0.14	-2.34	-159.98
365	F202D	558378.72	1.28	-2.38	-121.40	-160.01
366	F202C	558377.93	0.49	-0.10	-4.07	-13.15
367	F202Q	558378.61	1.17	0.17	-1.33	-158.04
368	F202E	558378.85	1.41	-2.75	-118.63	-158.05
369	F202G	558378.30	0.86	-0.14	-6.30	-90.83
370	F202H	558378.42	0.97	0.65	13.49	-149.94
371	F202I	558377.47	0.02	0.27	-2.36	38.43
372	F202L	558377.71	0.26	-0.16	-2.32	20.85
373	F202K	558378.77	1.33	2.97	140.36	-167.40
374	F202M	558378.51	1.06	0.38	-1.25	-24.46
375	F202P	558417.85	40.41	-0.20	-9.85	-115.92
376	F202S	558377.97	0.53	-0.12	-4.31	-97.23
377	F202T	558378.18	0.74	0.28	-3.43	-93.17
378	F202W	558378.56	1.12	0.07	2.79	-87.18
379	F202Y	558378.60	1.16	-0.08	0.54	-99.81
380	F202V	558377.45	0.00	-0.18	-3.35	29.12
381	C215C	558378.28	0.00	0.00	0.00	0.00
382	C215A	558372.00	-6.28	0.04	0.00	-2.47
383	C215R	559909.49	1531.20	2.85	-27.44	-18.31
384	C215N	558377.23	-1.06	0.54	-0.42	-16.56
385	C215D	558382.39	4.10	-1.77	15.47	-16.56
386	C215Q	558397.74	19.45	0.54	-0.57	-16.71
387	C215E	558429.22	50.94	0.30	1.24	-16.58
388	C215G	558372.36	-5.92	0.06	-0.05	-8.73
389	C215H	558468.32	90.04	0.52	-0.33	-15.39
390	C215I	558427.03	48.75	0.52	-0.36	6.03
391	C215L	568253.34	9875.05	0.53	-0.32	3.89
392	C215K	558727.59	349.30	2.22	-19.17	-17.03

#	Mutation	Stability/ kcal·mol^{-1}	ΔΔG/ kcal·mol^{-1}	Mobility/ cm^2·V·s^{-1}	Δ dipole/ D	Δ hydroph/ D
393	C215M	558453.95	75.66	0.53	-0.70	-1.46
394	C215F	2394447.42	1836069.13	0.53	-0.60	0.58
395	C215P	558471.42	93.13	0.52	0.06	-11.39
396	C215S	558372.87	-5.41	0.03	-0.10	-9.52
397	C215T	558395.53	17.25	0.53	-0.27	-9.15
398	C215W	559635.58	1257.30	0.51	-0.63	-8.83
399	C215Y	580503.10	22124.82	0.53	-0.67	-11.15
400	C215V	558395.16	16.87	0.53	-0.25	5.01
401	E232E	558385.36	0.00	0.00	0.00	0.00
402	E232A	558385.52	0.16	3.14	17.97	-89.35
403	E232R	558385.39	0.03	5.52	89.99	16.88
404	E232N	558385.86	0.49	3.15	18.67	0.93
405	E232D	558386.25	0.89	0.46	9.59	0.93
406	E232C	558385.60	0.24	3.07	17.54	-102.82
407	E232Q	558385.63	0.26	0.83	46.32	-0.16
408	E232G	558385.68	0.32	3.14	17.72	-50.91
409	E232H	558386.18	0.81	3.17	23.50	-6.50
410	E232I	558385.05	-0.32	3.17	18.70	-133.97
411	E232L	558385.23	-0.14	3.17	18.68	-123.56
412	E232K	558386.17	0.80	5.53	81.51	7.43
413	E232M	558385.65	0.28	3.17	19.08	-94.89
414	E232F	558385.21	-0.15	3.16	19.13	-110.53
415	E232P	560211.69	1826.32	0.80	46.57	-32.76
416	E232S	558385.72	0.35	3.14	18.24	-46.24
417	E232T	558385.50	0.14	3.15	18.47	-49.09
418	E232W	558385.69	0.32	0.83	46.48	-52.47
419	E232Y	558385.65	0.28	3.15	19.34	-43.05
420	E232V	558385.10	-0.27	3.15	18.43	-128.67
421	Y265Y	558377.27	0.00	0.00	0.00	0.00
422	Y265A	558379.20	1.93	0.15	-1.75	-10.40
423	Y265R	558378.05	0.78	2.81	28.67	12.14
424	Y265N	558379.17	1.90	0.10	-0.94	9.00
425	Y265D	558379.84	2.57	-2.62	-33.76	9.00
426	Y265C	558379.11	1.84	-1.20	-18.25	-12.87
427	Y265Q	558378.92	1.65	0.08	-0.84	8.71
428	Y265E	558379.51	2.24	-2.60	-23.58	8.30
429	Y265G	558379.74	2.47	0.15	-1.89	-2.53
430	Y265H	558379.81	2.54	0.33	-0.56	7.58
431	Y265I	558378.29	1.02	0.10	-1.15	-18.97
432	Y265L	558378.21	0.94	0.10	-1.16	-17.03
433	Y265K	558378.71	1.44	3.05	27.82	9.86
434	Y265M	558378.62	1.35	0.09	-0.81	-11.31
435	Y265F	558377.74	0.47	0.03	-0.15	-13.80
436	Y265P	558384.90	7.63	0.11	-4.66	1.49
437	Y265S	558379.28	2.01	0.13	-1.47	-1.48
438	Y265T	558378.81	1.54	0.12	-1.30	-2.20
439	Y265W	558377.72	0.45	-0.04	0.70	-1.57
440	Y265V	558378.05	0.78	0.12	-1.34	-17.99
441	E266E	558383.77	0.00	0.00	0.00	0.00
442	E266A	558384.49	0.71	3.61	16.84	-20.32
443	E266R	558383.55	-0.22	5.70	38.50	3.79

#	Mutation	Stability/ kcal·mol^{-1}	ΔΔG/ kcal·mol^{-1}	Mobility/ cm^2·V·s^{-1}	Δ dipole/ D	Δ hydroph/ D
444	E266N	558384.38	0.61	3.54	17.34	0.68
445	E266D	558384.70	0.93	2.70	9.92	0.63
446	E266C	558384.27	0.50	3.61	17.12	-23.42
447	E266Q	558383.91	0.13	2.74	17.01	0.41
448	E266G	558385.21	1.44	3.13	16.35	-11.58
449	E266H	558384.35	0.58	2.90	16.94	-1.35
450	E266I	558382.85	-0.93	3.54	17.39	-29.85
451	E266L	558382.96	-0.82	3.56	17.30	-27.86
452	E266K	558384.16	0.39	5.70	46.21	1.80
453	E266M	558383.49	-0.29	3.56	17.40	-21.95
454	E266F	558383.24	-0.53	2.75	17.05	-25.47
455	E266P	571427.38	13043.61	3.56	16.08	-7.50
456	E266S	558384.66	0.89	3.60	17.08	-10.62
457	E266T	558384.06	0.29	3.58	17.24	-11.36
458	E266W	558383.39	-0.38	2.73	17.34	-12.95
459	E266Y	558383.78	0.01	2.74	17.55	-10.48
460	E266V	558383.30	-0.47	3.58	17.22	-28.76
461	I273I	558375.98	0.00	0.00	0.00	0.00
462	I273A	558377.94	1.96	0.06	-0.87	18.24
463	I273R	558376.88	0.90	2.94	56.83	67.55
464	I273N	558378.04	2.06	0.00	-0.13	59.05
465	I273D	558378.55	2.57	-2.59	-24.41	59.06
466	I273C	558377.82	1.84	-0.05	-1.37	12.49
467	I273Q	558377.63	1.65	0.48	0.38	59.04
468	I273E	558378.09	2.11	-2.30	-36.02	59.01
469	I273G	558378.07	2.10	0.06	-1.23	35.07
470	I273H	558378.22	2.24	0.63	6.06	56.19
471	I273L	558376.90	0.92	0.51	0.03	4.26
472	I273K	558377.31	1.33	2.99	52.35	62.63
473	I273M	558377.30	1.32	0.50	0.45	16.44
474	I273F	558376.80	0.83	0.43	0.94	10.22
475	I273P	558378.66	2.69	0.04	-4.03	43.29
476	I273S	558378.12	2.14	0.05	-0.61	37.17
477	I273T	558377.69	1.71	0.02	-0.23	35.93
478	I273W	558377.81	1.84	0.35	2.23	36.11
479	I273Y	558377.13	1.15	0.39	1.14	39.84
480	I273V	558377.06	1.08	0.02	-0.33	1.96
481	D275D	558385.19	0.00	0.00	0.00	0.00
482	D275A	558385.36	0.16	3.09	23.63	-52.55
483	D275R	558385.49	0.30	5.84	79.86	8.66
484	D275N	558385.60	0.41	3.06	24.41	0.00
485	D275C	558385.17	-0.02	1.00	3.78	-60.56
486	D275Q	558385.88	0.69	3.06	24.77	-0.63
487	D275E	558385.79	0.60	0.00	-4.41	-0.67
488	D275G	558385.75	0.56	3.09	23.27	-30.07
489	D275H	558385.86	0.67	3.05	28.89	-4.51
490	D275I	559921.48	1536.28	1.23	59.51	-78.89
491	D275L	558385.68	0.49	3.06	24.42	-72.69
492	D275K	558385.91	0.72	5.41	87.42	3.59
493	D275M	558385.30	0.10	3.06	24.78	-56.14
494	D275F	558385.06	-0.13	3.03	25.14	-65.28

#	Mutation	Stability/ kcal·mol^{-1}	ΔΔG/ kcal·mol^{-1}	Mobility/ cm^2·V·s^{-1}	Δ dipole/ D	Δ hydroph/ D
495	D275P	558386.58	1.39	3.07	21.82	-19.52
496	D275S	558385.32	0.13	3.08	23.90	-27.44
497	D275T	558390.62	5.42	1.24	59.42	-29.13
498	D275W	558385.60	0.40	2.99	25.95	-31.73
499	D275Y	558385.35	0.16	3.01	25.20	-26.20
500	D275V	558432.25	47.06	1.24	59.42	-75.63
501	S277S	558377.35	0.00	0.00	0.00	0.00
502	S277A	558378.03	0.68	0.01	-0.02	-16.53
503	S277R	558454.20	76.85	2.82	13.20	23.46
504	S277N	558379.45	2.10	0.46	0.31	18.02
505	S277D	558380.67	3.32	-2.45	-5.65	18.03
506	S277C	558379.47	2.11	0.50	0.12	-21.62
507	S277Q	558378.94	1.59	0.46	0.29	17.43
508	S277E	558385.46	8.11	-1.85	-4.63	17.63
509	S277G	558378.80	1.45	0.86	-1.57	-1.75
510	S277H	558381.95	4.59	0.33	0.49	15.59
511	S277I	558745.30	367.95	0.45	0.23	-34.28
512	S277L	558413.34	35.99	0.45	0.32	-29.88
513	S277K	558383.81	6.46	2.81	12.72	20.18
514	S277M	558381.57	4.22	0.46	0.36	-18.38
515	S277F	558808.05	430.70	-1.45	51.34	-24.68
516	S277P	558648.18	270.83	0.00	1.30	4.99
517	S277T	558398.30	20.95	0.48	0.06	-1.06
518	S277W	558440.03	62.68	0.28	0.73	-1.58
519	S277Y	558521.65	144.30	0.30	0.58	1.96
520	S277V	558405.94	28.59	0.49	0.07	-32.18
521	Y282Y	558370.28	0.00	0.00	0.00	0.00
522	Y282A	558368.47	-1.81	-0.14	-1.78	13.21
523	Y282R	558375.44	5.16	2.68	17.02	-15.88
524	Y282N	558369.35	-0.93	-0.24	-0.88	-11.94
525	Y282D	558369.63	-0.65	-0.61	-2.81	-11.91
526	Y282C	558368.41	-1.87	-0.17	-1.31	17.53
527	Y282Q	558372.54	2.26	-0.28	-0.70	-11.64
528	Y282E	558405.12	34.84	-0.74	-3.57	-11.61
529	Y282G	558369.14	-1.14	-0.12	-1.78	1.85
530	Y282H	558370.55	0.27	-0.30	-0.52	-9.89
531	Y282I	558451.45	81.17	-0.24	-0.87	28.10
532	Y282L	558392.91	22.63	-0.25	-1.00	24.28
533	Y282K	558379.75	9.47	0.52	2.33	-13.71
534	Y282M	558373.10	2.82	-0.24	-0.88	15.11
535	Y282F	558372.66	2.38	-0.13	0.01	20.11
536	Y282P	558386.21	15.93	-0.21	-3.12	-3.14
537	Y282S	558368.82	-1.46	-0.16	-1.49	0.65
538	Y282T	558377.76	7.48	-0.19	-1.19	1.57
539	Y282W	558372.18	1.90	0.07	0.64	2.62
540	Y282V	558393.60	23.32	-0.19	-1.20	26.10
541	D314D	558385.70	0.00	0.00	0.00	0.00
542	D314A	558385.43	-0.27	2.53	-51.17	-123.63
543	D314R	558385.20	-0.49	3.48	-27.83	19.58
544	D314N	558385.79	0.09	2.55	-51.53	0.07
545	D314C	558385.37	-0.33	2.49	-51.10	-143.92

#	Mutation	Stability/ kcal·mol^{-1}	ΔΔG/ kcal·mol^{-1}	Mobility/ cm^2·V·s^{-1}	Δ dipole/ D	Δ hydroph/ D
546	D314Q	558385.88	0.18	0.76	-22.51	-1.62
547	D314E	558386.32	0.63	-1.96	52.14	-1.53
548	D314G	558385.49	-0.20	2.53	-50.86	-69.00
549	D314H	558386.36	0.67	1.20	-27.83	-9.94
550	D314I	558385.27	-0.42	2.56	-51.56	-192.69
551	D314L	558385.37	-0.32	2.56	-51.55	-176.07
552	D314K	558386.14	0.45	3.70	-32.50	8.03
553	D314M	558385.80	0.10	2.61	-51.60	-132.65
554	D314F	558385.31	-0.39	0.72	-23.04	-156.05
555	D314P	11988871.94	11430486.24	2.52	-50.92	-44.10
556	D314S	558385.50	-0.20	2.53	-51.34	-62.55
557	D314T	558385.35	-0.35	2.54	-51.46	-66.50
558	D314W	558385.36	-0.34	0.71	-23.57	-71.56
559	D314Y	558385.50	-0.20	0.72	-23.08	-59.36
560	D314V	558385.18	-0.51	2.54	-51.45	-184.06
561	S340S	558377.62	0.00	0.00	0.00	0.00
562	S340A	558378.20	0.58	0.01	-0.71	37.18
563	S340R	558377.60	-0.02	2.63	74.37	-49.33
564	S340N	558378.62	0.99	-0.35	1.27	-37.05
565	S340D	558379.11	1.48	-3.17	-70.15	-37.08
566	S340C	558378.18	0.56	-0.51	-0.28	49.38
567	S340Q	558378.38	0.76	-0.03	1.79	-36.12
568	S340E	558378.80	1.18	-2.71	-62.13	-36.17
569	S340G	558378.40	0.78	-0.01	-1.45	3.96
570	S340H	558379.13	1.51	0.67	23.85	-31.23
571	S340I	558378.84	1.22	-0.01	1.16	80.11
572	S340L	558377.71	0.08	-0.03	1.17	69.72
573	S340K	558378.55	0.93	2.42	86.61	-41.90
574	S340M	558378.31	0.69	-0.02	1.76	42.64
575	S340F	558378.09	0.47	0.01	2.88	57.36
576	S340P	574234.19	15856.57	-0.02	-5.69	-10.86
577	S340T	558381.02	3.40	-0.29	0.63	2.28
578	S340W	558376.86	-0.76	0.00	3.61	2.85
579	S340Y	558377.70	0.08	-0.02	2.50	-3.62
580	S340V	558391.68	14.06	-0.02	0.56	74.77
581	E348E	558384.41	0.00	0.00	0.00	0.00
582	E348A	558384.71	0.30	2.55	67.10	102.89
583	E348R	558384.88	0.47	5.39	166.86	-16.92
584	E348N	558384.95	0.53	2.57	68.60	-1.33
585	E348D	558385.51	1.09	-0.10	4.71	-1.32
586	E348C	558384.83	0.41	1.90	50.66	120.19
587	E348Q	558384.80	0.39	2.56	68.78	-0.61
588	E348G	558385.29	0.87	2.53	66.27	56.59
589	E348H	558385.78	1.36	3.04	75.02	5.85
590	E348I	558383.52	-0.89	2.58	68.51	162.08
591	E348L	558383.73	-0.68	2.59	68.45	147.47
592	E348K	558384.52	0.11	5.43	142.70	-8.73
593	E348M	558384.71	0.30	2.58	69.28	110.44
594	E348F	558383.86	-0.56	2.61	69.51	129.28
595	E348P	617167.21	58782.79	2.55	64.34	35.30
596	E348S	558384.78	0.37	2.54	67.65	51.04

#	Mutation	Stability/ kcal·mol^{-1}	ΔΔG/ kcal·mol^{-1}	Mobility/ cm^2·V·s^{-1}	Δ dipole/ D	Δ hydroph/ D
597	E348T	558384.40	-0.01	2.56	68.08	54.19
598	E348W	558384.95	0.54	2.68	70.58	56.69
599	E348Y	558384.21	-0.20	2.62	69.69	46.43
600	E348V	558383.81	-0.61	2.57	68.01	154.78
601	V349V	558376.33	0.00	0.00	0.00	0.00
602	V348	558377.44	1.11	0.00	-1.09	-59.81
603	V349R	558376.93	0.60	3.06	85.95	-198.27
604	V349N	558377.69	1.36	0.00	0.56	-179.13
605	V349D	558378.02	1.69	-2.45	-64.70	-179.06
606	V349C	558377.56	1.23	-0.07	-1.97	-39.97
607	V349Q	558377.67	1.34	0.01	1.10	-177.86
608	V349E	558377.95	1.62	-2.33	-68.36	-177.40
609	V349G	558377.67	1.34	0.01	-1.53	-113.03
610	V349H	558377.82	1.49	0.67	8.05	-169.96
611	V349I	558376.98	0.65	0.00	0.58	8.61
612	V349L	558376.93	0.60	0.01	0.55	-8.14
613	V349K	558377.94	1.61	3.05	96.64	-186.61
614	V349M	558377.23	0.90	0.01	1.47	-51.05
615	V349F	558377.04	0.71	0.04	2.06	-28.47
616	V349P	558378.16	1.83	0.01	-4.56	-136.91
617	V349S	558377.70	1.37	0.00	-0.51	-119.14
618	V349T	558377.48	1.15	0.00	0.03	-115.34
619	V349W	558376.42	0.09	0.03	4.10	-110.90
620	V349Y	558376.75	0.42	0.01	2.04	-123.10
621	T350T	558378.74	0.00	0.00	0.00	0.00
622	T350A	558379.07	0.33	-0.07	-1.08	60.60
623	T350R	558379.10	0.37	3.04	92.53	-89.37
624	T350N	558379.56	0.83	0.07	0.41	-69.33
625	T350D	558380.21	1.47	-2.33	-41.28	-69.33
626	T350C	558379.24	0.51	-0.10	-1.85	82.48
627	T350Q	558379.83	1.09	0.00	0.91	-67.70
628	T350E	558380.16	1.43	-2.32	-40.77	-67.71
629	T350G	558378.82	0.08	-0.12	-1.48	2.48
630	T350H	558380.12	1.38	0.86	10.28	-58.99
631	T350I	558378.98	0.25	0.08	0.42	135.52
632	T350L	558379.11	0.38	0.07	0.42	117.40
633	T350K	558379.91	1.17	3.12	88.69	-77.49
634	T350M	558379.51	0.78	0.00	1.05	70.34
635	T350F	558379.43	0.69	0.20	1.56	95.73
636	T350P	559270.45	891.71	-0.08	-4.33	-23.59
637	T350S	558379.20	0.47	-0.06	-0.53	-4.21
638	T350W	558380.33	1.60	0.23	2.87	5.47
639	T350Y	558380.01	1.28	0.24	1.85	-7.36
640	T350V	558379.16	0.43	0.01	-0.11	126.00

9.7.4 Sorting system for the single point saturation screening (Stage 3)

The mutants were sorted in MOE by using the protein property descriptors. Mutants with a hydrophobic moment >0 D, dipole moment <0 D, mobility >-1 $cm^2 \cdot V \cdot s^{-1}$ and ΔΔG (Stability) <2 $kcal \cdot mol^{-1}$ were included in the selection for Stage 4 (**Figure 63**).

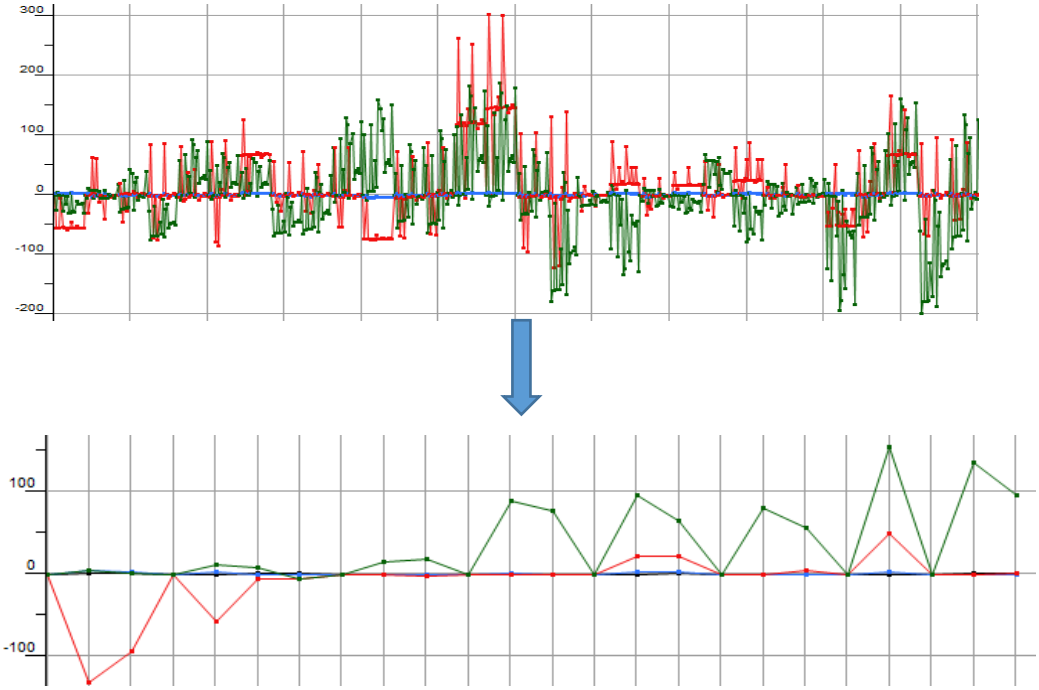

Figure 63: Sorting of mutant in MOE using protein descriptors. First frame shows all variants with their properties and second frame shows the residual variants after sorting.

9.7.5 Final sorting (Stage 4)

In this phase, only a few mutation options remain, whereas the last selection takes place. From the initial 36 sites, only 8 sites with multiple options remain. The best mutation in terms of descriptor values were now selected for each position (**Table 86**). The increase of the hydrophobic moment and the decrease of the dipole moment with little or no influence on the stability is the selection criterion.

Table 86: Mutants and their protein properties in comparison after sorting (stage 4).

#	Mutation	Stability / kcal·mol^{-1}	ΔΔG / kcal·mol^{-1}	Mobility / cm^2·V·s^{-1}	Δ dipole / D	Δ hydroph / D
1	H23H	303285.1	0.0	0.0	0.0	0.0
2	H23R	303284.6	-0.4	2.8	-72.6	24.4
3	H23K	303285.3	0.2	2.8	-72.2	14.7
4	P25P	303280.3	0.0	0.0	0.0	0.0
5	P25R	303280.2	-0.1	2.5	-109.2	55.1
6	P25K	303280.5	0.2	2.8	-119.3	45.1
7	E37E	305208.05	0.00	0.00	0.00	0.00
8	E37R	305208.66	0.60	5.38	-131.90	5.10
9	E37Q	305208.53	0.47	2.38	-93.64	0.57
10	S39S	305202.20	0.00	0.00	0.00	0.00
11	S39R	305202.18	-0.02	2.32	-57.57	11.24
12	S39N	305203.08	0.88	0.01	-5.88	7.52
13	S39C	305202.77	0.57	-0.06	-4.95	-5.23
14	T135T	82956.43	0.00	0.00	0.00	0.00
15	T135M	82955.67	-0.77	-0.13	-1.31	14.32
16	T135C	82956.52	0.09	-0.11	-1.92	17.89
17	T209T	305200.54	0.00	0.00	0.00	0.00
18	T209I	305200.63	0.09	0.51	-0.59	88.75
19	T209L	305200.68	0.14	0.00	-0.53	76.34
20	E331E	305207.06	0.00	0.00	0.00	0.00
21	E331I	305206.88	-0.18	2.77	21.67	96.38
22	E331M	305207.62	0.56	2.78	22.11	64.92
23	S340S	305202.78	0.00	0.00	0.00	0.00
24	S340I	305202.64	-0.14	-0.19	-1.17	79.79
25	S340F	305202.57	-0.21	-0.58	5.19	55.81
26	E348E	305207.20	0.00	0.00	0.00	0.00
27	E348V	305206.75	-0.45	2.57	48.75	154.77
28	T350T	305205.99	0.00	0.00	0.00	0.00
29	T350I	305206.45	0.46	0.07	-0.77	135.53
30	T350F	305207.31	1.32	0.20	1.95	95.73

In the last step the best single point mutations were chosen to generate a 10 fold-mutant (2 mutations from the previous calculation regarding OxdB-Sol) and calculate its properties and compare it with the wild type (**Table 87**).

Table 87: Computational site directed mutagenesis of constructed variants in comparison to the wild type. Showing stablilty, interaction and property changes in a symetric calculation from WT to Mutant.

Mutation	Variant	ΔΔG / kcal·mol^{-1}	Δ Mobility / cm^2·V·s^{-1}	Δ dipole / D	Δ hydroph / D
WT	-	0	0	0	0
M19K. P20R, P36R	BSol1	+1.10	+8.61	-189.10	+173.73
H23R, P25R, E37Q, S39R, T135M, T209I, E331I, S340I, E348V, T350I	3DMSet1	-8.91	+14.79	-139.75	652.91
P25R, T135M, T209I, E331I	3DMSet1a	-2.73	+4.46	-79.99	+255.48
S349I, E348V, T350I	3DMSet1b	-1.54	+2.95	+45.55	+371.90
P25R, E37Q, S39R, T135M, T209I, E331I	3DMSet2	-3.91	+10.45	-116.14	+259.79

Splitting mutation to ensure false positive prediction before going into laboratory experiments. 3DM-Set 2 was designed after proving correct mutations.

Table 88: All 3DM and MOE based mutants.

3DM-Set-1	3DM-Set-1a	3DM-Set-1b	3DM-Set-2
H23R *(H8R)*			
P25R *(P10R)*	P25R *(P10R)*		P25R *(P10R)*
E37Q *(E22Q)*			E37Q *(E22Q)*
S39R *(S24R)*			S39R *(S24R)*
T135M *(T118M)*	T135M *(T118M)*		T135M *(T118M)*
T209I *(T192I)*	T209I *(T192I)*		T209I *(T192I)*
E331I *(E317I)*	E331I *(E317I)*		E331I *(E317I)*
S340I *(S326I)*		S340I *(S326I)*	
E348V *(E334V)*		E348V *(E334V)*	
T350I *(T336I)*		T350I *(T336I)*	

Table 89: Comparison of WT with all tested variants of OxdB showing calculated protein properties and the mutation site.

Enzyme	Hydroph. moment / D	Dipole moment / D	Dipole-/ Hydrophobicity moment	Mobility / $cm^2 \cdot V.s^{-1}$	Mut.	Site
OxdB-WT	788	340	0.43	-17	0	-
OxdB-Sol1	1025	304	0.30	-13	3	Loops
OxdB-Sol2	1125	483	0.43	-20	3	Helix
OxdB-Sol3	1171	726	0.61	-15	6	Both
OxdB-Set1a	1046	274	0.26	-16	4	Surface (not helix)
OxdB-Set2	1049	201	0.19	-14	6	Surface (not helix)

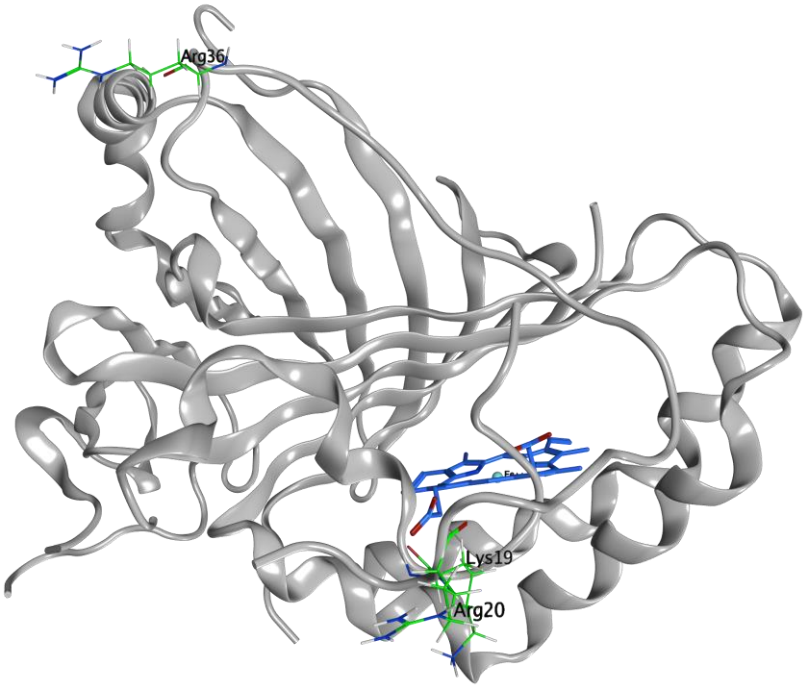

Figure 64: Illustration of OxdB-Sol1 (M19L/P20R/P36R), whereas the mutations are located on the first loop and indicated in green. The heme is shown in blue.

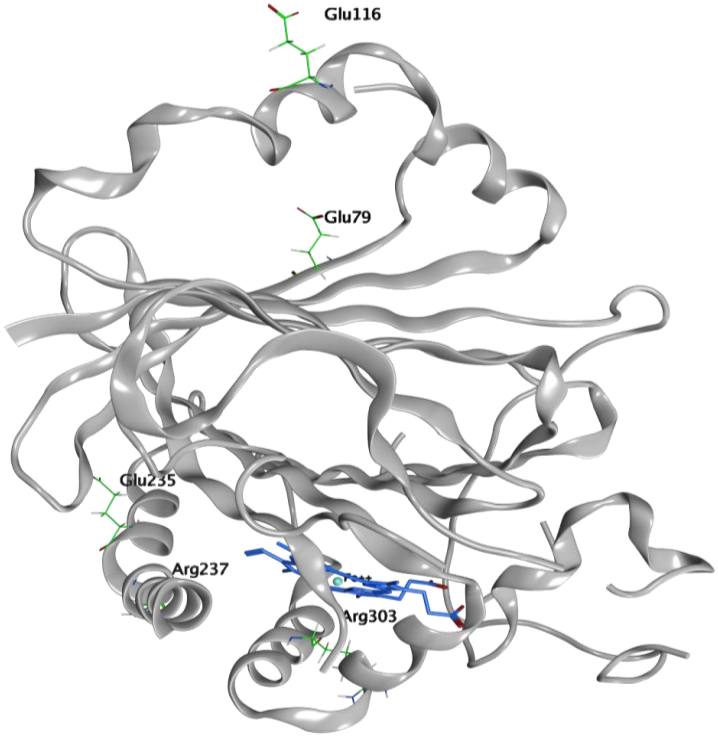

Figure 65: Illustration of OxdB-Sol2 (K79E/I116E/L235E/L237R/Y303R), whereas the mutations are displayed in green and located on helices with K79E as an exception being on the β-strand. Heme is shown in blue.

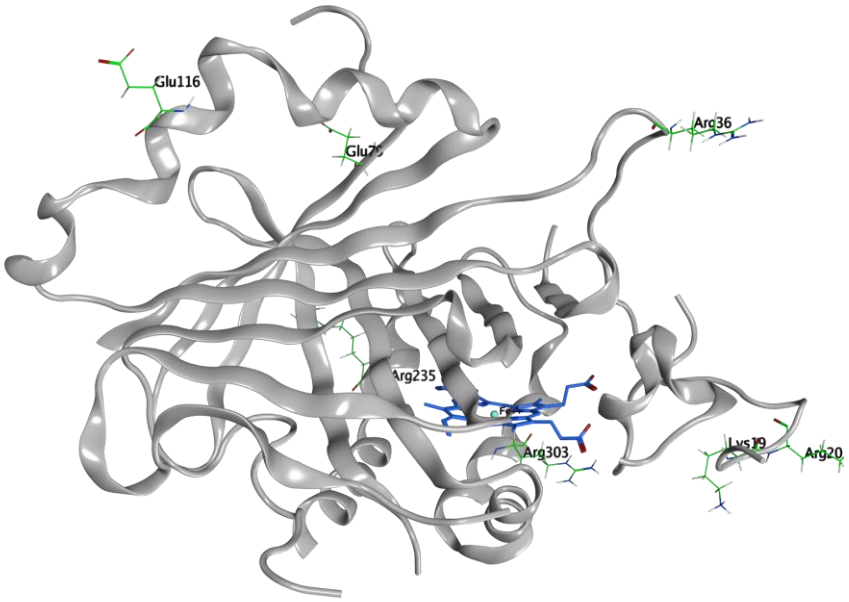

Figure 66: OxdB-Sol3 (M19L/P20R/P36R/K79E/I116E/L235R/Y303R). Combination of selected mutations from OxdB-Sol1 and OxdBSol2 shown in green. Heme is shown in blue.

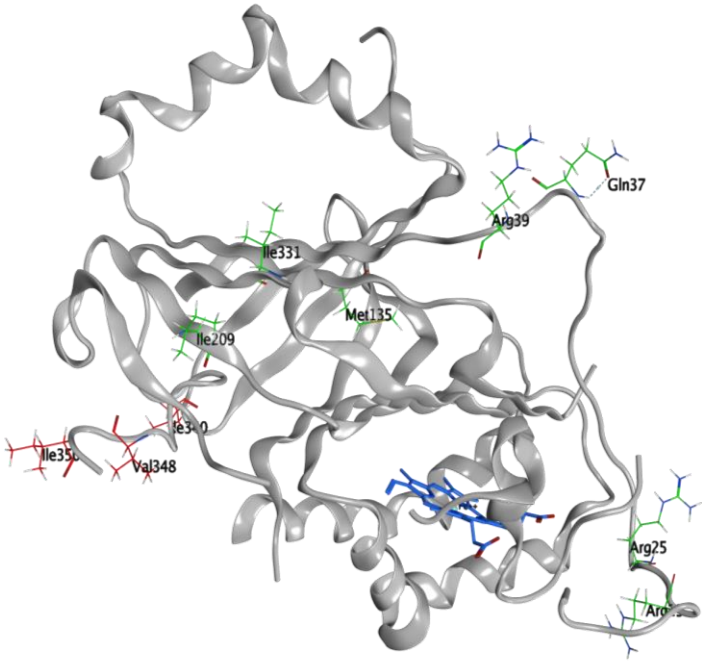

Figure 67: Model of OxdB-Set1(H23R/P25R/E37Q/S39R/T135M/T209I/E331I/S340I/E348V/T350I). Mutations are highlighted (red and green). OxdB-Set1b (S340I/E348V/T350I) mutations highlighted in red. Heme is shown in blue.

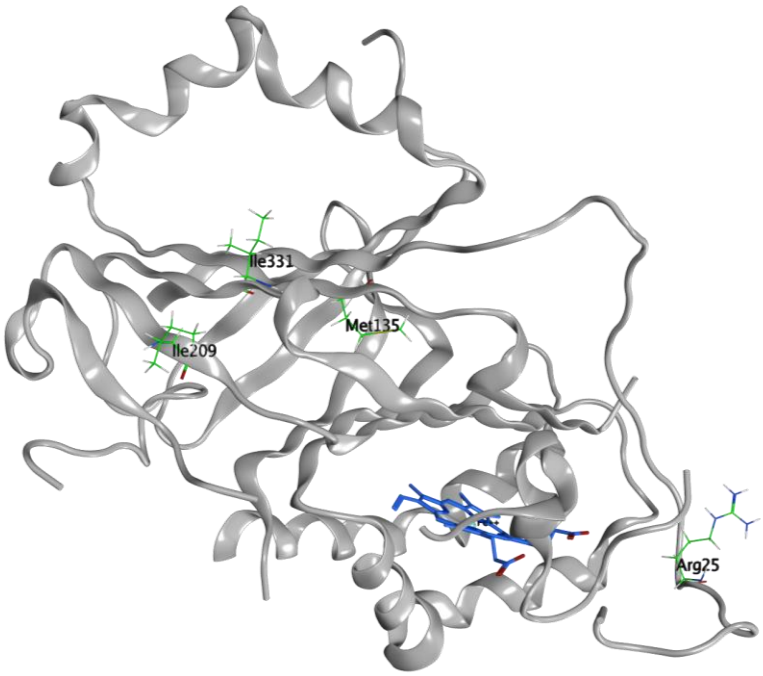

Figure 68: Model of OxdB-Set1a (P25R/T135M/T209I/E331I), whereas the mutations are highlighted in green and heme in blue.

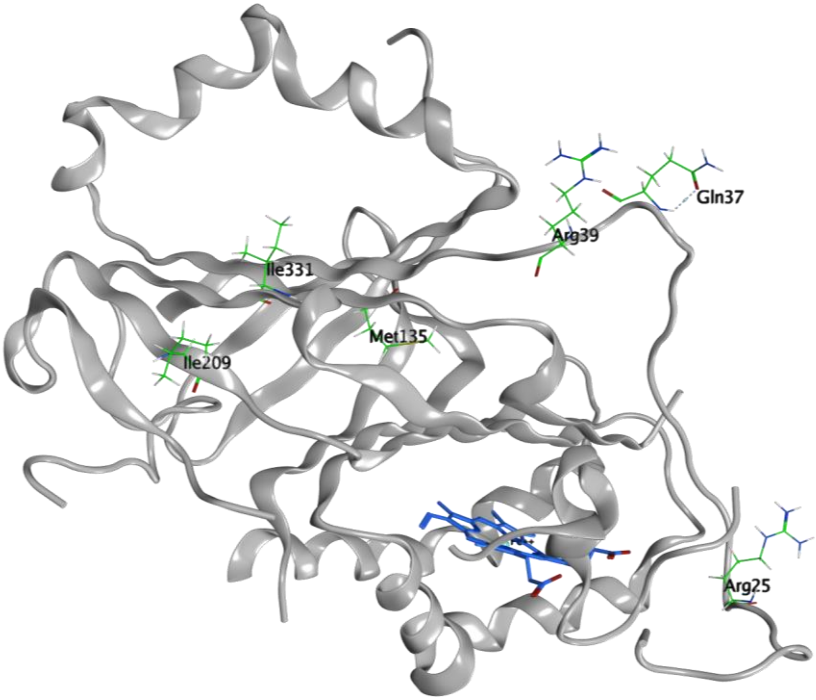

Figure 69: Model of OxdB-Set2 (P25R/E37Q/S39R/T135M/T209I/E331), whereas the mutations are highlighted in green and heme in blue.

9.7.6 Characterization of BSol-Variants

9.7.6.1 General procedure 10 (GP10): Biotransformation with purified OxdB-WT and OxdB-Sol-variants

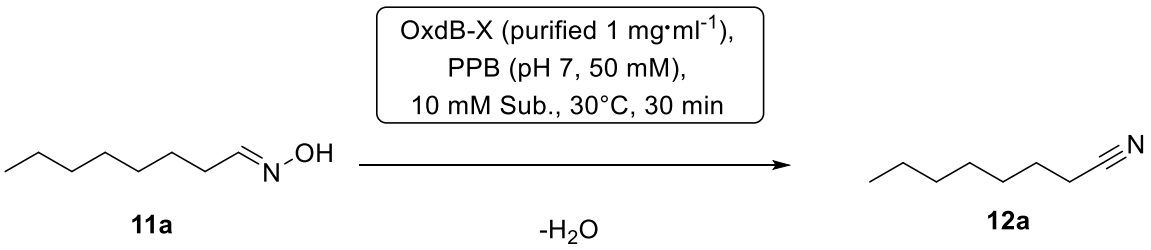

For the biotransformation the respective enzyme (1 mg·mL^{-1}) was first placed into a 2 mL Eppendorf tubes along with PPB (pH 7, 50 mM). For activity measurements the reaction was started without prior incubation. For stability measurements the enzymes were first incubated for an hour at the investigated temperature. The reaction was started by the addition of octanal oxime (10 mM, 10% *v/v* ethanol). After 30 min at 30 °C the 500 µL reaction solution were extracted with ethyl acetate (500 µL). The conversion was determined via GC.

9.7.6.2 Specific activity of OxdB-Sol variants

The specific activity was determined according to GP11 without prior incubation using 10 mM octanal oxime as substrate.

Table 90: Specific activity and conversion of purified OxdB-WT and OxdB-Sol1-variants with Octanal oxime.

Enzyme	Conv. with C8-oxime / %	Specific Activity / mU·mg^{-1}
OxdB-Sol1	86	286
OxdB-Sol2	14	46
OxdB-Sol3	70	233
OxdB-WT	66	220

9.7.6.3 Temperature stability of OxdB-Sol-variants

The thermostability of OxdB and OxdB-Sol variants were determined according to GP11 with prior incubation at the investigated temperature. The reaction itself was carried out at 30 °C.

Table 91: Thermostability investigation of OxdB-WT and OxdB-Sol-variants with purified enzymes.

#	Enzyme	temp / °C	Incubation / °C	Solvent / %	Conversion / %
1	B-WT	30	-	10	66
2	B-Sol1	30	-	10	86
3	B-Sol2	30	-	10	14
4	B-Sol3	30	-	10	70
5	B-WT	30	40	10	47
6	B-Sol1	30	40	10	73
7	B-Sol2	30	40	10	2
8	B-Sol3	30	40	10	62
9	B-WT	30	50	10	16
10	B-Sol1	30	50	10	44
11	B-Sol2	30	50	10	1
12	B-Sol3	30	50	10	3
13	B-WT	30	40	20	43
14	B-Sol1	30	40	20	68
15	B-Sol2	30	40	20	1
16	B-Sol3	30	40	20	2
17	B-WT	30	50	20	1
18	B-Sol1	30	50	20	1
19	B-Sol2	30	50	20	1
20	B-Sol3	30	50	20	1
21	B-WT	30	40	30	0
22	B-Sol1	30	40	30	0
23	B-Sol2	30	40	30	0
24	B-Sol3	30	40	30	0
25	B-WT	30	50	30	0
26	B-Sol1	30	50	30	0
27	B-Sol2	30	50	30	0
28	B-Sol3	30	50	30	0

9.7.7 Characterization of OxdB-Variants

9.7.7.1 General procedure 11 (GP11): Biotransformation with whole cell catalyst

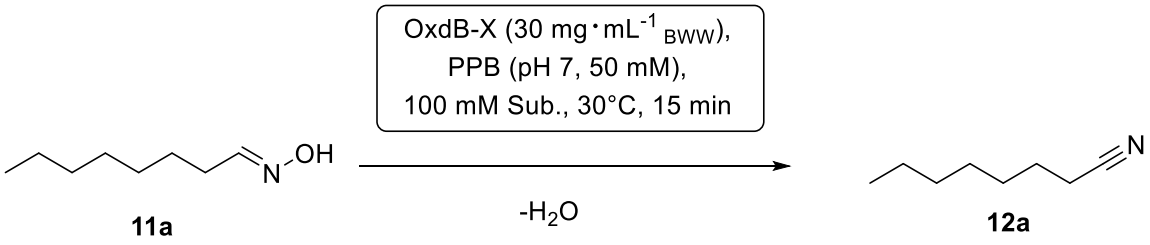

For the biotransformation the respective enzyme (30 mg·mL^{-1} $_{BWW}$) was first placed into a 2 mL Eppendorf tubes along with PPB (pH 7, 50 mM). After an incubation period of 30 minutes with the parameters to be investigated (temperature 30-50 °C, solvent content: 10- 40%), if not stated otherwise ethanolic octanal oxime solution (100 mM, 10% *v/v*) was added to start the reaction. After 15 min the 1 mL reaction solution was extracted with 800 µL ethyl acetate. The conversion was determined via GC (**Table 92**, **Table 93**, **Table 94**).

Table 92: Temperature tolerance of OxdB-WT, B-Sol1, 3DM-Set1a and 3DM-Set2 octanal oxime as substrate. The reaction was performed with 15 min reaction time and a pre incubation time at the given temperature for 30 mins. Cell concentration was set to 30 mg·mL^{-1}.

#	Enzyme	temp / °C	Incubation / °C	Conversion / %	Conversion / %	Mean / %
1	B-WT	30	30	63	60	62
2	Set1a	30	30	50	47	48
3	Set2	30	30	45	47	46
4	B-WT	30	40	42	46	44
5	Set1a	30	40	46	42	44
6	Set2	30	40	46	44	45
7	B-WT	30	45	34	34	34
8	Set1a	30	45	32	37	34
9	Set2	30	45	38	42	40
10	B-WT	30	50	21	21	21
11	Set1a	30	50	27	28	27
12	Set2	30	50	27	26	26
13	B-WT	30	55	1	1	1
14	Set1a	30	55	2	2	2
15	Set2	30	55	2	2	2

Table 93: Solvent tolerance of OxdB-Set2 and octanal oxime as substrate. The reaction was performed with 15 min reaction time and a pre incubation time of 30 mins with the given solvent concentration.

#	Enzyme	temp / °C	Solvent / %	Solvent	Conversion / %	Conversion / %	Mean/ %
1	Set2	30	10	ETOH	89	95	92
2	Set2	30	20	ETOH	60	60	60
3	Set2	30	30	ETOH	32	32	32
4	Set2	30	40	ETOH	0	3	1.5
5	Set2	30	10	ISO	76	70	73
6	Set2	30	20	ISO	57	57	57
7	Set2	30	30	ISO	0	2	1
8	Set2	30	40	ISO	0	0	0

Table 94: OxdB-WT and OxdB-Sol variants as whole cells investigating the solvent tolerance using different ethanol ratios for the reaction with octanal oxime.

#	Enzyme	Ethanol ratio / %	Substrate	Concentration / mM	Conversion / %
1	BSol1	10	C8	100	95%
2	BSol1	20	C8	100	88%
3	BSol1	30	C8	100	83%
4	BSol1	40	C8	100	42%
5	BSol2	10	C8	100	45%
6	BSol2	20	C8	100	43%
7	BSol2	30	C8	100	14%
8	BSol2	40	C8	100	7%
9	BSol3	10	C8	100	84%
10	BSol3	20	C8	100	81%
11	BSol3	30	C8	100	35%
12	BSol3	40	C8	100	10%
13	B-WT	10	C8	100	86%
14	B-WT	20	C8	100	82%
15	B-WT	30	C8	100	70%
16	B-WT	40	C8	100	28%

9.8 Increasing the activity of OxdB by rational design

9.8.1 Molecular modeling

Docking was performed as described in GDP1. As model enzyme OxdRE and as ligands non specified *E*/*Z*-conformers of fatty aldoximes were used. The resulting data were tabulated indicating the energy and RMSD-values of 5 poses (**Table 95**).

Table 95: docking results with fatty aldoximes using OxdRE as model enzyme

#	Ligand	ΔG/ kcal·mol-1	RMSD-refine
1	C8	-11.1	1.4
2	C8	-10.7	1.0
3	C8	-10.6	1.6
4	C8	-10.5	1.1
5	C8	-10.5	1.1
6	C9	-11.1	2.0
7	C9	-11.1	1.2
8	C9	-11.0	1.2
9	C9	-11.0	1.0
10	C9	-10.9	0.7
11	C10	-11.7	1.3
12	C10	-11.2	1.5
13	C10	-11.0	1.6
14	C10	-10.9	1.7
15	C10	-10.9	0.7
16	C11	-11.6	1.2
17	C11	-11.5	1.3
18	C11	-11.4	1.2
19	C11	-11.2	1.0
20	C11	-11.0	1.3
21	C12	-12.5	1.7
22	C12	-12.1	0.8
23	C12	-11.5	1.1
24	C12	-10.6	1.3
25	C12	-9.9	1.0
26	C13	-11.9	1.9
27	C13	-11.6	1.2
28	C13	-11.6	1.9
29	C13	-11.5	0.7
30	C13	-11.2	1.2
31	C14	-12.2	1.4
32	C14	-11.7	1.3
33	C14	-11.7	1.3
34	C14	-11.7	1.5
35	C14	-11.6	1.0
36	C15	-11.9	1.1
37	C15	-11.8	2.9
38	C15	-11.8	1.6
39	C15	-11.7	1.7
40	C15	-11.7	1.5
41	C16	-12.3	1.9
42	C16	-12.2	1.6
43	C16	-12.1	1.6
44	C16	-11.7	1.1
45	C16	-11.7	1.8
46	C17	-12.0	1.9
47	C17	-11.8	1.9
48	C17	-11.7	1.6

#	Ligand	ΔG/ kcal·mol-1	RMSD-refine
49	C17	-11.7	2.4
50	C17	-11.6	2.0
51	C18	-12.8	2.0
52	C18	-12.2	1.9
53	C18	-12.0	1.3
54	C18	-11.8	3.8
55	C18	-11.5	3.0

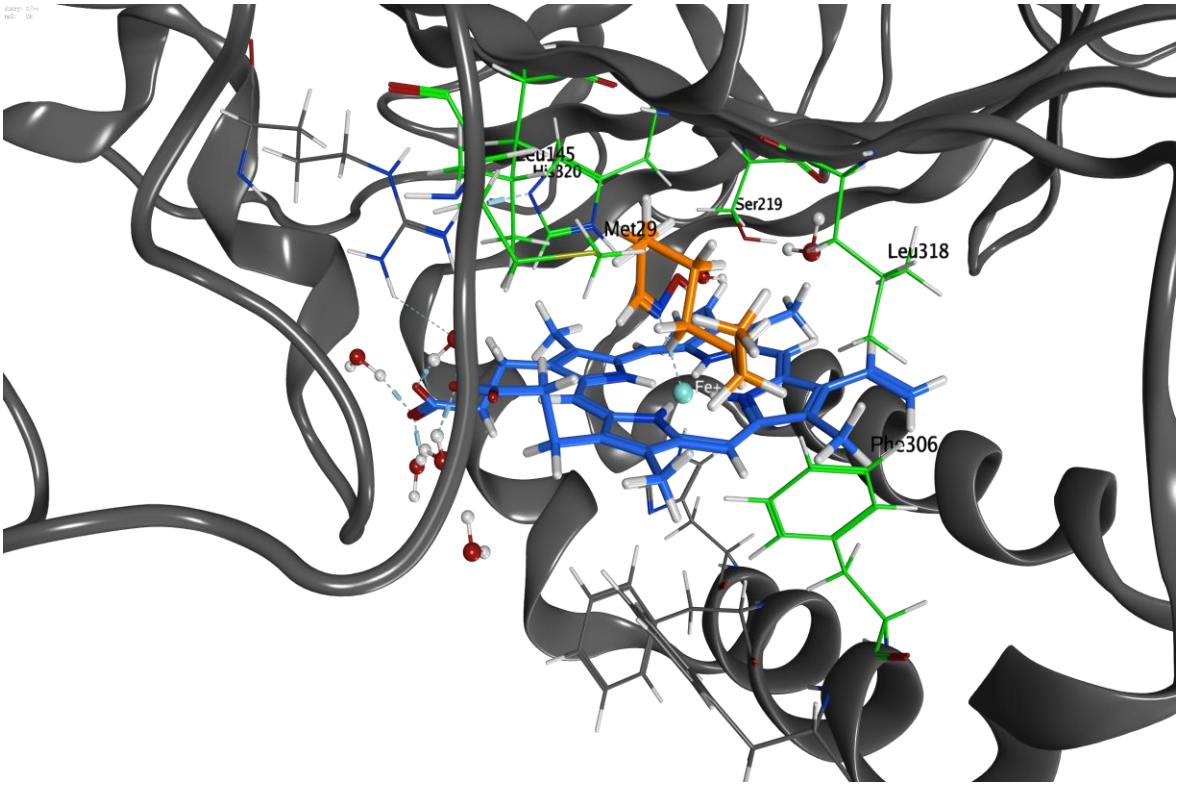

Figure 70: Docked structure of octanal oxime in OxdRE showing a complete incorporation in the active site.

The docking results were compared visually in terms of correct pose and incorporation into the active site. Afterwards a homology model of OxdB was used to identify the crucial positions, which would lead to an increased active site or entrance. In silico site directed mutagenesis and surface calculation were performed to validate the mutational purpose. Afterwards the experiments were continued in vitro.

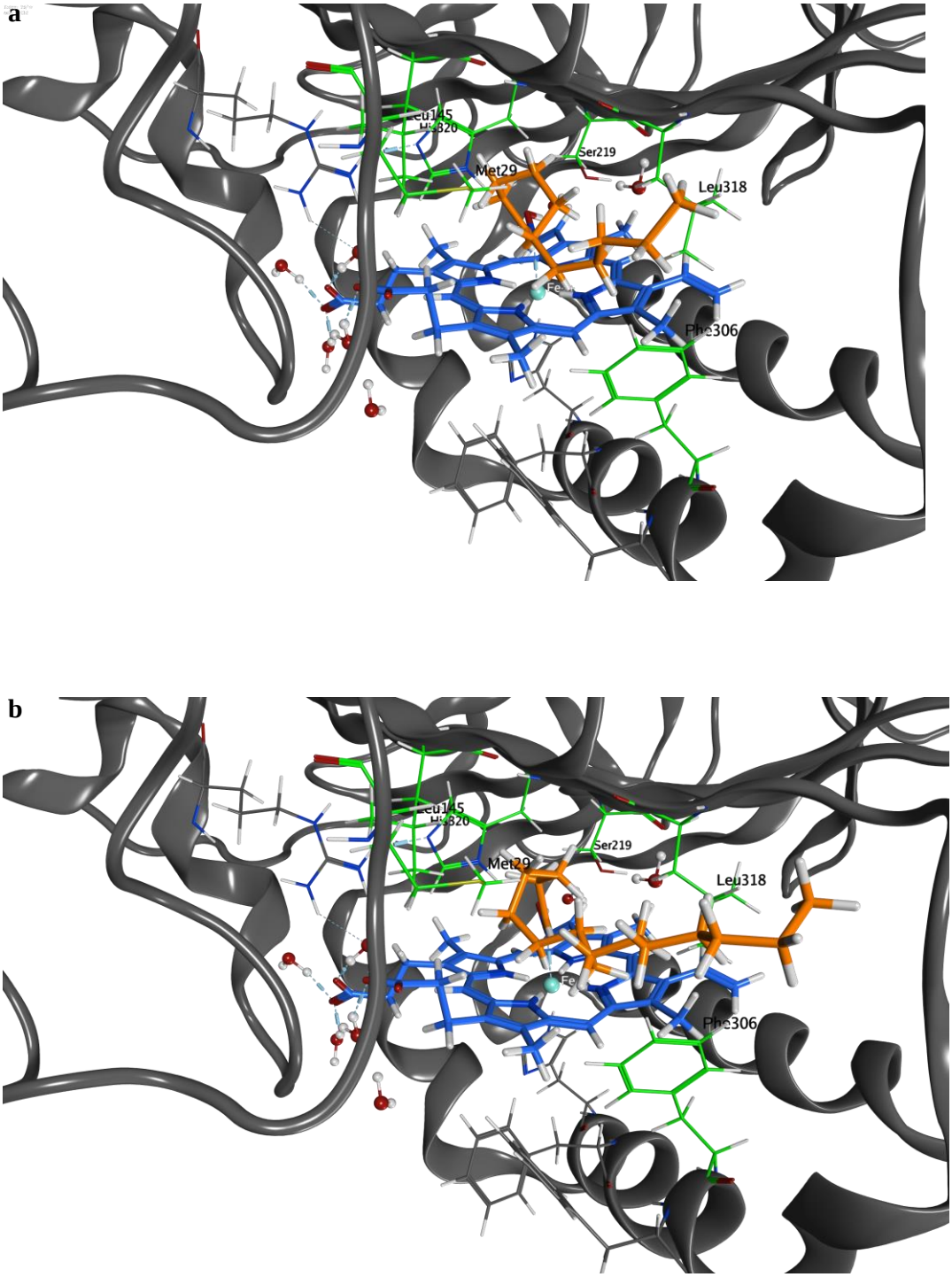

Figure 71: Molecular docking using MOE as software. **Frame a** shows dodecanal oxime inside the active site. **Frame b** showing hexadecanal oxime in the active site showing same pose as dodecanal oxime with only the alkyl rest merging further out.

9.8.2 Surface modification

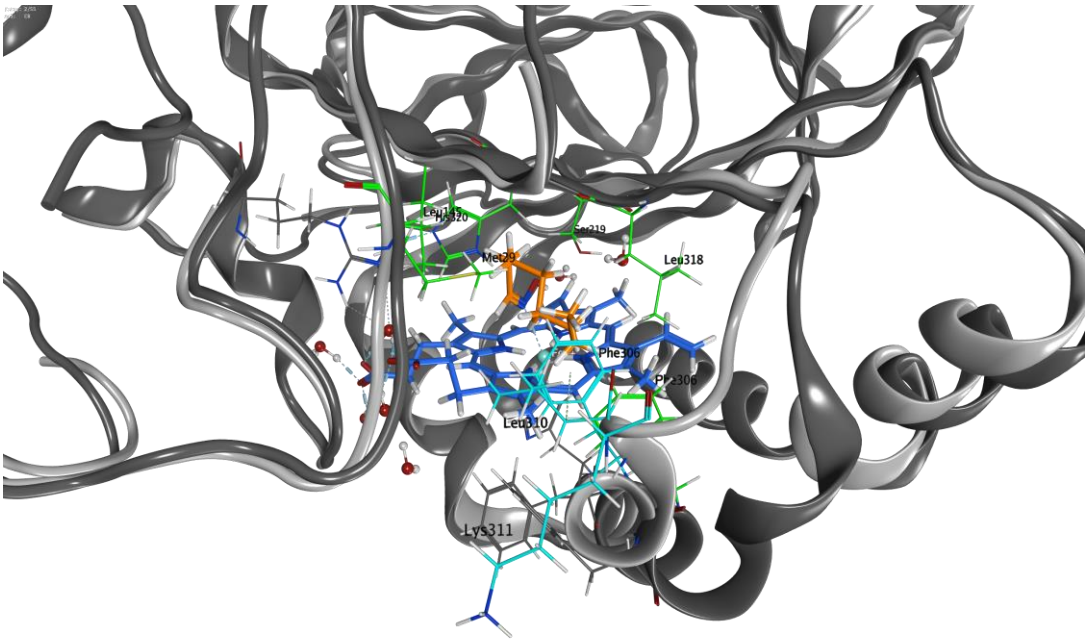

Figure 72: superposed structure of OxdRE and OxdB homology model. OxdRE crystal structure with bound octanal oxime (dark grey). OxdB as homology model superposed (light grey).

a

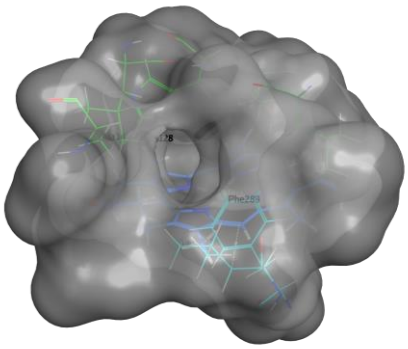

b

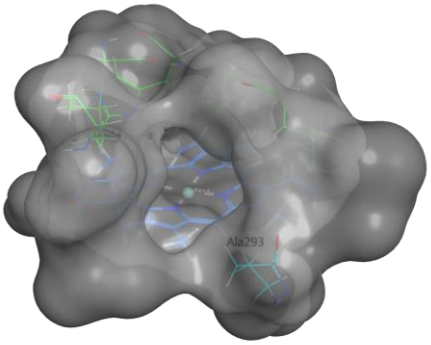

Figure 73: Modeled surface of OxdB-WT (**Frame a**) and OxdB5 (F290A-L294A) (**Frame b**). Showing enhanced entrance site for the mutant compared to the wild type.

9.8.3 Solubility calculation

The solubilities were calculated using the web-based tool ACD/I-Lab.[148]

Table 96: Calculated solubilities of aldoximes in water at 25 °C. The ACD/I-Lab programme was used to calculate the solubilities.

Aldoxime	solubility / µg·ml^{-1}	LogSw	Reliability:	Conc. / mM
C7	59.00	-3.34	0.65	0.45666
C8	39.00	-3.57	0.55	0.27216
C9	24.00	-3.81	0.55	0.15261
C10	18.00	-3.99	0.67	0.10510
C11	11.00	-4.22	0.69	0.05938
C12	6.20	-4.50	0.68	0.03011
C13	2.90	-4.87	0.63	0.01360
C14	0.37	-5.79	0.56	0.00163
C15	0.17	-6.16	0.53	0.00070
C16	0.07	-6.54	0.48	0.00027
C17	0.02	-7.02	0.45	0.00007
C18	0.01	-7.29	0.45	0.00004

9.8.4 Genera procedure 14 (GP14): Biotransformation with whole cell catalyst

Biotransformation's were carried out with whole cell catalyst (33 mg·mL^{-1} $_{BWW}$) in PPB (pH7, 50 mM) and ethanol (10%, *v/v*) at 30 °C. The cell suspension as well as the buffer were placed first and the reaction was started by addition of the substrate (100 mM). After the stated reaction period the suspension was extracted with ethyl acetate, which simultaneously stops the reaction. The conversion was determined via GC.

9.8.4.1 Activity assay of OxdB-Variants

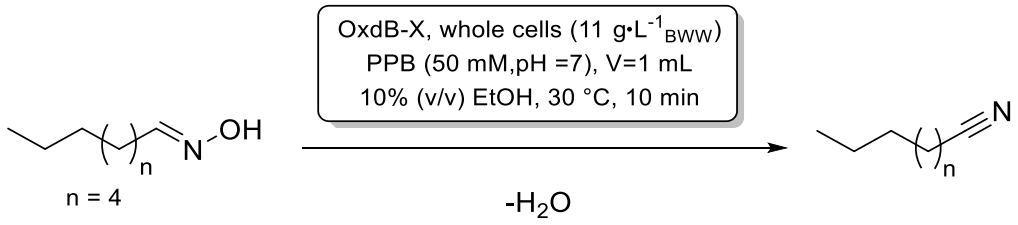

Biotransformation's was carried out according to GP14 using whole cell catalyst (11 mg·mL^{-1} $_{BWW}$), octanal oxime (100 mM) as substrate, 10 min reaction time and 1 mL reaction volume. For work up the suspension was extracted with ethyl acetate (800 µL) and the conversion was determined via GC (**Table 97**).

Table 97: Activity assay of OxdB-WT with OxdB-Set2 (thermostable) and OxdB5 (increased entrance) .

#	Enzyme	Conc. / mM	Temperature / °C	Time / min	Conv. / %	Conv. / %	Mean / %	Activity / mU·mg^{-1}
1	OxdB-WT	100	30	10	22	22	22	200
2	OxdB-Set2	100	30	10	20	20	20	180
3	OxdB5	100	30	10	54	53	54	490

9.8.4.2 Performance of OxdB-Variants at different reaction temperatures

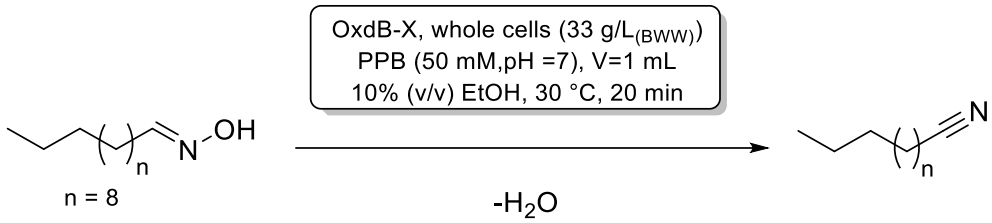

Biotransformation's was carried out according to GP1 using whole cell catalyst (33 mg · mL^{-1}, $_{BWW}$), dodecanal oxime (100 mM) as substrate, 20 min reaction time and 1 mL reaction volume. For work up the suspension was extracted with ethyl acetate (800 µL) and the conversion was determined via GC (**Table 98**).

Table 98: Comparison of OxdB-WT with OxdB-Set2 (thermostable) and OxdB5 (increased entrance) in their perfomance for the conversion of dodecanal oxime.

#	Enzyme	Conc. / mM	Temperature / °C	Time / min	Conv. / %	Conv. / %	Mean / %
1	OxdB-WT	100	30	20	2	1	2
2	OxdB-Set2	100	30	20	1	5	3
3	OxdB5	100	30	20	6	6	6
4	OxdB-WT	100	40	20	14	16	15
5	OxdB-Set2	100	40	20	27	23	25
6	OxdB5	100	40	20	28	22	25
7	OxdB-WT	100	50	20	8	9	9
8	OxdB-Set2	100	50	20	22	12	17
9	OxdB5	100	50	20	1	1	1

9.9 Pickering emulsion mediated biotransformation

9.9.1 General Procedure 15 (GP15): Pickering emulsions mediated biotransformation of dodecanal oxime

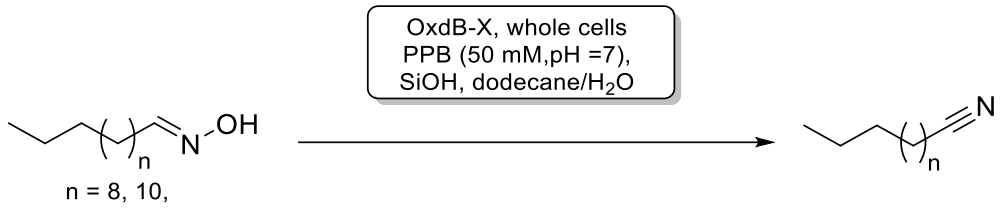

The Pickering emulsion were prepared according to *Bago Rodriguez et al*.[146] Silica particles (1 wt%, 52 mg) were added into a 10 mL beaker. Subsequently, the particles were dissolved by the addition of dodecanal oxime solution in dodecane (3 mL, 50 mM). As aqueous phase the cell solution (33 mg·mL^{-1}) in PPB buffer (50 mM, pH 7) was added. The emulsions were prepared according to the protocol[146] using ultra-turrax homogenisation (IKA T25 Digital and a dispersing element with 8 mm stator diameter) for 2 min at 13.000 rpm. For all emulsions, a drop test was performed to verify the emulsion type (w/o or o/w) and in some cases pictures of the emulsion were taken with a digital camera (Canon EOS 1100D) to assess the emulsion stability. For the extraction 100 µL of the emulsion were taken and diluted with 700 µL ethyl acetate. After vortexing, centrifugation was performed (1 min, 11000 rpm) and the organic phase was filtered through silica gel. The conversion was determined via GC.

9.9.2 Pickering emulsion characterization

The Pickering emulsion were performed as described in GP15 using particles with different hydrophobicity. The particle amount, substrate concentration and cell amount were constant in all emulsion. The emulsion type was determined via droplet test. The hydrophobic particles (15%-25%) formed w/o emulsions and the hydrophilic (65%-100%) once o/w emulsions (**Figure 74**).

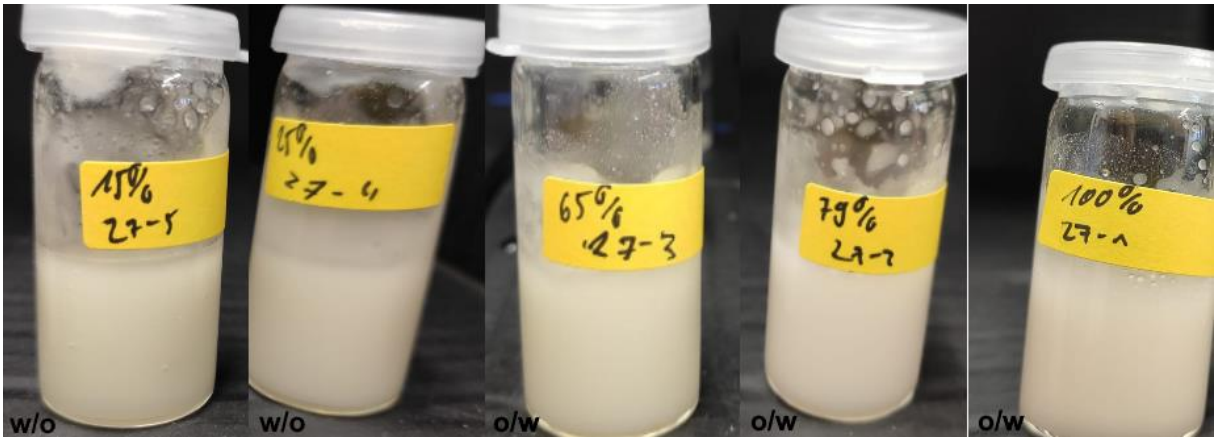

Figure 74: Pickering emulsion with different silica particles after 1 hour.

9.9.3 Synthesis of dodecane nitril in different Pickering emulsions

The reactions were performed according to GP15 using silica particles with different grade of methylation. The reaction was also condemned with 1 mL reaction volume using 2 mL-Eppendorf-Tubess and shaking at 1000 rpm.

Table 99: Dodecanal oxime transformation with OxdB-WT with different PE particles at RT and 24 hours reaction time.

PE	Concentration / mM	Conversion / %	Conversion / %	Mean / %
15%	50	40	37	39
25%	50	44	29	37
65%	50	46	34	40
79%	50	80	65	73
100%	50	57	49	53

Table 100: Dodecanal oxime transformation with OxdB-WT with different PE particles at RT and 24 hour reaction time. The reactions were conducted in a thermoshaker using 1 mL reaction tubes at 1000 rpm.

PE	Concentration / mM	Conversion / %
15%	50	10
25%	50	11
65%	50	13
79%	50	15
100%	50	9

9.9.4 Comparison of OxdB-WT and OxdB5 performed biotransformation of fatty aldoximes in Pickering emulsions

The reaction was carried out according to GP15 using OxdB5 and OxdB-WT (33 mg·mL^{-1}, $_{BWW}$) and silica particles (79% SiOH, 1 wt%, 52 mg). As substrates dodecanal oxime and tetradecanal oxime (100 mM) in dodecane were used. The substrates were applied as suspensions in dodecane before the emulsifying process.

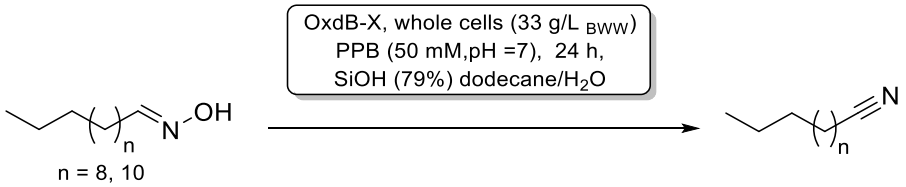

Table 101: Biotransformation in Pickering emulsion as alternative for insolbule substrates with dodecanal- and tetradecanal oxime as substrate

#	Enzyme	Substrate	Conc. / mM	BWW / mg·ml^{-1}	Conversion / %
1	B-WT	C12	100	33	99
2	B-5	C12	100	33	99
3	B-WT	C14	100	33	19
4	B-5	C14	100	33	31

9.10 Combining Flow chemistry and Pickering emulsion with OxdB catalyzed octane nitrile synthesis

9.10.1 Flow set up for the Pickering emulsion mediated cascade reaction

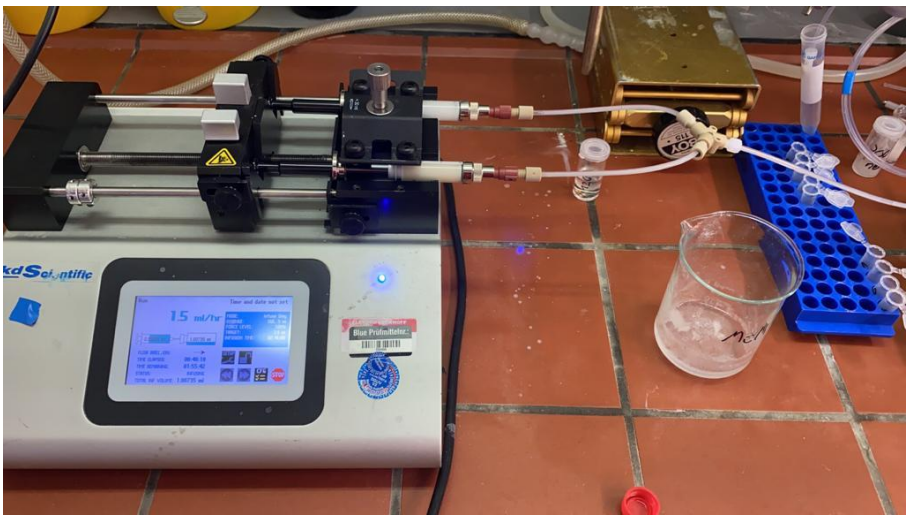

Figure 75: Foto of the flow setup showing the syringe pump with the two installed glass syringes, a T-piece and the reactor on the right. The Eppendorf tubes were used to take samples. The bottom Pickering emulsion (PE2) contained the enzyme.

For the flow reaction, two 5 mL glass syringes with Teflon traction and an inner diameter of 10.4 mm were used. The microreactor and the short T-piece used to connect the two syringes into the microreactor were made of Teflon tubes. The microreactor had an inner diameter of 1/16" and a volume of 3 mL. All reactions were performed at room temperature. A Syringe pump type Legat® 200 from KD Scientific Inc (address: 84 October Hill Road, Holliston, Ma 01756, USA, internet www.kdscietific.com) was used (**Figure 75**).

9.10.2 Investigation of Pickering emulsion mediated cascade reaction of octane nitrile starting from octanal

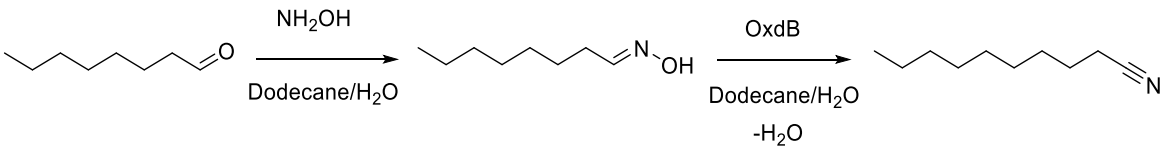

Pickering emulsion 1 (PE1) was prepared by dispersed silica particles (1 wt%, 52 mg, SiOH 51%) in dodecane (3 mL) and adding hydroxylamine solution (3 mL, 120 mM, pH = 6.4) as aqueous phase. The second emulsion (PE2) was prepared dispersed silica particles (1 wt%, 52 mg, SiOH 51%) and octanal (43 µL, 100 mM) in dodecane (3 mL). Then adding OxdB-Sol1 (0.3 ml, 30 mg·mL^{-1}) with PPB (2.7 mL, 50 mM, pH 7) . The emulsions were prepared according to the standard protocol[146] using a homogenizer (2 min, 13000 rpm) and afterwards filled in two separate syringes, then placed in the syringe pump and the reaction started by injecting the emulsions in the reactor using a T-piece for mixing. In addition, a batch reaction was performed for 1 h using 100 µL of each emulsion and suspending it in an Eppendorf tubes (2 mL). Each sample (80 µL) was diluted with 720 µL ethyl

acetate and after mixing (vortex) phase separation was induced by pulse centrifugation, filtered through a silica pad and the organic phase analyzed via GC. The settings and results of the reaction are in the tables below.

Table 102: Pickering emulsion mediated synthesis of octane nitrile starting from octanal (100 mM) and hydroxylamine (120 mM) in a flow system.

Sample time/ min	Flow rate / mL·h^{-1}	Reactor volume / ml	Residence time / min	Aldehyde / %	Oxime / %	Nitrile / %
Equil.	1.5	3	60	57	7	36
15	1.5	3	60	70	6	22
30	1.5	3	60	53	15	31
45	1.5	3	60	70	10	18

9.10.3 Investigation of octanal oxime formation in Pickering emulsion

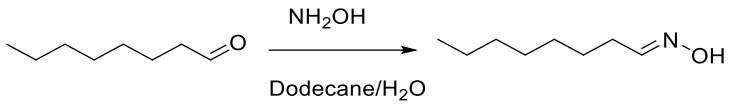

Pickering emulsion 1 (PE1) was prepared by dispersed silica particles (1 wt%, 52 mg, SiOH 51%) in dodecane (3 mL) and adding hydroxylamine solution (3 mL, 0-300 mM, pH = 6.4) as aqueous phase. The second emulsion (PE2) was prepared dispersed silica particles (1 wt%, 52 mg, SiOH 25%) and octanal (43 µL, 100 mM) in dodecane (3 mL). Then adding *E.coli* BL21 (empty) (0.3 ml, 30 mg·mL^{-1} with PPB (2.7 mL, 50 mM, pH 7) . The emulsions were prepared according to the standard protocol using a homogenizer (2 min, 13000 rpm) and afterwards filled in two separate syringes, then placed in the syringe pump and the reaction started by injecting the emulsions in the reactor using a T-piece for mixing. In addition, a batch reaction was performed for 1 h using 100 µL of each emulsion and suspending it in an Eppendorf tubes (2 mL). Each sample (80 µL) was diluted with 720 µL ethyl acetate and after mixing (vortex) phase separation was induced by pulse centrifugation, filtered through a silica pad and the organic phase analyzed via GC. The settings and results of the reaction are in the tables below.

Table 103: Pickering emulsion mediated synthesis of octanal oxime starting from octanal (100 mM) and hydroxylamine (120 mM) in a flow system.

Sample time/ min	Flow rate/ mL·h^{-1}	Reactor volume/ ml	Residence time / min	Aldehyde /%	Oxime / %
Equil.	1.5	3	60	10	90
15	1.5	3	60	4	96
30	1.5	3	60	2	98

Table 104: Pickering emulsion mediated synthesis of octanal oxime starting from octanal (100 mM) and hydroxylamine (120 mM) in a flow system.

Sample time/ min	Flow rate/ mL·h^{-1}	Reactor volume/ ml	Residence time / min	Aldehyde /%	Oxime / %
Equil.	1.5	3	60	90	10
15	1.5	3	60	80	20
30	1.5	3	60	89	11
45	1.5	3	60	94	6
60	1.5	3	60	84	16
Batch	-	-	60	39	61

9.10.4 Hydroxylamine influence towards OxdB catalyzed octane nitrile synthesis in Pickering emulsions

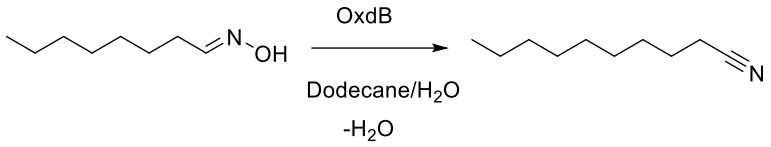

Pickering emulsion 1 (PE1) was prepared by dispersed silica particles (1 wt%, 52 mg, SiOH 51%) in dodecane (3 mL) and octanal oxime (100 mM) as organic phase. Then adding hydroxylamine solution (3 mL, 0-300 mM, pH = 6.4) as aqueous phase. The second emulsion (PE2) was prepared by dispersed silica particles (1 wt%, 52 mg, SiOH 25%) in dodecane (3 mL) and adding OxdB-Sol1 (0.3 ml, 30 mg·mL^{-1}) with PPB (2.7 mL, 50 mM, pH7). The emulsions were prepared according to the standard protocol using a homogenizer (2 min, 13000 rpm) and afterwards filled in two separate syringes, then placed in the syringe pump and the reaction started by injecting the emulsions in the reactor using a T-piece for mixing. In addition, a batch reaction was performed for 1 h using 100 µL of each emulsion and suspending it in an Eppendorf tubes (2 mL). Each sample (80 µL) was diluted with 720 µL ethyl acetate and after mixing (vortex) phase separation was induced by pulse centrifugation, filtered through a silica pad and the organic phase analyzed via GC. The settings and results of the reaction are in the tables below.

Table 105: Pickering emulsion mediated synthesis of octane nitrile starting from octanal oxime (100 mM)

Sample time/ min	Flow rate/ mL·h^{-1}	Reactor volume/ ml	Residence time / min	Oxime / %	Nitrile / %
Equil.	1.5	3	60	18	82
15	1.5	3	60	20	80
30	1.5	3	60	15	85
45	1.5	3	60	17	83
60	1.5	3	60	13	87
Batch	-	-	60	9	91

Table 106: Pickering emulsion mediated synthesis of octane nitrile starting from octanal oxime (100 mM) in presence of hydroxylamine (120 mM)

Sample time/ min	Flow rate/ mL·h^{-1}	Reactor volume/ ml	Residence time / min	Oxime / %	Nitrile / %
Equil.	1.5	3	60	80	20
15	1.5	3	60	83	17
30	1.5	3	60	94	6
45	1.5	3	60	83	17
60	1.5	3	60	81	19
Batch	-	-	60	90	10

Table 107: Pickering emulsion mediated synthesis of octane nitrile starting from octanal oxime (100 mM) in presence of hydroxylamine (300 mM)

Sample time/ min	Flow rate/ mL·h^{-1}	Reactor volume/ ml	Residence time / min	Oxime / %	Nitrile / %
Equil.	1.5	3	60	93	7
15	1.5	3	60	96	4
30	1.5	3	60	96	4
45	1.5	3	60	92	8
60	1.5	3	60	97	3
Batch	-	-	60	100	0

9.10.5 OxdB catalyzed octane nitrile synthesis in Pickering emulsions with aldehyde and hydroxylamine being in the same emulsion

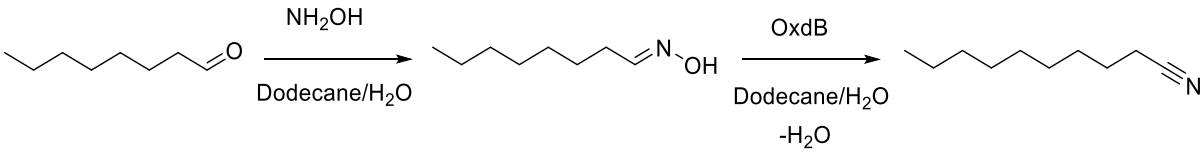

Pickering emulsion 1 (PE1) was prepared by dispersed silica particles (1 wt%, 52 mg, SiOH 51%) in dodecane (3 mL) and octanal oxime (100 mM) as organic phase. Then adding a hydroxylamine solution (3 mL, 120 mM, pH = 6.4) as aqueous phase. The emulsions were prepared according to the standard protocol using a homogenizer (2 min, 13000 rpm). The second emulsion (PE2) was prepared using silica particles (1 wt%, 52 mg, SiOH 25%) dissolved in dodecane (3 mL) and PPB (2.7 mL, 50 mM, pH7) and OxdB-Sol1 (0.3 ml, 30 mg·mL^{-1}). The two emulsions were filled in two separate syringes, then placed in the syringe pump and the reaction started by injecting the emulsions in the reactor. In addition, a batch reaction was performed for 1h using 100 µL of each emulsion and suspending it in an Eppendorf tubes (2 mL). Each sample (80 µL) was diluted with 720 µL ethyl acetate and after mixing (vortex) phase separation was induced by pulse centrifugation, filtered through a silica pad and the organic phase analyzed via GC. The settings and results of the reaction are in the table below.

Table 108: Results and settings of the flow reaction with 120 mM hydroxylamine and octanal in one emulsion

Sample time/ min	Flow rate/ mL·h^{-1}	Reactor volume/ ml	Residence time / min	Aldehyde /%	Oxime / %	Nitrile / %
Equil.	1.5	3	60	23	61	15
15	1.5	3	60	26	22	51
30	1.5	3	60	25	17	56
45	1.5	3	60	25	19	55
60	1.5	3	60	22	47	30
Batch	-	-	60	24	33	42

9.12 Analytic

9.12.1 Nuclear magnetic resonance spectroscopy (NMR)

The ^{1}H-NMR spectra were recorded on a Bruker Avance AV500 HD (^{1}H: 500 MHz) spectrometer. Deuterated chloroform ($CDCl_3$), DMSO-d_6 and D_2O were used as solvents. The chemical shift (δ) is given in parts per million (ppm) and referenced to the solvent signals ($CDCl_3$: 7.26 ppm, DMSO 2.50 ppm). For the determination of solubility D_2O was used as reference and with ethanol or methanol as an internal standard. The spectra were processed with MestReNova.

9.12.2 High performance liquid chromatography (HPLC)

The conversion and enantiomeric excess were determined using a calibration curve for the SFC HPLC. The OB-H column from *Chiracel*^{TM} served as stationary phase. The mobile phase consisted of CO_2/isopropanol mixture (98:2, *v/v*). The method ran for 30 mins at 1.0 ml/min, the injection volume was 20 µL and the measurement ran at 20 °C. The absorbance was measured at 210 nm (**Table 109**).

Table 109: HPLC-methods and rention times of phenyl propanal oxime and nitrile derivatives.

Fatty aldoxime/ nitrile	Method	Retention times /min
Phenylpropanal oxime /nitrile	98:2 for 33 min, 1 mL·min^{-1}	(*S*)-nitrile: 9.51 (*R*)-nitrile: 12.32 *(S,E)*-oxime: 19.35 *(R,E)*-oxime: 21.44 (*Z*)-oxime: 22.30; 23.83
2-fluoro-phenylpropanal oxime /nitrile	98:2 for 33 min, 1 mL·min^{-1}	(*S*)-nitrile: 6.77 (*R*)-nitrile: 7.47 *rac*-(*E/Z*)-oxime: 14.95
3-fluoro-phenylpropanal oxime /nitrile	98:2 for 33 min, 1 mL·min^{-1}	(*S*)-nitrile: 7.30 (*R*)-nitrile: 8.15 *rac*-(*E/Z*)-oxime: 12.13
4-fluoro-phenylpropanal oxime /nitrile	98:2 for 33 min, 1 mL·min^{-1}	(*S*)-nitrile: 8.12 (*R*)-nitrile: 9.08 *rac*-(*E/Z*)-oxime: 14.65
2-fluoro-phenylpropanal oxime /nitrile	92:8 to 84:16 in 0.5 min, 1.5 mL·min^{-1} 84:16 to 75:25 in 3.5 min, 1.5 mL·min^{-1} 75:25 to 70:30 in 1 min, 1.5 mL·min^{-1} 70:30 to 95:5 in 0.5 min, 1.5 mL·min^{-1} 95:5 for 0.4 min, 1.5 mL·min^{-1}	(*S*)-nitrile: 3.63 (*R*)-nitrile: 3.92 (*E*)-oxime 4.30 (*Z*)-oxime 4.74

.

9.12.3 Gas chromatography (GC)

The conversion of fatty aldoximes into fatty nitrile was determined via gas chromatography using the GC-2010 from *Shimadzu* and FID for detection. As stationary phase the column Zebron ZB-FAME (0.25 mm ID, 0.2 µm film thickness and 30 m length) was used. Injection volume was set to 1 µL, the flow control at 96.7 kPa, the injection temperature to 200 °C and the detection temperature to 220 °C. The Methods for each fatty aldoxime are listed in **Table 110**.

Table 110: GC-Methods and retention times for fatty aldoximes and corresponding nitriles

Fatty aldoxime/ nitrile	Method	Retention times /min
Octadecanal oxime /nitrile	120 °C to 150 °C in 10 °C/min,	Nitrile: 3.08
	150 °C to 200 °C in 100 °C/min	Oxime 3.49
	200 °C for 1.5 min	
Dodecanal oxime /nitrile	150 °C for 0.5 min	Nitrile: 2.73
	150 °C to 190 °C in 57 °C/min	Oxime 2.91
	190 °C for 3 min	
Tetradecanal oxime / nitrile	150 °C for 0.5 min	Nitrile: 3.80
	150 °C to 190 °C in 57 °C/min	Oxime 4.30
	190 °C for 3 min	
Hexadecanal oxime/ nitrile	170 °C for 1 min	Nitrile: 7.02
(column: BGB-174)	170 °C to 200 °C in 30 °C/min	Oxime 8.60
	200 for 11 min	

9.12.4 Column chromatography and thin layer chromatography

Silica gel 60 (0.04-0.063 mm) from *Merck* served as a stationary phase for column chromatography. A cyclohexane/ethyl acetate mixture (98: 2, *v/v*) was used as the mobile phase. Depending on the *Rf* value, different gradients were set for chromatography. For TLC chromatography, TLC Silica gel 60 F254 from *Merck* was used.

9.12.5 MS and HRMS

The routine MS-spectra were measured via Esquire 3000. The Agilent Techn. 6220 TOF LCMS with ESI as ionization method was used for the accurate mass measurement.

9.12.6 *E/Z*-separation:

The FPPOX derivatives were separated into the *E* and *Z*-isomers via automated column chromatography (**Figure 76**). Isomer purity was confirmed with ^{1}H-NMR in deuterated DMSO-d_6. (The isomers are not stable in chloroform ($CDCl_3$)).

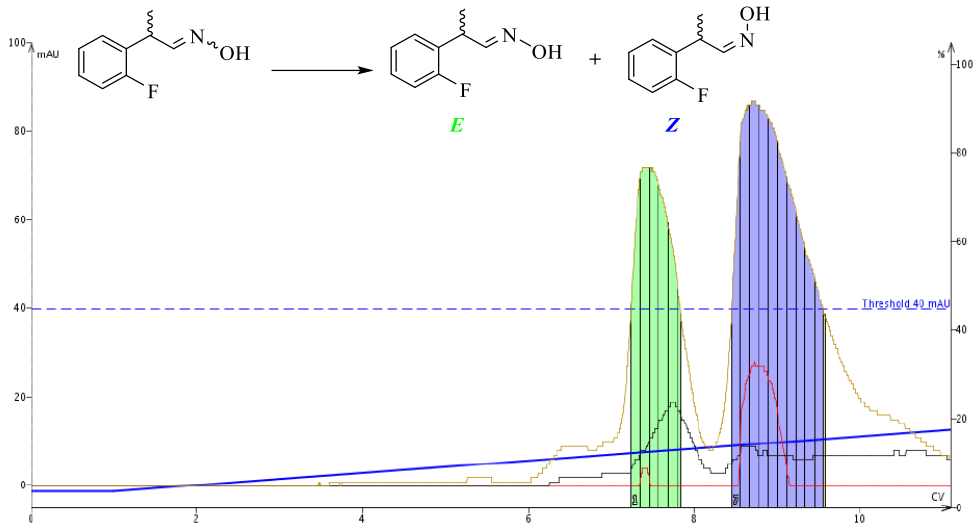

Figure 76:Chromatogram of the automated column chromatography for the *E/Z*-separation of 2-FPPOX as example.

10 List of abbreviations

APS	Ammonium peroxo disulfate
dH_2O	distilled water
E. coli	*Escherichia coli*
ee.	enantiomeric excess
eq.	equivalent
g	acceleration of gravity
HPLC	high performance liquid chromatography
J	coupling constant [Hz]
kDa	Kilodalton
PPB	Potassium phosphate buffer
LB-Medium	Luria-Bertani Medium
NMR	nuclear magnetic resonance
OD	optical density
OxdA	Aldoxime dehydratase from *Pseudomonas chlororaphis*
OxdRE	Aldoxime dehydratase from *Rhodococcus erythropolis*
OxdB	Aldoxime dehydratase from *Rhodococcus erythropolis*
pH	pondus Hydrogenii
rac	racemate
rpm	rounds per minute
SDS-PAGE	Sodium dodecyl sulfate -polyacrylamide gel electrophoresis
TB-Medium	terrific broth Medium
TEMED	Tetramethylethylendiamine
TLC	thin layer chromatography
v/v	volume ratio
PPOX	phenylpropanal oxime
FPPOX	fluoro-phenylpropanal oxime

11 Plasmids

11.1 OxdB aldoxime dehydratase from *Bacillus sp.* as pUC18 construct

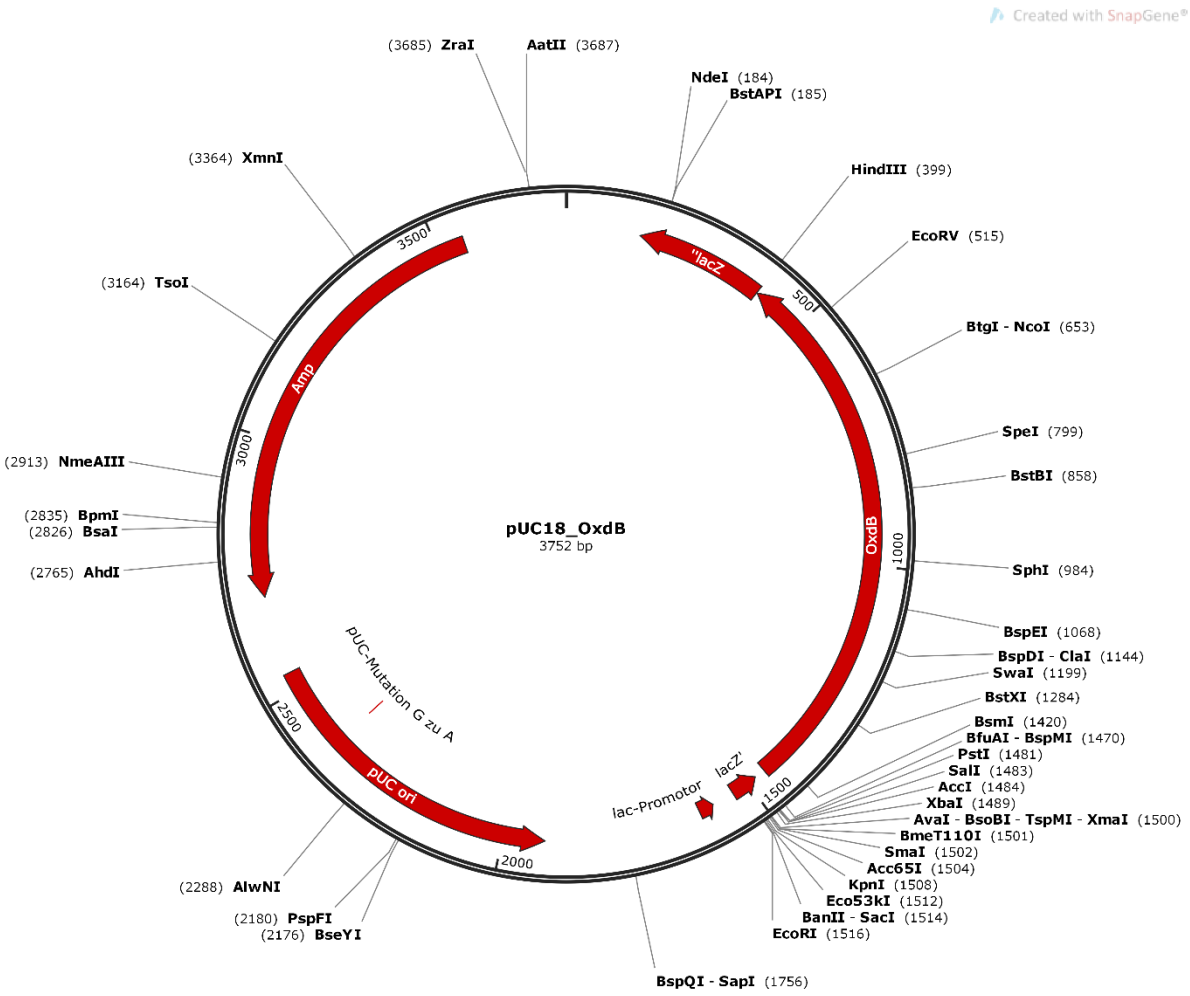

11.1.1 Base sequence of the aldoxime dehydratase from *Bacillus sp.* OxB-1 (OxdB) (Accession number: GenBank: AP013294.1

ATGAAAAATATGCCGGAAAATCACAATCCACAAGCGAATGCCTGGACTGCCGAATTTCCTCCTGAAATGAGCTATGTAGTATTTGCGCAGATTG
GGATTCAAAGCAAGTCTTTGGATCACGCAGCGGAACATTTGGGAATGATGAAAAAGAGTTTCGATTTGCGGACAGGCCCCAAACATGTGGATCG
AGCCTTGCATCAAGGAGCCGATGGATACCAAGATTCCATCTTTTTAGCCTACTGGGATGAGCCTGAAACATTTAAATCATGGGTTGCGGATCCTG
AAGTACAAAAGTGGTGGTCGGGTAAAAAAATCGATGAAAATAGTCCAATCGGGTATTGGAGTGAGGTAACGACCATTCCGATTGATCACTTTGA
GACTCTTCATTCCGGAGAAAATTACGATAATGGGGTTTCACACTTTGTACCGATCAAGCATACAGAAGTCCATGAATATTGGGGAGCAATGCGC
GACCGCATGCCGGTGTCTGCCAGTAGTGATTTGGAAAGCCCCCTTGGCCTTCAATTACCGGAACCCATTGTCCGGGAGTCTTTCGGAAAACGGCT
AAAAGTCACGGCGCCGGATAATATTTGCTTGATTCGAACCGCTCAAAATTGGTCTAAATGTGGTAGCGGGGAAAGGGAAACGTATATAGGACTA
GTGGAACCGACCCTCATAAAAGCGAATACGTTTCTTCGTGAAAATGCTAGTGAAACAGGCTGTATTAGTTCAAAATTAGTCTATGAACAGACCC
ATGACGGCGAAATAGTAGATAAATCATGTGTCATCGGATATTATCTCTCCATGGGGCATCTTGAACGCTGGACGCATGATCATCCAACACATAA
AGCGATCTACGGAACCTTTTATGAGATGTTGAAAAGGCATGATTTTAAGACCGAACTTGCTTTATGGCACGAGGTTTCGGTGCTTCAATCCAAAG
ATATCGAGCTTATCTATGTCAACTGCCATCCGAGTACTGGATTTCTTCCATTCTTTGAAGTGACAGAAATTCAAGAGCCTTTACTGAAAAGCCCTA
GCGTCAGGATCCAGTGA

11.1.2 Amino acid sequence

MKNMPENHNPQANAWTAEFPPEMSYVVFAQIGIQSKSLDHAAEHLGMMKKSFDLRTGPKHVDRALHQGADGYQDSIFLAYWDEPETFKSWVADPE
VQKWWSGKKIDENSPIGYWSEVTTIPIDHFETLHSGENYDNGVSHFVPIKHTEVHEYWGAMRDRMPVSASSDLESPLGLQLPEPIVRESFGKRLKVTAP
DNICLIRTAQNWSKCGSGERETYIGLVEPTLIKANTFLRENASETGCISSKLVYEQTHDGEIVDKSCVIGYYLSMGHLERWTHDHPTHKAIYGTFYEMLK
RHDFKTELALWHEVSVLQSKDIELIYVNCHPSTGFLPFFEVTEIQEPLLKSPSVRIQ*

11.1.3 Base sequence OxdB-F288-mutant (OxdB2)

ATGAAAAATATGCCGGAAAATCACAATCCACAAGCGAATGCCTGGACTGCCGAATTTCCTCCTGAAATGAGCTATGTAGTATTTGCGCAGATTG
GGATTCAAAGCAAGTCTTTGGATCACGCAGCGGAACATTTGGGAATGATGAAAAAGAGTTTCGATTTGCGGACAGGCCCCAAACATGTGGATCG
AGCCTTGCATCAAGGAGCCGATGGATACCAAGATTCCATCTTTTTAGCCTACTGGGATGAGCCTGAAACATTTAAATCATGGGTTGCGGATCCTG
AAGTACAAAAGTGGTGGTCGGGTAAAAAAATCGATGAAAATAGTCCAATCGGGTATTGGAGTGAGGTAACGACCATTCCGATTGATCACTTTGA
GACTCTTCATTCCGGAGAAAATTACGATAATGGGGTTTCACACTTTGTACCGATCAAGCATACAGAAGTCCATGAATATTGGGGAGCAATGCGC
GACCGCATGCCGGTGTCTGCCAGTAGTGATTTGGAAAGCCCCCTTGGCCTTCAATTACCGGAACCCATTGTCCGGGAGTCTTTCGGAAAACGGCT
AAAAGTCACGGCGCCGGATAATATTTGCTTGATTCGAACCGCTCAAAATTGGTCTAAATGTGGTAGCGGGGAAAGGGAAACGTATATAGGACTA
GTGGAACCGACCCTCATAAAAGCGAATACGTTTCTTCGTGAAAATGCTAGTGAAACAGGCTGTATTAGTTCAAAATTAGTCTATGAACAGACCC
ATGACGGCGAAATAGTAGATAAATCATGTGTCATCGGATATTATCTCTCCATGGGGCATCTTGAACGCTGGACGCATGATCATCCAACACATAA
AGCGATCTACGGAACCCGCTATGAGATGTTGAAAAGGCATGATTTTAAGACCGAACTTGCTTTATGGCACGAGGTTTCGGTGCTTCAATCCAAAG
ATATCGAGCTTATCTATGTCAACTGCCATCCGAGTACTGGATTTCTTCCATTCTTTGAAGTGACAGAAATTCAAGAGCCTTTACTGAAAAGCCCTA
GCGTCAGGATCCAGTGA

11.1.4 Amino acid sequence

MKNMPENHNPQANAWTAEFPPEMSYVVFAQIGIQSKSLDHAAEHLGMMKKSFDLRTGPKHVDRALHQGADGYQDSIFLAYWDEPETFKSWVADPE
VQKWWSGKKIDENSPIGYWSEVTTIPIDHFETLHSGENYDNGVSHFVPIKHTEVHEYWGAMRDRMPVSASSDLESPLGLQLPEPIVRESFGKRLKVTAP
DNICLIRTAQNWSKCGSGERETYIGLVEPTLIKANTFLRENASETGCISSKLVYEQTHDGEIVDKSCVIGYYLSMGHLERWTHDHPTHKAIYGTAYEML
KRHDFKTELALWHEVSVLQSKDIELIYVNCHPSTGFLPFFEVTEIQEPLLKSPSVRIQ*

11.1.5 Base sequence OxdB-F288/L293A/K294G mutant (OxdB4)

ATGAAAAATATGCCGGAAAATCACAATCCACAAGCGAATGCCTGGACTGCCGAATTTCCTCCTGAAATGAGCTATGTAGTATTTGCGCAGATTG
GGATTCAAAGCAAGTCTTTGGATCACGCAGCGGAACATTTGGGAATGATGAAAAAGAGTTTCGATTTGCGGACAGGCCCCAAACATGTGGATCG
AGCCTTGCATCAAGGAGCCGATGGATACCAAGATTCCATCTTTTTAGCCTACTGGGATGAGCCTGAAACATTTAAATCATGGGTTGCGGATCCTG
AAGTACAAAAGTGGTGGTCGGGTAAAAAAATCGATGAAAATAGTCCAATCGGGTATTGGAGTGAGGTAACGACCATTCCGATTGATCACTTTGA
GACTCTTCATTCCGGAGAAAATTACGATAATGGGGTTTCACACTTTGTACCGATCAAGCATACAGAAGTCCATGAATATTGGGGAGCAATGCGC
GACCGCATGCCGGTGTCTGCCAGTAGTGATTTGGAAAGCCCCCTTGGCCTTCAATTACCGGAACCCATTGTCCGGGAGTCTTTCGGAAAACGGCT
AAAAGTCACGGCGCCGGATAATATTTGCTTGATTCGAACCGCTCAAAATTGGTCTAAATGTGGTAGCGGGGAAAGGGAAACGTATATAGGACTA
GTGGAACCGACCCTCATAAAAGCGAATACGTTTCTTCGTGAAAATGCTAGTGAAACAGGCTGTATTAGTTCAAAATTAGTCTATGAACAGACCC
ATGACGGCGAAATAGTAGATAAATCATGTGTCATCGGATATTATCTCTCCATGGGGCATCTTGAACGCTGGACGCATGATCATCCAACACATAA
AGCGATCTACGGAACCGCGTATGAGATGGCGGCAAGGCATGATTTTAAGACCGAACTTGCTTTATGGCACGAGGTTTCGGTGCTTCAATCCAAA
GATATCGAGCTTATCTATGTCAACTGCCATCCGAGTACTGGATTTCTTCCATTCTTTGAAGTGACAGAAATTCAAGAGCCTTTACTGAAAAGCCCT
AGCGTCAGGATCCAGTGA

11.1.6 Amino acid sequence

MKNMPENHNPQANAWTAEFPPEMSYVVFAQIGIQSKSLDHAAEHLGMMKKSFDLRTGPKHVDRALHQGADGYQDSIFLAYWDEPETFKSWVADPE
VQKWWSGKKIDENSPIGYWSEVTTIPIDHFETLHSGENYDNGVSHFVPIKHTEVHEYWGAMRDRMPVSASSDLESPLGLQLPEPIVRESFGKRLKVTAP
DNICLIRTAQNWSKCGSGERETYIGLVEPTLIKANTFLRENASETGCISSKLVYEQTHDGEIVDKSCVIGYYLSMGHLERWTHDHPTHKAIYGTAYEMA
GRHDFKTELALWHEVSVLQSKDIELIYVNCHPSTGFLPFFEVTEIQEPLLKSPSVRIQ*

11.2 OxdB aldoxime dehydratase from *Bacillus sp.* as pET28a construct

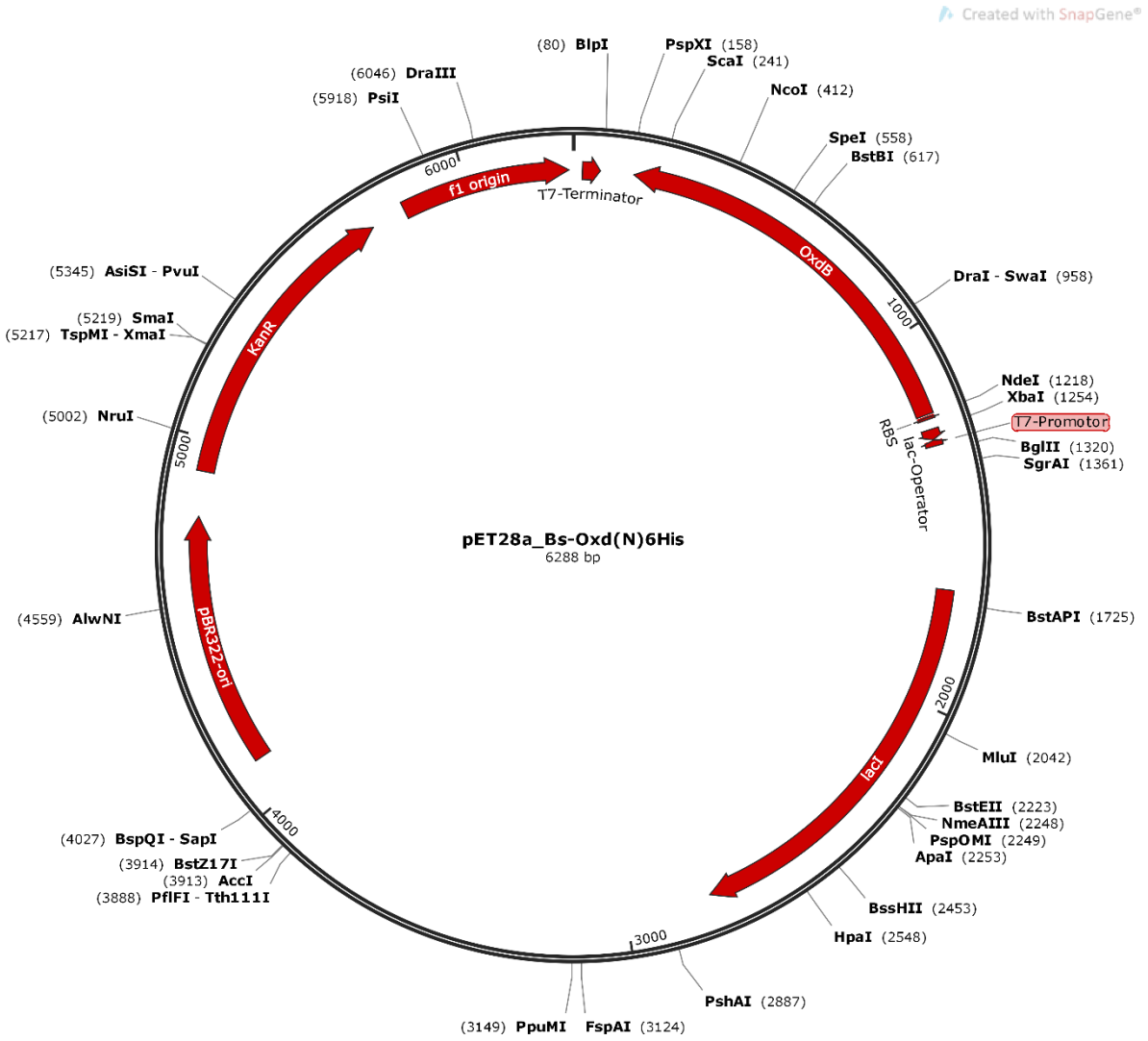

11.2.1 Base sequence of the aldoxime dehydratase from *Bacillus sp.* OxB-1 (OxdB-WT) (Accession number: GenBank: AP013294.1

GGCAGCAGCCATCATCATCATCATCACAGCAGCGGCCTGGTGCCGCGCGGCAGCCATATGGGCAGCAGCCATCATCATCATCATCACAGCAGCG
GCCTGGTGCCGCGCGGCAGCCATATGAAAAATATGCCGGAAAATCACAATCCACAAGCGAATGCCTGGACTGCCGAATTTCCTCCTGAAATGAG
CTATGTAGTATTTGCGCAGATTGGGATTCAAAGCAAGTCTTTGGATCACGCAGCGGAACATTTGGGAATGATGAAAAAGAGTTTCGATTTGCGG
ACAGGCCCCAAACATGTGGATCGAGCCTTGCATCAAGGAGCCGATGGATACCAAGATTCCATCTTTTTAGCCTACTGGGATGAGCCTGAAACAT
TTAAATCATGGGTTGCGGATCCTGAAGTACAAAAGTGGTGGTCGGGTAAAAAAATCGATGAAAATAGTCCAATCGGGTATTGGAGTGAGGTAAC
GACCATTCCGATTGATCACTTTGAGACTCTTCATTCCGGAGAAAATTACGATAATGGGGTTTCACACTTTGTACCGATCAAGCATACAGAAGTCC
ATGAATATTGGGGAGCAATGCGCGACCGCATGCCGGTGTCTGCCAGTAGTGATTTGGAAAGCCCCCTTGGCCTTCAATTACCGGAACCCATTGTC
CGGGAGTCTTTCGGAAAACGGCTAAAAGTCACGGCGCCGGATAATATTTGCTTGATTCGAACCGCTCAAAATTGGTCTAAATGTGGTAGCGGGG
AAAGGGAAACGTATATAGGACTAGTGGAACCGACCCTCATAAAAGCGAATACGTTTCTTCGTGAAAATGCTAGTGAAACAGGCTGTATTAGTTC
AAAATTAGTCTATGAACAGACCCATGACGGCGAAATAGTAGATAAATCATGTGTCATCGGATATTATCTCTCCATGGGGCATCTTGAACGCTGG
ACGCATGATCATCCAACACATAAAGCGATCTACGGAACCTTTTATGAGATGTTGAAAAGGCATGATTTTAAGACCGAACTTGCTTTATGGCACGA
GGTTTCGGTGCTTCAATCCAAAGATATCGAGCTTATCTATGTCAACTGCCATCCGAGTACTGGATTTCTTCCATTCTTTGAAGTGACAGAAATTCA
AGAGCCTTTACTGAAAAGCCCTAGCGTCAGGATCCAGTAA

11.2.2 Amino acid sequence OxdB (B-WT)

MGSSHHHHHHSSGLVPRGSHMKNMPENHNPQANAWTAEFPPEMSYVVFAQIGIQSKSLDHAAEHLGMMKKSFDLRTGPKHVDRALHQGADGYQDS
IFLAYWDEPETFKSWVADPEVQKWWSGKKIDENSPIGYWSEVTTIPIDHFETLHSGENYDNGVSHFVPIKHTEVHEYWGAMRDRMPVSASSDLESPLG
LQLPEPIVRESFGKRLKVTAPDNICLIRTAQNWSKCGSGERETYIGLVEPTLIKANTFLRENASETGCISSKLVYEQTHDGEIVDKSCVIGYYLSMGHLER
WTHDHPTHKAIYGTFYEMLKRHDFKTELALWHEVSVLQSKDIELIYVNCHPSTGFLPFFEVTEIQEPLLKSPSVRIQ*

11.2.3 Base sequence OxdBSol1

ATGGGCAGCAGCCATCATCATCATCATCACAGCAGCGGCCTGGTGCCGCGCGGCAGCCATATGAAAAACAAACGCGAGAATCATAATCCGCAG
GCAAATGCATGGACCGCAGAATTTCCGCGTGAAATGAGCTATGTTGTTTTTGCCCAGATTGGCATTCAGAGCAAAAGCCTGGATCATGCAGCAG
AACATCTGGGTATGATGAAAAAATCATTTGATCTGCGTACCGGTCCGAAACATGTTGATCGTGCACTGCATCAGGGTGCAGATGGTTATCAGGAT
AGCATTTTTCTGGCATATTGGGATGAACCGGAAACCTTTAAAAGCTGGGTTGCAGATCCGGAAGTTCAGAAATGGTGGTCAGGCAAAAAAATCG
ATGAAAATAGCCCGATTGGTTATTGGAGCGAAGTTACCACCATTCCGATTGATCATTTTGAAACCCTGCATAGCGGTGAGAATTATGATAATGGT
GTTAGCCATTTCGTGCCGATCAAACATACCGAAGTTCATGAATATTGGGGTGCAATGCGTGATCGTATGCCGGTTAGCGCAAGCAGCGATCTGG
AAAGTCCGCTGGGTCTGCAGCTGCCTGAACCGATTGTTCGTGAAAGCTTTGGTAAACGTCTGAAAGTTACCGCACCGGATAACATTTGTCTGATT
CGTACCGCACAGAATTGGAGCAAATGTGGTAGCGGTGAACGTGAAACCTATATTGGTCTGGTTGAACCGACACTGATTAAAGCAAATACCTTTC
TGCGTGAAAATGCAAGCGAAACCGGTTGTATTAGCAGCAAACTGGTTTATGAACAGACCCATGATGGTGAGATTGTTGATAAAAGCTGCGTGAT
TGGCTATTATCTGAGCATGGGTCATCTGGAACGTTGGACACATGATCATCCGACACATAAAGCAATTTATGGCACCTTTTACGAGATGCTGAAAC
GCCATGATTTCAAAACCGAACTGGCACTGTGGCATGAAGTTAGCGTTCTGCAGAGCAAAGATATTGAACTGATTTACGTTAATTGCCATCCGAGC
ACCGGTTTTCTGCCGTTTTTTGAAGTTACCGAAATTCAAGAACCGCTGCTGAAAAGCCCGAGCGTTCGTATTCAGTAA

11.2.4 Amino acid sequence OxdBSol1

MGSSHHHHHHSSGLVPRGSHMKNKRENHNPQANAWTAEFPREMSYVVFAQIGIQSKSLDHAAEHLGMMKKSFDLRTGPKHVDRALHQGADGYQDS
IFLAYWDEPETFKSWVADPEVQKWWSGKKIDENSPIGYWSEVTTIPIDHFETLHSGENYDNGVSHFVPIKHTEVHEYWGAMRDRMPVSASSDLESPLG
LQLPEPIVRESFGKRLKVTAPDNICLIRTAQNWSKCGSGERETYIGLVEPTLIKANTFLRENASETGCISSKLVYEQTHDGEIVDKSCVIGYYLSMGHLER
WTHDHPTHKAIYGTFYEMLKRHDFKTELALWHEVSVLQSKDIELIYVNCHPSTGFLPFFEVTEIQEPLLKSPSVRIQ*

11.2.5 Base sequence OxdBSol2

ATGGGCAGCAGCCATCATCATCATCATCACAGCAGCGGCCTGGTGCCGCGCGGCAGCCATATGAAGAACATGCCGGAAAATCATAATCCGCAGG
CAAATGCATGGACCGCAGAATTTCCGCCTGAAATGAGCTATGTTGTTTTTGCCCAGATTGGCATTCAGAGCAAAAGCCTGGATCATGCAGCAGA
ACATCTGGGTATGATGAAAAAATCATTTGATCTGCGTACCGGTCCGAAACATGAAGATCGTGCACTGCATCAGGGTGCAGATGGTTATCAGGAT
AGCATTTTTCTGGCATATTGGGATGAACCGGAAACCTTTAAAAGCTGGGTTGCAGATCCGGAAGTTCAAGAATGGTGGTCAGGCAAAAAAATCG
ATGAAAATAGCCCGATTGGTTATTGGAGCGAAGTTACCACAATTCCGATCGATCATTTTGAAACCCTGCATAGCGGTGAGAATTATGATAATGGT
GTTAGCCATTTCGTGCCGATCAAACATACCGAAGTTCATGAATATTGGGGTGCAATGCGTGATCGTATGCCGGTTAGCGCAAGCAGCGATCTGG
AAAGTCCGCTGGGTCTGCAGCTGCCTGAACCGATTGTTCGTGAAAGTTTTGGTAAACGTCTGAAAGTTACCGCACCGGATAACATTTGTCTGATT
CGTACCGCACAGAATTGGAGCAAATGTGGTAGCGGTGAACGTGAAACCTATGAAGGTCGTGTTGAACCGACACTGATTAAAGCAAATACCTTTC
TGCGTGAAAATGCAAGCGAAACCGGTTGTATTAGCAGCAAACTGGTTTATGAACAGACCCATGATGGTGAGATTGTTGATAAAAGCTGCGTGAT
TGGCTATTATCTGAGCATGGGTCATCTGGAACGTTGGACACATGATCATCCGACACATAAAGCAATTCGTGGCACCTTTTATGAAATGCTGAAAC
GCCATGATTTCAAAACCGAACTGGCACTGTGGCATGAAGTTAGCGTTCTGCAGAGCAAAGATATTGAACTGATTTACGTTAATTGCCATCCGAGC
ACCGGTTTTCTGCCGTTTTTTGAAGTTACCGAAATTCAAGAACCGCTGCTGAAAAGCCCGAGCGTTCGTATTCAGTAA

11.2.6 Amino acid sequence OxdBSol2

MGSSHHHHHHSSGLVPRGSHMKNMPENHNPQANAWTAEFPPEMSYVVFAQIGIQSKSLDHAAEHLGMMKKSFDLRTGPKHEDRALHQGADGYQDSI
FLAYWDEPETFKSWVADPEVQEWWSGKKIDENSPIGYWSEVTTIPIDHFETLHSGENYDNGVSHFVPIKHTEVHEYWGAMRDRMPVSASSDLESPLGL
QLPEPIVRESFGKRLKVTAPDNICLIRTAQNWSKCGSGERETYEGRVEPTLIKANTFLRENASETGCISSKLVYEQTHDGEIVDKSCVIGYYLSMGHLER
WTHDHPTHKAIRGTFYEMLKRHDFKTELALWHEVSVLQSKDIELIYVNCHPSTGFLPFFEVTEIQEPLLKSPSVRIQ*

11.2.7 Base sequence OxdBSol3

ATGGGCAGCAGCCATCATCATCATCATCACAGCAGCGGCCTGGTGCCGCGCGGCAGCCATATGAAAAACAAACGCGAGAATCATAATCCGCAG
GCAAATGCATGGACCGCAGAATTTCCGCGTGAAATGAGCTATGTTGTTTTTGCCCAGATTGGCATTCAGAGCAAAAGCCTGGATCATGCAGCAG
AACATCTGGGTATGATGAAAAAATCATTTGATCTGCGTACCGGTCCGAAACATGAAGATCGTGCACTGCATCAGGGTGCAGATGGTTATCAGGA
TAGCATTTTTCTGGCATATTGGGATGAACCGGAAACCTTTAAAAGCTGGGTTGCAGATCCGGAAGTTCAAGAATGGTGGTCAGGCAAAAAAATC
GATGAAAATAGCCCGATTGGTTATTGGAGCGAAGTTACCACAATTCCGATCGATCATTTTGAAACCCTGCATAGCGGTGAGAATTATGATAATG
GTGTTAGCCATTTCGTGCCGATCAAACATACCGAAGTTCATGAATATTGGGGTGCAATGCGTGATCGTATGCCGGTTAGCGCAAGCAGCGATCTG
GAAAGTCCGCTGGGTCTGCAGCTGCCTGAACCGATTGTTCGTGAAAGCTTTGGTAAACGTCTGAAAGTTACCGCACCGGATAACATTTGTCTGAT
TCGTACCGCACAGAATTGGAGCAAATGTGGTAGCGGTGAACGTGAAACCTATCGTGGTCTGGTTGAACCGACACTGATTAAAGCAAATACCTTT
CTGCGTGAAAATGCAAGCGAAACCGGTTGTATTAGCAGCAAACTGGTTTATGAACAGACCCATGATGGTGAGATTGTTGATAAAAGCTGCGTGA
TTGGCTATTATCTGAGCATGGGTCATCTGGAACGTTGGACACATGATCATCCGACACATAAAGCAATTCGTGGCACCTTTTATGAAATGCTGAAA
CGCCATGATTTCAAAACCGAACTGGCACTGTGGCATGAAGTTAGCGTTCTGCAGAGCAAAGATATTGAACTGATTTACGTTAATTGCCATCCGAG
CACCGGTTTTCTGCCGTTTTTTGAAGTTACCGAAATTCAAGAACCGCTGCTGAAAAGCCCGAGCGTTCGTATTCAGTAA

11.2.8 Amino acid sequence OxdBSol3

MGSSHHHHHHSSGLVPRGSHMKNKRENHNPQANAWTAEFPREMSYVVFAQIGIQSKSLDHAAEHLGMMKKSFDLRTGPKHEDRALHQGADGYQDSI
FLAYWDEPETFKSWVADPEVQEWWSGKKIDENSPIGYWSEVTTIPIDHFETLHSGENYDNGVSHFVPIKHTEVHEYWGAMRDRMPVSASSDLESPLGL
QLPEPIVRESFGKRLKVTAPDNICLIRTAQNWSKCGSGERETYRGLVEPTLIKANTFLRENASETGCISSKLVYEQTHDGEIVDKSCVIGYYLSMGHLER
WTHDHPTHKAIRGTFYEMLKRHDFKTELALWHEVSVLQSKDIELIYVNCHPSTGFLPFFEVTEIQEPLLKSPSVRIQ*

11.2.9 Base sequence OxdB-Set1

ATGGGCAAAAATATGCCGGAAAATCGAAATCGACAAGCGAATGCCTGGACTGCCGAATTTCCTCCTCAGATGCGATATGTAGTATTTGCGCAGA
TTGGGATTCAAAGCAAGTCTTTGGATCACGCAGCGGAACATTTGGGAATGATGAAAAAGAGTTTCGATTTGCGGACAGGCCCCAAACATGTGGA
TCGAGCCTTGCATCAAGGAGCCGATGGATACCAAGATTCCATCTTTTTAGCCTACTGGGATGAGCCTGAAACATTTAAATCATGGGTTGCGGATC
CTGAAGTACAAAAGTGGTGGTCGGGTAAAAAAATCGATGAAAATAGTCCAATCGGGTATTGGAGTGAGGTAATGACCATTCCGATTGATCACTT
TGAGACTCTTCATTCCGGAGAAAATTACGATAATGGGGTTTCACACTTTGTACCGATCAAGCATACAGAAGTCCATGAATATTGGGGAGCAATG
CGCGACCGCATGCCGGTGTCTGCCAGTAGTGATTTGGAAAGCCCCCTTGGCCTTCAATTACCGGAACCCATTGTCCGGGAGTCTTTCGGAAAACG
GCTAAAAGTCATTGCGCCGGATAATATTTGCTTGATTCGAACCGCTCAAAATTGGTCTAAATGTGGTAGCGGGGAAAGGGAAACGTATATAGGA
CTAGTGGAACCGACCCTCATAAAAGCGAATACGTTTCTTCGTGAAAATGCTAGTGAAACAGGCTGTATTAGTTCAAAATTAGTCTATGAACAGA
CCCATGACGGCGAAATAGTAGATAAATCATGTGTCATCGGATATTATCTTTCAATGGGGCATCTTGAACGCTGGACGCATGATCATCCAACACAT
AAAGCGATCTACGGAACCTTTTATGAGATGTTGAAAAGGCATGATTTTAAGACCGAACTTGCTTTATGGCACGAGGTTTCGGTGCTTCAATCCAA
AGATATCATTCTTATCTATGTCAACTGCCATCCGATTACTGGATTTCTTCCATTCTTTGTGGTGATTGAAATTCAAGAGCCTTTACTGAAAAGCCC
TAGCGTCAGGATCCAGTAA

11.2.10 Amino acid sequence OxdB-Set1

MGKNMPENRNRQANAWTAEFPPQMRYVVFAQIGIQSKSLDHAAEHLGMMKKSFDLRTGPKHVDRALHQGADGYQDSIFLAYWDEPETFKSWVADP
EVQKWWSGKKIDENSPIGYWSEVMTIPIDHFETLHSGENYDNGVSHFVPIKHTEVHEYWGAMRDRMPVSASSDLESPLGLQLPEPIVRESFGKRLKVIA
PDNICLIRTAQNWSKCGSGERETYIGLVEPTLIKANTFLRENASETGCISSKLVYEQTHDGEIVDKSCVIGYYLSMGHLERWTHDHPTHKAIYGTFYEML
KRHDFKTELALWHEVSVLQSKDIILIYVNCHPITGFLPFFVVIEIQEPLLKSPSVRIQ*

11.2.11 Base sequence OxdB-Set1a

ATGGGCAAAAATATGCCGGAAAATCACAATCGACAAGCGAATGCCTGGACTGCCGAATTTCCTCCTGAAATGCGATATGTAGTATTTGCGCAGA
TTGGGATTCAAAGCAAGTCTTTGGATCACGCAGCGGAACATTTGGGAATGATGAAAAAGAGTTTCGATTTGCGGACAGGCCCCAAACATGTGGA
TCGAGCCTTGCATCAAGGAGCCGATGGATACCAAGATTCCATCTTTTTAGCCTACTGGGATGAGCCTGAAACATTTAAATCATGGGTTGCGGATC
CTGAAGTACAAAAGTGGTGGTCGGGTAAAAAAATCGATGAAAATAGTCCAATCGGGTATTGGAGTGAGGTAACGACCATTCCGATTGATCACTT
TGAGACTCTTCATTCCGGAGAAAATTACGATAATGGGGTTTCACACTTTGTACCGATCAAGCATACAGAAGTCCATGAATATTGGGGAGCAATG
CGCGACCGCATGCCGGTGTCTGCCAGTAGTGATTTGGAAAGCCCCCTTGGCCTTCAATTACCGGAACCCATTGTCCGGGAGTCTTTCGGAAAACG
GCTAAAAGTCATTGCGCCGGATAATATTTGCTTGATTCGAACCGCTCAAAATTGGTCTAAATGTGGTAGCGGGGAAAGGGAAACGTATATAGGA
CTAGTGGAACCGACCCTCATAAAAGCGAATACGTTTCTTCGTGAAAATGCTAGTGAAACAGGCTGTATTAGTTCAAAATTAGTCTATGAACAGA
CCCATGACGGCGAAATAGTAGATAAATCATGTGTCATCGGATATTATCTCAGTATGGGCCACCTGGAGCGTTGGACCCACGACCACCCAACACA

TAAAGCGATCTACGGAACCTTTTATGAGATGTTGAAAAGGCATGATTTTAAGACCGAACTTGCTTTATGGCACGAGGTTTCGGTGCTTCAATCCA
AAGATATCGAGCTTATCTATGTCAACTGCCATCCGAGTACTGGATTTCTTCCATTCTTTGAAGTGACAGAAATTCAAGAGCCTTTACTGAAAAGC
CCTAGCGTCAGGATCCAGTAA

11.2.12 Amino acid sequence OxdB-Set1a

MGKNMPENHNRQANAWTAEFPPEMRYVVFAQIGIQSKSLDHAAEHLGMMKKSFDLRTGPKHVDRALHQGADGYQDSIFLAYWDEPETFKSWVADP
EVQKWWSGKKIDENSPIGYWSEVTTIPIDHFETLHSGENYDNGVSHFVPIKHTEVHEYWGAMRDRMPVSASSDLESPLGLQLPEPIVRESFGKRLKVIAP
DNICLIRTAQNWSKCGSGERETYIGLVEPTLIKANTFLRENASETGCISSKLVYEQTHDGEIVDKSCVIGYYLSMGHLERWTHDHPTHKAIYGTFYEMLK
RHDFKTELALWHEVSVLQSKDIELIYVNCHPSTGFLPFFEVTEIQEPLLKSPSVRIQ*

11.2.13 Base sequence OxdB-Set1b

ATGGGCAAAAATATGCCGGAAAATCACAATCCACAAGCGAATGCCTGGACTGCCGAATTTCCTCCTGAAATGAGCTATGTAGTATTTGCGCAGA
TTGGGATTCAAAGCAAGTCTTTGGATCACGCAGCGGAACATTTGGGAATGATGAAAAAGAGTTTCGATTTGCGGACAGGCCCCAAACATGTGGA
TCGAGCCTTGCATCAAGGAGCCGATGGATACCAAGATTCCATCTTTTTAGCCTACTGGGATGAGCCTGAAACATTTAAATCATGGGTTGCGGATC
CTGAAGTACAAAAGTGGTGGTCGGGTAAAAAAATCGATGAAAATAGTCCAATCGGGTATTGGAGTGAGGTAACGACCATTCCGATTGATCACTT
TGAGACTCTTCATTCCGGAGAAAATTACGATAATGGGGTTTCACACTTTGTACCGATCAAGCATACAGAAGTCCATGAATATTGGGGAGCAATG
CGCGACCGCATGCCGGTGTCTGCCAGTAGTGATTTGGAAAGCCCCCTTGGCCTTCAATTACCGGAACCCATTGTCCGGGAGTCTTTCGGAAAACG
GCTAAAAGTCACGGCGCCGGATAATATTTGCTTGATTCGAACCGCTCAAAATTGGTCTAAATGTGGTAGCGGGGAAAGGGAAACGTATATAGGA
CTAGTGGAACCGACCCTCATAAAAGCGAATACGTTTCTTCGTGAAAATGCTAGTGAAACAGGCTGTATTAGTTCAAAATTAGTCTATGAACAGA
CCCATGACGGCGAAATAGTAGATAAATCATGTGTCATCGGATATTATCTGTCGATGGGACATCTTGAACGCTGGACGCATGATCATCCAACACAT
AAAGCGATCTACGGAACCTTTTATGAGATGTTGAAAAGGCATGATTTTAAGACCGAACTTGCTTTATGGCACGAGGTTTCGGTGCTTCAATCCAA
AGATATCATTCTTATCTATGTCAACTGCCATCCGATTACTGGATTTCTTCCATTCTTTGTGGTGATTGAAATTCAAGAGCCTTTACTGAAAAGCCC
TAGCGTCAGGATCCAGTAA

11.2.14 Amino acid sequence OxdB-Set1b

MGKNMPENHNPQANAWTAEFPPEMSYVVFAQIGIQSKSLDHAAEHLGMMKKSFDLRTGPKHVDRALHQGADGYQDSIFLAYWDEPETFKSWVADP
EVQKWWSGKKIDENSPIGYWSEVTTIPIDHFETLHSGENYDNGVSHFVPIKHTEVHEYWGAMRDRMPVSASSDLESPLGLQLPEPIVRESFGKRLKVTA
PDNICLIRTAQNWSKCGSGERETYIGLVEPTLIKANTFLRENASETGCISSKLVYEQTHDGEIVDKSCVIGYYLSMGHLERWTHDHPTHKAIYGTFYEML
KRHDFKTELALWHEVSVLQSKDIILIYVNCHPITGFLPFFVVIEIQEPLLKSPSVRIQ*

11.2.15 Base sequence OxdB-Set2

ATGGGCAAAAATATGCCGGAAAATCACAATCGACAAGCGAATGCCTGGACTGCCGAATTTCCTCCTGAAATGCGATATGTAGTATTTGCGCAGA
TTGGGATTCAAAGCAAGTCTTTGGATCACGCAGCGGAACATTTGGGAATGATGAAAAAGAGTTTCGATTTGCGGACAGGCCCCAAACATGTGGA
TCGAGCCTTGCATCAAGGAGCCGATGGATACCAAGATTCCATCTTTTTAGCCTACTGGGATGAGCCTGAAACATTTAAATCATGGGTTGCGGATC
CTGAAGTACAAAAGTGGTGGTCGGGTAAAAAAATCGATGAAAATAGTCCAATCGGGTATTGGAGTGAGGTAACGACCATTCCGATTGATCACTT
TGAGACTCTTCATTCCGGAGAAAATTACGATAATGGGGTTTCACACTTTGTACCGATCAAGCATACAGAAGTCCATGAATATTGGGGAGCAATG
CGCGACCGCATGCCGGTGTCTGCCAGTAGTGATTTGGAAAGCCCCCTTGGCCTTCAATTACCGGAACCCATTGTCCGGGAGTCTTTCGGAAAACG
GCTAAAAGTCATTGCGCCGGATAATATTTGCTTGATTCGAACCGCTCAAAATTGGTCTAAATGTGGTAGCGGGGAAAGGGAAACGTATATAGGA
CTAGTGGAACCGACCCTCATAAAAGCGAATACGTTTCTTCGTGAAAATGCTAGTGAAACAGGCTGTATTAGTTCAAAATTAGTCTATGAACAGA
CCCATGACGGCGAAATAGTAGATAAATCATGTGTCATCGGATATTATCTCAGTATGGGCCACCTGGAGCGTTGGACCCACGACCACCCAACACA
TAAAGCGATCTACGGAACCTTTTATGAGATGTTGAAAAGGCATGATTTTAAGACCGAACTTGCTTTATGGCACGAGGTTTCGGTGCTTCAATCCA
AAGATATCGAGCTTATCTATGTCAACTGCCATCCGAGTACTGGATTTCTTCCATTCTTTGAAGTGACAGAAATTCAAGAGCCTTTACTGAAAAGC
CCTAGCGTCAGGATCCAGTAA

11.2.16 Amino acid sequence OxdB-Set2

MGKNMPENHNRQANAWTAEFPPQMRYVVFAQIGIQSKSLDHAAEHLGMMKKSFDLRTGPKHVDRALHQGADGYQDSIFLAYWDEPETFKSWVADP
EVQKWWSGKKIDENSPIGYWSEVMTIPIDHFETLHSGENYDNGVSHFVPIKHTEVHEYWGAMRDRMPVSASSDLESPLGLQLPEPIVRESFGKRLKVIA
PDNICLIRTAQNWSKCGSGERETYIGLVEPTLIKANTFLRENASETGCISSKLVYEQTHDGEIVDKSCVIGYYLSMGHLERWTHDHPTHKAIYGTFYEML
KRHDFKTELALWHEVSVLQSKDIILIYVNCHPSTGFLPFFEVTEIQEPLLKSPSVRIQ*

11.2.17 Base sequence OxdB-F288/L293A mutant (B5)

ATGGGCAAGAACATGCCCGAGAACCATAACCCGCAGGCTAACGCTTGGACCGCAGAGTTTCCCCCGGAGATGAGTTACGTTGTGTTCGCACAAA
TCGGCATCCAGTCGAAAAGCTTAGACCATGCTGCCGAGCACCTGGGCATGATGAAGAAAAGCTTTGACTTACGCACTGGACCGAAGCACGTTGA
CCGCGCGTTACACCAGGGTGCTGACGGTTATCAGGACTCGATTTTCCTTGCTTATTGGGACGAACCGGAGACGTTCAAGAGCTGGGTGGCTGACC
CCGAGGTCCAGAAATGGTGGTCAGGCAAGAAGATTGACGAGAACTCGCCTATTGGCTACTGGTCGGAAGTTACCACAATCCCTATCGACCATTT
CGAAACCCTGCACTCCGGGGAGAACTATGACAACGGAGTGAGTCATTTCGTCCCCATTAAACACACTGAGGTTCACGAGTACTGGGGCGCTATG
CGTGATCGTATGCCAGTCTCCGCATCTTCAGACCTGGAGTCTCCGCTCGGTCTGCAGCTGCCTGAGCCGATCGTACGCGAAAGCTTTGGCAAGCG
TTTGAAGGTTACAGCTCCCGACAACATCTGTCTGATCCGCACTGCGCAGAACTGGTCAAAGTGCGGCAGTGGCGAGCGTGAGACCTACATTGGT
CTGGTTGAGCCTACATTAATTAAGGCTAACACTTTCCTGCGCGAGAACGCAAGCGAGACCGGATGCATCAGCTCCAAGCTCGTTTACGAGCAAA
CTCACGATGGAGAGATTGTTGACAAGAGCTGCGTAATTGGTTACTACCTGTCGATGGGCCACCTGGAGCGTTGGACTCACGACCACCCCACGCA
CAAGGCCATTTATGGTACTGCCTACGAAATGGCAAAGCGTCACGACTTCAAAACTGAGCTGGCGCTGTGGCATGAAGTGTCCGTTTTGCAGTCG
AAGGACATTGAATTGATTTACGTTAATTGTCACCCCTCAACCGGCTTCCTGCCGTTCTTCGAGGTTACGGAGATCCAGGAACCGCTGCTTAAGTC
TCCGAGTGTTCGTATTCAATGA

11.2.18 Amino acid sequence

MGKNMPENHNPQANAWTAEFPPEMSYVVFAQIGIQSKSLDHAAEHLGMMKKSFDLRTGPKHVDRALHQGADGYQDSIFLAYWDEPETFKSWVADP
EVQKWWSGKKIDENSPIGYWSEVTTIPIDHFETLHSGENYDNGVSHFVPIKHTEVHEYWGAMRDRMPVSASSDLESPLGLQLPEPIVRESFGKRLKVTA
PDNICLIRTAQNWSKCGSGERETYIGLVEPTLIKANTFLRENASETGCISSKLVYEQTHDGEIVDKSCVIGYYLSMGHLERWTHDHPTHKAIYGTAYEM
AKRHDFKTELALWHEVSVLQSKDIELIYVNCHPSTGFLPFFEVTEIQEPLLKSPSVRIQ

11.3 OxdRE aldoxime dehydratase from *Rhodococcss erythropolis* as pET28a construct

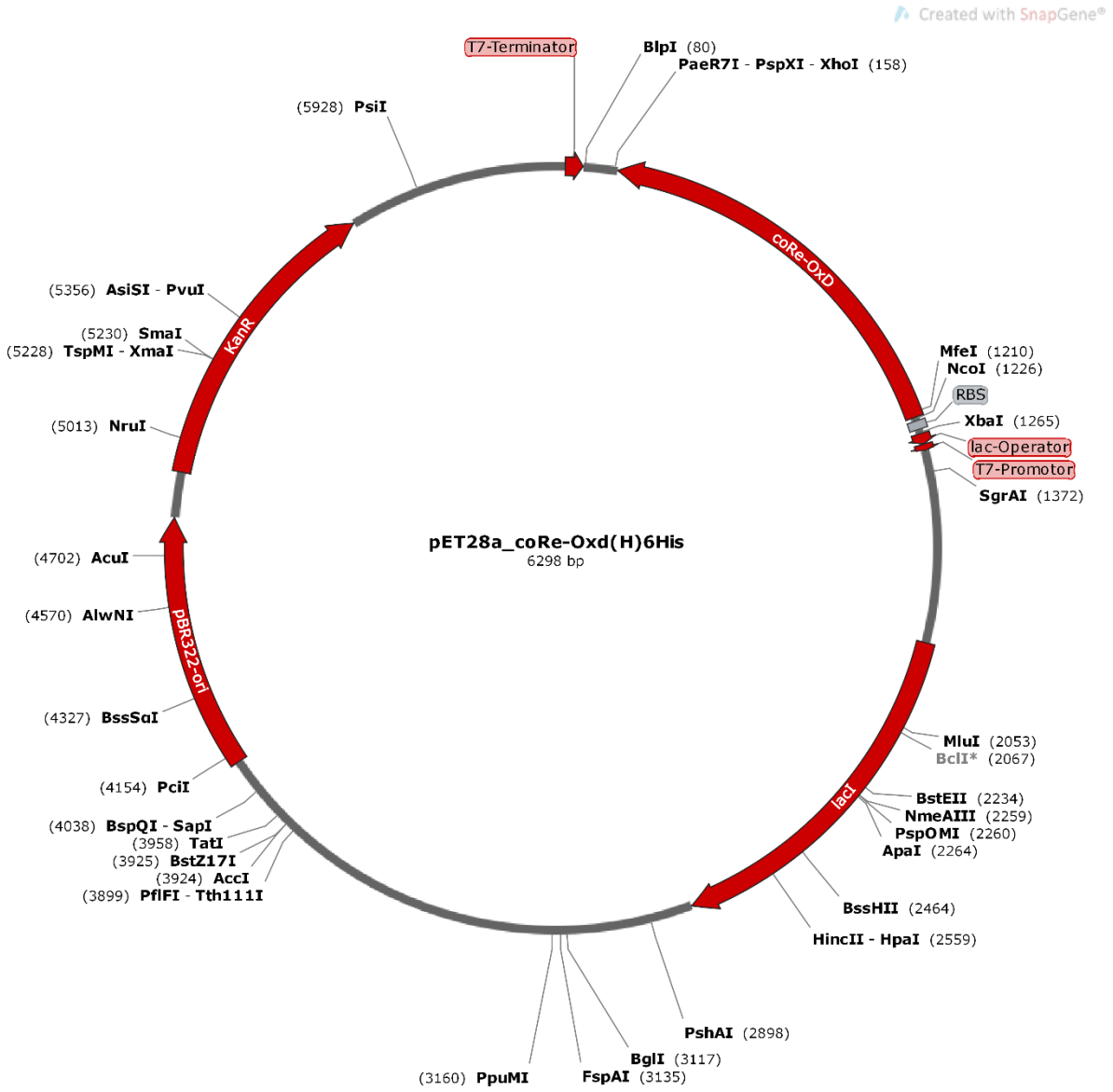

11.3.1 Aldoxime dehydratase from *Rhodococcss erythropolis* (*Rhodococcss sp*. N-771, OxdRE) Base sequence (Accession number: GenBank: AB094201.1)

ATGGGCAGCAGCCATCATCATCATCATCACAGCAGCGGCCTGGTGCCGCGCGGCAGCCATATGGAAAGCGCAATTGGTGAACATCTGCAGTGTC
CGCGTACCCTGACCCGTCGTGTTCCGGATACCTATACCCCTCCGTTTCCGATGTGGGTTGGTCGTGCAGATGATGCACTGCAGCAGGTTGTTATG
GGTTATCTGGGTGTTCAGTTTCGTGATGAAGATCAGCGTCCGGCAGCACTGCAGGCAATGCGTGATATTGTTGCAGGTTTTGATCTGCCGGATGG
TCCGGCACATCATGATCTGACCCATCATATTGATAATCAGGGCTATGAAAACCTGATTGTGGTGGGTTATTGGAAAGATGTTAGCAGCCAGCATC
GTTGGAGCACCAGCACCCCGATTGCAAGTTGGTGGGAAAGCGAAGATCGTCTGAGTGATGGTCTGGGTTTTTTTCGTGAAATTGTGGCACCGCGT
GCAGAACAGTTTGAAACCCTGTATGCATTTCAAGAAGATCTGCCTGGCGTTGGTGCAGTTATGGATGGTATTAGCGGTGAAATTAACGAACATG
GTTATTGGGGTAGCATGCGTGAACGTTTTCCGATTAGCCAGACCGATTGGATGCAGGCAAGCGGTGAACTGCGTGTTATTGCCGGTGATCCGGCA
GTTGGTGGTCGTGTTGTTGTTCGTGGTCATGATAACATTGCACTGATTCGTAGCGGTCAGGATTGGGCAGATGCCGAAGCAGATGAACGTAGCCT
GTATCTGGATGAAATTCTGCCGACCCTGCAGAGCGGTATGGATTTTCTGCGTGATAATGGTCCTGCAGTTGGTTGTTATAGCAATCGTTTTGTGCG
CAACATTGATATCGATGGCAATTTTCTGGATCTGAGCTATAACATTGGTCATTGGGCAAGCCTGGATCAGCTGGAACGTTGGAGCGAAAGCCATC
CGACCCATCTGCGTATTTTTACCACCTTTTTTCGCGTTGCAGCCGGTCTGAGCAAACTGCGTCTGTATCATGAAGTTAGCGTTTTTGATGCAGCAG
ATCAGCTGTATGAATACATTAATTGTCATCCGGGTACAGGTATGCTGCGTGATGCAGTTACCATTGCAGAACATTAA

11.3.2 Amino acid sequence (Uniprot: Q76K71)

MESAIGEHLQCPRTLTRRVPDTYTPPFPMWVGRADDALQQVVMGYLGVQFRDEDQRPAALQAMRDIVAGFDLPDGPAHHDLTHHIDNQGYENLIVV
GYWKDVSSQHRWSTSTPIASWWESEDRLSDGLGFFREIVAPRAEQFETLYAFQEDLPGVGAVMDGISGEINEHGYWGSMRERFPISQTDWMQASGEL
RVIAGDPAVGGRVVVRGHDNIALIRSGQDWADAEADERSLYLDEILPTLQSGMDFLRDNGPAVGCYSNRFVRNIDIDGNFLDLSYNIGHWASLDQLER
WSESHPTHLRIFTTFFRVAAGLSKLRLYHEVSVFDAADQLYEYINCHPGTGMLRDAVTIAEH*

11.3.3 Base sequence OxdRE-L145F

TTAATGTTCTGCAATGGTAACTGCATCACGCAGCATACCTGTACCCGGATGACAATTAATGTATTCATACAGCTGATCTGCTGCATCAAAAACGC
TAACTTCATGATACAGACGCAGTTTGCTCAGACCGGCTGCAACGCGAAAAAAGGTGGTAAAAATACGCAGATGGGTCGGATGGCTTTCGCTCCA
ACGTTCCAGCTGATCCAGGCTTGCCCAATGACCAATGTTATAGCTCAGATCCAGAAAATTGCCATCGATATCAATGTTGCGCACAAAACGATTGC
TATAACAACCAACTGCAGGACCATTATCACGCAGAAAATCCATACCGCTCTGCAGGGTCGGCAGAATTTCATCCAGATACAGGCTACGTTCATCT
GCTTCGGCATCTGCCCAATCCTGACCGCTACGAATCAGTGCAATGTTATCATGACCACGAACAACAACACGACCACCAACTGCCGGATCACCGG
CAATAACACGCAGTTCACCGCTTGCCTGCATCCAATCGGTCTGGCTAATCGGAAAACGTTCACGCATGCTACCCCAATAACCATGTTCGTTAATT
TCACCGCTAATACCATCCATAACTGCACCAACGCCAGGCAGATCTTCTTGAAATGCATAGAAGGTTTCAAACTGTTCTGCACGCGGTGCCACAAT
TTCACGAAAAAAACCCAGACCATCACTCAGACGATCTTCGCTTTCCCACCAACTTGCAATCGGGGTGCTGGTGCTCCAACGATGCTGGCTGCTAA
CATCTTTCCAATAACCCACCACAATCAGGTTTTCATAGCCCTGATTATCAATATGATGGGTCAGATCATGATGTGCCGGACCATCCGGCAGATCA
AAACCTGCAACAATATCACGCATTGCCTGCAGTGCTGCCGGACGCTGATCTTCATCACGAAACTGAACACCCAGATAACCCATAACAACCTGCT
GCAGTGCATCATCTGCACGACCAACCCACATCGGAAACGGAGGGGTATAGGTATCCGGAACACGACGGGTCAGGGTACGCGGACACTGCAGAT
GTTCACCAATTGCGCTTTCCAT

11.3.4 Amino acid sequence OxdRE-L145F

MESAIGEHLQCPRTLTRRVPDTYTPPFPMWVGRADDALQQVVMGYLGVQFRDEDQRPAALQAMRDIVAGFDLPDGPAHHDLTHHIDNQGYENLIVV
GYWKDVSSQHRWSTSTPIASWWESEDRLSDGLGFFREIVAPRAEQFETFYAFQEDLPGVGAVMDGISGEINEHGYWGSMRERFPISQTDWMQASGELR
VIAGDPAVGGRVVVRGHDNIALIRSGQDWADAEADERSLYLDEILPTLQSGMDFLRDNGPAVGCYSNRFVRNIDIDGNFLDLSYNIGHWASLDQLERW
SESHPTHLRIFTTFFRVAAGLSKLRLYHEVSVFDAADQLYEYINCHPGTGMLRDAVTIAEH*

11.3.5 Base sequence OxdRE-10-(3M)-M28-L145A-A147G

TTAATGTTCTGCAATGGTAACTGCATCACGCAGCATACCTGTACCCGGATGACAATTAATGTATTCATACAGCTGATCTGCTGCATCAAAAACGC
TAACTTCATGATACAGACGCAGTTTGCTCAGACCGGCTGCAACGCGAAAAAAGGTGGTAAAAATACGCAGATGGGTCGGATGGCTTTCGCTCCA
ACGTTCCAGCTGATCCAGGCTTGCCCAATGACCAATGTTATAGCTCAGATCCAGAAAATTGCCATCGATATCAATGTTGCGCACAAAACGATTGC
TATAACAACCAACTGCAGGACCATTATCACGCAGAAAATCCATACCGCTCTGCAGGGTCGGCAGAATTTCATCCAGATACAGGCTACGTTCATCT
GCTTCGGCATCTGCCCAATCCTGACCGCTACGAATCAGTGCAATGTTATCATGACCACGAACAACAACACGACCACCAACTGCCGGATCACCGG
CAATAACACGCAGTTCACCGCTTGCCTGCATCCAATCGGTCTGGCTAATCGGAAAACGTTCACGCATGCTACCCCAATAACCATGTTCGTTAATT
TCACCGCTAATACCATCCATAACTGCACCAACGCCAGGCAGATCTTCTTGAAAGCCATATGCGGTTTCAAACTGTTCTGCACGCGGTGCCACAAT
TTCACGAAAAAAACCCAGACCATCACTCAGACGATCTTCGCTTTCCCACCAACTTGCAATCGGGGTGCTGGTGCTCCAACGATGCTGGCTGCTAA
CATCTTTCCAATAACCCACCACAATCAGGTTTTCATAGCCCTGATTATCAATATGATGGGTCAGATCATGATGTGCCGGACCATCCGGCAGATCA
AAACCTGCAACAATATCACGCATTGCCTGCAGTGCTGCCGGACGCTGATCTTCATCACGAAACTGAACACCCAGATAACCCATAACAACCTGCT
GCAGTGCATCATCTGCACGACCAACCCACGCCGGAAACGGAGGGGTATAGGTATCCGGAACACGACGGGTCAGGGTACGCGGACACTGCAGAT
GTTCACCAATTGCGCTTTCCAT

11.3.6 Amino acid sequence OxdRE-10-(3M)-M28-L145A-A147G

MESAIGEHLQCPRTLTRRVPDTYTPPFPAWVGRADDALQQVVMGYLGVQFRDEDQRPAALQAMRDIVAGFDLPDGPAHHDLTHHIDNQGYENLIVV
GYWKDVSSQHRWSTSTPIASWWESEDRLSDGLGFFREIVAPRAEQFETAYGFQEDLPGVGAVMDGISGEINEHGYWGSMRERFPISQTDWMQASGEL
RVIAGDPAVGGRVVVRGHDNIALIRSGQDWADAEADERSLYLDEILPTLQSGMDFLRDNGPAVGCYSNRFVRNIDIDGNFLDLSYNIGHWASLDQLER
WSESHPTHLRIFTTFFRVAAGLSKLRLYHEVSVFDAADQLYEYINCHPGTGMLRDAVTIAEH*

11.3.7 Base sequence OxdRE-25-(3G)-M29G-L145G-A147G

TTAATGTTCTGCAATGGTAACTGCATCACGCAGCATACCTGTACCCGGATGACAATTAATGTATTCATACAGCTGATCTGCTGCATCAAAAACGC
TAACTTCATGATACAGACGCAGTTTGCTCAGACCGGCTGCAACGCGAAAAAAGGTGGTAAAAATACGCAGATGGGTCGGATGGCTTTCGCTCCA
ACGTTCCAGCTGATCCAGGCTTGCCCAATGACCAATGTTATAGCTCAGATCCAGAAAATTGCCATCGATATCAATGTTGCGCACAAAACGATTGC
TATAACAACCAACTGCAGGACCATTATCACGCAGAAAATCCATACCGCTCTGCAGGGTCGGCAGAATTTCATCCAGATACAGGCTACGTTCATCT
GCTTCGGCATCTGCCCAATCCTGACCGCTACGAATCAGTGCAATGTTATCATGACCACGAACAACAACACGACCACCAACTGCCGGATCACCGG
CAATAACACGCAGTTCACCGCTTGCCTGCATCCAATCGGTCTGGCTAATCGGAAAACGTTCACGCATGCTACCCCAATAACCATGTTCGTTAATT
TCACCGCTAATACCATCCATAACTGCACCAACGCCAGGCAGATCTTCTTGAAAGCCATAGCCGGTTTCAAACTGTTCTGCACGCGGTGCCACAAT
TTCACGAAAAAAACCCAGACCATCACTCAGACGATCTTCGCTTTCCCACCAACTTGCAATCGGGGTGCTGGTGCTCCAACGATGCTGGCTGCTAA
CATCTTTCCAATAACCCACCACAATCAGGTTTTCATAGCCCTGATTATCAATATGATGGGTCAGATCATGATGTGCCGGACCATCCGGCAGATCA
AAACCTGCAACAATATCACGCATTGCCTGCAGTGCTGCCGGACGCTGATCTTCATCACGAAACTGAACACCCAGATAACCCATAACAACCTGCT
GCAGTGCATCATCTGCACGACCAACCCACCCCGGAAACGGAGGGGTATAGGTATCCGGAACACGACGGGTCAGGGTACGCGGACACTGCAGAT
GTTCACCAATTGCGCTTTCCAT

11.3.8 Amino acid sequence OxdRE-10-(3M)-M29G-L145G-A147G

MESAIGEHLQCPRTLTRRVPDTYTPPFPGWVGRADDALQQVVMGYLGVQFRDEDQRPAALQAMRDIVAGFDLPDGPAHHDLTHHIDNQGYENLIVV
GYWKDVSSQHRWSTSTPIASWWESEDRLSDGLGFFREIVAPRAEQFETGYGFQEDLPGVGAVMDGISGEINEHGYWGSMRERFPISQTDWMQASGEL
RVIAGDPAVGGRVVVRGHDNIALIRSGQDWADAEADERSLYLDEILPTLQSGMDFLRDNGPAVGCYSNRFVRNIDIDGNFLDLSYNIGHWASLDQLER
WSESHPTHLRIFTTFFRVAAGLSKLRLYHEVSVFDAADQLYEYINCHPGTGMLRDAVTIAEH*´

11.4 OxdA Plasmid aldoxime dehydratase from *Pseudomonas chlororaphis* as pET28a construct

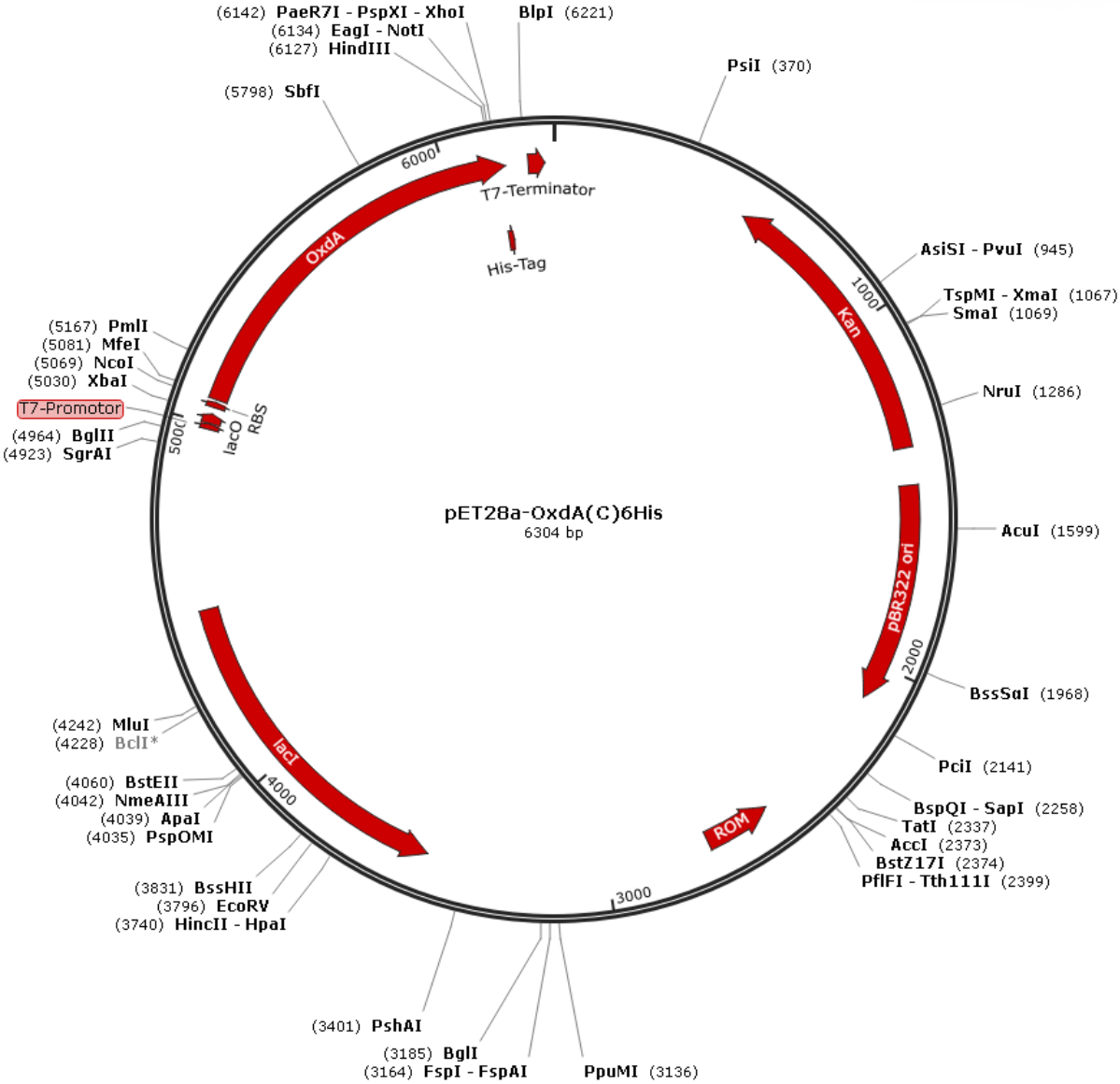

11.4.1 Aldoxime dehydratase from *Pseudomonas chlororaphis* B23 (OxdA) Base sequence (Accession number: GenBank: AB093544.1)

ATGGAAAGCGCAATTGATACCCATCTGAAATGTCCGCGTACCCTGAGCCGTCGTGTTCCGGAAGAATATCAGCCTCCGTTTCCGATGTGGGTTGC
ACGTGCCGATGAACAGCTGCAGCAGGTTGTTATGGGTTATCTGGGTGTTCAGTATCGTGGTGAAGCACAGCGTGAAGCAGCACTGCAGGCAATG
CGTCATATTGTTAGCAGCTTTAGCCTGCCGGATGGTCCGCAGACCCATGATCTGACCCATCATACCGATAGCAGCGGTTTTGATAATCTGATGGT
TGTGGGTTATTGGAAAGATCCGGCAGCACATTGTCGTTGGCTGCGTAGTGCCGAAGTTAATGATTGGTGGACCAGCCAGGATCGTCTGGGTGAA
GGTCTGGGTTATTTTCGTGAAATTAGCGCACCGCGTGCAGAACAGTTTGAAACCCTGTATGCATTTCAGGATAATCTGCCTGGTGTTGGTGCAGT
TATGGATAGCACCAGCGGTGAAATTGAAGAACATGGTTATTGGGGTAGCATGCGTGATCGTTTTCCGATTAGCCAGACCGATTGGATGAAACCG
ACCAATGAACTGCAGGTTGTTGCCGGTGATCCGGCAAAGGTGGTCGTGTTGTTATTATGGGTCATGATAACATTGCACTGATTCGTAGCGGTCAG
GATTGGGCAGATGCAGAAGCAGAAGAACGTAGCCTGTATCTGGATGAAATTCTGCCGACCCTGCAGGATGGTATGGATTTTCTGCGTGATAATG
GTCAGCCGCTGGGTTGTTATAGCAATCGTTTTGTTCGTAATATCGATCTGGATGGCAATTTTCTGGATGTGAGCTATAACATTGGTCATTGGCGTA
GCCTGGAAAAACTGGAACGTTGGGCAGAAAGCCATCCGACCCATCTGCGTATTTTTGTTACCTTTTTTCGTGTTGCAGCCGGTCTGAAAAAACTG

CGTCTGTATCATGAAGTTAGCGTGAGTGATGCAAAAAGCCAGGTGTTTGAATATATCAACTGTCATCCGCATACCGGCATGCTGCGTGATGCAGT
TGTTGCACCGACCAAGCTTGCGGCCGCACTCGAGC ACCACCACCACCACCACTGA

11.4.2 Amino acid sequence (Uniprot: Q7WSJ4)

MESAIDTHLKCPRTLSRRVPEEYQPPFPMWVARADEQLQQVVMGYLGVQYRGEAQREAALQAMRHIVSSFSLPDGPQTHDLTHHTDSSGFDNLMVV
GYWKDPAAHCRWLRSAEVNDWWTSQDRLGEGLGYFREISAPRAEQFETLYAFQDNLPGVGAVMDSTSGEIEEHGYWGSMRDRFPISQTDWMKPTNE
LQVVAGDPAKGGRVVIMGHDNIALIRSGQDWADAEAEERSLYLDEILPTLQDGMDFLRDNGQPLGCYSNRFVRNIDLDGNFLDVSYNIGHWRSLEKL
ERWAESHPTHLRIFVTFFRVAAGLKKLRLYHEVSVSDAKSQVFEYINCHPHTGMLRDAVVAPT

11.4.3 Base sequence OxdA-L145F

ATGGAAAGCGCAATTGATACCCATCTGAAATGTCCGCGTACCCTGAGCCGTCGTGTTCCGGAAGAATATCAGCCTCCGTTTCCGATGTGGGTTGC
ACGTGCCGATGAACAGCTGCAGCAGGTTGTTATGGGTTATCTGGGTGTTCAGTATCGTGGTGAAGCACAGCGTGAAGCAGCACTGCAGGCAATG
CGTCATATTGTTAGCAGCTTTAGCCTGCCGGATGGTCCGCAGACCCATGATCTGACCCATCATACCGATAGCAGCGGTTTTGATAATCTGATGGT
TGTGGGTTATTGGAAAGATCCGGCAGCACATTGTCGTTGGCTGCGTAGTGCCGAAGTTAATGATTGGTGGACCAGCCAGGATCGTCTGGGTGAA
GGTCTGGGTTATTTTCGTGAAATTAGCGCACCGCGTGCAGAACAGTTTGAAACCTTTTATGCATTTCAGGATAATCTGCCTGGTGTTGGTGCAGTT
ATGGATAGCACCAGCGGTGAAATTGAAGAACATGGTTATTGGGGTAGCATGCGTGATCGTTTTCCGATTAGCCAGACCGATTGGATGAAACCGA
CCAATGAACTGCAGGTTGTTGCCGGTGATCCGGCAAAAGGTGGTCGTGTTGTTATTATGGGTCATGATAACATTGCACTGATTCGTAGCGGTCAG
GATTGGGCAGATGCAGAAGCAGAAGAACGTAGCCTGTATCTGGATGAAATTCTGCCGACCCTGCAGGATGGTATGGATTTTCTGCGTGATAATG
GTCAGCCGCTGGGTTGTTATAGCAATCGTTTTGTTCGTAATATCGATCTGGATGGCAATTTTCTGGATGTGAGCTATAACATTGGTCATTGGCGTA
GCCTGGAAAAACTGGAACGTTGGGCAGAAAGCCATCCGACCCATCTGCGTATTTTTGTTACCTTTTTTCGTGTTGCAGCCGGTCTGAAAAAACTG
CGTCTGTATCATGAAGTTAGCGTGAGTGATGCAAAAAGCCAGGTGTTTGAATATATCAACTGTCATCCGCATACCGGCATGCTGCGTGATGCAGT
TGTTGCACCGACCAAGCTTGCGGCCGCACTCGAGCACCACCACCACCACCACTGA

11.4.4 Amino acid sequence OxdA-L145F

MESAIDTHLKCPRTLSRRVPEEYQPPFPMWVARADEQLQQVVMGYLGVQYRGEAQREAALQAMRHIVSSFSLPDGPQTHDLTHHTDSSGFDNLMVV
GYWKDPAAHCRWLRSAEVNDWWTSQDRLGEGLGYFREISAPRAEQFETFYAFQDNLPGVGAVMDSTSGEIEEHGYWGSMRDRFPISQTDWMKPTNE
LQVVAGDPAKGGRVVIMGHDNIALIRSGQDWADAEAEERSLYLDEILPTLQDGMDFLRDNGQPLGCYSNRFVRNIDLDGNFLDVSYNIGHWRSLEKL
ERWAESHPTHLRIFVTFFRVAAGLKKLRLYHEVSVSDAKSQVFEYINCHPHTGMLRDAVVAPTKLAAALEHHHHHH*

12 References

[1] H.-J. Arpe, *Industrial organic chemistry*, Wiley-VCH Verlag, Weinheim, **2016**.

[2] R. A. Reck, *J. Am. Oil Chem. Soc.* **1985**, *62*, 355.

[3] H. Surburg, J. Panten, *Common fragrance and flavor materials. Preparation, properties and uses*, Wiley-VCH, Weinheim, **2010**.

[4] a) E. B. Villhauer, J. A. Brinkman, G. B. Naderi, B. F. Burkey, B. E. Dunning, K. Prasad, B. L. Mangold, M. E. Russell, T. E. Hughes, *J. Med. Chem.* **2003**, *46*, 2774; b) L. Pellegatti, J. Sedelmeier, *Org. Process Res. Dev.* **2015**, *19*, 551; c) S. A. Savage, G. S. Jones, S. Kolotuchin, S. A. Ramrattan, T. Vu, R. E. Waltermire, *Org. Process Res. Dev.* **2009**, *13*, 1169; d) Y.-H. Wang, F. Zhang, H. Diao, R. Wu, *ACS Catal.* **2019**, *9*, 2292.

[5] S. S. Joshi, A. Bhatnagar, V. V. Ranade in *Industrial Catalytic Processes for Fine and Specialty Chemicals* (Eds.: V. V. Ranade, S. S. Joshi), Elsevier, Amsterdam, **2016**, pp. 317–392.

[6] William, C. D., Richard, V. L., JR., US3496215, **1965**.

[7] H. Gröger, Y. Asano, *J. Org. Chem.* **2020**, *85*, 6243.

[8] Y. Asano, Y. Kato, *FEMS Microbiol. Lett.* **1998**, *158*, 185.

[9] Y. Asano, *J. Biotechnol.* **2002**, *94*, 65.

[10] M. Sørensen, E. H. J. Neilson, B. L. Møller, *Mol. Plant.* **2018**, *11*, 95.

[11] Y. Asano, S. Okazaki in *Future Directions in Biocatalysis (Second Edition)* (Ed.: T. Matsuda), Elsevier, **2017**, pp. 173–187.

[12] Y. Kato, T. Tsuda, Y. Asano, *Eur. J. Biochem.* **1999**, *263*, 662.

[13] Y. Kato, K. Nakamura, H. Sakiyama, S. G. Mayhew, Y. Asano, *Biochemistry* **2000**, *39*, 800.

[14] H. Sawai, H. Sugimoto, Y. Kato, Y. Asano, Y. Shiro, S. Aono, *J. Biol. Chem.* **2009**, *284*, 32089.

[15] X.-L. Pan, F.-C. Cui, W. Liu, J.-Y. Liu, *J. Phys. Chem. B* **2012**, *116*, 5689.

[16] J. Nomura, H. Hashimoto, T. Ohta, Y. Hashimoto, K. Wada, Y. Naruta, K.-I. Oinuma, M. Kobayashi, *PNAS* **2013**, *110*, 2810.

[17] K. Kobayashi, M. Kubo, S. Yoshioka, T. Kitagawa, Y. Kato, Y. Asano, S. Aono, *ChemBioChem* **2006**, *7*, 2004.

[18] Y. Kato, Y. Asano, *Appl. Microbiol. Biotechnol.* **2006**, *70*, 92.

[19] K. Kobayashi, S. Yoshioka, Y. Kato, Y. Asano, S. Aono, *J. Biol. Chem.* **2005**, *280*, 5486.

[20] R.-Z. Liao, W. Thiel, *J. Phys. Chem. B* **2012**, *116*, 9396.

[21] R. Rädisch, M. Chmátal, L. Rucká, P. Novotný, L. Petrásková, P. Halada, M. Kotik, M. Pátek, L. Martínková, *Int. J. Biol. Macromol.* **2018**, *115*, 746.

[22] J. E. Choi, S. Shinoda, Y. Asano, H. Gröger, *Catalysts* **2020**, *10*, 362.

[23] T. Betke, J. Higuchi, P. Rommelmann, K. Oike, T. Nomura, Y. Kato, Y. Asano, H. Gröger, *ChemBioChem* **2018**, *19*, 768.

[24] K.-I. Oinuma, Y. Hashimoto, K. Konishi, M. Goda, T. Noguchi, H. Higashibata, M. Kobayashi, *J. Biol. Chem.* **2003**, *278*, 29600.

[25] Y. Kato, Y. Asano, *Biosci. Biotechnol. Biochem.* **2005**, *69*, 2254.

[26] Y. Kato, S. Yoshida, S.-X. Xie, Y. Asano, *J. Biosci. Bioeng.* **2004**, *97*, 250.

[27] S.-X. Xie, Y. Kato, H. Komeda, S. Yoshida, Y. Asano, *Biochemistry* **2003**, *42*, 12056.

[28] A. Hinzmann, S. Glinski, M. Worm, H. Gröger, *J. Org. Chem.* **2019**.

[29] a) K. Kühnel, S. C. Maurer, Y. Galeyeva, W. Frey, S. Laschat, V. B. Urlacher, *Adv. Synth. Catal.* **2007**, *349*, 1451; b) D. Zehentgruber, F. Hannemann, S. Bleif, R. Bernhardt, S. Lütz, *ChemBioChem* **2010**, *11*, 713.

[30] H. Yamada, M. Kobayashi, *Biosci. Biotechnol. Biochem.* **1996**, *60*, 1391.

[31] S. Wu, R. Snajdrova, J. C. Moore, K. Baldenius, U. T. Bornscheuer, *Angew. Chem. Int. Ed.* **2021**, *60*, 88.

[32] William, C. D., J. R, Richard, V. L., JR., US3536748, **1967**.

[33] T. Betke, M. Maier, H. Gruber-Wölfler, H. Gröger, *Nat. Commun.* **2018**, *9*, 5112.

[34] a) R. Plagemann, J. Langermann, U. Kragl, *Eng. Life Sci.* **2014**, *14*, 493; b) D. Uhrich, J. von Langermann, *Front. Microbiol.* **2017**, *8*, 2111; c) M. Frese, N. Sewald, *Angew. Chem. Int. Ed.* **2015**, *54*, 298; d) J. Löwe, A. A. Ingram, H. Gröger, *Bioorg. Med. Chem.* **2018**, *26*, 1387.

[35] a) A. Idris, A. Bukhari, *Biotechnol. Adv.* **2012**, *30*, 550; b) D.-X. Jia, T. Wang, Z.-J. Liu, L.-Q. Jin, J.-J. Li, C.-J. Liao, D.-S. Chen, Y.-G. Zheng, *J. Biosci. Bioeng.* **2018**, *126*, 176.

[36] A. Hinzmann, M. Stricker, H. Gröger, *Catalysts* **2020**, *10*, 1073.

[37] A. Hinzmann, N. Adebar, T. Betke, M. Leppin, H. Gröger, *Eur. J. Org. Chem.* **2019**, *41*, 6911.

[38] N. Adebar, H. Gröger, *Eur. J. Org. Chem.* **2020**, *38*, 6062.

[39] C. Plass, A. Hinzmann, M. Terhorst, W. Brauer, K. Oike, H. Yavuzer, Y. Asano, A. J. Vorholt, T. Betke, H. Gröger, *ACS Catal.* **2019**, *9*, 5198.

[40] a) M. Kirihara, T. Okada, Y. Sugiyama, M. Akiyoshi, T. Matsunaga, Y. Kimura, *Org. Process Res. Dev.* **2017**, *21*, 1925; b) T. Okada, T. Asawa, Y. Sugiyama, T. Iwai, M. Kirihara, Y. Kimura, *Tetrahedron* **2016**, *72*, 2818; c) T. Okada, T. Asawa, Y. Sugiyama, M. Kirihara, T. Iwai, Y. Kimura, *Synlett* **2014**, *25*, 596.

[41] A. Hinzmann, M. Stricker, J. Busch, S. Glinski, K. Oike, H. Gröger, *Eur. J. Org. Chem.* **2020**, *16*, 2399.

[42] A. Hinzmann, M. Stricker, H. Gröger, *ACS Sustainable Chem. Eng.* **2020**, *8*, 17088.

[43] J. E. Choi, S. Shinoda, R. Inoue, D. Zheng, H. Gröger, Y. Asano, *Biocatal. Biotransformation* **2019**, *37*, 414.

[44] T. J. Jennings, US3260731, **1964**.

[45] A. Hinzmann, T. Betke, Y. Asano, H. Gröger, *Chemistry* **2021**, *27*, 5313.

[46] R. Metzner, S. Okazaki, Y. Asano, H. Gröger, *ChemCatChem* **2014**, *6*, 3105.

[47] T. Betke, P. Rommelmann, K. Oike, Y. Asano, H. Gröger, *Angew. Chem. Int. Ed.* **2017**, *56*, 12361.

[48] H. Yavuzer, Y. Asano, H. Gröger, *Angew. Chem. Int. Ed.* **2021**.

[49] R. M. Neyyappadath, R. Chisholm, M. D. Greenhalgh, C. Rodríguez-Escrich, M. A. Pericàs, G. Hähner, A. D. Smith, *ACS Catal.* **2018**, *8*, 1067.

[50] P. Hoyos, M. Fernández, J. V. Sinisterra, A. R. Alcántara, *J. Org. Chem.* **2006**, *71*, 7632.

[51] F. Kühn, S. Katsuragi, Y. Oki, C. Scholz, S. Akai, H. Gröger, *Chem. Commun.* **2020**, *56*, 2885.

[52] K. Higashio, S. Katsuragi, D. Kundu, N. Adebar, C. Plass, F. Kühn, H. Gröger, S. Akai, *Eur. J. Org. Chem.* **2020**, *2020*, 1961.

[53] K. Yasukawa, R. Hasemi, Y. Asano, *Adv. Synth. Catal.* **2011**, *353*, 2328.

[54] B. M. Nestl, S. C. Hammer, B. A. Nebel, B. Hauer, *Angew. Chem. Int. Ed.* **2014**, *53*, 3070.

[55] C. Li, R. Zhang, J. Wang, L. M. Wilson, Y. Yan, *Trends Biotechnol.* **2020**, *38*, 729.

[56] U. T. Bornscheuer, M. Höhne (Eds.) *Protein engineering. Methods and protocols*, Humana Press; Springer, New York, NY, **2018**.

[57] U. T. Bornscheuer, G. W. Huisman, R. J. Kazlauskas, S. Lutz, J. C. Moore, K. Robins, *Nature* **2012**, *485*, 185.

[58] F. H. Arnold, *Acc. Chem. Res.* **1998**, *31*, 125.

[59] P. A. Romero, F. H. Arnold, *Nat. Rev. Mol. Cell Biol.* **2009**, *10*, 866.

[60] S. Lutz, *Curr. Opin. Biotechnol.* **2010**, *21*, 734.

[61] B. Seelig, J. W. Szostak, *Nature* **2007**, *448*, 828.

[62] G. Kiss, N. Çelebi-Ölçüm, R. Moretti, D. Baker, K. N. Houk, *Angew. Chem. Int. Ed.* **2013**, *52*, 5700.

[63] M. T. Reetz, *J. Am. Chem. Soc.* **2013**, *135*, 12480.

[64] M. T. Reetz, *Angew. Chem. Int. Ed.* **2011**, *50*, 138.

[65] M. T. Reetz, *PNAS* **2004**, *101*, 5716.

[66] S. F. Sousa, P. A. Fernandes, M. J. Ramos, *Proteins* **2006**, *65*, 15.

[67] a) J. L. Medina-Franco, O. Méndez-Lucio, J. Yoo, *Int. J. Mol. Sci.* **2014**, *15*, 3253; b) D. B. Kitchen, H. Decornez, J. R. Furr, J. Bajorath, *Nat. Rev. Drug Discov.* **2004**, *3*, 935.

[68] V. L. Schramm, *Arch. Biochem. Biophys.* **2005**, *433*, 13.

[69] D. Ghislieri, A. P. Green, M. Pontini, S. C. Willies, I. Rowles, A. Frank, G. Grogan, N. J. Turner, *J. Am. Chem. Soc.* **2013**, *135*, 10863.

[70] a) M. Alexeeva, A. Enright, M. J. Dawson, M. Mahmoudian, N. J. Turner, *Angew. Chem. Int. Ed.* **2002**, *41*, 3177; b) R. Carr, M. Alexeeva, A. Enright, T. S. C. Eve, M. J. Dawson, N. J. Turner, *Angew. Chem. Int. Ed.* **2003**, *42*, 4807.

[71] a) Y. Gumulya, J. Sanchis, M. T. Reetz, *ChemBioChem* **2012**, *13*, 1060; b) D. Li, Q. Wu, M. T. Reetz, *Meth. Enzymol.* **2020**, *643*, 225.

[72] M. Höhne, S. Schätzle, H. Jochens, K. Robins, U. T. Bornscheuer, *Nat. Chem. Biol.* **2010**, *6*, 807.

[73] E. Z. Eisenmesser, D. A. Bosco, M. Akke, D. Kern, *Science* **2002**, *295*, 1520.

[74] J. A. McCammon, B. R. Gelin, M. Karplus, *Nature* **1977**, *267*, 585.

[75] H. J. Wijma, S. J. Marrink, D. B. Janssen, *J. Chem. Inf. Model.* **2014**, *54*, 2079.

[76] H. J. Wijma, R. J. Floor, S. Bjelic, S. J. Marrink, D. Baker, D. B. Janssen, *Angew. Chem. Int. Ed.* **2015**, *127*, 3797.

[77] a) F. Steffen-Munsberg, C. Vickers, A. Thontowi, S. Schätzle, T. Meinhardt, M. Svedendahl Humble, H. Land, P. Berglund, U. T. Bornscheuer, M. Höhne, *ChemCatChem* **2013**, *5*, 154; b) U. T. Bornscheuer, *Eng. Life Sci.* **2004**, *4*, 539; c) U. T. Bornscheuer, B. Hauer, K. E. Jaeger, U. Schwaneberg, *Angew. Chem. Int. Ed.* **2019**, *58*, 36; d) A. Nobili, Y. Tao, I. V. Pavlidis, T. van den Bergh, H.-J. Joosten, T. Tan, U. T. Bornscheuer, *ChemBioChem* **2015**, *16*, 805.

[78] A. Nobili, M. G. Gall, I. V. Pavlidis, M. L. Thompson, M. Schmidt, U. T. Bornscheuer, *FEBS J.* **2013**, *280*, 3084.

[79] M. Voss, D. Das, M. Genz, A. Kumar, N. Kulkarni, J. Kustosz, P. Kumar, U. T. Bornscheuer, M. Höhne, *ACS Catal.* **2018**, *8*, 11524.

[80] a) S. A. Adcock, J. A. McCammon, *Chem. Rev.* **2006**, *106*, 1589; b) M. C. Childers, V. Daggett, *Mol. Syst. Des. Eng.* **2017**, *2*, 9.

[81] X. Sheng, F. Himo, *J. Am. Chem. Soc.* **2019**, *141*, 11230.

[82] J. D. Bloom, S. T. Labthavikul, C. R. Otey, F. H. Arnold, *PNAS* **2006**, *103*, 5869.

[83] K. A. Bava, M. M. Gromiha, H. Uedaira, K. Kitajima, A. Sarai, *Nucleic Acids Res.* **2004**, *32*, D120-1.

[84] a) I. V. Korendovych, *Methods Mol. Biol.* **2018**, *1685*, 15; b) A. V. Gribenko, M. M. Patel, J. Liu, S. A. McCallum, C. Wang, G. I. Makhatadze, *PNAS* **2009**, *106*, 2601.

[85] M. T. Reetz, J. D. Carballeira, A. Vogel, *Angew. Chem. Int. Ed.* **2006**, *45*, 7745.

[86] D. J. Tantillo, C. Jiangang, K. N. Houk, *Curr. Opin. Chem. Biol.* **1998**, *2*, 743.

[87] L. Jiang, E. A. Althoff, F. R. Clemente, L. Doyle, D. Röthlisberger, A. Zanghellini, J. L. Gallaher, J. L. Betker, F. Tanaka, C. F. Barbas et al., *Science* **2008**, *319*, 1387.

[88] D. Röthlisberger, O. Khersonsky, A. M. Wollacott, L. Jiang, J. DeChancie, J. Betker, J. L. Gallaher, E. A. Althoff, A. Zanghellini, O. Dym et al., *Nature* **2008**, *453*, 190.

[89] M. Linder, A. J. Johansson, T. S. G. Olsson, J. Liebeschuetz, T. Brinck, *J. Chem. Inf. Model.* **2011**, *51*, 1906.

[90] A. Kleemann, J. Engel, B. Kutscher, D. Reichert, *Pharmaceutical substances*, Thieme, Stuttgart, New York, **2001**.

[91] H. Gröger, K. Drauz, O. May (Eds.) *Enzyme catalysis in organic synthesis*, WiVCH, Weinheim, New York, **2012**.

[92] H. Gröger, Y. Asano, *J. Org. Chem.* **2020**, *85*, 6243.

[93] S. X. Xie, Y. Kato, Y. Asano, *Biosci. Biotechnol. Biochem.* **2001**, *65*, 2666.

[94] Molecular Operating Environment (MOE) 2019.01 (Chemical Computing Group ULC, Montreal, QC, Canada, 2019).

[95] J. Davila-Calderon, N. N. Patwardhan, L.-Y. Chiu, A. Sugarman, Z. Cai, S. R. Penutmutchu, M.-L. Li, G. Brewer, A. E. Hargrove, B. S. Tolbert, *Nat. Commun.* **2020**, *11*, 4775.

[96] a) A. B. Bueno, B. Sun, F. S. Willard, D. Feng, J. D. Ho, D. B. Wainscott, A. D. Showalter, M. Vieth, Q. Chen, C. Stutsman et al., *Nat. Chem. Biol.* **2020**, *16*, 1105; b) F.-A. Khan, N. Nasim, Y. Wang, A. Alhazmi, M. Sanam, Z. Ul-Haq, D. Yalamati, M. Ulanova, Z.-H. Jiang, *Eur. J. Med. Chem.* **2020**, *209*, 112863; c) J. K. Leman, B. D. Weitzner, S. M. Lewis, J. Adolf-Bryfogle, N. Alam, R. F. Alford, M. Aprahamian, D. Baker, K. A. Barlow, P. Barth et al., *Nat. Methods* **2020**, *17*, 665.

[97] T. Clairfeuille, K. R. Buchholz, Q. Li, E. Verschueren, P. Liu, D. Sangaraju, S. Park, C. L. Noland, K. M. Storek, N. N. Nickerson et al., *Nature* **2020**, *584*, 479.

[98] C. Czekelius, E. M. Carreira, *Angew. Chem. Int. Ed.* **2005**, *44*, 612.

[99] a) G. Sciortino, J. Rodríguez-Guerra Pedregal, A. Lledós, E. Garribba, J.-D. Maréchal, *J. Comput. Chem.* **2018**, *39*, 42; b) V. Muñoz Robles, E. Ortega-Carrasco, L. Alonso-Cotchico, J. Rodriguez-Guerra, A. Lledós, J.-D. Maréchal, *ACS Catal.* **2015**, *5*, 2469.

[100] Y. Miao, R. Metzner, Y. Asano, *ChemBioChem* **2017**, *18*, 451.

[101] H. Yavuzer, H. Gröger, Y. Asano, *Angew. Chem. Int. Ed.* **2021**.

[102] S. Nsikabaka, W. Harb, M. F. Ruiz-López, *J. Mol. Struct.* **2006**, *764*, 161.

[103] a) H. Stetter, *Angew. Chem. Int. Ed.* **1976**, *88*, 695; b) M. Christmann, *Angew. Chem. Int. Ed.* **2005**, *44*, 2632; c) H. Stetter, *Angew. Chem. Int. Ed.* **1976**, *15*, 639; d) O. Bortolini, G. Fantin, M. Fogagnolo, P. P. Giovannini, A. Massi, S. Pacifico, *Org. Biomol. Chem.* **2011**, *9*, 8437.

[104] a) D. Enders, O. Niemeier, T. Balensiefer, *Angew. Chem. Int. Ed.* **2006**, *45*, 1463; b) X. Linghu, J. S. Johnson, *Angew. Chem. Int. Ed.* **2003**, *42*, 2534; c) K. Dong, R. Sang, J.-F. Soule, C. Bruneau, R. Franke, R. Jackstell, M. Beller, *Chemistry* **2015**, *21*, 18033; d) D. Enders, U. Kallfass, *Angew. Chem. Int. Ed.* **2002**, *41*, 1743; e) C. A. Dvorak, V. H. Rawal, *Tetrahedron Lett.* **1998**, *39*, 2925.

[105] M. Paul, P. Sudkaow, A. Wessels, N. E. Schlörer, J.-M. Neudörfl, A. Berkessel, *Angew. Chem. Int. Ed.* **2018**, *57*, 8310.

[106] R. Breslow, *J. Am. Chem. Soc.* **1958**, *80*, 3719.

[107] A. L. E. Larsson, B. A. Persson, J.-E. Bäckvall, *Angew. Chem. Int. Ed.* **1997**, *36*, 1211.

[108] a) D. Belder, M. Ludwig, L.-W. Wang, M. T. Reetz, *Angew. Chem. Int. Ed.* **2006**, *45*, 2463; b) N. Adebar, A. Nastke, H. Gröger, *React. Chem. Eng.* **2021**; c) N. Adebar, H. Gröger, *Bioengineering (Basel, Switzerland)* **2019**, *6*.

[109] T. Betke, P. Rommelmann, K. Oike, Y. Asano, H. Gröger, *Angew. Chem. Int. Ed.* **2017**, *129*, 12533.

[110] R. Franke, D. Selent, A. Börner, *Chem. Rev.* **2012**, *112*, 5675.

[111] I. del Río, O. Pàmies, P. W. van Leeuwen, C. Claver, *J. Organomet. Chemistry* **2000**, *608*, 115.

[112] a) F. G. Delolo, E. N. dos Santos, E. V. Gusevskaya, *Green Chem.* **2019**, *21*, 1091; b) A. G. Panda, M. D. Bhor, S. S. Ekbote, B. M. Bhanage, *Catal Lett* **2009**, *131*, 649; c) A. C. Chen, L. Ren, A. Decken, C. M. Crudden, *Organometallics* **2000**, *19*, 3459; d) T. J. Kwok, D. J. Wink,

Organometallics **1993**, *12*, 1954; e) M. Miyazawa, S. Momose, K. Yamamoto, *Synlett* **1990**, *1990*, 711.

[113] a) O. Tissot, M. Gouygou, F. Dallemer, J.-C. Daran, G. G. A. Balavoine, *Eur. J. Inorg. Chem.* **2001**, *2001*, 2385; b) E. R. Nelsen, C. R. Landis, *Journal of the American Chemical Society* **2013**, *135*, 9636; c) K. Hamza, J. Blum, *Eur. J. Org. Chem.* **2007**, *2007*, 4706.

[114] T. H. Richardson, F. Jung, K. J. Griffin, M. Wester, J. L. Raucy, B. Kemper, L. M. Bornheim, C. Hassett, C. J. Omiecinski, E. F. Johnson, *Arch. Biochem. Biophys.* **1995**, *323*, 87.

[115] E. M. Gillam, Z. Guo, M. V. Martin, C. M. Jenkins, F. P. Guengerich, *Arch. Biochem. Biophys.* **1995**, *319*, 540.

[116] I. Jansson, I. Stoilov, M. Sarfarazi, J. B. Schenkman, *Toxicology* **2000**, *144*, 211.

[117] a) E. Verderber, L. J. Lucast, J. A. van Dehy, P. Cozart, J. B. Etter, E. A. Best, *J. Bacteriol.* **1997**, *179*, 4583; b) K. Sasaki, M. Watanabe, T. Tanaka, *Appl. Microbiol. Biotechnol.* **2002**, *58*, 23; c) G. Levicán, A. Katz, M. de Armas, H. Núñez, O. Orellana, *PNAS* **2007**, *104*, 3135; d) Z. Kang, J. Zhang, J. Zhou, Q. Qi, G. Du, J. Chen, *Biotechnol. Adv.* **2012**, *30*, 1533; e) P. M. McNicholas, G. Javor, S. Darie, R. P. Gunsalus, *FEMS Microbiol. Lett.* **1997**, *146*, 143; f) J. Zhang, Z. Kang, J. Chen, G. Du, *Sci. Rep.* **2015**, *5*, 8584.

[118] a) S. Strumilo, J. Czerniecki, P. Dobrzyn, *Biochem. Biophys. Res. Commun.* **1999**, *256*, 341; b) E. Naito, M. Ito, I. Yokota, T. Saijo, J. Matsuda, Y. Kuroda, *Eur. J. Pediatr.* **1998**, *157*, 648; c) D. S. Flournoy, P. A. Frey, *Biochemistry* **1989**, *28*, 9594.

[119] T. Hara, A. Koda, N. Nozawa, U. Ota, H. Kondo, H. Nakagawa, A. Kamiya, K. Miyashita, H. Itoh, M. Nakajima et al., *FEBS open bio* **2016**, *6*, 515.

[120] E. T. Farinas, U. Schwaneberg, A. Glieder, F. H. Arnold, *Adv. Synth. Catal.* **2001**, *343*, 601.

[121] a) P. Sandhu, T. Baba, F. P. Guengerich, *Arch. Biochem. Biophys.* **1993**, *306*, 443; b) Y. J. Chun, M. Y. Kim, F. P. Guengerich, *Biochem. Biophys. Res. Commun.* **1999**, *262*, 20.

[122] J. W. Dubendorf, F. Studier, *J. Mol. Biol.* **1991**, *219*, 45.

[123] G. L. Rosano, E. A. Ceccarelli, *Front. Microbiol.* **2014**, *5*, 172.

[124] P. J. Shilling, K. Mirzadeh, A. J. Cumming, M. Widesheim, Z. Köck, D. O. Daley, *Commun. Biol.* **2020**, *3*, 214.

[125] G. Hannig, S. C. Makrides, *Trends in Biotechnology* **1998**, *16*, 54.

[126] K. Chen, Z. Wang, K. Ding, Y. Chen, Y. Asano, *GCS* **2021**, 179.

[127] M. Goldsmith, D. S. Tawfik, *Curr. Opin. Struct. Biol.* **2012**, *22*, 406.

[128] E. O. McCullum, B. A. R. Williams, J. Zhang, J. C. Chaput, *Methods Mol. Biol.* **2010**, *634*, 103.

[129] C. G. Acevedo-Rocha, R. Agudo, M. T. Reetz, *J. Biotechnol.* **2014**, *191*, 3.

[130] K. L. Morley, R. J. Kazlauskas, *Trends Biotechnol.* **2005**, *23*, 231.

[131] a) P. Molina-Espeja, J. Viña-Gonzalez, B. J. Gomez-Fernandez, J. Martin-Diaz, E. Garcia-Ruiz, M. Alcalde, *Biotechnol. Adv.* **2016**, *34*, 754; b) O. Salazar, P. C. Cirino, F. H. Arnold, *ChemBioChem* **2003**, *4*, 891.

[132] Z. Luo, W. Zeng, G. Du, S. Liu, F. Fang, J. Zhou, J. Chen, *Bioprocess. Biosyst. Eng.* **2017**, *40*, 693.

[133] R. D. Gupta, D. S. Tawfik, *Nat. Methods* **2008**, *5*, 939.

[134] J.-M. Reymond, *Enzyme assays. High-throughput screening, genetic selection, and fingerprinting*, Wiley-VCH, Weinheim, Germany, **2006**.

[135] S. Lutz, *Curr. Opin. Biotechnol.* **2010**, *21*, 734.

[136] L. Sumbalova, J. Stourac, T. Martinek, D. Bednar, J. Damborsky, *Nucleic Acids Res.* **2018**, *46*, W356-W362.

[137] a) M. T. Reetz, J. D. Carballeira, *Nat. Protoc.* **2007**, *2*, 891; b) C. G. Acevedo-Rocha, S. Hoebenreich, M. T. Reetz, *Methods Mol. Biol.* **2014**, *1179*, 103.

[138] a) G. Qu, A. Li, C. G. Acevedo-Rocha, Z. Sun, M. T. Reetz, *Angew. Chem. Int. Ed.* **2020**, *59*, 13204; b) C. A. Denard, H. Ren, H. Zhao, *Curr. Opin. Chem. Biol.* **2015**, *25*, 55; c) J. Wang, A. Ilie, M. T. Reetz, *Adv. Synth. Catal.* **2017**, *359*, 2056; d) K. Wu, H. Wang, L. Chen, H. Fan, Z. Zhao, D. Wei, *Appl. Microbiol. Biotechnol.* **2016**, *100*, 8757; e) L. Biewenga, T. Saravanan, A. Kunzendorf, J.-Y. van der Meer, T. Pijning, P. G. Tepper, R. van Merkerk, S. J. Charnock, A.-M. W. H. Thunnissen, G. J. Poelarends, *ACS Catal.* **2019**, *9*, 1503.

[139] a) J. Pauly, H. Gröger, A. V. Patel, *J. Biotechnol.* **2018**, *280*, 42; b) J. Pauly, H. Gröger, A. V. Patel, *Green Chem.* **2018**, *20*, 5179; c) J. Pauly, H. Gröger, A. V. Patel, *Catalysts* **2019**, *9*, 547.

[140] F. H. Arnold, *Nature* **2001**, *409*, 253.

[141] L. M. Mayr, D. Bojanic, *Curr. Opin. Pharmacol.* **2009**, *9*, 580.

[142] H. J. Wijma, R. J. Floor, P. A. Jekel, D. Baker, S. J. Marrink, D. B. Janssen, *Protein Eng. Des. Sel.* **2014**, *27*, 49.

[143] J. Bendl, J. Stourac, E. Sebestova, O. Vavra, M. Musil, J. Brezovsky, J. Damborsky, *Nucleic Acids Res.* **2016**, 479.

[144] K. K. Yang, Z. Wu, F. H. Arnold, *Nat. Methods* **2019**, *16*, 687.

[145] a) M. T. Reetz, S. Wilensek, D. Zha, K.-E. Jaeger, *Angew. Chem. Int. Ed.* **2001**, *40*, 3589; b) M. T. Reetz, L.-W. Wang, M. Bocola, *Angew. Chem. Int. Ed.* **2006**, *45*, 1236.

[146] A. M. Bago Rodriguez, L. Schober, A. Hinzmann, H. Gröger, B. P. Binks, *Angew. Chem. Int. Ed.* **2021**, *60*, 1450.

[147] a) H. Zhu, R. Srivastava, J. Q. Brown, M. J. McShane, *Bioconjug. Chem.* **2005**, *16*, 1451; b) Z. Y. Zhao, J. Liu, M. Hahn, S. Qiao, A. P. J. Middelberg, L. He, *RSC Adv.* **2013**, *3*, 22008.

[148] ACD/I-Lab 2.0, Advanced Chemistry Development, Inc., Toronto, ON, Canada, www.acdlabs.com, 2021.

[149] a) J. M. Kwasigroch, D. Gilis, Y. Dehouck, M. Rooman, *Bioinformatics* **2002**, *18*, 1701; b) R. Guerois, J. E. Nielsen, L. Serrano, *J. Mol. Biol.* **2002**, *320*, 369; c) D. Gilis, M. Rooman, *Protein Eng.* **2000**, *13*, 849.

[150] a) E. Capriotti, P. Fariselli, R. Casadio, *Nucleic Acids Res.* **2005**, 306; b) E. Capriotti, P. Fariselli, I. Rossi, R. Casadio, *BMC Bioinform.* **2008**, 6; c) Y. Dehouck, A. Grosfils, B. Folch, D. Gilis, P. Bogaerts, M. Rooman, *Bioinformatics* **2009**, *25*, 2537; d) J. Schymkowitz, J. Borg, F. Stricher, R. Nys, F. Rousseau, L. Serrano, *Nucleic Acids Res.* **2005**, 382.

[151] S. Khan, M. Vihinen, *Hum. Mutat.* **2010**, *31*, 675.

[152] D. A. Drummond, C. O. Wilke, *Nat. Rev. Genet.* **2009**, *10*, 715.

[153] R. K. Kuipers, H.-J. Joosten, W. J. H. van Berkel, N. G. H. Leferink, E. Rooijen, E. Ittmann, F. van Zimmeren, H. Jochens, U. Bornscheuer, G. Vriend et al., *Proteins* **2010**, *78*, 2101.

[154] J. Kyte, R. F. Doolittle, *J. Mol. Biol.* **1982**, *157*, 105.

[155] J. Y. Kim, S. H. Ahn, S. T. Kang, B. J. Yoon, *J. Colloid Interface Sci.* **2006**, *299*, 486.

[156] D. J. Ericsson, A. Kasrayan, P. Johansson, T. Bergfors, A. G. Sandström, J.-E. Bäckvall, S. L. Mowbray, *J. Mol. Biol.* **2008**, *376*, 109.

[157] C. Ceccarelli, Z.-X. Liang, M. Strickler, G. Prehna, B. M. Goldstein, J. P. Klinman, B. J. Bahnson, *Biochemistry* **2004**, *43*, 5266.

[158] a) M. Sagermann, A. Ohtaki, K. Newton, N. Doukyu, *J. Struct. Biol.* **2010**, *170*, 32; b) D. G. Kellner, S.-C. Hung, K. E. Weiss, S. G. Sligar, *J. Biol. Chem.* **2002**, *277*, 9641.

[159] S.-Y. Park, K. Yamane, S. Adachi, Y. Shiro, K. E. Weiss, S. A. Maves, S. G. Sligar, *J. Inorg. Biochem.* **2002**, *91*, 491.

[160] a) I. Geronimo, C. A. Denning, W. E. Rogers, T. Othman, T. Huxford, D. K. Heidary, E. C. Glazer, C. M. Payne, *Biochemistry* **2016**, *55*, 3594; b) M. J. L. J. Fürst, B. Kerschbaumer, C. Rinnofner, A. K. Migglautsch, M. Winkler, M. W. Fraaije, *Adv. Synth. Catal.* **2019**.

[161] N. H. Schlieben, K. Niefind, J. Müller, B. Riebel, W. Hummel, D. Schomburg, *J. Mol. Biol.* **2005**, *349*, 801.

[162] B. J. Sullivan, T. Nguyen, V. Durani, D. Mathur, S. Rojas, M. Thomas, T. Syu, T. J. Magliery, *J. Mol. Biol.* **2012**, *420*, 384.

[163] Yang Jianing, Universität Bielefeld, **2021**.

[164] R. A. Sheldon, I. Arends, U. Hanefeld, *Green chemistry and catalysis*, Wiley-VCH, Weinheim, **2008**.

[165] a) A. A. Desai, *Angew. Chem. Int. Ed.* **2011**, *50*, 1974; b) M. J. Burk, S. van Dien, *Trends Biotechnol.* **2016**, *34*, 187; c) N. R. Barton, A. P. Burgard, M. J. Burk, J. S. Crater, R. E. Osterhout, P. Pharkya, B. A. Steer, J. Sun, J. D. Trawick, S. J. van Dien et al., *J. Ind. Microbiol. Biotechnol.* **2015**, *42*, 349.

[166] A. M. B. Rodriguez, B. P. Binks, *Soft matter* **2020**, *16*, 10221.

[167] L. Schober, H. Yavuzer, A. M. B. Rodriguez, H. Gröger, B. P. Binks, *manuscript in preparation* **2021**.

[168] M. M. Bradford, *Anal. Biochem.* **1976**, 248.